Load Sharing Mechanism of Piled-Raft Foundation in Sand

Rouzbeh Vakili

A Thesis

in the Department

of

Building, Civil and Environmental Engineering

Presented in Partial Fulfilment of the Requirements

for the Degree of

Doctor of Philosophy (Civil Engineering) at

Concordia University

Montreal, Quebec, CANADA

January 2015

CONCORDIA UNIVERSITY

School of Graduate Studies

This is to certify the thesis prepared

By: **Rouzbeh Vakili**

Entitled: **Load Sharing Mechanism of Piled Raft Foundation in Sand**

and submitted in partial fulfillment of the requirements for the degree of

Doctor of Philosophy (Civil Engineering)

complies with the regulations of the University and meets with the accepted standards with respect to originality and quality.

Signed by the final examining committee:

_____ Chair

_____ External Examiner
Dr. T.A. Newson

_____ External to program
Dr. Y.R. Shayan

_____ Examiner
Dr. O. Pekau

_____ Examiner
Dr. A. Zsaki

_____ Supervisor
Dr. A. Hanna

Approved by _____
Dr. M. Zaheeruddin, Chair, Department of Building, Civil & Environmental Engineering

_____2015 _____
Dr. A. Asif
Dean, Faculty of Engineering and Computer Science

ABSTRACT

Load Sharing Mechanism of Piled Raft Foundation in Sand

Rouzbeh Vakili, Ph.D.
Concordia University, 2015

The application of piled raft foundations for supporting high rise buildings has significantly increased over the last few years. The economic benefits of piled raft foundations in comparison with alternative approaches have encouraged this popularity, but this comes with additional complexity for load sharing calculations in a multi-parameter problem. These parameters are, but not limited to: soil density, pile length, pile spacing, raft geometry, and pile installation technique. The complexity of piled raft foundation design demands further research in a range of different engineering aspects.

In this study, the load sharing mechanism of a piled raft foundation in sandy soil was investigated through small scale tests and three dimensional numerical analyses. The effects of density in homogeneous and layered soil, sand particle size distribution, pile installation method, and raft width were studied through experimental analyses. Experimental tests were performed on a shallow footing, single pile and single piled raft unit in clean Silica sand. The results of small scale tests reveal that soil density changes the load sharing mechanism of a displacement piled raft—the pile share increases in denser soil. However, this result does not hold in non-displacement piled rafts where load sharing is independent of soil density. Furthermore, it is observed that particle size distribution has inconsiderable effects on piled raft behavior.

One of the experimental tests on non-displacement piled rafts was employed to calibrate the 3D numerical model, which was further expanded into 2x2 and 3x3 piled raft

foundations. The load sharing outputs of the aforementioned models were compared for a given settlement ratio. This comparison reveals that the number of piles has an inconsiderable impact on the load sharing of non-displacement piled raft given that the piles are identical in size and a minimum spacing among them is respected. The numerical analysis confirms that the conducted experimental tests on non-displacement piled rafts are applicable to predict the load sharing in practical cases. Therefore, an empirical model was developed to achieve this goal under various settlement ratio and pile spacing. The proposed empirical models were validated against the available centrifuge and field test results in the literature.

A widely accepted analytical model in the literature was modified based on the previously conducted experimental results. The proposed model calculates the load sharing as a function of settlement and pile spacing ratio in homogeneous and layers soils.

ACKNOWLEDGEMENTS

Throughout my PhD program, I have been blessed with support and friendship of many whose insights and advices have tremendously enlightened my way of thinking. First, I would like to express my deepest gratitude to my supervisor, Dr. Adel Hanna, for his consistent support, guidance, patience, and encouragement. I have been extremely fortunate to have a supervisor who made the arduous journey through graduate school a continuous learning experience that would last with me forever. Without his vast knowledge, great experience, and remarkable insights, this dissertation would have never been successful.

I have been blessed to receive unconditional guidance and support from my colleagues at Concordia University, Dr. Anup Sinha, Mr. Fabrizio Di Camilio and Mr. Ibrahim Mashhour. I am thankful to the technical staff at Concordia University, including Mr. Joseph Hrib, and Mr. Jaime Yeargans, for the consultation and technical assistance.

Finally, I extend my most gratefulness to my parents, Farah & Ghodrat, who supported me emotionally and financially throughout my studies. Special thanks to my brother, Arash, for his friendship, encouragement, and advices.

TO MY FAMILY

&

TO THE SOUL OF MY BELOVED AUNT

Parivash

TABLE OF CONTENTS

List of Figures

List of Tables

List of Symbols

B_r = Breath of raft

BE = Boundary Elements

C_c = Coefficient of curvature

CCC = Circular cast-in-place concrete pile

C_{ps} = Coefficient of pile spacing

c_u = Coefficient of uniformity

d_{grain} = Diameter of soil particle

d_r = Width of single piled raft unit or effective width of the raft associated with each pile

d_p = Pile diameter

DAS = Data acquisition system

DP = Displacement pile

DPR = Displacement piled raft

D_r = Relative density

D_{10} = Effective particle size

D_{30} = Diameter corresponding to 30% finer in the particle size curve

D_{50} = Average particle size

D_{60} = Diameter corresponding to 60% finer in the particle size curve

e = Void ratio

E = Modulus of elasticity

e_{max} = Maximum void ratio

e_{min} = Minimum void ratio

E_r = Elastic modulus of raft

E_S = Elastic modulus of soil

FE = Finite Elements

G = Shear modulus

G_S = Specific gravity of soil solids

K_p = Stiffness of pile group

K_{pr} = Stiffness of piled raft

K_r = Stiffness of raft

K_{rs} = Raft-soil stiffness ratio

L = Pile length

L_r = Length of raft

$LVDT$ = Linear vertical displacement transducer

M = Pile installation method coefficient

NDP = Non-displacement pile

$NDPR$ = Non-displacement piled raft

NR = Not reported

OCR = Over consolidation ratio

OD = Outer diameter

PDR = Poulos-Davis-Randolph Method

P_p = Ultimate capacity of piles in a piled raft footing

P_1 = Total applied load on a piled raft footing at the pile group failure point

Q_p = Ultimate bearing capacity of single pile

Q_{PG} = Ultimate bearing capacity of pile group

Q_{PR} = Ultimate bearing capacity of piled raft

Q_R = Ultimate bearing capacity of raft

R = Raft (shallow footing)

r_m = Influence radius of pile

S = Pile spacing

t_r = Thickness of raft

$USCS$ = Unified soil classification system

VEE = Visual engineering environment

W = Settlement (displacement)

W_P = Settlement of pile

W_R = Settlement of raft

W_{PR} = Settlement of piled raft

X = Raft share in a piled raft foundation

XCC = X-section cast-in-place concrete pile

α_{rp} = Pile-raft interaction factor proposed by Randolph (1983)

α' = Pile sharing factor proposed by Akinmusuru (1980)

γ = Shear strain

$\gamma_{\max}$ = Maximum dry unit weight

$\gamma_{\min}$ = Minimum dry unit weight

δ = Friction angle between soil particles and sand paper

ε = Normal strain

ν_r = Poisson ratio of raft

ν_s = Poisson ratio of soil

η_{PG} = Pile group efficiency

σ = Normal stress

τ = Shear stress

ϕ = Soil friction angle

$2D$ = Two dimensional

$3D$ = Three dimensional

Chapter 1

Introduction

1.1 General

The piled raft foundation system is a combination of shallow and deep foundations (Figure 1-1), which is mainly used under high rise buildings. The conventional design method for this type of foundation was based on the assumption that the piles carry the entire external load—the raft's contribution was ignored. Burland et al. (1977) initially suggested considering the contribution of the raft in bearing capacity and applying the piles below the raft for controlling the settlement. This idea has since been studied by many other researchers (e.g., Viggiani 2001, Poulos 2001a and b, Mandolini 2003, Randolph et al. 2004). Viggiani et al. (2012) divided piled raft foundations into two main categories: "small" and "large" piled rafts. Small piled rafts are those in which the raft width (B_r) is small in comparison to the pile length (L). In this case, adding piles not only satisfies the appropriate safety factor for bearing capacity, but it also controls the settlement. In large piled rafts ($B_r/L>1$), the raft is usually enough to provide the required bearing capacity and additional piles are used to reduce both total and differential settlements. Either of these pile raft foundations transfers the superstructure load to the soil by a complex soil-structure interaction. The interacting mechanism among foundation elements and their surrounding soil is illustrated schematically in Figure 1-2 and could be classified into two categories: (1) pile-soil-pile and (2) pile-soil-raft.

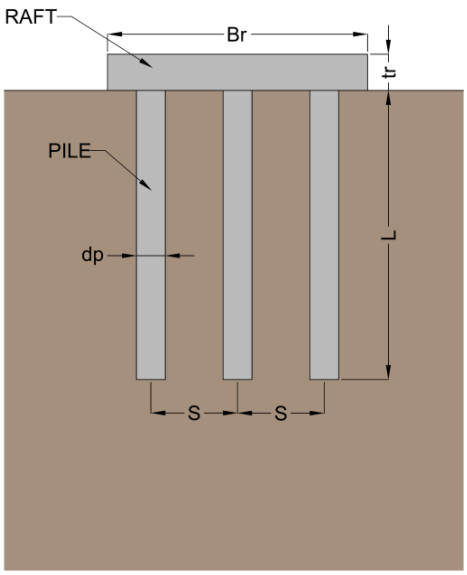

Figure 1-1 Schematic view of a piled raft foundation

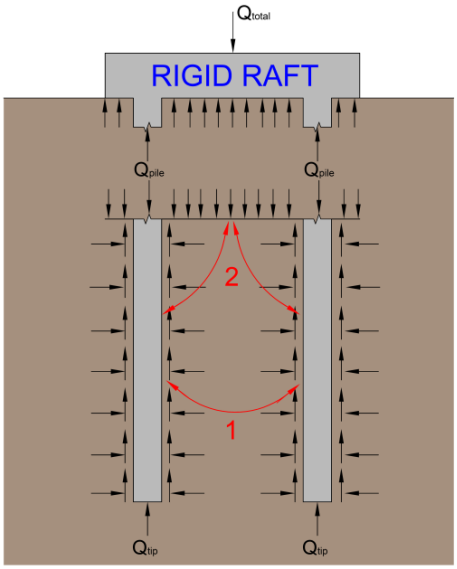

Figure 1-2 Schematic view of load sharing mechanism between pile and rafts in a piled raft foundation (1) pile-soil-pile interaction and (2) pile-soil-raft interaction

The pile-soil-pile interaction is the same as the free standing pile group and is a function of pile spacing and pile installation method. The interaction effect in the pile group design is considered by defining the group efficiency as follows:

$$\eta_{PG} = \frac{Q_{PG}}{n \times Q_P} \tag{1.1}$$

Where Q_{PG} is the pile group's ultimate load, $Q_{P,}$ is the ultimate load of a single pile under equal soil conditions, and n is the number of piles in the group.

Liu et al. (1985) illustrated that for bored piles in sandy soils, the group efficiency is very close to unity and is independent of pile spacing (Phung 1993). The group efficiency of driven piles in cohessionless soil with the usual values of the pile spacing ($2.5 \le s/d_p \le 3.5$) is always greater than 1 (Viggiani et al. 2012). In the design concept of pile groups, for typical pile spacing in loose to dense sand ($3d_p$ to $3.5d_p$), the efficiency is conservatively assumed to be equal to unity.

Pile-soil-raft interaction could have favorable and unfavorable effects on bearing capacity and the settlement of piled rafts, respectively. The pressure between the cap and the soil favorably increases the horizontal stress on the pile shaft and consequently increases the shaft resistance. Whereas, this pressure induces negative skin friction on the piles which increases the settlement. The pile-soil-raft interaction mainly controls the load sharing mechanism of piled raft foundations when pile spacing (S) is more than $3.5d_p$.

The behavior of piled raft foundations in sand has been extensively studied in the literature through experimental and numerical analyses. However, the effect of raft-soil contact on the load sharing mechanism of piled raft footings is not very well understood.

1.2 Purpose of this study

The parameters that could impact the load sharing mechanism of piled raft foundation are, but not limited to: piled raft settlement, soil density, pile length, pile spacing, raft geometry, and pile installation techniques. Different researchers studied the effect of pile length, number of piles,

pile configuration, and cap geometry on piled raft behavior, but less attention has been paid to the other aforementioned parameters. Therefore, the main goal of this study is investigating the effect of soil density, soil stratification, pile installation method, raft width ratio, and piled raft settlement on load sharing mechanism between piles and rigid raft in non-cohesive soil and also developing settlement based methods for estimating the load sharing of piled raft foundations.

1.3 Thesis Outline

The present thesis consists of the following nine chapters.

Chapter 2 covers the background on piled raft foundation behavior including experimental and numerical studies, as well as the field observations.

In Chapter 3 the characteristics of the experimental set up, test soil, and modeled foundations are explained, in addition to a detailed description of testing procedures.

Chapter 4 presents the result of each experimental test in the form of load-settlement and load sharing-settlement curves. The load-settlement curves are analyzed and the ultimate capacity is obtained.

In Chapter 5, parametric study on the experimental results was conducted, the effect of each parameter on load sharing and group efficiency of piled raft footing is studied. The experimental observations are compared with previous studies to shows the consistency of the results.

In Chapter 6, the effect of pile number on the shared load between the piles and the raft is studied through a series of three dimensional numerical analyses. The model is calibrated by the result of a conducted experimental test on a non-displacement piled raft. The validated model is employed to estimate the load sharing of 2x2 and 3x3 non-displacement piled raft in homogeneous sand.

In Chapter 7, empirical design charts for estimating the load sharing and group efficiency of non-displacement piled raft are presented. The proposed empirical models are validated against the available centrifuge and field test results in the literature.

In Chapter 8, Randolph (1983)'s simplified method for load sharing estimation is adjusted to incorporate the effect of settlement on pile-raft interaction factor in homogeneous and layered soil. The proposed analytical model is validated by experimental tests conducted in this study.

Finally, Chapter 9 concludes this thesis with some discussion and potential future research directions.

Chapter 2

Literature Review

2.1 General

The concept of piled raft foundations was originally described by Sievert (1957) and encouraged designers to adopt this approach for high-rise building foundations. Conventionally, the pile group was designed to carry the total applied load notwithstanding the bearing capacity of the raft. Such design is proven to be over-engineered due to the fact that the ratio of the ultimate bearing capacities of piled rafts over pile groups is always greater than one as illustrated in Figure 2-1. Consequently, Hanson et al. (1973) and Borland et al. (1977) proposed a new design philosophy to consider the raft as the main bearing element and to apply the pile group as the settlement reducer. Following this idea, the implemented piles below the raft are designed to operate typically at 70-80% of their ultimate load or even at their full load capacity.

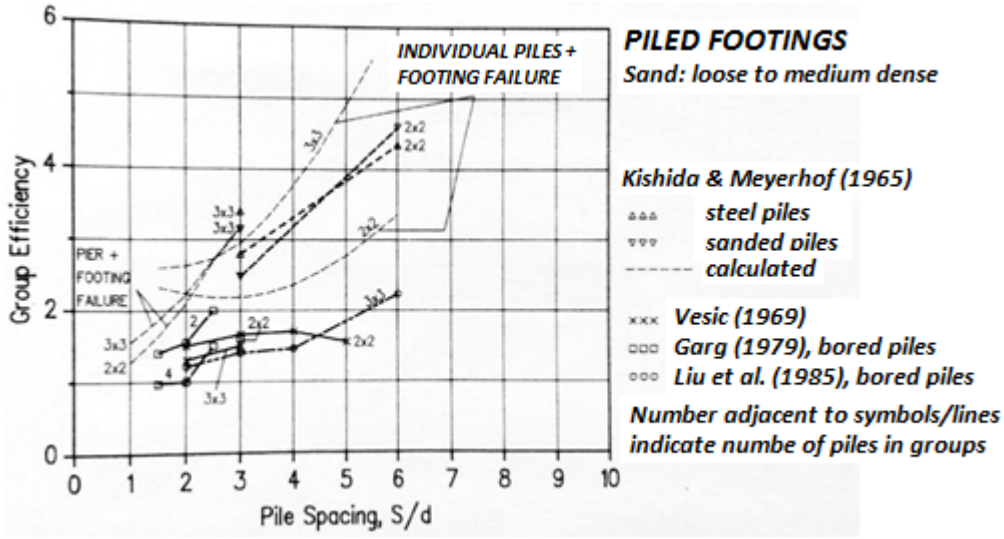

Figure 2-1 Group efficiency of piled raft foundations in loose to medium dense sand, adapted from Phuong (1993)

The aforementioned design approach was widely recognized in the nineties when the demand for constructing high-rise buildings rose (Franke 1991; Hanson 1993; Clancy and Randolph 1993; Poulson 1994; Franke et al. 1994; Ta and Small 1996; and Wang 1996). Poulson (2001b) illustrated that the adoption of such a design approach ultimately results in a more economical solution due to a reduction in the number of piles pursuant to bearing capacity and settlement requirements. Figure 2-2 compares the load-settlement curves of piled rafts under the conventional and the aforementioned approach and conveys that the number of piles could be gradually decreased till an acceptable settlement under a given design load is achieved.

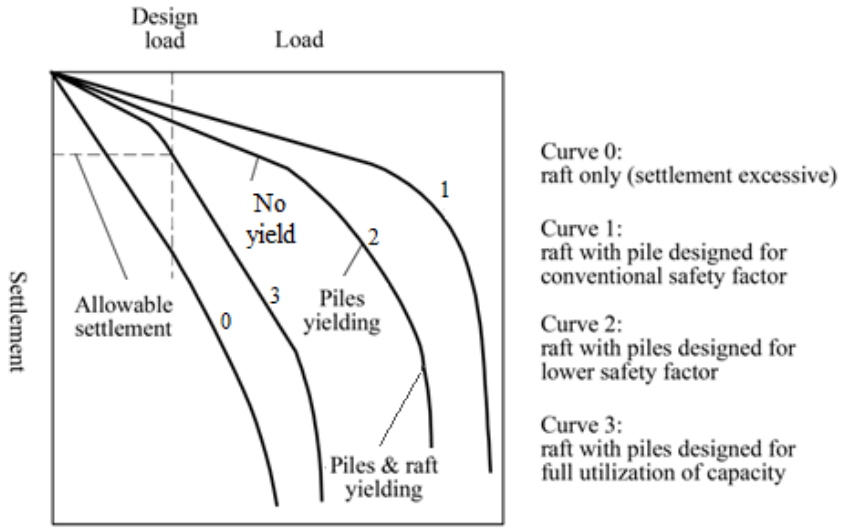

Figure 2-2 Load settlement curves for piled rafts according to various design philosophies, adapted from Poulson (2001b)

In the following sections of this chapter, a comprehensive literature review is conducted on experimental and analytical studies on piled raft foundation. Since the main focus of this study is the load-sharing mechanism of piled raft footing in sand, only the conducted investigations on sandy soils are highlighted herein. At the end of this chapter, the available case studies on piled raft footing in sand are presented.

2.2 Experimental works

This subsection describes the following three main categories of experimental works: 1g model test, centrifuge test, and field large test.

2.2.1 1g Model Tests

In the literature, numerous experimental results are reported which analyze the performance of pile groups under various loading and soil conditions (e.g., Al-Mahdi 2004, Lee and Chung 2005, Al-Mahdi 2006). Furthermore, several small scale tests have been conducted to study the behavior of piled raft foundations which is summarized as follows.

Akinmusuru (1980) demonstrated that the bearing capacity of the piled raft foundations exceeds the sum of the bearing capacity of the raft and pile group through a series of experiments on shallow footing, pile group and piled raft under identical soil conditions. It was further illustrated that the bearing capacity of the raft in the piled raft foundation is similar to that of a shallow footing. Based on these observations, the following correlation was proposed for the piled raft bearing capacity determination:

$$Q_{PR} = \alpha' Q_{PG} + Q_R \tag{2.1}$$

where Q_{PG} is the ultimate capacity of pile group, Q_R is the raft's ultimate capacity, and α' is the pile sharing factor which incorporates the effect of pile-soil-raft interaction on the pile group ultimate capacity. It was shown that α' is always greater than unity and decreases by increasing the pile length.

Akinmusuru (1980) also displayed the effect of pile length and raft geometry on the piled raft load sharing. Experimental results on a single piled raft unit (Figure 2-3) revealed that the raft

share increases extensively by enlarging the raft width, whereas the pile length has inconsiderable impact on the load sharing.

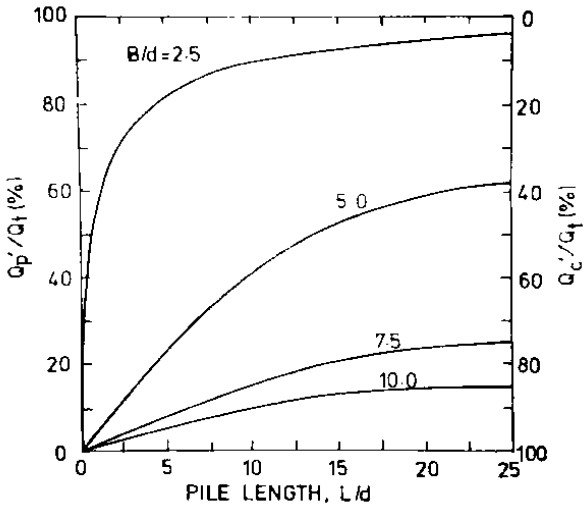

Figure 2-3 Load sharing between single pile and cap, adapted from Akinmusuru (1980)

Cao et al. (2004) verified the effectiveness of unconnected piles in reducing a raft's settlement by conducting experimental tests in plane-strain condition. The model raft was founded on sand with relative density of 70% and different parameters such as raft rigidity, pile length, pile arrangement, and number of piles were varied in this study. The experimental results revealed that disconnected piles below the raft are efficient in reducing settlement and carry around 30% of the applied load on the raft at high pressures (Figure 2-4).

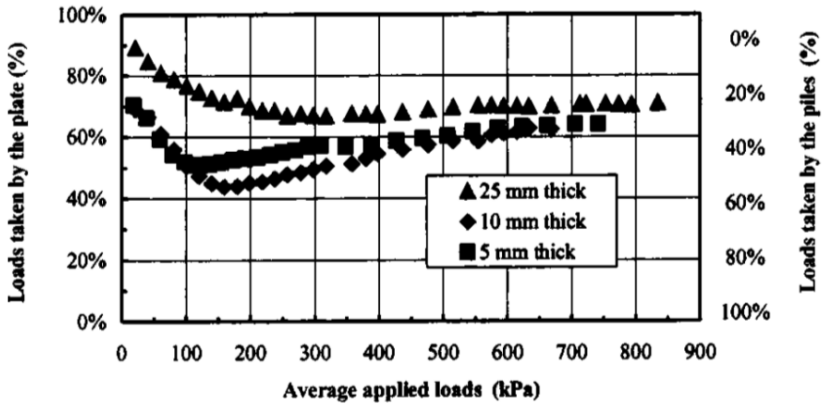

Figure 2-4 Fraction of loads taken by plates and piles for 500mm long piles, adapted from Cao et al. (2004)

Lee and Chung (2005) executed small scale model tests on isolated single pile, single-loaded pile in a pile group, un-piled footing, freestanding pile group and piled raft. All the pile groups in this study consist of nine piles (3x3) driven into a dense sand deposit (Figure 2-5). The experimental results illustrated that the contact between the raft and the underlying soil increases the piles skin friction as a function of pile spacing and pile position (Figure 2-6). It was also observed that the raft share in piled raft foundations is similar to un-piled raft behavior.

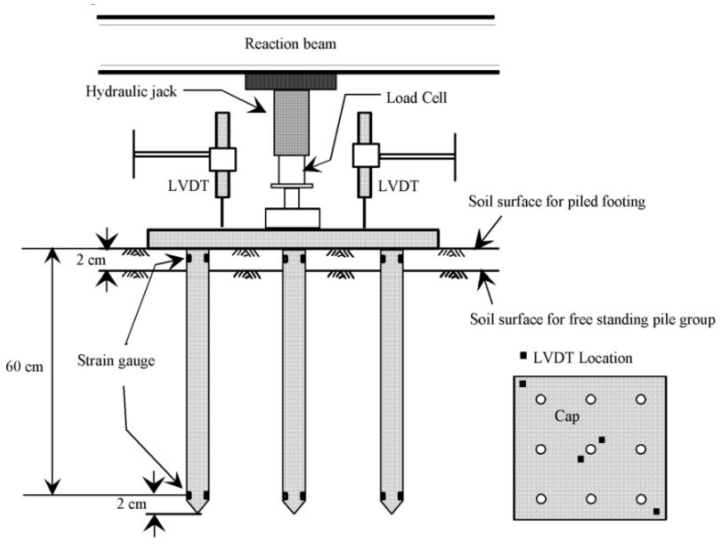

Figure 2-5 Schematic of test setup, adapted from Lee and Chung (2005)

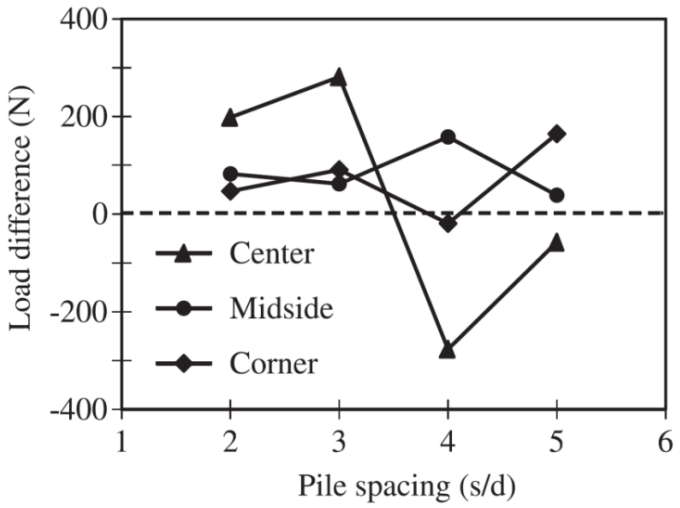

Figure 2-6 Difference in shaft friction between piles in free standing pile group and piled footing at the settlement of 3mm or post-yield condition, adapted from Lee and Chung (2005)

El Sawwaf (2010) performed an experimental investigation on connected and unconnected displacement piled raft footings under axial load and overturning moment (Figure 2-7). The effects of pile length, number of piles, relative density of sand, and load eccentricity on the load-settlement behavior of piled raft were investigated through this study. The experimental tests were conducted in three different relative densities: 35, 55, and 80%. The concluding points of this study are as follows: the efficiency of the piled raft system depends on the load eccentricity ratio, pile arrangement and relative density; increasing the number of piles could only lead to reduction of settlement until reaches a certain value; the greatest improvement in the raft behavior was observed when the sand is in dense condition and the piles are connected to the raft (Figure 2-8).

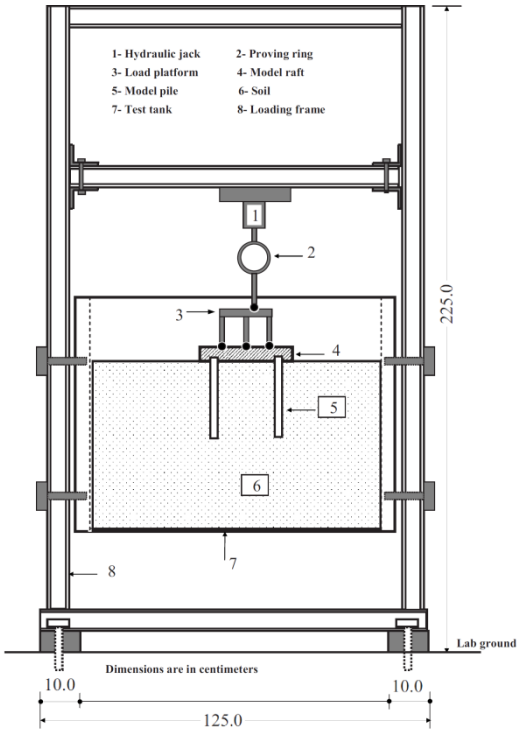

Figure 2-7 Schematic view of the experimental apparatus, adapted from El Sawwaf (2010)

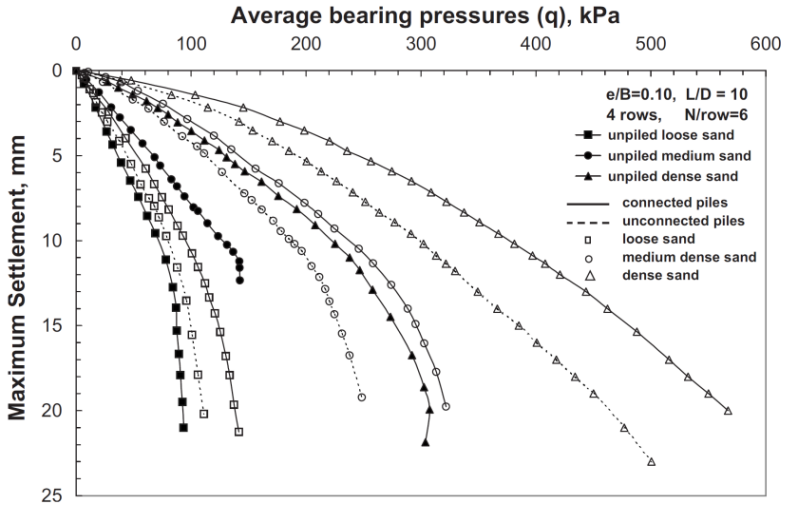

Figure 2-8 Variation of average bearing pressures versus maximum settlement for different relative densities of sand, adapted from El Sawwaf (2010)

El-Garhy et al. (2013) studied the behavior of piled raft foundations in sand by conducting a series of small scale tests. In the test program, the pile spacing was kept unchanged ($S=3.5d_p$); while, the pile length, number of piles, and raft thickness were varied. The test results revealed

that: the raft thickness and the pile length have inconsiderable effects on the piled raft load sharing (Figure 2-9 and 2-10); the pile share increases by increasing the number of piles when the pile spacing and the raft size are constant (Figure 2-10).

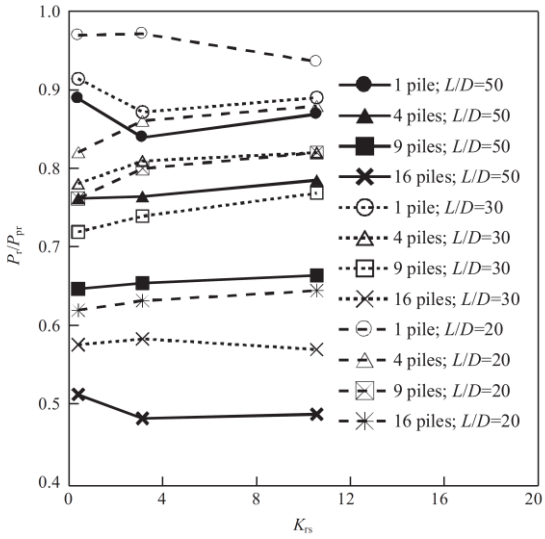

Figure 2-9 Variation of raft share versus raft relative stiffness for piled raft with different number of piles and slenderness ratios, adapted from El-Garhy et al. (2013)

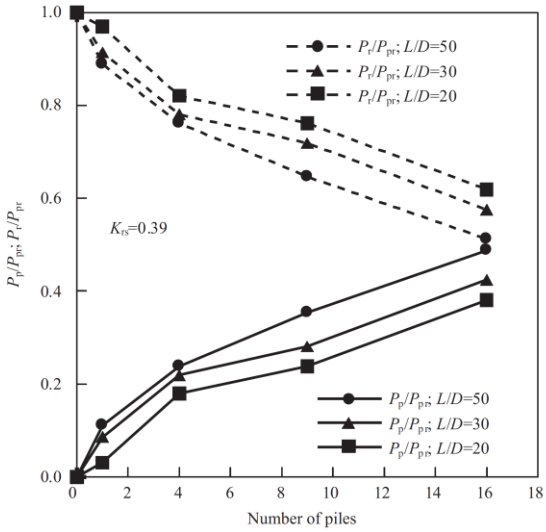

Figure 2-10 Load sharing of a piled raft with different number of piles and also various slenderness ratio, adapted from El-Garhy et al. (2013)

Supplementary information about the test tanks and the model piled rafts in the aforementioned experimental studies are provided in Table 2-1.

Table 2-1 The properties of test box, raft, pile, and soil in small scale tests on piled raft footing in sand

	Test Box			Raft		Pile		
Reference	Wide (mm)	Long (mm)	Height (mm)	Dimension (mm)	Thickness (mm)	Size (mm)	Thickness (mm)	Length (mm)
Akinmusuru (1980)	NR	NR	NR	Rec.: 8x16 d_p Sq.: 2.5-10 d_p	16	19 OD	NR	up to 25 d_p
Cao et al. (2004)	240	1700	800	220x440	5, 10, 25	9.5x9.5	1	350, 500
Lee and Chung (2005)	1000	1400	2500	365x365	20	32 OD	1.2	600
El Sawwaf (2010)	900	400	500	398x200	10	12 OD	1	60, 120, 180
El-Garhy et al. (2013)	1000	1000	1000	300x300	5,10,15	10 OD	1.5	200,300,500

OD: outer diameter, d_p: pile diameter, NR: not reported, Rec.: rectangular, Sq.: square

2.2.2 Centrifuge Model Tests

Geotechnical centrifuge modeling is an accurate technique to track the behavior of piled raft footings in sandy soil. Although the results of centrifuge tests are more reliable than small scale tests, its inaccessibility and high associated expenses restrict its applications.

Giretti (2010) performed two series of centrifuge tests to examine the behavior of rigid raft on settlement reducing piles subjected to axial loading.

- The first series of experimental tests was executed on rigid circular raft lying on a bed of fully saturated loose sand (D_r=30%) and supported by either displacement or non-displacement piles. The testing program included the experiments on raft and piled raft with 1, 3, 7 and 13 piles (Figure 2-11). The model raft was 88mm in diameter and 15mm in thickness. The model piles employed in these tests were close ended and free headed with the diameter of 8mm and the length of 160mm. The centrifuge test results demonstrated the settlement reducing effect of piles and revealed that the number of displacement piles

required to reduce the settlement to an acceptable limit is lower than that of non-displacement piles (Fioravante et al. 2008). The variations of load sharing versus settlement for different piled raft configurations are illustrated in Figure 2-12. It is observed that load sharing varies non-linearly with settlement ratio (W/d_r) and the pile share increases by increasing the number of piles.

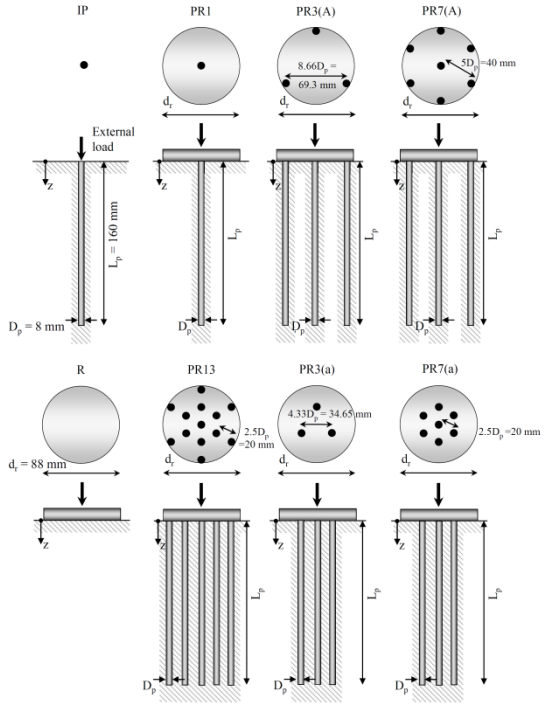

Figure 2-11 Piled raft configurations in the centrifuge tests, adapted from Giretti (2010)

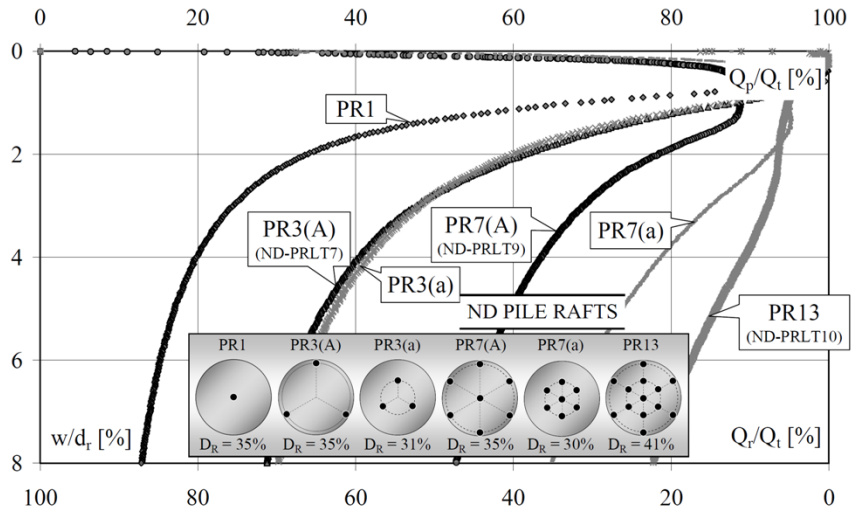

Figure 2-12 Variation of load sharing versus raft relative settlement (settlement of piled raft over raft diameter), adapted from Giretti (2010)

- The second series of centrifuge tests was performed under two scenarios where a rigid raft was either connected or detached from the driven piles in the dry sand deposit (Dr=60%). The testing program included the tests on raft, single pile, and piled rafts with 1, 4 and 9 displacement piles (Figure 2-13). The model raft was a square with 115mm width and 25mm height. The employed model piles were close ended and free headed with the diameter of 8mm and the length of 292mm. The test results revealed that the connected piles act as settlement reducers by transferring the applied load on their heads to deeper soil volume; whereas, the non-connected piles mainly perform as soil reinforcement. Furthermore, it was concluded that the pile-soil-raft interaction produces negative skin friction on the upper part of pile shafts and the stiffness modulus of connected piled raft reduces by settlement until it reaches the raft stiffness at pile group failure point (Fioravante 2011).

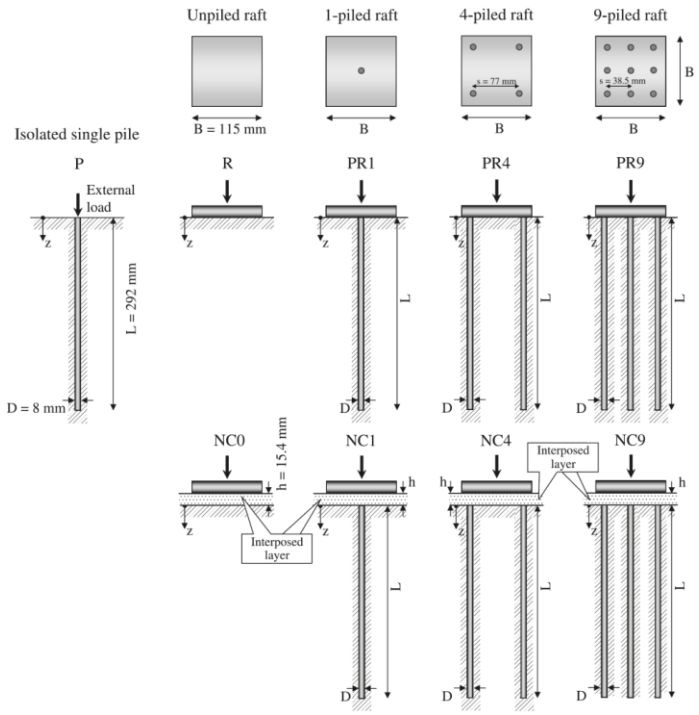

Figure 2-13 Schematic view of model foundations in the serious #2 of centrifuge tests, adapted from Fioravante and Giretti (2010)

2.2.3 Field Large Model Tests

The field large scale test is the most reliable method for evaluating foundation performance; however, its associated cost limits its applications.

Liu et al. (1985) executed field tests on piled raft foundations in sand and concluded that block failure does not occur for groups of bored piles in sand. The following empirical equation was proposed for piled raft bearing capacity determination:

$$Q_{PR} = n\left(\beta_s \delta_s Q_{ss} + \beta_b \delta_b Q_{sb}\right) + Q_R \tag{2.2}$$

Where: Q_{PR} = the ultimate capacity of piled raft foundation.

n is the number of piles in the group, Q_{ss} and Q_{sb} are the shaft and base capacity of single pile, and Q_R is the raft ultimate capacity.

Where: δ and β are coefficients represent the effects of pile-soil-pile and pile-soil-raft interactions, respectively.

Phuong (2010) performed large scale tests on shallow footing, pile group, and piled raft footing that consisted of a square raft and five displacement piles (Figure 2-14). The following conclusions were drawn from the analyses. The pile-soil-raft interaction governs the piled raft behavior through pile shaft capacity expansion; the recorded pile share in a piled raft footing is much greater than the carried load by a free standing pile group in identical soil condition; the pile position does not have a considerable impact on the amount of the carried load by the pile in a piled raft system (Figure 2-18); prior to the piles failure, the majority of applied load is absorbed by the pile and it is later transferred to the raft after the failure point; the load-settlement behavior of the raft in a piled raft footing is similar to that of a corresponding shallow foundation.

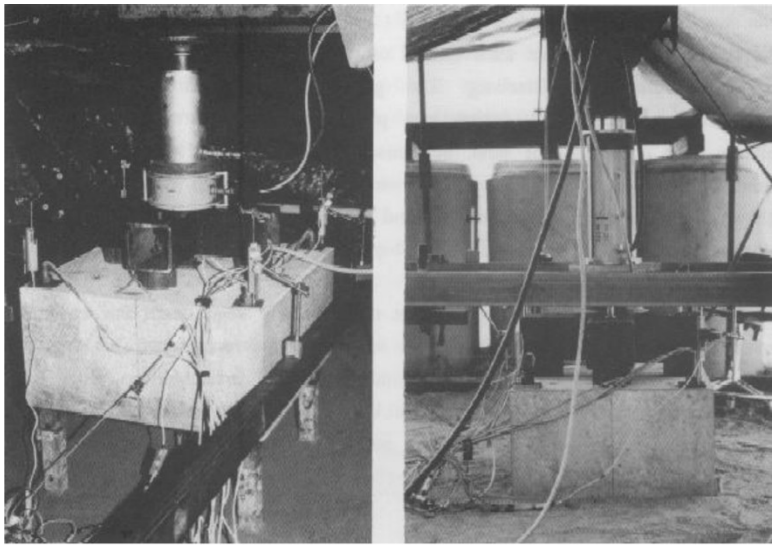

Figure 2-14 Field large-model tests set up: a) Test on a free-standing pile group; b) Test on a piled footing with the cap in contact with soil, adapted from (Phuong 2010)

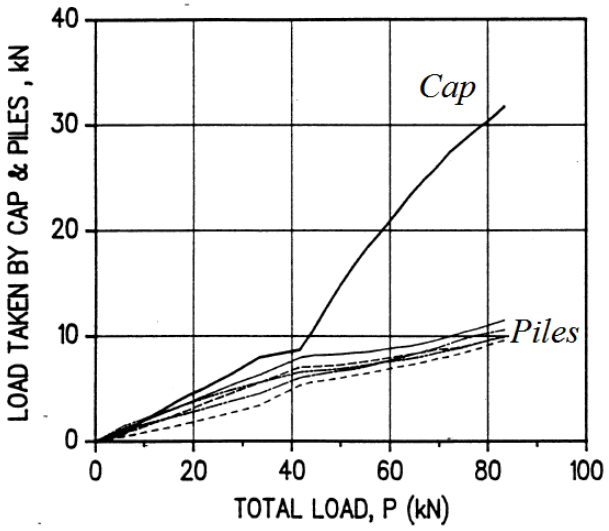

Figure 2-15 Load share between cap and individual piles when the sand density and pile length are 38% and 2.3m respectively, adapted from Phuong (1993)

2.3 Analytical Works

Several analytical methods have been proposed for piled raft foundation; some of those were summarized by Poulson et al. (1997), and Poulson (2001a and b). All the analytical methods could be categorized in four classes:

- **Simplified analysis method**, which involves a number of simplifications in relation to the modeling of the soil profile and the loading conditions on the raft.
- **Approximate computer–based method**, which includes the following approaches:
  - Strip-on-springs approach, in which the raft is represented by a series of strip footings, and the piles are represented by springs with appropriate stiffness (Poulson 1991, Poulson 2001b),
  - Plate-on-springs approach, in which the raft and the soil are represented by an elastic plate and continuum, respectively and the piles are modeled as interacting springs (Poulson 1994, Viggiani 1998, Anagnostopoulos and Georgiadis 1998).
- **More rigorous computer–based method**, such as:
  - Boundary element technique, in which both the raft and the piles are modeled with boundary elements (Sinha 1997 and Hartmann and Jahn 2001),

- Mixed technique, presents a method that combines boundary element (BE) and finite element (FE) analysis. The raft is modeled by FE as a plate supported by non-linear elastic springs at each node of the mesh. These springs collectively represent the underlying soil and the piles. The transferred pressure from raft and pile to the soil is modeled by BE (Franke et al. 1994).

- **Accurate Numerical Method**
  - Two-dimensional (2D) numerical analyses,
  - Three-dimensional (3D) numerical analyses.

The simplified and numerical methods are explained in more detail below.

2.3.1 Simplified Analysis Method

Several simplified solutions have been proposed to analyze piled raft foundations (e.g., Poulson and Davis 1980, Randolph 1994, Van Impe and Clerq 1995, and Borland 1995). More recently, Lee et al. (2014) proposed a model for load sharing determination which took into account the settlement dependent variation of load sharing behavior. Although this method is more advanced, the fundamental assumptions of the model limit its applications. The most widely acceptable simplified technique is the Poulson-Davis-Randolph method which is described in the following section.

Poulson–Davis–Randolph (PDR) method

Randolph (1983) proposed a simplified method for estimating the load sharing of a piled raft foundation. The method was developed for a single piled raft unit with a floating pile which is attached to a rigid circular cap and resting on an elastic semi-infinite mass. Based on this approach, the stiffness of the piled raft is estimated as follows:

$$K_{pr} = \frac{K_p + K_r\left(1 - 2\alpha_{rp}\right)}{1 - \alpha_{rp}^2 \frac{K_r}{K_p}} \tag{2.3}$$

Where K_{pr}, K_p, K_r, and α_{rp} represent the piled raft stiffness, the pile group stiffness, the raft stiffness, and raft-pile interaction factor, respectively.

The raft and pile group stiffness, K_r and K_p, can be estimated via elastic theory, using approaches such as those described by Poulson and Davis (1980), Mayne and Poulson (1999), and Fleming et al. (2009).

The following equation was proposed to determine the proportion of the total applied load which is carried by the raft in a piled raft system:

$$X = \frac{P_r}{P_t} = \frac{K_r\left(1 - \alpha_{rp}\right)}{K_p + K_r\left(1 - 2\alpha_{rp}\right)} \tag{2.4}$$

Where P_r is the load carried by the raft, and P_t is the total applied load on the piled raft. The pile-raft interaction factor in Eq. 2.4, α_{rp}, is estimated as follows:

$$\alpha_{rp} = 1 - \frac{\ln\left(\frac{d_r}{d_p}\right)}{\zeta} \tag{2.5}$$

Where d_r is the effective diameter of the raft associated with each pile.

d_p, is the pile diameter, and the parameter ζ is defined by the following equation:

$$\zeta = \ln\left(\frac{2r_m}{d_p}\right) \tag{2.6}$$

Where r_m represents the radius of influence of the pile which is a function of Young's modulus and Poisson's ratio of the soil, as well as the pile length.

It was shown by Clancy and Randolph (1996) that increasing the number of piles raises the pile-raft interaction factor until it reaches the saturation point of 0.85 (Figure 2-19). They further concluded that α_{rp} is independent of slenderness ratio, and raft stiffness ratio. Fleming et al. (2009) confirmed the validity of the Randolph's simplified method by comparing the estimated load sharing values with the field measurement results reported by Cooke et al. (1981). An important factor was left out in Randolph's model and subsequently in Fleming et al. (2009)'s study, which was the effect of settlement on load sharing of the piled raft. Comodromos et al. (2009) stated that the pile-raft interaction factor decreases be increasing the applied load on the piled raft foundation. Therefore, a settlement based analytical model was developed based on Randolph's model in this thesis and is discussed in chapter 8.

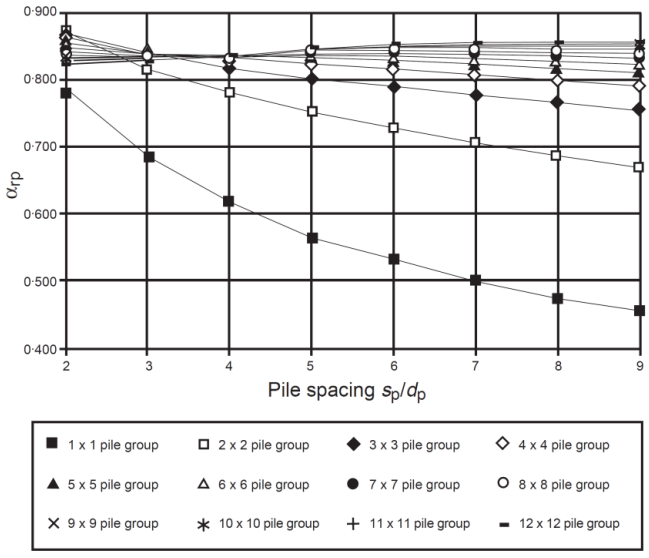

Figure 2-16 Values of interaction factor α_{rp} for various size with $L_p/d_p = 25$, $K_{ps} = 1000$ and $k_{rs} = 10$, adapted from Clancy and Randolph (1996)

Poulson and Davis established a tri-linear load-settlement curve for the piled raft footing based on Randolph's method (Figure 2-17). The piled raft stiffness was calculated according to Eq. 2.3

and assumed to be valid until the pile group capacity is fully mobilized (point A). The corresponding load at point A is determined by the following equation:

$$P_1 = \frac{P_p}{(1-X)} \tag{2.6}$$

Where P_p is the ultimate load capacity of the piles in the group and X is the proportion of the carried load by the raft (Eq. 2.4).

The stiffness of piled raft system after pile group failure is identical to that of the raft alone (K_r), and this holds until the piled raft system is no longer able to carry additional load (point B). Beyond point B, the load-settlement curve becomes stable.

Poulson and Davis (1980) recommended that the ultimate load capacity of a piled raft can generally be taken as the lesser of the following two values:

- The sum of the ultimate capacities of the raft plus all the piles,
- The ultimate capacity of a block containing the piles and the raft.

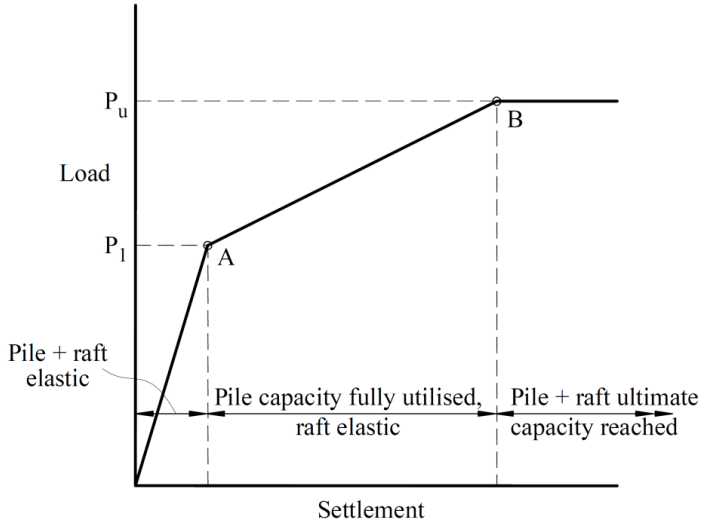

Figure 2-17 Simplified load-settlement curve for preliminary analysis, adapted from Poulus (2001b)

2.3.2 Numerical Methods

2-dimensional numerical analysis

The piled raft foundation elements are modeled as a plane-strain or an axially symmetric problem through a 2-dimensional (2D) numerical analysis. Although 3D modeling is the ideal choice for analyzing piled raft foundations, simpler 2D numerical models are widely used in the literature which is explained briefly in the following section.

Prakoso and Kulhawy (2001) analyzed the behavior of vertically loaded piled raft foundations using elastic and elastic-plastic models. The effects of the raft and pile group geometries on the settlement and raft bending moment were investigated through this study. The numerical results revealed that the ratio of pile group to raft width, and pile depth are the most influential elements.

Poulson (2001b) compared the results of plane-strain analyses with those obtained from the PDR approach and 3D analysis. It was concluded that 2D analysis over predicts settlements due to the implicit assumption of plane-strain in the analysis.

Oh et al. (2008a) investigated the performance of piled raft foundations in sand by conducting finite element analysis. The results of this study revealed that the raft thickness affects differential settlement and bending moments, but has minor impact on load sharing and maximum settlement. A parametric study was also conducted on a piled raft with 16 piles spaced in a range of $3d_p$ to$7d_p$, while the pile diameter, pile length, and raft thickness were kept constant. The numerical results revealed that the maximum settlement increases by enlarging the pile spacing.

Omeman (2012) studied the effect of different parameters on load sharing of piled raft foundation in sandy soil by conducting a series of 2D finite element analyses. Five different pile group configurations were considered as illustrated in Figure 2-18. The numerical results revealed that the raft share decreases by increasing the pile diameter, and number of piles (Figure 2-19), while the pile length has inconsiderable impact on piled raft load sharing (Figure 2-20).

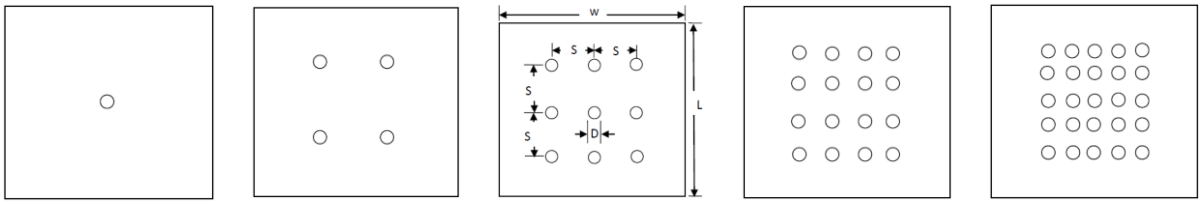

Figure 2-18 The considered pile raft configuration in 2D analyses by Omeman (2012)

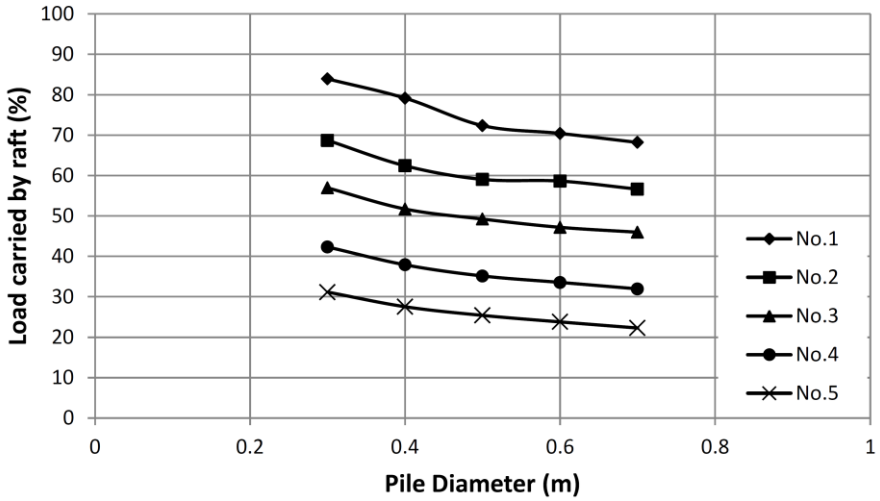

Figure 2-19 Variation of raft share versus pile diameter at a constant load for 5 different piled raft configurations, adapted from Omeman (2012)

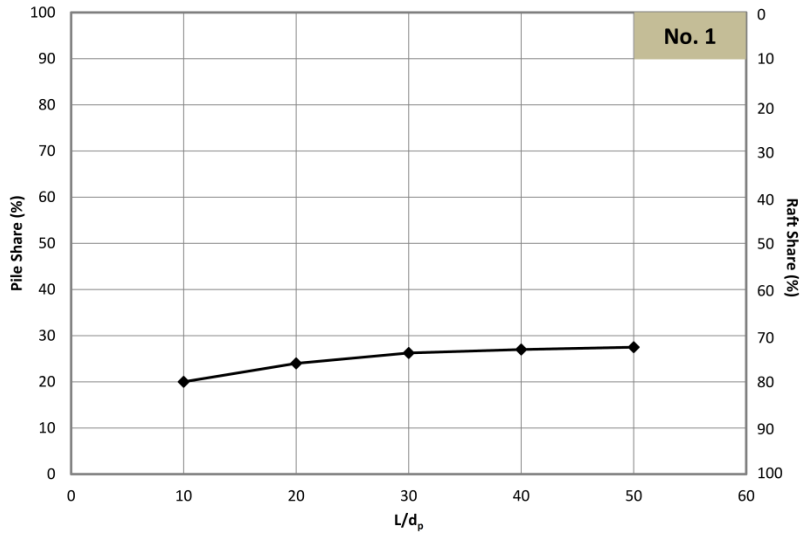

Figure 2-20 The load sharing of single piled raft unit at 600kPa in different slenderness ratio reported by Omeman (2012)

3-dimensional numerical analysis

3D finite element and finite difference analyses have the highest level of accuracy and also complexity among the available analytical methods for studying the piled raft behavior. Numerous studies could be found in the literature based on 3D numerical analysis and in the following a few of them that are related to topic of this study are highlighted.

Oh et al. (2008b) conducted a detailed 3D analysis on piled raft foundation in sand using the PLAXIS software. Soil profile and soil properties were kept unchanged through the numerical study and an extensive parametric study was performed by varying the pile spacing, the number of piles, the pile diameter, the raft dimension ratio, and the raft thickness. The results of this study revealed that the maximum settlement of the piled rafts depends on the pile spacing and number of piles and is independent of the raft thickness. Whereas, the differential settlement of piled rafts decreases by increasing the raft thickness.

Sinha (2013) performed a series of 3D numerical analyses on non-displacement piled raft foundation. The effect of different parameters on settlement, bearing capacity and load sharing of

piled rafts were studied through this numerical study. For studying the effect of pile spacing on load sharing mechanism, the length over diameter ratio was kept unchanged (L/d_p=15) and the pile spacing varied from $2d_p$ to $7d_p$. More information about geometry of piled raft is provided in Table 2-2. Figure 2-21 shows the effect of pile spacing on load-settlement curve and it is observed that the settlement of piled raft increases by increasing the pile spacing. Based on this observation, Sinha (2013) recommended not using piled raft with pile spacing more than $6d_p$.

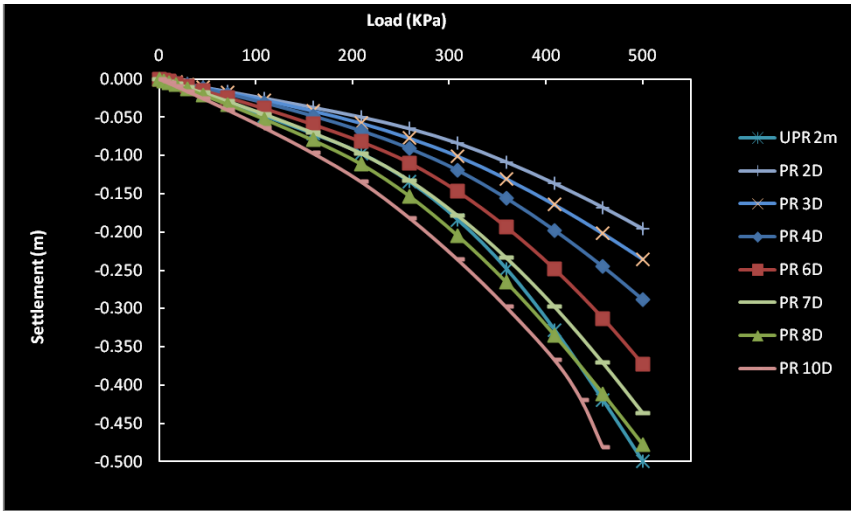

Figure 2-21 Influence of pile spacing on load settlement behavior, adapted from Sinha (2013)

Table 2-2 The geometrical information of piled raft models and the recorded load sharing at 0.5MPa

Pile Spacing	Raft Size $(B_r \times L_r \times t_r)$	No. of Piles	Length of Pile (m)	Pile Diameter (m)	Applied Load (MPa)	Load Share (%)	
						Raft	Pile
2D	24x24x2m	144	15	1	0.5	14	86
3D	24x24x2m	64	15	1	0.5	15	85
4D	24x24x2m	36	15	1	0.5	37	63
6D	24x24x2m	16	15	1	0.5	66	34
7D	28x28x2m	16	15	1	0.5	67	33

Figure 2-22 shows the variation of load sharing versus pile spacing. This figure illustrates that the piles carry 90% of the applied load when the pile spacing is less than $3d_p$. Furthermore, it is observed that for pile spacing greater than $3d_p$ the raft share increases until it reaches the saturation point (70%) at $S/d_p=6$.

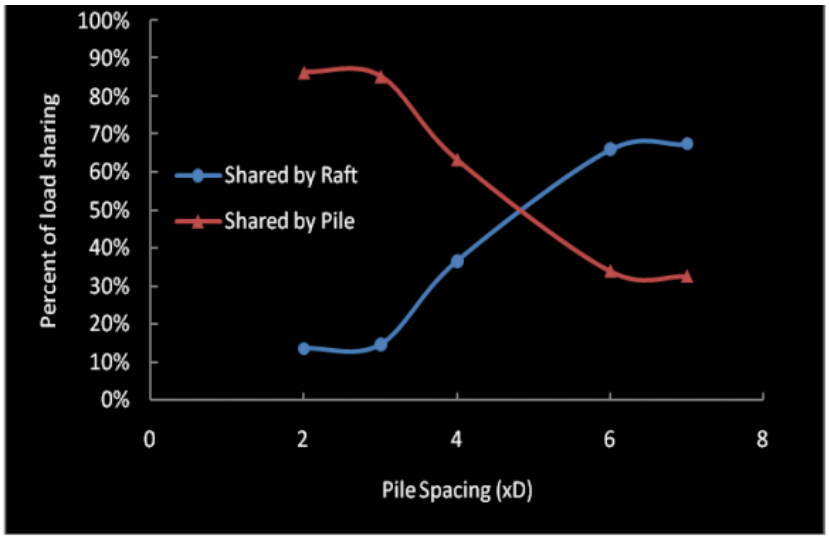

Figure 2-22 Variation of load sharing versus pile spacing, adapted from Sinha (2013)

Neto et al. (2014) applied the finite element method to simulate four case histories available in the literature. The soil was considered elastic in this study and the effect of different parameters such as S/d_p, L/d_p, and stiffness ratio on piled raft behavior were studied through the numerical analyses. It was concluded that the relative spacing (S/d_p) has a significant effect on load distribution between the raft and the piles. In addition, it was illustrated that for the pile spacing of $3d_p$, the foundation acts as a group of piles which absorbs 94 to 98% of the total applied load. The amount of carried load by the piles decreases by increasing the pile spacing ratio.

Lv et al. (2014) studied the effect of the pile cross sectional shape on the load sharing mechanism of piled raft foundation. The behavior of piled raft with X-section cast-in-place concrete pile (XCC) was compared with traditional circular cast-in-place concrete (CCC) piled

raft. It was demonstrated that XCC piles carry more load than circular piles (66% versus 46%) for the applied load on identical piled raft systems in the study. The cause of this load sharing difference is the greater side resistance of XCC piles.

2.4 Case Studies

In the last decade, some super high-rise buildings have been constructed upon piled raft foundations in non-cohesive soils. However, most of these structures are not monitored for settlement and the load sharing between the piles and raft (Katzenbach et al. 2000, Yamashita and Yamada 2007). There are only a few real life case studies available in the literature, which investigate the behavior of piled raft foundation of high-rise buildings in sand. These cases, reported by El-Mossallamy et al. (2006) and Yamashita et al. (2011) are briefly discussed in the following.

2.4.1 Nineteen story residential tower

The geotechnical investigation of this project revealed that there is a loose to medium sand layer up to 63m in depth lying on top of another layer of medium to dense sand (Figure 2-23). It was further determined that the water level stands at the depth of 3m from the ground surface. A piled raft foundation was recommended for this project to reduce the overall and differential settlement. More specifically, 28 cast-in-place concrete piles with a length of 63m, shaft diameter of 1.2 to 1.3m, and toe diameter of 1.8 to 2.2m were constructed for this project. A liquefiable silty-sand layer approximately 10m thick was found in the depth of 8m. In order to eliminate the large shear deformation of the foundation, due to the presence of liquefiable layer, the soil in the depth of 8-18m was improved by grid-form soil cement walls. The recorded measurement on pile P1 revealed that the ratio of pile toe load to the pile head load was 0.42 both at the end of construction and 15 months after the construction phase. The ratios of the load

carried by the piles to the net load on the tributary area were 0.63 for the pile P1 and 0.66 for the pile P2 at the end of construction (Figure 2-23). These ratios increased to 0.69 and 0.77 in 15 months after the construction for the piles P1 and P2, respectively.

2.4.2 Eleven story office building

Figure 2-24 shows the elevation and foundation plan of the eleven story office building as well as the underlying soil profile. Piled raft foundation system was adopted for this project to control the differential settlement. The raft was founded on loose sand with SPT-N values of about 10 and the pile toes were embedded in the dense sand and gravel layer. The cast-in-place concrete piles are employed for this project with a shaft diameter of 1.1-1.5m. The toe diameter of pile is 1.4-1.8m and the length of pile is 27.5m. The ratio of the pile toe load to the pile head load was 0.25 at the end of construction and slightly decrease to 0.2 in 32 months after the end of construction. The ratio of the load carried by the piles to the total applied load was 0.54 at the end of construction and 0.65 at the last observation (32 months after construction).

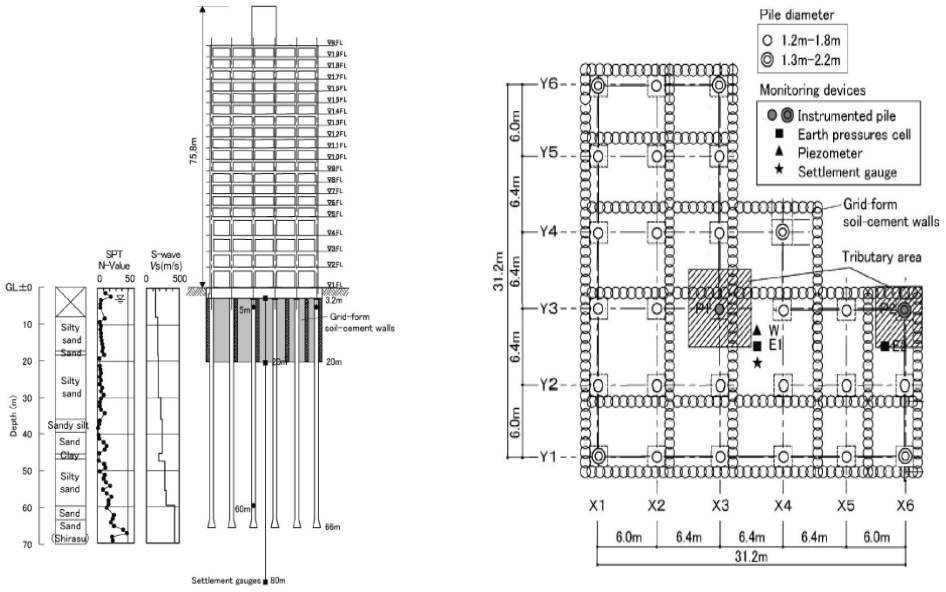

Figure 2-23 Soil profile, foundation plan and elevation of nineteen story residential tower, adapted from Yamashita et al. (2011)

2.4.3 Hadron experimental hall

The foundation plan, elevation of the foundation, and the soil profile below the foundation are illustrated in Figure 2-25. The raft was founded on dense sand and gravel in the center of the building and rested on medium to dense sand on the sides. Because of the presence of a thick saturated cohesive layer in the depth of 23m, the mat foundation could not provide the allowable settlement and the piled raft foundation was suggested for this building. 371 bored pre-cast concrete piles with 0.6-0.8m in diameter and 22-25.7m in length were used in this project. Two years after the construction, the ratio of the load carried by the piles to the net load for the piles P1 and P2 was 0.86 and 0.67, respectively (Figure 2-25).

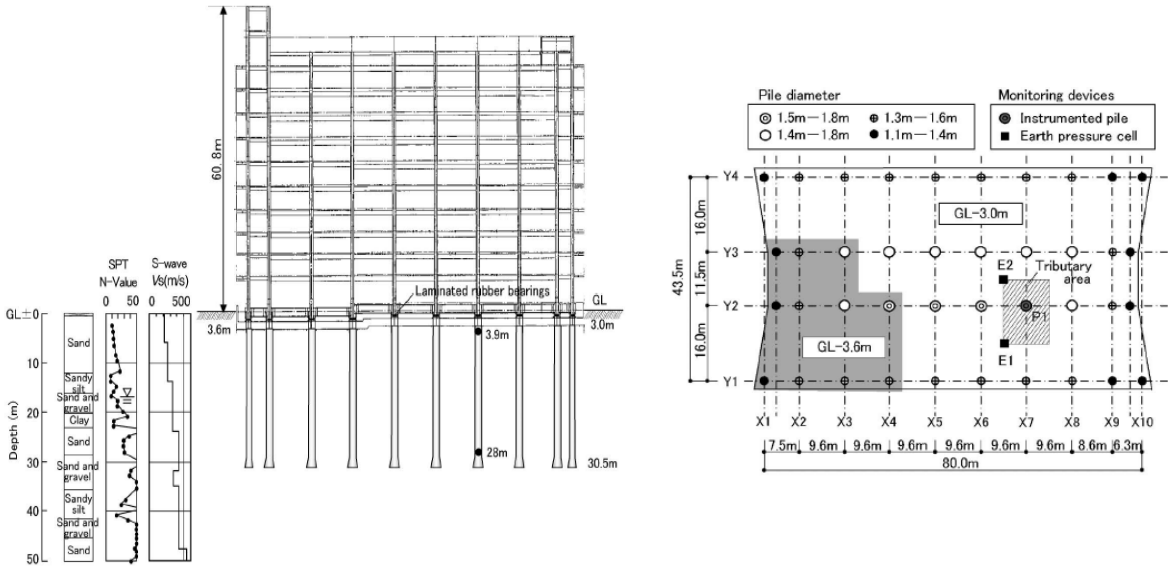

Figure 2-24 Soil profile, foundation plan and elevation of eleven story base-isolated office building, adapted from Yamashita et al. (2011)

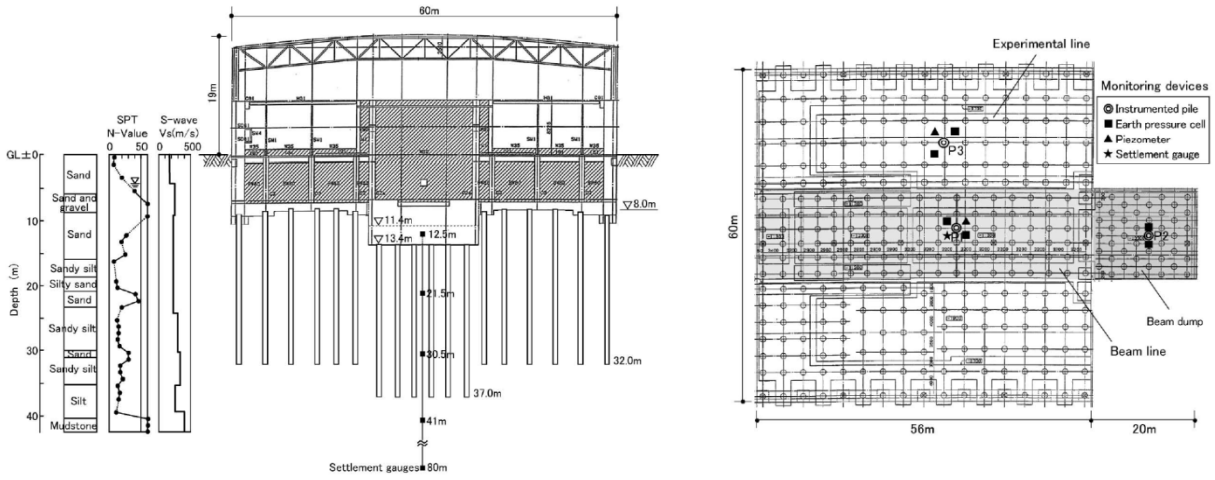

Figure 2-25 Soil profile, foundation plan and elevation of Hardon experimental hall, adapted from Yamashita et al. (2011)

2.4.4 Forty seven story residential tower

The foundation plan and the soil profile below the forty seven story residential tower are shown in Figure 2-26. The raft was founded in the depth of 4.3m on medium sand and gravel and the pile group, consisted of 50m long cast-in-place concrete piles, were embedded in very dense sand and gravel. Two piles, 5D and 7D, were instrumented by LVDT and strain gages to monitor the load sharing during and after the construction. Before casting the foundation slab, the initial values of displacement were recorded at the reference point (depth of 70m). Then, the variation of vertical displacement by time was measured at different depth relative to the reference point (Figure 2-27). The measured displacement at the depth of 5.3m is approximately equal to foundation settlement (Yamashita et al. 2010). The pile share, 8 months after the end of construction, was reported to be 0.93 and 0.87 for the pile 5D and 7D, respectively.

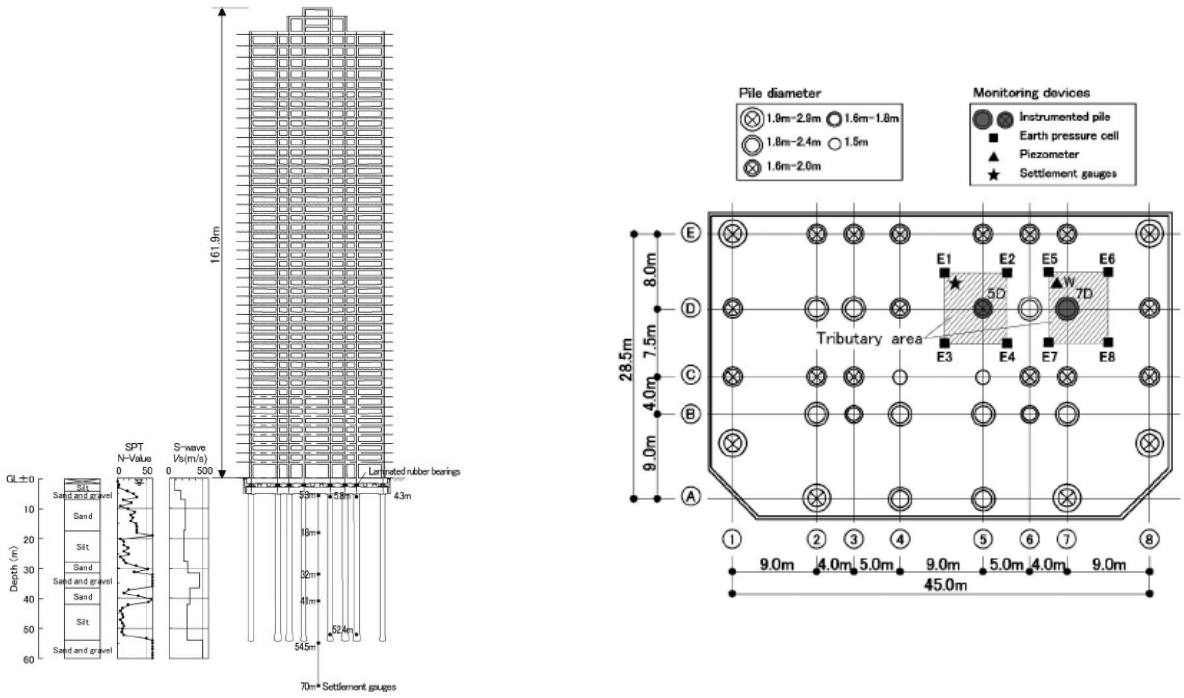

Figure 2-26 The soil profile and the foundation plan of 47 story residential tower, adapted from Yamashita et al. (2011)

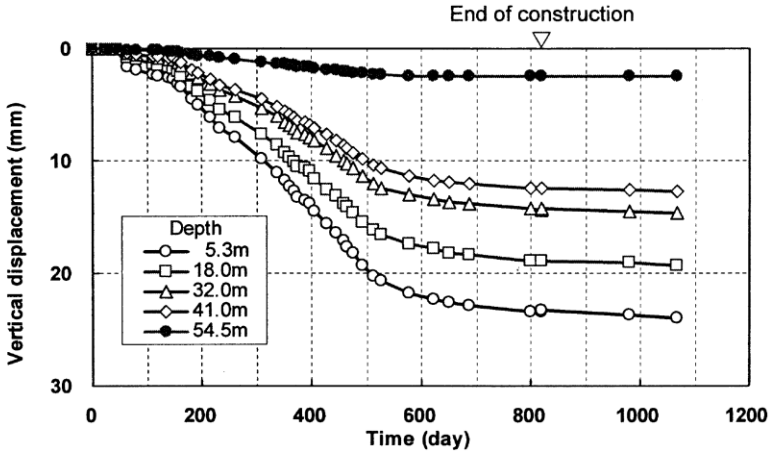

Figure 2-27 Variation of vertical displacement versus time, adapted from Yamashita et al. (2010)

Yamashita et al. (2011) used the above reported field measurements to plot the variation of pile share versus the average spacing between the instrumented pile and the adjacent piles (Figure 2-28). This comparison revealed that the ratio of the load carried by piles to the net load generally decreases by increasing pile spacing and becomes almost constant for S/d_p above six.

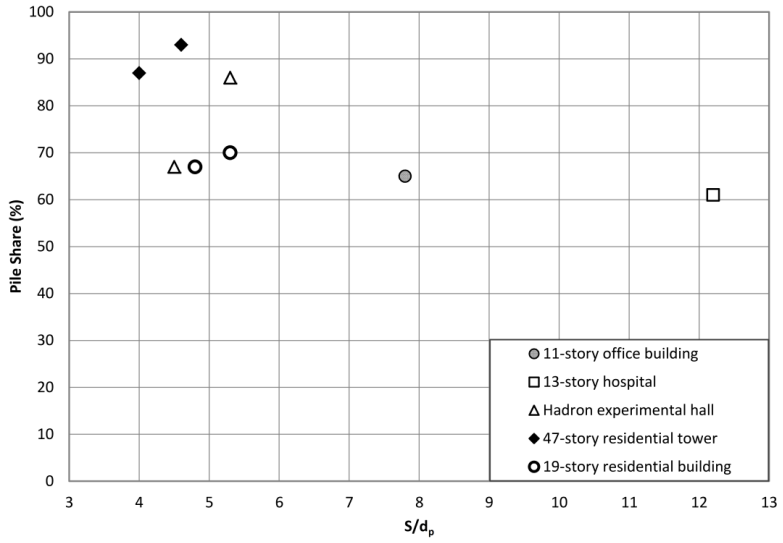

Figure 2-28 Variation of pile share versus pile spacing in piled raft foundation, after Yamashita et al. (2011)

2.5 Research objectives

The conducted literature review in this chapter includes the studies that have been performed on piled raft foundations in sand. Although, the available information in the literature about piled raft foundations is valuable, it is not sufficient for developing a comprehensive method for load sharing estimation. For instance, Akinmusuru (1980) and El-Garhy et al. (2013) studied the effect of some limited parameters such as pile length and raft thickness on the piled raft load sharing, El Sawwaf (2010) and Lee and Chung (2005) only performed experimental tests on displacement (driven) piled rafts, and Giretti (2010) and Phuong (2010) mainly focused on developing a model for estimating piled raft settlement in their studies and gave less attention to piled raft load sharing. In addition, the conducted numerical studies on piled raft load sharing are mostly based on two dimensional analyses, which is not a realistic simulation of piled raft behavior and the effect of some important parameters such as foundation settlement was completely neglected in the available analytical models for piled raft load sharing estimation.

Besides the parameters which were studied in the literature, there are some other factors such as subsoil condition, pile installation method, and number of piles which have not received enough attention before and their effects on the behavior of piled raft foundations are unknown. Therefore, the objectives of this thesis could be listed as follows:

- Building an experimental setup which is capable of determining the piled raft load sharing.
- Conducting experimental investigations to examine the effect of the following factors on piled raft load sharing:
    - Particle size distribution
    - Soil relative density
    - Piled raft settlement
    - Pile installation method
    - Raft width ratio
    - Dissimilarity in soil density (homogeneous and layered sand).
- Conducting three dimensional numerical analyses to study the effect of number of piles on load sharing mechanism.
- Developing settlement-based models for determining the piled raft load sharing in homogeneous and layered sand.
- Presenting a design procedure for piled raft foundations by taking into consideration the contribution of both pile group and raft in the bearing capacity.

Chapter 3

Experimental Investigation

3.1 General

The experimental tests were carried out in the Geotechnical Lab of Concordia University. The main purpose of the small scale tests was to study the effect of different parameters such as soil density in homogeneous and layered soil, particle size distribution, pile spacing, and pile installation method on load sharing mechanism of piled raft foundation in sand. The experimental tests were conducted on single pile, shallow footing and piled raft foundation (Figure 3-1). Pile number, pile length and pile diameter were kept constant in all tests. The following sections provide detailed descriptions of the sand properties, model pile and model raft.

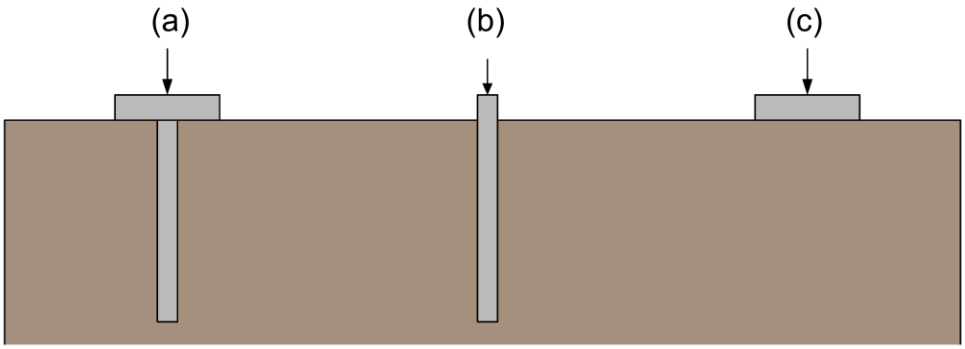

Figure 3-1 Different types of foundation that are tested in this study (a) single piled raft unit, (b) Single pile, (c) shallow footing

3.2 Model Pile and Raft

Steel mechanical pipe with an outer diameter of 28.6mm (d_p), 6.35mm thickness, and 290mm length (L) was used as the model pile. The pile was instrumented with pressure transducers and

mechanical pistons on the head and the tip. The compressed oil inside the pistons transferred the applied pressure to the transducers (Figure 3-2). The recorded outputs of the sensors were used to estimate the applied pressure according to the initial calibration.

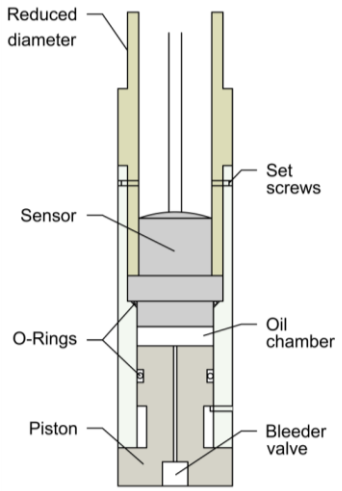

Figure 3-2 Specifications of designed piston for instrumenting the model pile

Square steel plates with 100 and 150mm length (d_r) and 25.4mm thickness (t_r) were used to simulate the model rigid rafts. The raft-soil stiffness ratio (K_{rs}) was calculated by Eq. 3.1 to confirm the rigidity of raft ($K_{rs} >> 5$) based on the suggestions of Horikoshi and Randolph (1997).

$$K_{rs} = \frac{E_r}{E_S}\frac{1-\nu_s^2}{1-\nu_r^2}\left(\frac{t_r}{d_r/2}\right)^3 \tag{3.1}$$

Where E_r is the modulus of elasticity of steel plate ($2.1\times10^5 MPa$), E_s is soil modulus at depth of $d_r/2$ (10-50MPa), d_r is the raft diameter, t_r is raft thickness, ν_s is the soil Poisson's ratio (0.25-0.4) and ν_r is steel Poisson's ratio (0.3).

The head of the pile was fitted in the center of the raft and fasten by two screws. Two small holes were drilled in the raft to pass the pressure transducers' wires. A load cell with a maximum capacity of 500kgf was mounted on the raft to measure the applied load on the model piled raft. To measure the settlement of the piled raft a linear vertical displacement transducer (LVDT) was used. The recorded excitation voltage of load cell and LVDT were used to determine the total force and corresponding settlement according to the calibration equations. A schematic view of the instrumented piled raft is shown in Figure 3-3.

The surface of the pile and the raft was covered with sand paper (grit 150) to simulate a concrete-sand interface (Figure 3-4). Direct shear tests were conducted to determine the friction angle between soil particles and sand paper (δ) at different densities. It is illustrated in Figure 3-5 that the ratio of soil-sand paper friction angle (δ) to soil friction angle (ϕ) was almost equal to unity (δ/ϕ =1). Several tests were conducted to find the appropriate sand paper grit which provides the desired roughness (Appendix A).

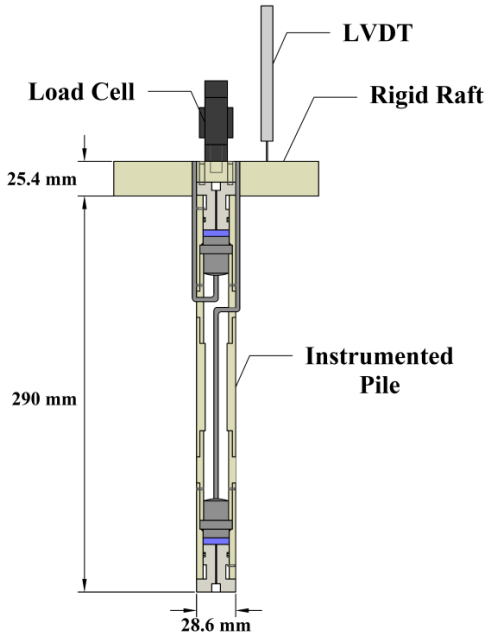

Figure 3-3 Schematic view of instrumented pile, raft and measuring devices

Figure 3-4 The covered instrumented pile and rafts with sand paper grit 150

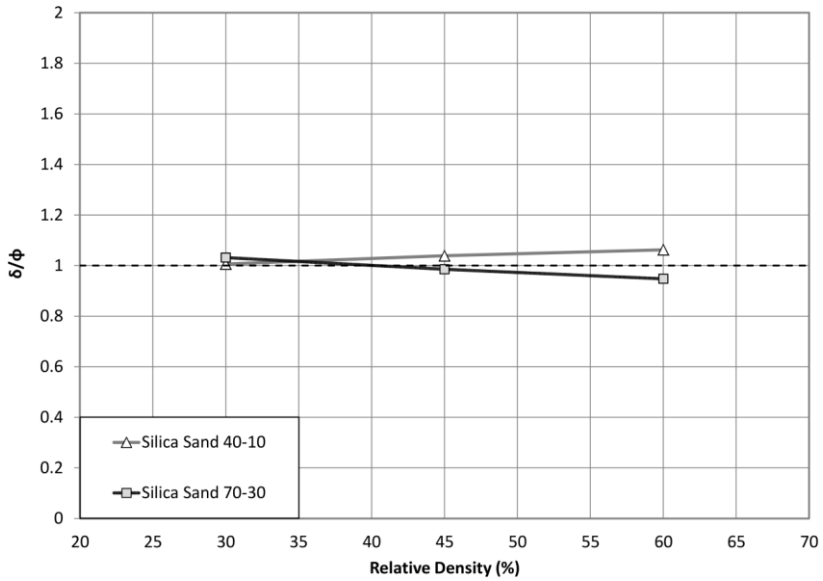

Figure 3-5 Variation of δ/ϕ versus relative density for 40-10 and 70-30 Silica sand

3.3 Test setup

3.3.1 Tank and frame

The size of the tank was chosen by considering the dimensions of the pile and the raft to minimize the boundary effects in the small scale tests. The size of the tank was 500x500mm^2 in plane and 600mm in height. Two sides of the tank were built with aluminum profiles and other

sides were made of transparent acrylic plastic (Plexiglas) which were reinforced with L profile steel sections to minimize deflection (Figure 3-6). The test tank was placed on a steel frame which was built with C channel profiles. The general side view of the experimental setup is shown in Figure 3-7.

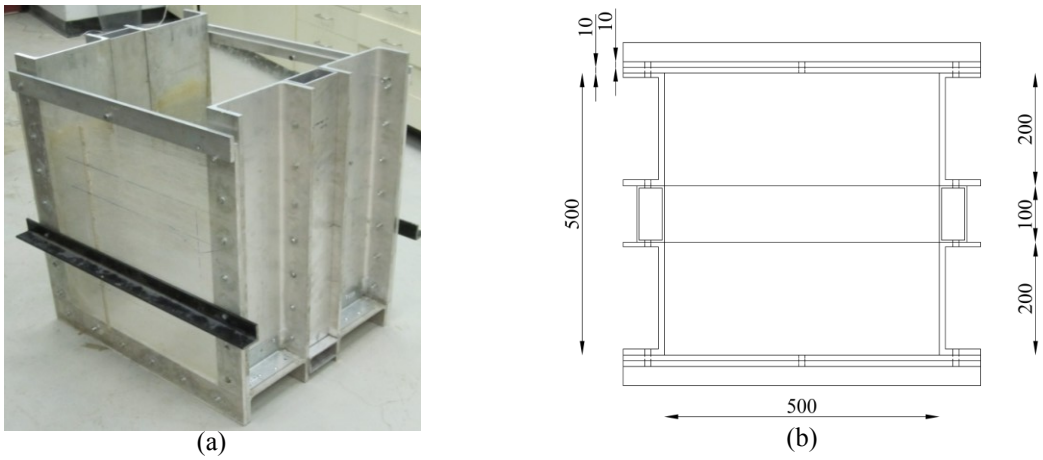

Figure 3-6 (a) General view and (b) top view of test tank (all the dimensions are in mm)

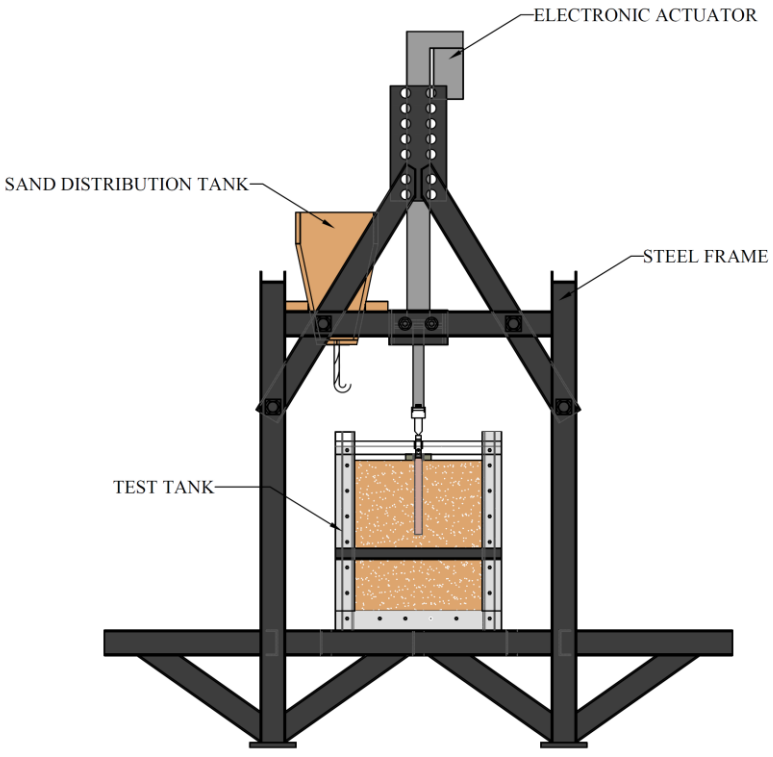

Figure 3-7 Side view of experimental setup

3.3.2 Sand distribution system

The test tank was filled with 4 layers of sand with a thickness of 150mm per layer. The sand was distributed into the test tank through a hose at a relatively low height to mitigate the effect of falling height of soil particles on soil density. A compaction plate of 500x500mm in dimension equipped with 7.12kg hammer and a maximum drop height of 20cm was used to compress each layer (Figure 3-8). The number of drops on individual layer was varied in order to obtain a homogeneous or layered sand deposit. A series of preliminary tests were conducted to determine the required number of drops to achieve constant relative density of 30%, 45%, and 60% in homogeneous pattern and desired density in the layered soil patterns. Three different patterns of layered soil were examined through this study (Figure 3-9). In the preliminary compaction tests, the distribution of relative density in depth was obtained by placing density cans with known weights and volumes at the corner of the tank, half way through each layer. At the end of each test, the cans were meticulously retrieved. The unit weight and density of each layer was determined based on the weight of the compacted soil inside the cans (Figure 3-8d). A single can was sufficient to accurately determine the soil density of each layer since the compact plate was rigid enough to equally distribute the compaction energy on soil surface. Figures 3-10 and 3-11 show the number of drops that were applied to each layer to prepare the homogeneous and layered deposits, respectively. Appendix B provides compaction test results.

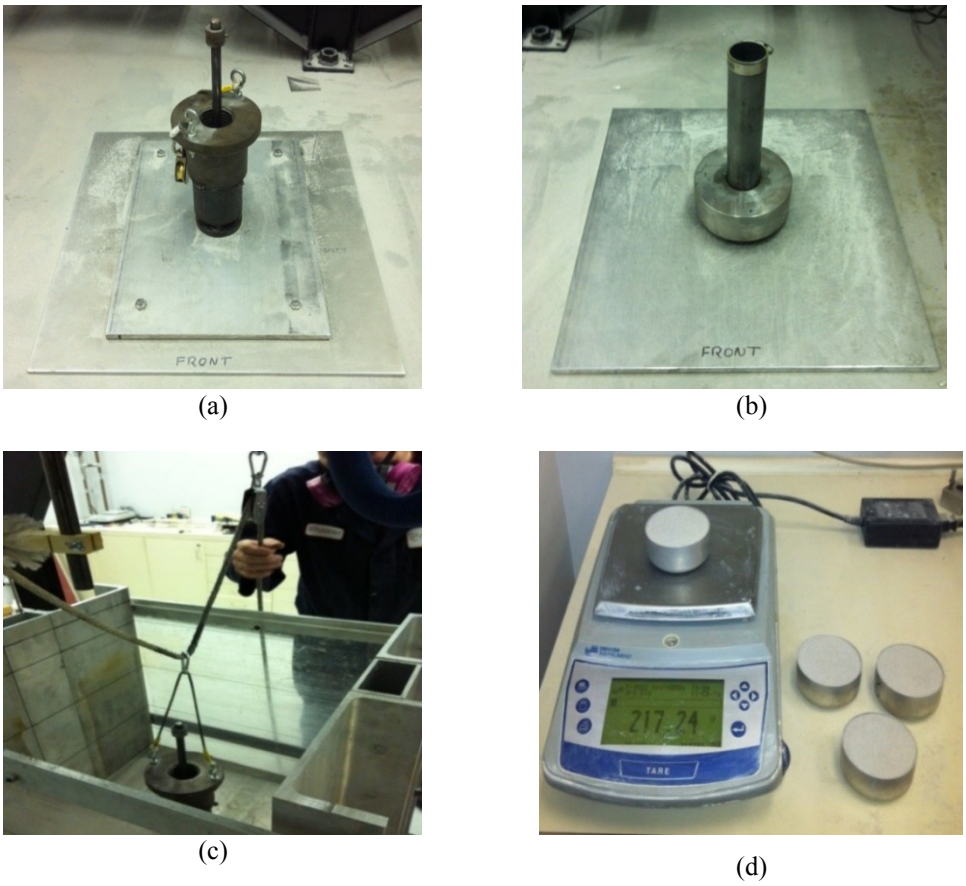

(a) (b) (c) (d)

Figure 3-8 (a and b) Compaction plates, (c) compaction mechanism, and (d) unit weight cans and high precision electronic scale

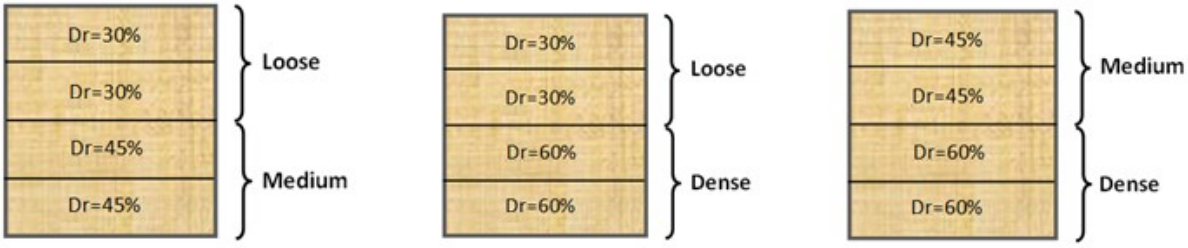

Figure 3-9 The pattern of relative density in layered soil (a) loose on medium, (b) loose on dense, and (c) medium on dense

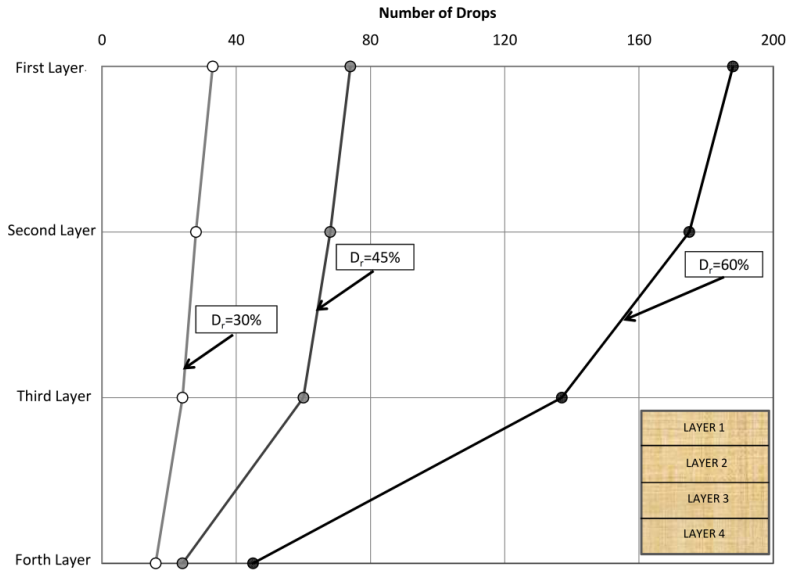

Figure 3-10 The required number of drops for each layer to reach the desired relative density in homogenous sand

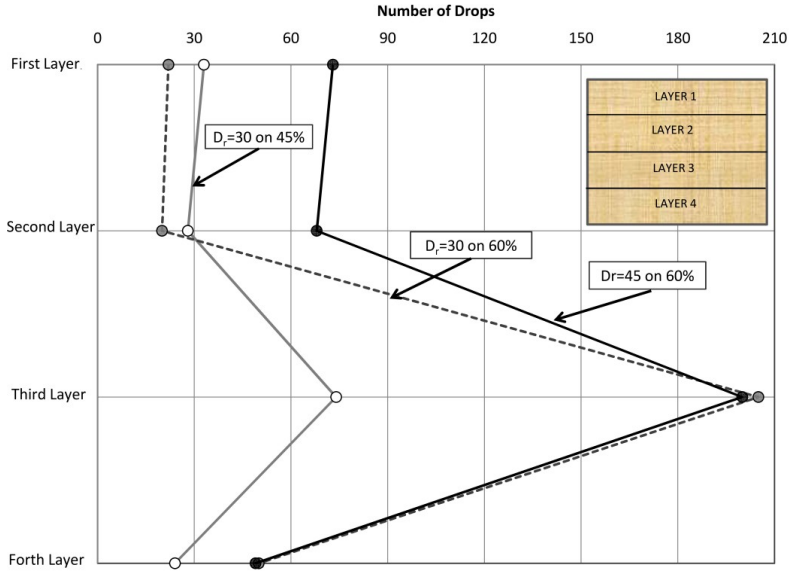

Figure 3-11 The required number of drops for each layer to reach the desired relative density in layered soil

3.3.3 Loading system

The implemented loading system in this study was a TH4-Series Electric Cylinder Actuator, a Servo Drive and a power supply. The Actuator is capable of applying a maximum load of 10kN at 5amp and 60V. The Servo Drive transmits the low energy signal from the controller, in this case being the Data Acquisition System, into a high energy signal to the motor. The driver was

configured to operate in a voltage control mode which allowed for a strain controlled testing procedure. The actuator was fixed on reaction beam that is connected to the steel frame.

3.3.4 Data acquisition system

A Data Acquisition System manufactured by Agilent Technologies was used in this study for collecting data from S load cell, instrumented pile and LVDT. Several computer programs using Visual Engineering Environment (VEE) were developed in order to control the data acquisition system and also dictate commands to the loading mechanism. A general view of written computer program is shown in Appendix C. Figure 3-12 shows schematically the connection between DAS and the other experimental instruments.

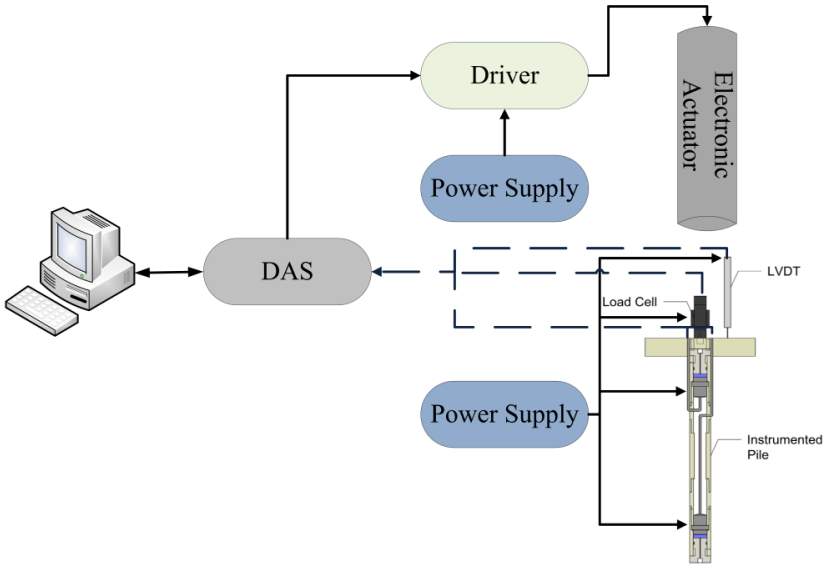

Figure 3-12 General view of the connection between instrumented pile, S load cell, LVDT, and electronic actuator with DAS

3.4 Sand properties

Clean Silica sand, composed of quartz grains, with two different particle size distribution were implemented in this study: Silica sand 40-10 and 70-30. Microscopic pictures of sand particles, categorized as sub-rounded, are shown in Figure 3-13. Soil properties of Silica sands,

summarized in Table 3-1, were determined by running preliminary soil mechanics tests such as sieve analysis, specific gravity, and maximum and minimum densities. Figure 3-14 illustrates the particles size distribution curves for both sands.

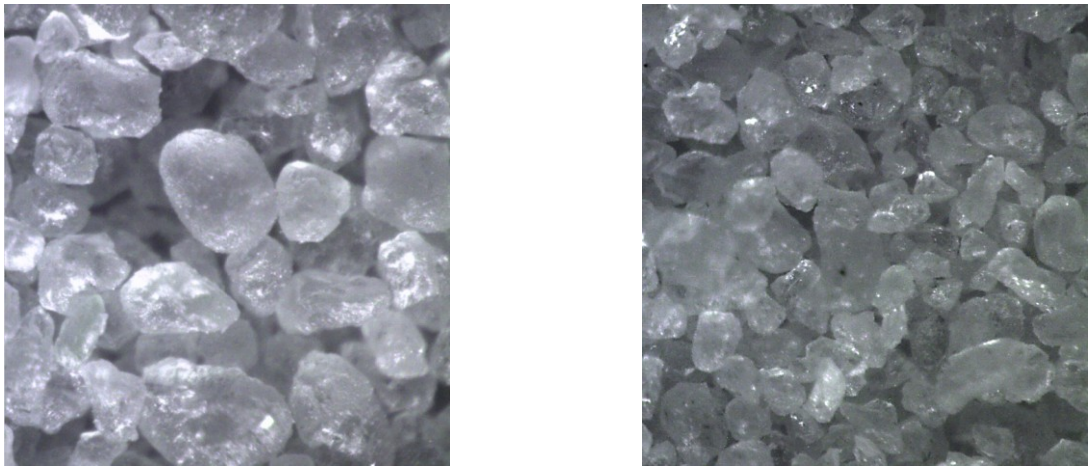

(a) (b)

Figure 3-13 Microscopic picture of sand particles (a) 40-10 Silica sand, (b) 70-30 Silica sand

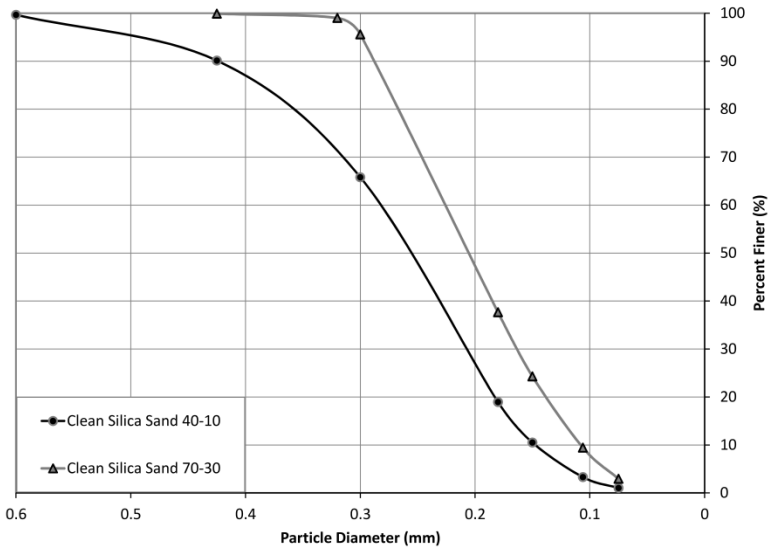

Figure 3-14 Particle size distribution of 40-10 and 70-30 Silica sand

Table 3-1 Basic soil mechanics properties of Silica sand 40-10 and Silica sand 70-30

Soil Property	Silica sand 40-10	Silica sand 70-30
D_{10}(mm)	0.155	0.105
D_{30}(mm)	0.213	0.162
D_{50} (mm)	0.26	0.21
D_{60}(mm)	0.291	0.224
Coefficient of uniformity (C_u)	1.88	2.133
Coefficient of curvature (C_c)	1.01	1.116
Soil Classification (USCS)	SP	SP
Maximum Dry Unit Weight (kN/m^3)	17.16	17.22
Minimum Dry Unit Weight (kN/m^3)	13.98	13.64
Minimum Void Ratio (e_{min})	0.4978	0.5097
Maximum Void Ratio (e_{max})	0.8385	0.9060
Specific Gravity (G_s)	2.62	2.65

Direct shear tests were conducted to determine the internal friction angles of test soils at different densities. The tests were performed in 4 different densities to show the range of peak friction angle (ϕ) from loose to very dense condition. The values of friction angle and void ratio in different relative densities are presented in Table 3-2.

Table 3-2 Void ratio and friction angle of 40-10 and 70-30 Silica sand at different densities

	Silica sand 40-10		Silica sand 70-30	
D_r (%)	e	ϕ	e	ϕ
30.00	0.74	32.96	0.79	33.21
45.00	0.69	34.93	0.73	37.59
60.00	0.63	36.80	0.67	40.06
75.00	0.58	38.79	0.61	41.22

3.5 Test procedure

3.4.1 Shallow footing

The shallow footing tests were executed on 100x100mm and 150x150mm rafts founded on sandy soil with 30, 45, and 60% densities (Figure 3-15). After the sand deposit preparation, the raft was place precisely in the center of the tank and the S load cell and LVDT were mounted on top of the raft. The point load was applied by the electronic actuator to the attached connection on the top of the S-load cell. The tests were conducted in strain control condition and continued until the displacement reached 25mm. The applied loads and corresponding settlements were recorded as the test outputs.

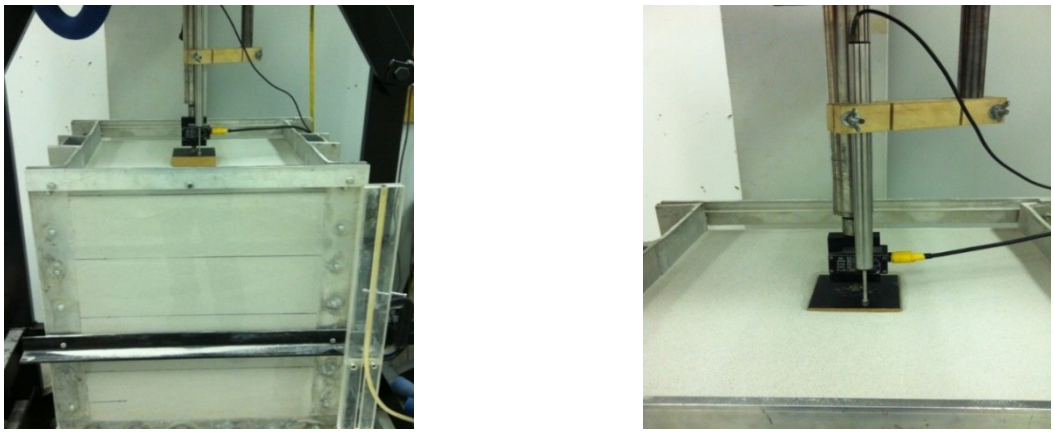

(a) (b)

Figure 3-15 Experimental tests on 100x100mm shallow footing (a) before running test, (b) after running test

3.4.2 Displacement pile and displacement piled raft

Upon completion of soil deposit, the model pile was connected to the actuator and inserted vertically into the soil mass till the embedded length of the pile reached 290mm. The center of the raft was fasten to the pile's head through the designated screw holes. The pressure transducers' wires were passed through the holes in the raft. The S load cell and the LVDT were mounted on top of the raft to measure the applied load and piled raft displacement, respectively.

The tests were commenced by applying the load through the actuator to the S load cell in a strain control condition. The VEE program in conjunction with the data acquisition system was used to control the actuator and collect the following outputs over constant displacement intervals: the amount of the total applied load on piled raft, the applied load on pile head and pile tip, as well as the corresponding settlement. The test was completed once the displacement of the pile raft reached 25mm. A general view of the experimental procedure is shown in Figure 3-16. Besides driving the pile for 285mm and running the test for maximum settlement of 15mm, the rest of the procedure was the same for tests on displacement pile.

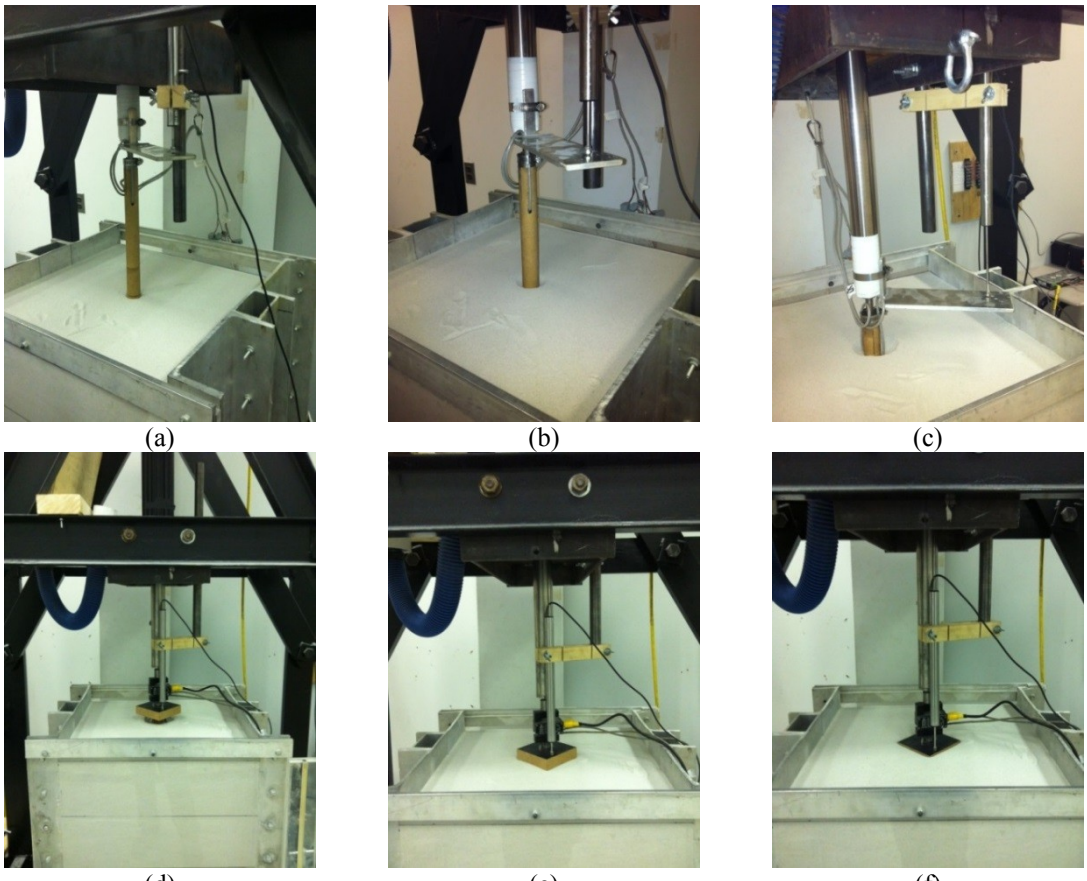

(a) (b) (c)

(d) (e) (f)

Figure 3-16 Step by step test procedure on displacement piled raft

3.4.3 Non-displacement pile and non-displacement piled raft

The test procedure began by filling and compacting the first two sand layers. In order to fix the position of the non-displacement pile in the middle of the test tank, the pile was connected to the actuator and founded on the surface of the second layer. Prior to connecting the pile to the actuator, the compacting plate was hung on top of the tank, with the actuator passing through an opening in the middle of the plate. Upon filling and compacting the remaining two layers, the actuator was disconnected and the compaction plate was removed in order to place the raft on the pile. Finally, the actuator was connected to the S load cell and the tests were conducted similar to the displacement piled raft procedure. The step by step test procedure is illustrated in Figure 3-17. The pile load test was executed for 15mm and the same procedure was followed for running it.

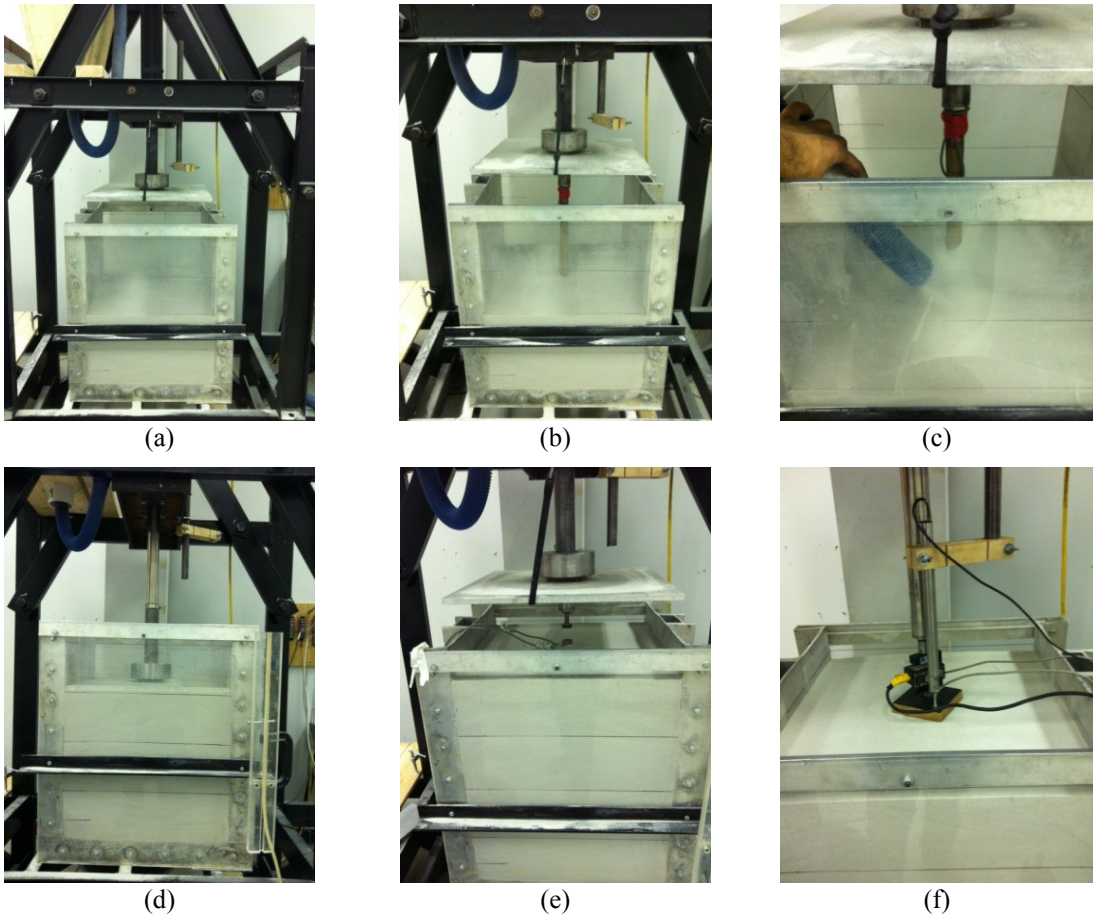

Figure 3-17 Step by step test procedure on non-displacement piled raft

3.6 Testing program

Tables 3-3 and 3-4 present the testing programme followed in this study. The experimental tests were divided into two main categories; the tests on homogeneous sand (Table 3-3) and the tests on layered sand (Table 3-4). Five series of small scale tests were performed on dry homogeneous sand; shallow footing (R), displacement pile (DP), non-displacement pile (NDP), displacement piled raft (DPR), and non-displacement piled raft (NDPR). Each series consists of 3 tests, which were conducted on different densities. In the aforementioned tables, the tests were labelled based on the foundation type followed by the soil relative density and soil type (40-10 or 70-30 Silica sand). The experimental tests on homogeneous sand were conducted on 40-10 Silica sand; moreover, the tests on the non-displacement piled raft were executed on 70-30 Silica sand.

The conducted tests on layered sand include two series; non-displacement pile (NDP) and non-displacement piled raft (NDPR). Since three different patterns of layered soil were examined in this study, each series consists of 3 tests (Table 3-4). In Table 3-4, the tests are specified by the foundation symbol followed by the relative density of the tow top and two bottom layers. Table 3-5 presents the list of the repeated tests to ensure the repeatability of the test results.

Table 3-3 Test program on dry homogeneous soil

	Test name	Sand type	Relative Density
RAFT	R10-30-40-10	40-10 Silica Sand	30
	R10-45-40-10		45
	R10-60-40-10		60
RAFT	R15-30-40-10	40-10 Silica Sand	30
	R15-45-40-10		45
	R15-60-40-10		60
DISPLACEMENT PILE	DP30-40-10	40-10 Silica Sand	30
	DP45-40-10		45
	DP60-40-10		60
NON-DISPLACEMENT PILE	NDP30-40-10	40-10 Silica Sand	30
	NDP45-40-10		45
	NDP60-40-10		60
DISPLACEMENT PILED RAFT	DPR30-40-10-R10	40-10 Silica Sand	30
	DPR45-40-10-R10		45
	DPR60-40-10-R10		60
NON-DISPLACEMENT PILED RAFT	NDPR30-40-10-R10	40-10 Silica Sand	30
	NDPR45-40-10-R10		45
	NDPR60-40-10-R10		60
NON-DISPLACEMENT PILED RAFT	NDPR30-40-10-R15	40-10 Silica Sand	30
	NDPR45-40-10-R15		45
	NDPR60-40-10-R15		60
NON-DISPLACEMENT PILED RAFT	NDPR30-70-30-R10	70-30 Silica Sand	30
	NDPR45-70-30-R10		45
	NDPR60-70-30-R10		60

R10: 10x10cm raft, R15: 15x15cm raft, DP: Displacement pile, NDP: Non-displacement pile, DPR: Displacement piled raft, NDPR: Non-displacement piled raft.

Table 3-4 Test program on dry layered sand

	Test name	Sand type	Thickness of each layer (mm)	Density of upper layer (%)	Density of lower layer (%)
NON-DISPLACEMENT PILE	NDP30/45-40-10	40-10 Silica Sand	300	30	45
	NDP30/60-40-10		300	30	60
	NDP45/60-40-10		300	45	60
NON-DISPLACEMENT PILED RAFT	NDPR30/45-40-10-R10	40-10 Silica Sand	300	30	45
	NDPR30/60-40-10-R10		300	30	60
	NDPR45/60-40-10-R10		300	45	60
NON-DISPLACEMENT PILED RAFT	NDPR30/45-40-10-R15	40-10 Silica Sand	300	30	45
	NDPR30/60-40-10-R15		300	30	60
	NDPR45/60-40-10-R15		300	45	60

NDP: Non-displacement pile, NDPR: Non-displacement piled raft.

Table 3-5 Test program for study the repeatability of the test results

Test name	Sand type	Relative Density
NDPR45-40-10-R10	40-10 Silica Sand	45
NDP60-40-10	40-10 Silica Sand	60

NDP: Non-displacement pile, NDPR: Non-displacement piled raft.

Chapter 4

Experimental Tests Results

4.1 General

The results of the experimental tests on homogeneous and layered sand are presented in this chapter. As mentioned previously, the amount of the total applied load on piled raft, the applied load on the pile head and pile tip, as well as the corresponding settlement were recorded during the tests. The result of each test is presented in the form of load-settlement curves and the derived ultimate capacities are summarized in tabular format. The ultimate load was defined at the point that either the curve suddenly turns downward (the plunging point) or a small increase of load produces a large amount of settlement. In the case of general shear failure, the peak point of load-settlement curve defined the ultimate bearing capacity. The alteration of load sharing with settlement is also illustrated for the tests on the rigid piled raft footing. To determine the amount of the raft share, the pile head measurement was subtracted from the applied load on the S load cell. For this purpose, the best fit non-linear equations, based on the coefficient of determination (R^2), were used to represent the collected data on the total load and pile head pressure. The same strategy was implemented to determine the frictional resistance of the pile where the best-fit non-linear equation of the pile tip measurements was subtracted from that of the pile head data.

The load settlement curves of shallow footing, single pile, and piled raft are compared herein to show the efficiency of the piled raft in controlling the settlement. Based on the experimental results, the piled raft efficiency was determined as the ratio of piled raft bearing capacity over single pile ultimate load.

4.2 Homogeneous Sand

The experimental results on homogeneous sand are categorized and presented in this section based on the soil relative density.

4.2.1 Loose sand (D_r=30%)

R10-30-40-10

The load settlement curve of shallow footing (Figure 4-1) illustrates that the foundation experienced punching shear failure, manifested by the steepness of the curve beyond the ultimate point (85kgf).

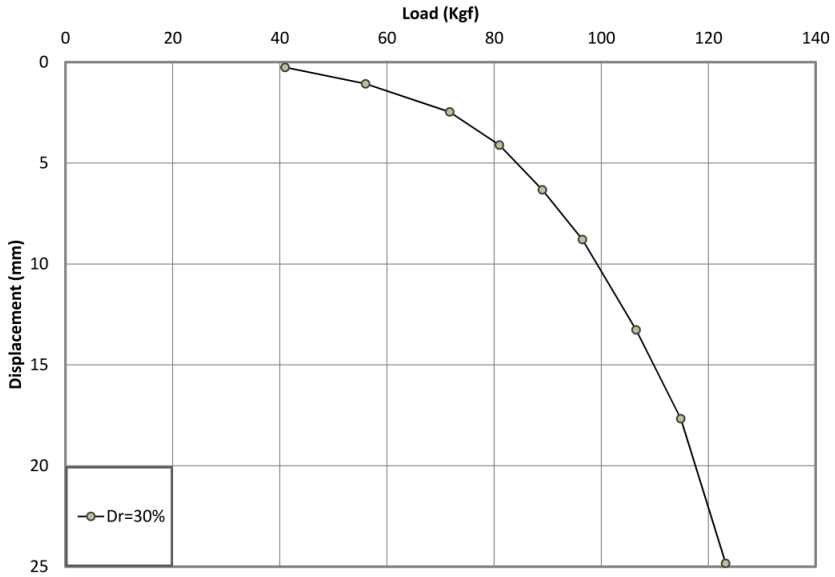

Figure 4-1 Test results on the shallow footing R10-30-40-10 (load-settlement curve)

R15-30-40-10

Comparing the performance of R15-30-40-10 (Figure 4-2) with R10-30-40-10 (Figure 4-1) clearly shows that increasing the raft width increases the ultimate capacity and reduces the settlement without making any changes in the failure mechanism.

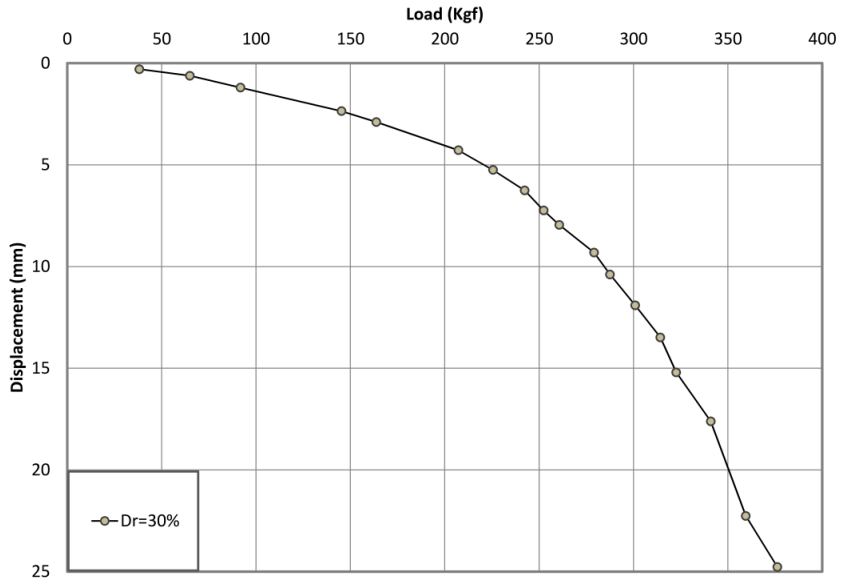

Figure 4-2 Test results on the shallow footing R15-30-40-10 (load-settlement curve)

DP30-40-10

The test results (Figure 4-3) illustrate that the displacement pile failed at 96.4kgf and the measured skin friction at the failure point was around 8kgf.

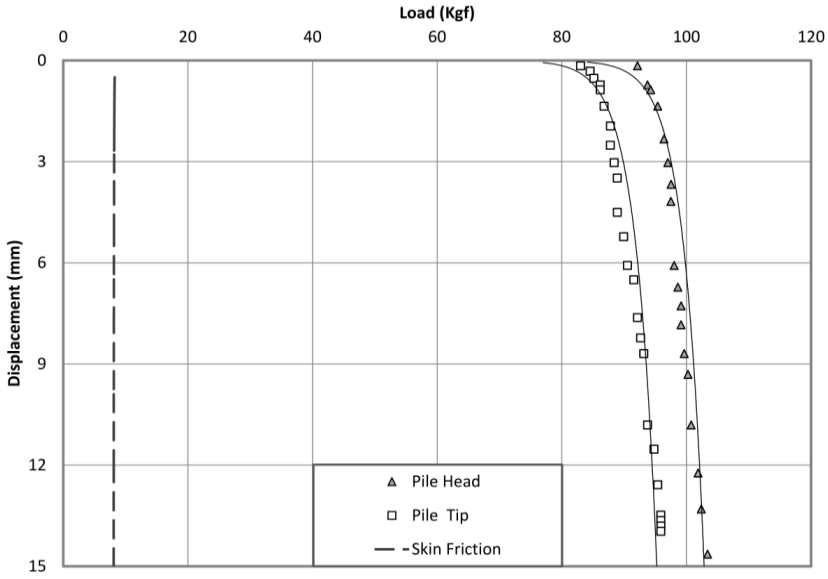

Figure 4-3 Test results on single displacement pile DP30-40-10 (load-settlement curve)

NDP30-40-10

The results of the test on non-displacement pile are demonstrated in Figure 4-4. The skin friction of non-displacement pile was fully mobilized at a small settlement and decreased as more settlement took place.

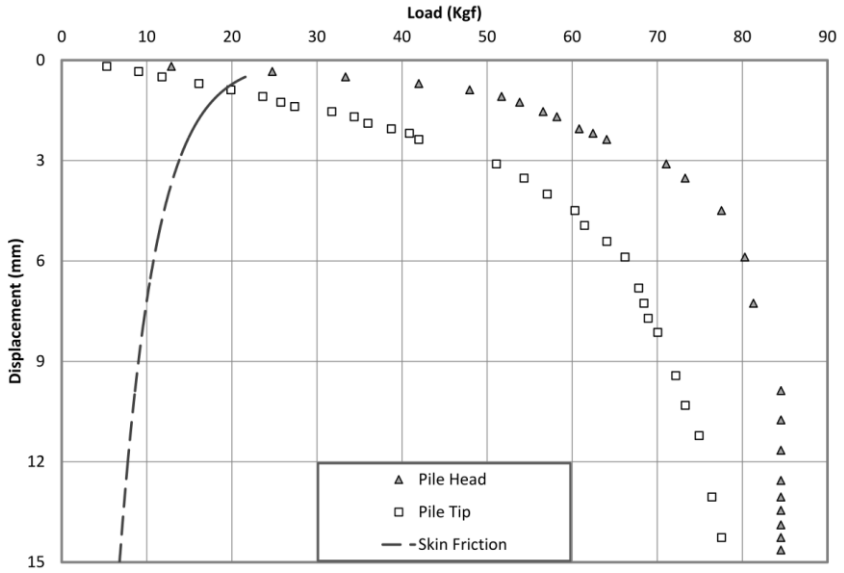

Figure 4-4 Test results on single non-displacement pile NDP30-40-10 (load-settlement curve)

DPR30-40-10-R10

The load-settlement curves of the displacement piled raft are presented in Figure 4-5. The variation of skin friction at various stages of settlement (Figure 4-5) shows that the frictional resistance increases with greater settlement which is a consequence of the pile-soil-raft interaction. Figure 4-6 illustrates the variations of the pile and raft load sharing by settlement: the pile takes most of the load at a small settlement and the raft share increases gradually with more settlement. Figure 4-7 illustrates the efficiency of piled raft footing in controlling the settlement.

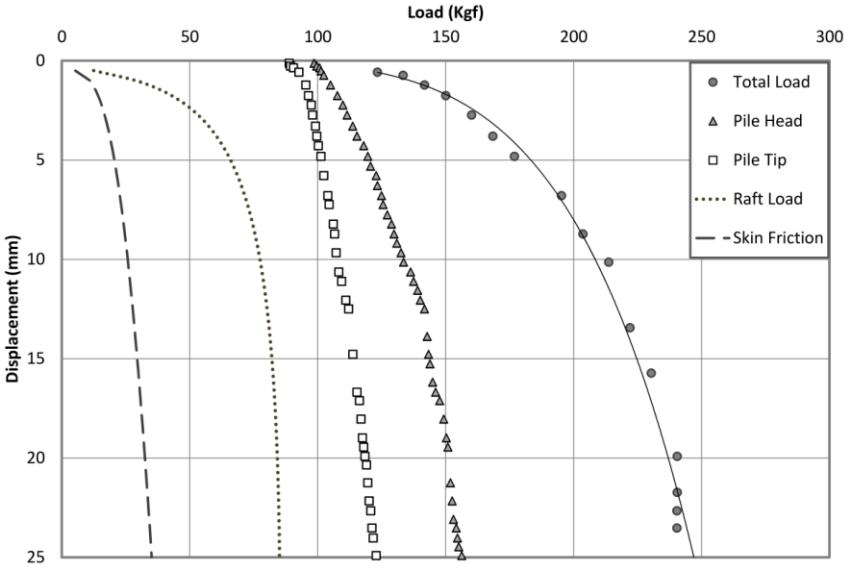

Figure 4-5 Test results on displacement piled raft DPR30-40-10-R10 (load-settlement curve)

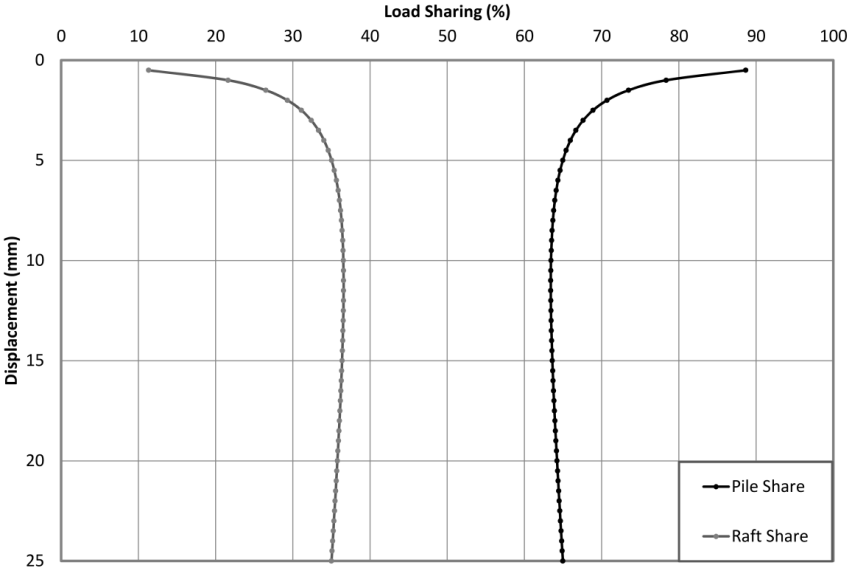

Figure 4-6 Test results on displacement piled raft DPR30-40-10-R10 (load sharing-settlement curve)

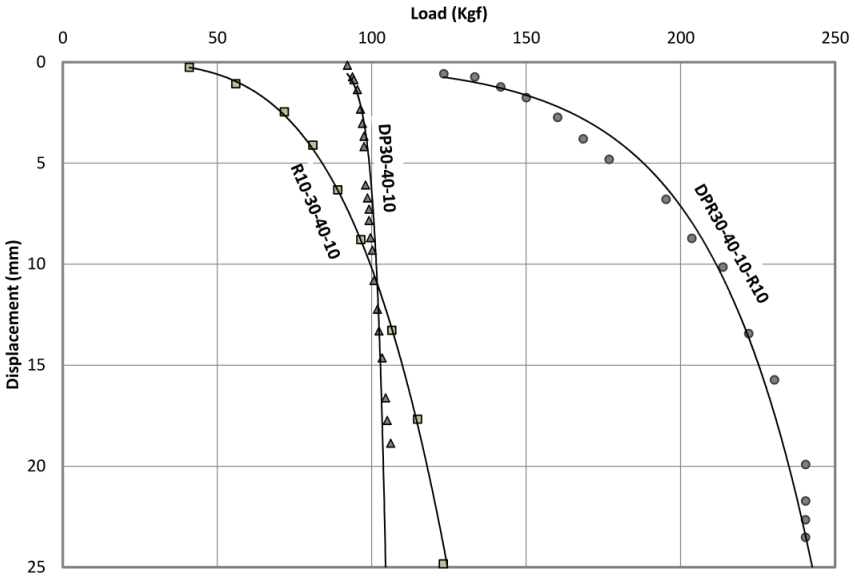

Figure 4-7 The load-settlement curves of shallow footing R10-30-40-10, single displacement pile DP30-40-10, and displacement piled raft DPR30-40-10-R10

NDPR30-40-10-R10

The behavior of non-displacement piled raft is similar to that of displacement piled raft; however, the amounts of measured load sharing are different.

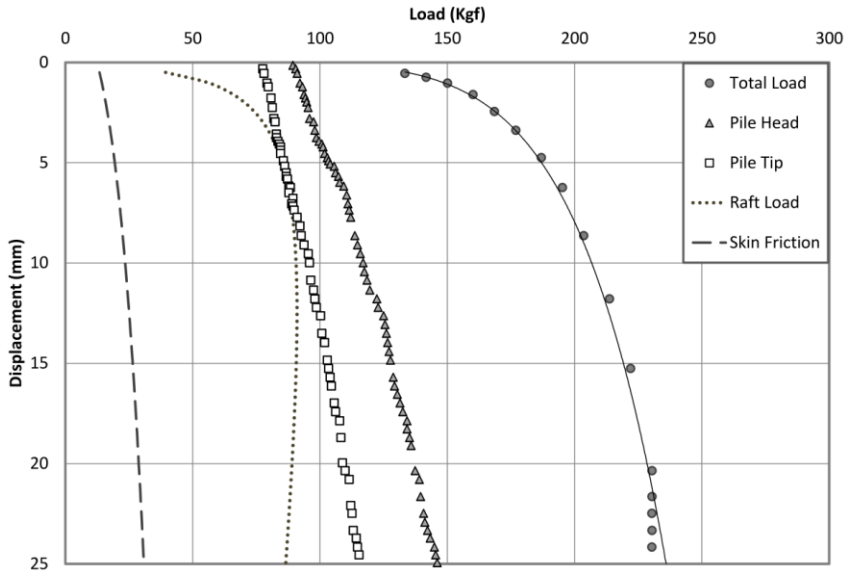

Figure 4-8 Test results on non-displacement piled raft NDPR30-40-10-R10 (load-settlement curve)

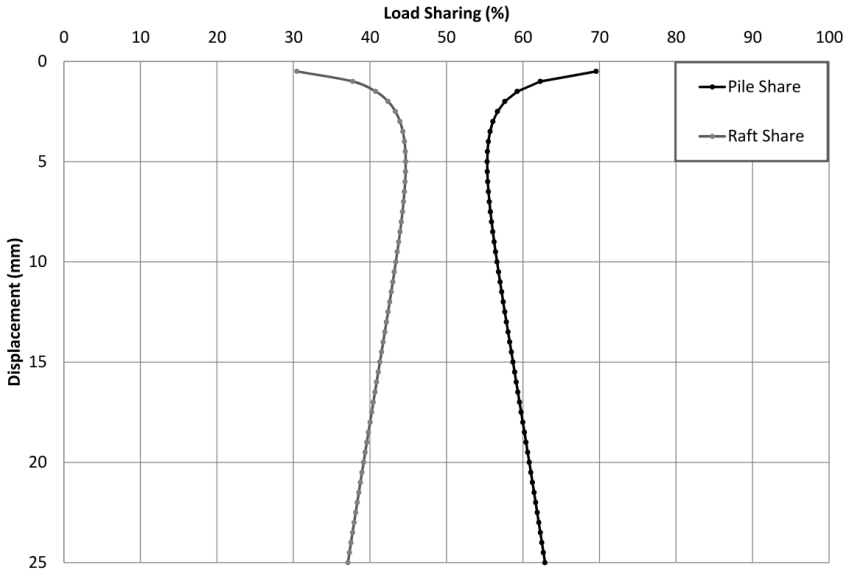

Figure 4-9 Test results on non-displacement piled raft NDPR30-40-10-R10 (load sharing-settlement curve)

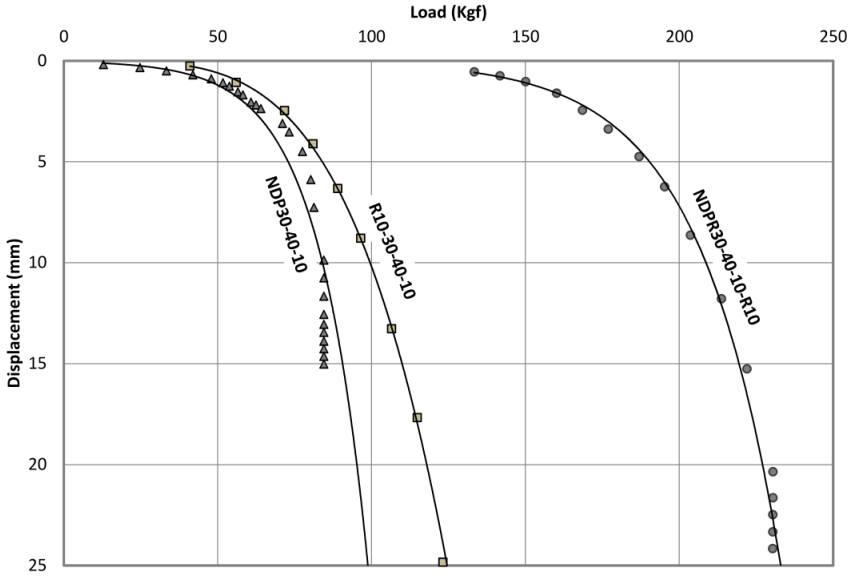

Figure 4-10 The load-settlement curves of shallow footing R10-30-40-10, single non-displacement pile NDP30-40-10, and non-displacement piled raft NDPR30-40-10-R10

NDPR30-40-10-R15

Figure 4-11 illustrates that the raft mainly provides the bearing capacity of the foundation in this test due to the fact that the raft width is much larger than the pile diameter (d_r=5.2d_p). When a large portion of the load transfers to the underlying soil by the raft, the effect of pile-soil-raft

interaction is more significant. As a result, the recorded skin friction in this test is more than the skin friction in NDPR30-40-10-R10 (Figure 4-8).

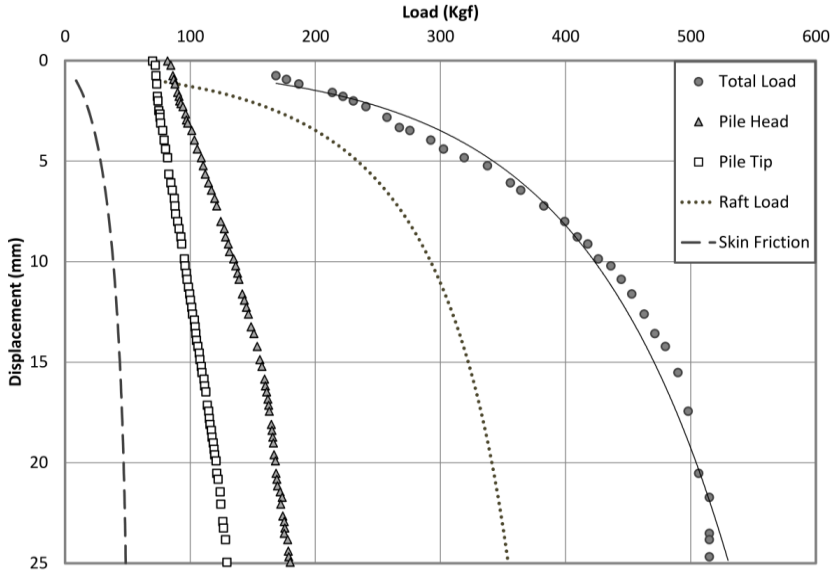

Figure 4-11 Test results on non-displacement piled raft NDPR30-40-10-R15 (load-settlement curve)

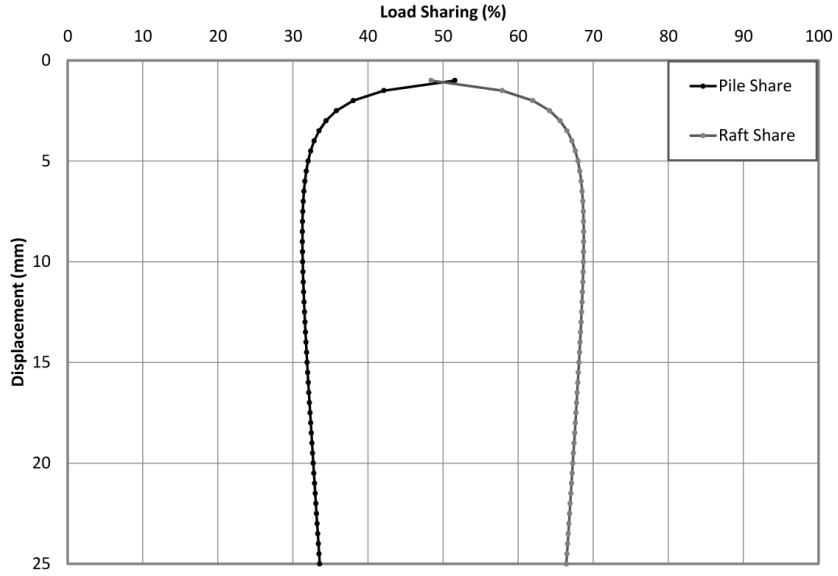

Figure 4-12 Test results on non-displacement piled raft NDPR30-40-10-R15 (load sharing-settlement curve)

NDPR30-70-30-R10

The following figures show the behavior of non-displacement piled raft in 70-30 Silica sand.

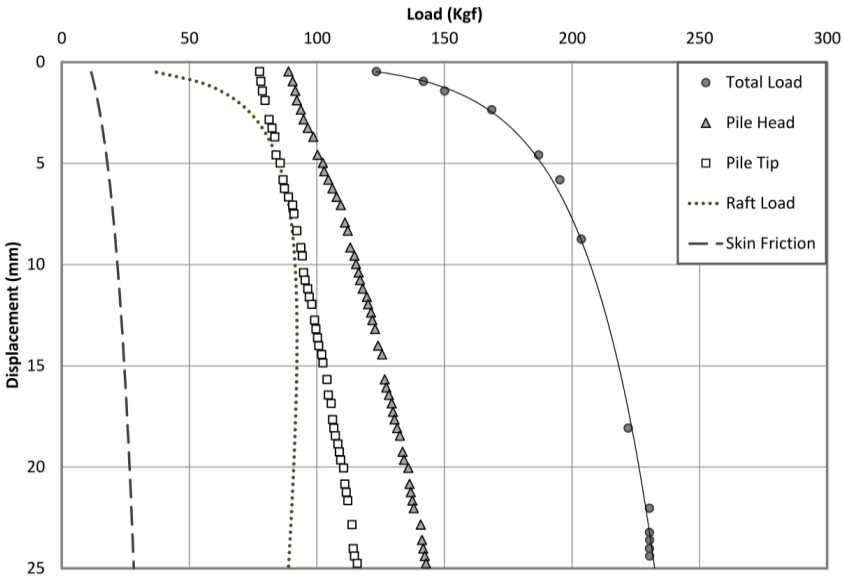

Figure 4-13 Test results on non-displacement piled raft NDPR30-70-30-R10 (load-settlement curve)

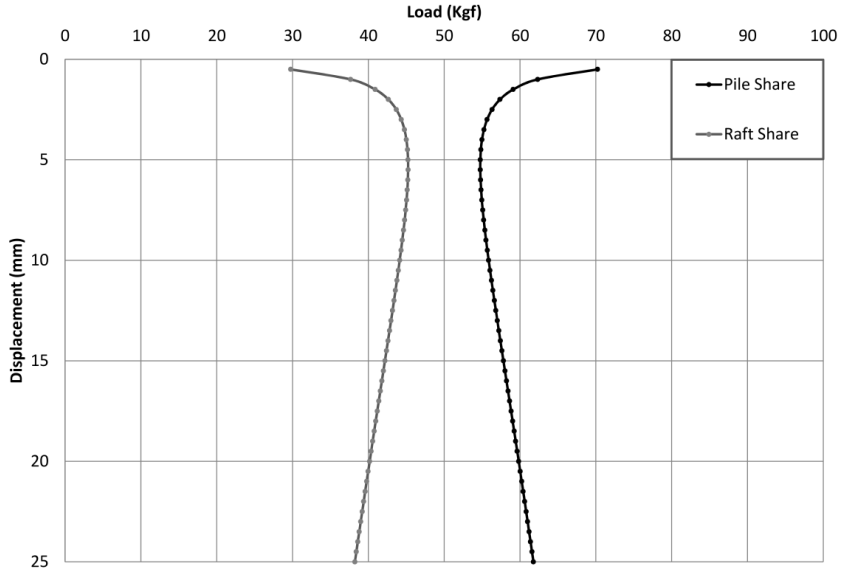

Figure 4-14 Test results on non-displacement piled raft NDPR30-70-30-R10 (load sharing-settlement curve)

4.2.2 Medium sand (D_r=45%)

R10-45-40-10

Significant change in the slope of load-settlement curve is observed in Figure 4-15 meaning that the foundation experienced the local shear failure. The ultimate bearing capacity was obtained as 139kgf at 5.2mm settlement.

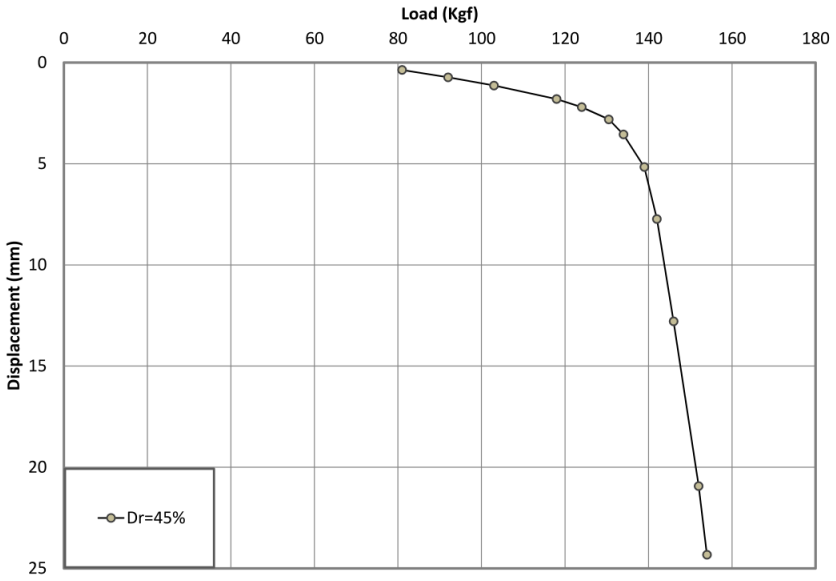

Figure 4-15 Test results on the shallow footing R10-45-40-10 (load-settlement curve)

R15-45-40-10

The failure mechanism of 150x150mm shallow footing was similar to R10-45-40-10 and the ultimate capacity was recorded as 531.6kgf.

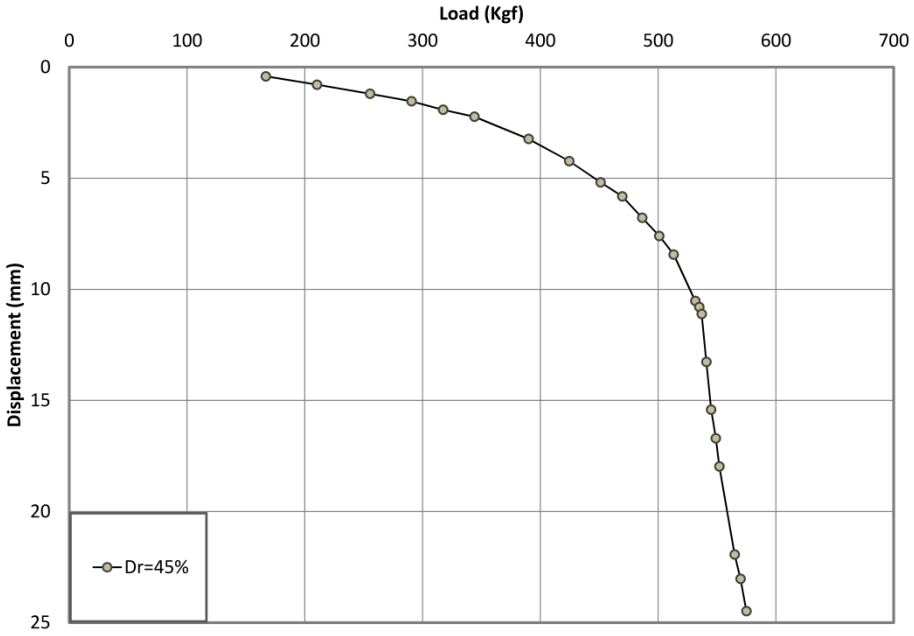

Figure 4-16 Test results on the shallow footing R15-45-40-10 (load-settlement curve)

DP45-40-10

Figure 4-17 shows that the displacement pile experienced the plunging failure at 171.1kgf. As expected, the skin and tip resistance of driven pile in medium sand were greater than those in loose sand.

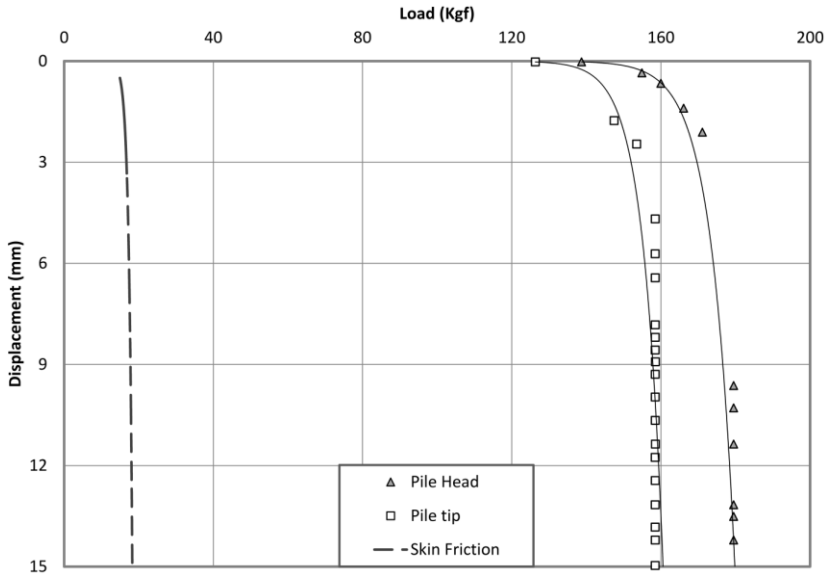

Figure 4-17 Test results on single displacement pile DP45-40-10 (load-settlement curve)

NDP45-40-10

The load-settlement curve of non-displacement pile is illustrated in Figure 4-18. The recorded ultimate capacity for non-displacement pile is less than that obtained for displacement pile in the same soil condition. This observation is related to the effect of pile driving on OCR of sandy soils.

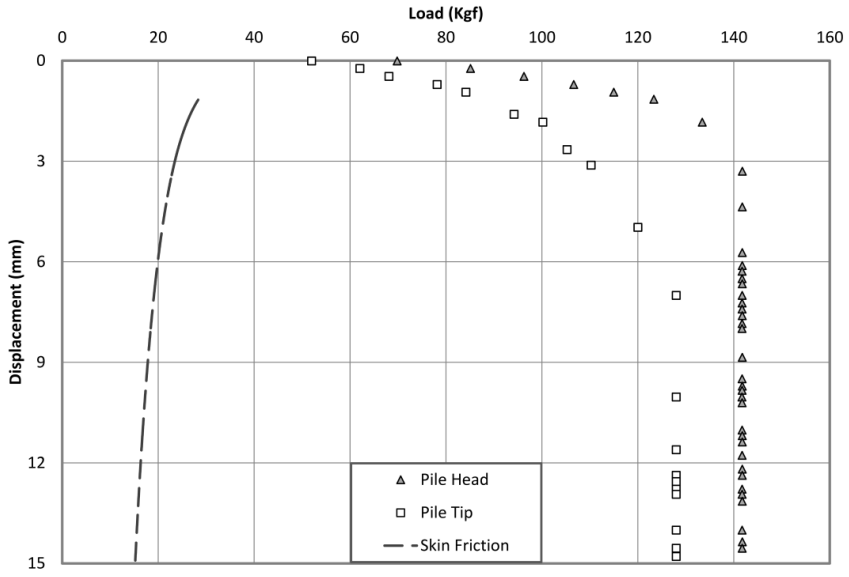

Figure 4-18 Test results on single non-displacement pile NDP45-40-10 (load-settlement curve)

DPR45-40-10-R10

The local shear failure was observed in the load-settlement curve of displacement piled raft in medium sand (Figure 4-19) and the obtained ultimate load was 310.7kgf.

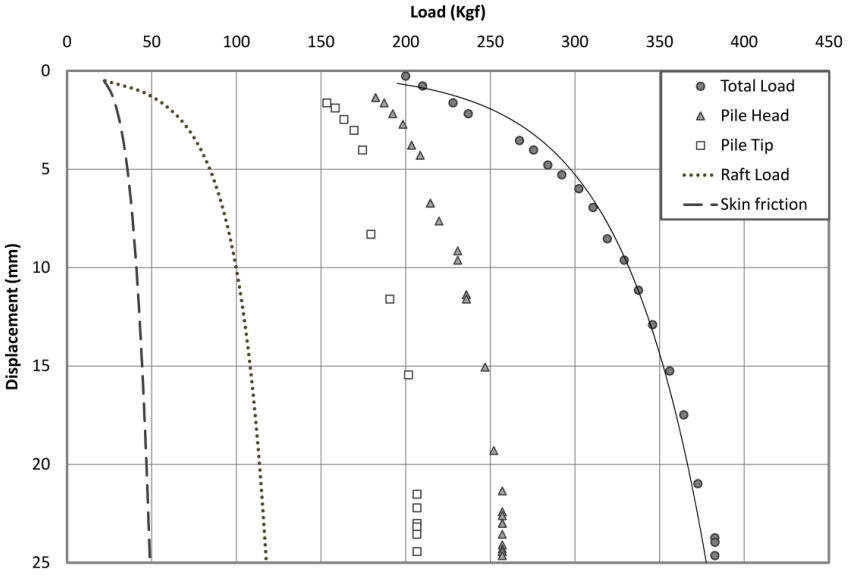

Figure 4-19 Test results on displacement piled raft DPR45-40-10-R10 (load-settlement curve)

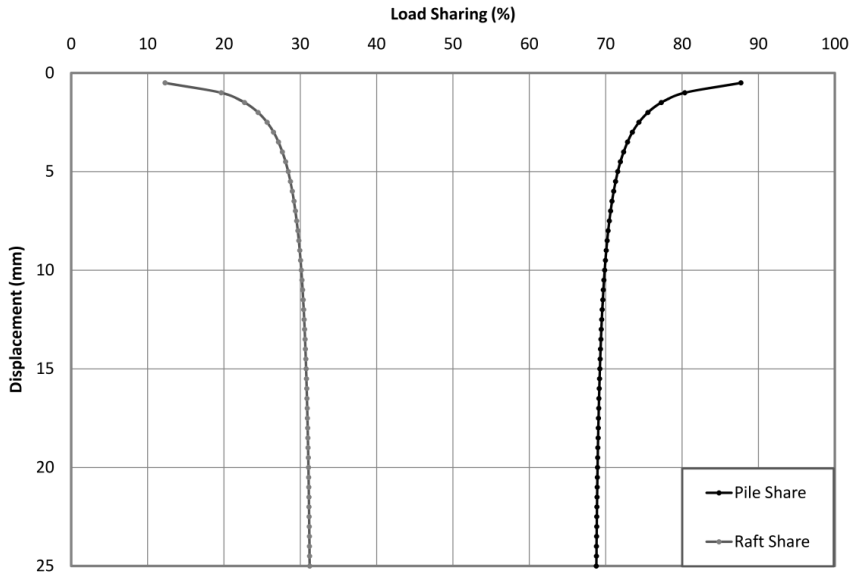

Figure 4-20 Test results on displacement piled raft DPR45-40-10-R10 (load sharing-settlement curve)

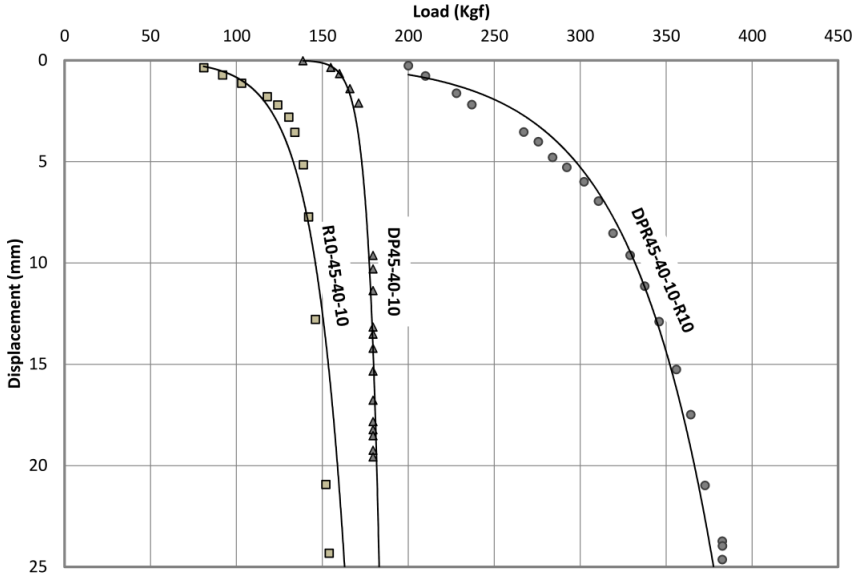

Figure 4-21 The load-settlement curves of shallow footing R10-45-40-10, single displacement pile DP45-40-10, and displacement piled raft DPR45-40-10-R10

NDPR45-40-10-R10

The load settlement curve of non-displacement piled raft in medium density (Figure 4-22) illustrates an excessive settlement at the failure point notwithstanding the addition of applied load. This observation demonstrates the occurrence of general shear failure. In other words, the failure surfaces extended to the ground and the heave was observed around the raft.

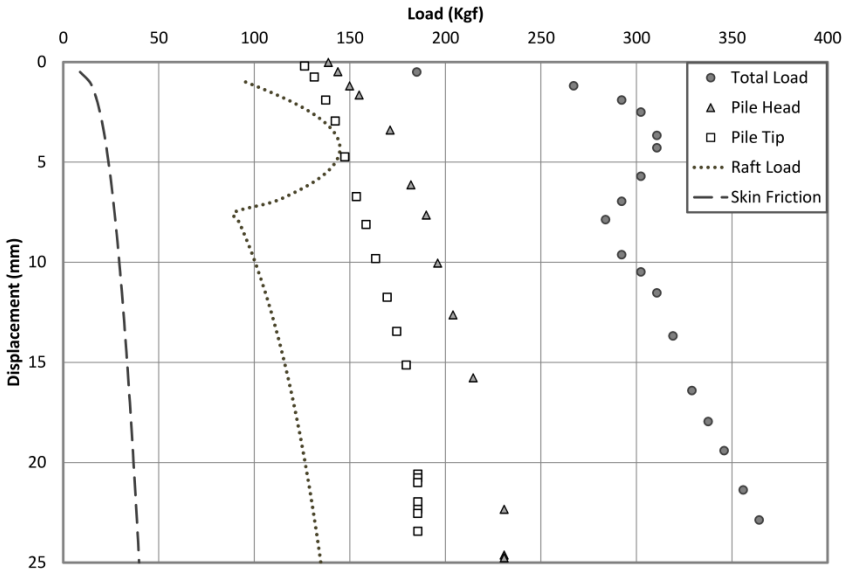

Figure 4-22 Test results on non-displacement piled raft NDPR45-40-10-R10 (load-settlement curve)

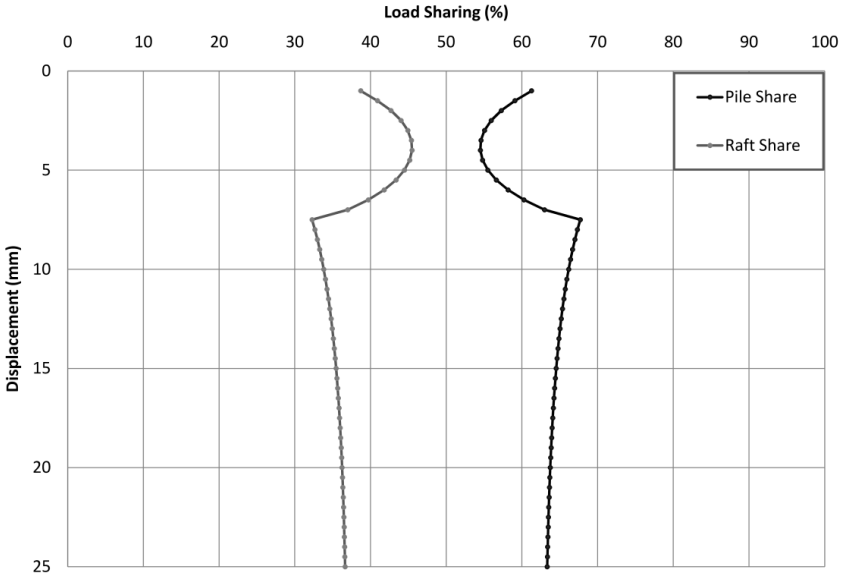

Figure 4-23 Test results on non-displacement piled raft NDPR45-40-10-R10 (load sharing-settlement curve)

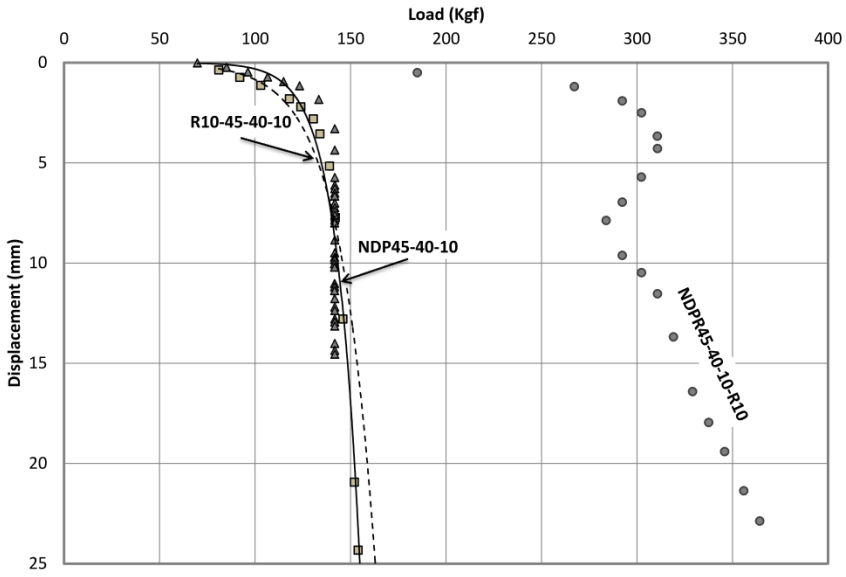

Figure 4-24 The load-settlement curves of shallow footing R10-45-40-10, single non-displacement pile NDP45-40-10, and non-displacement piled raft NDPR45-40-10-R10

NDPR45-40-10-R15

The experimental results show that the general shear failure occurred at the failure point (Figure 4-25) and the raft contribution in carrying the applied load was significant (Figure 4-26).

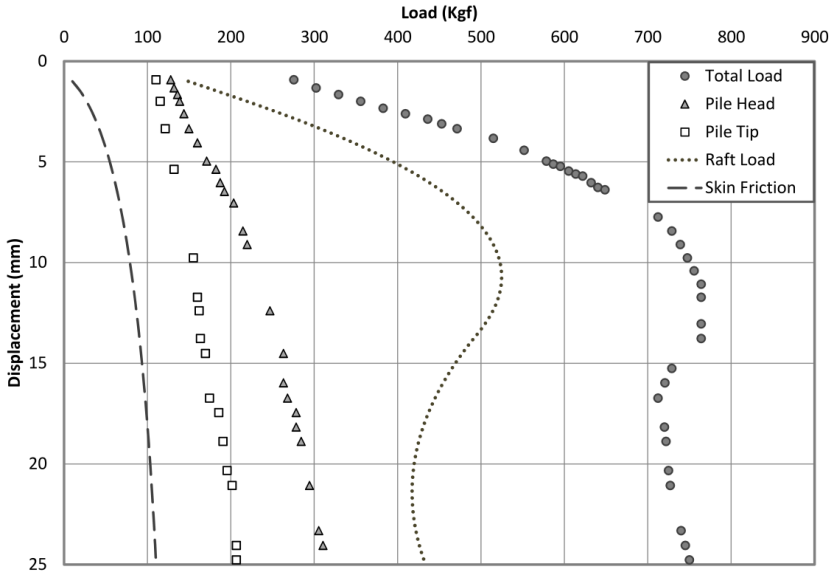

Figure 4-25 Test results on non-displacement piled raft NDPR45-40-10-R15 (load-settlement curve)

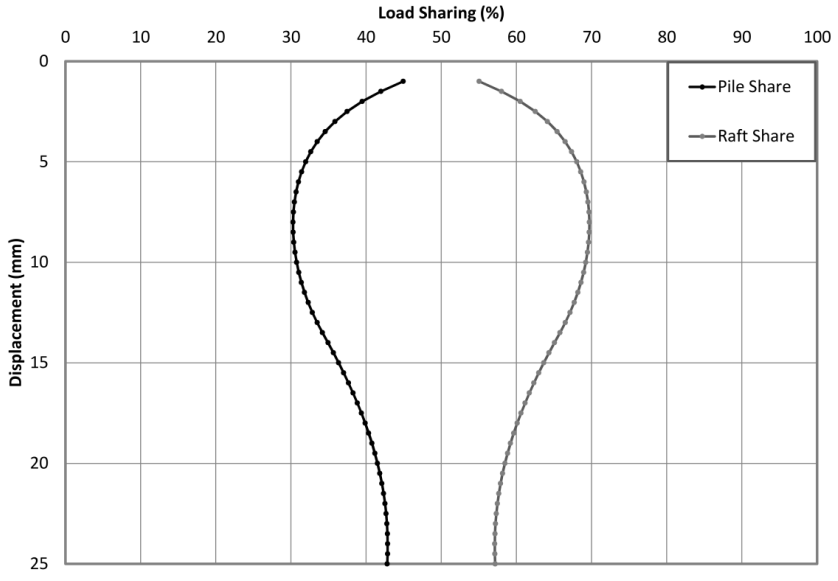

Figure 4-26 Test results on non-displacement piled raft NDPR45-40-10-R15 (load sharing-settlement curve)

NDPR45-70-30-R10

The following figures illustrate the behavior of non-displacement piled raft in 70-30 Silica sand.

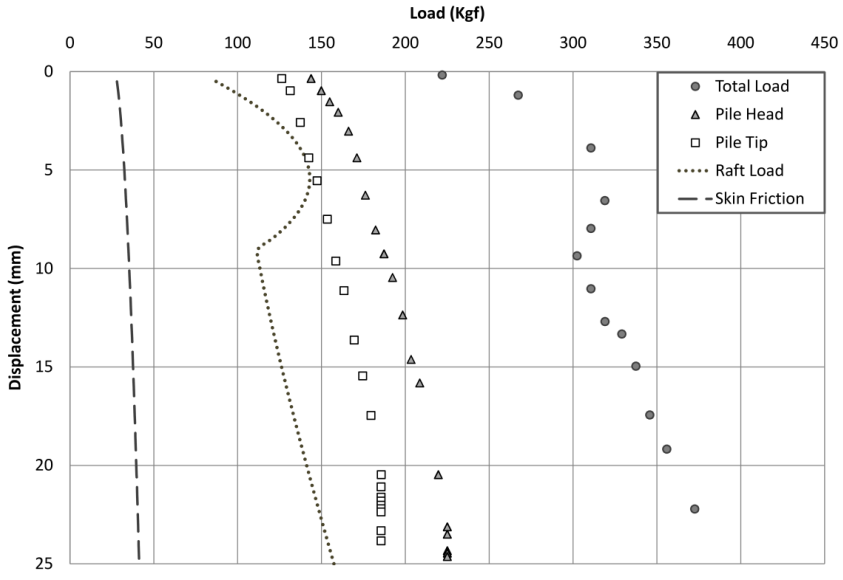

Figure 4-27 Test results on non-displacement piled raft NDPR45-70-30-R10 (load-settlement curve)

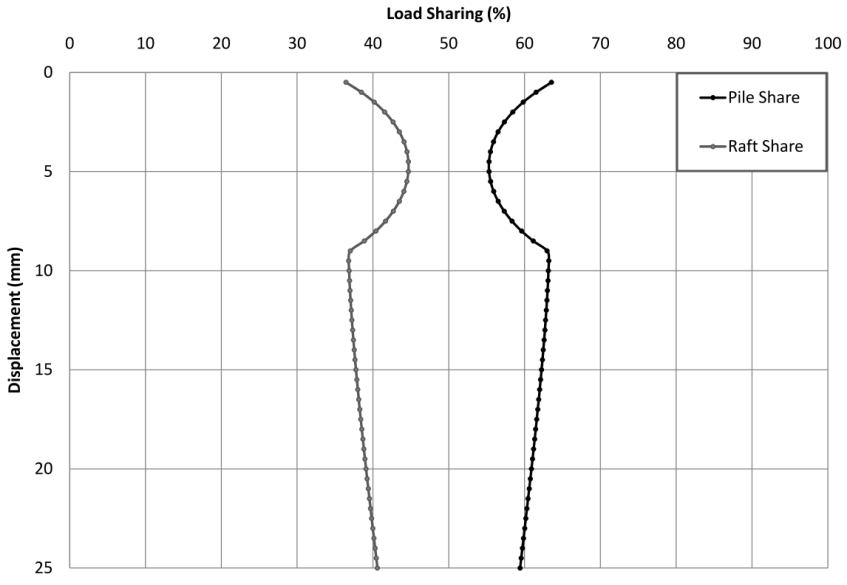

Figure 4-28 Test results on non-displacement piled raft NDPR45-70-30-R10 (load sharing-settlement curve)

4.2.3 Dense sand (D_r=60%)

R10-60-40-10

The general shear failure was observed on shallow footing founded on dense sand (Figure 4-29).

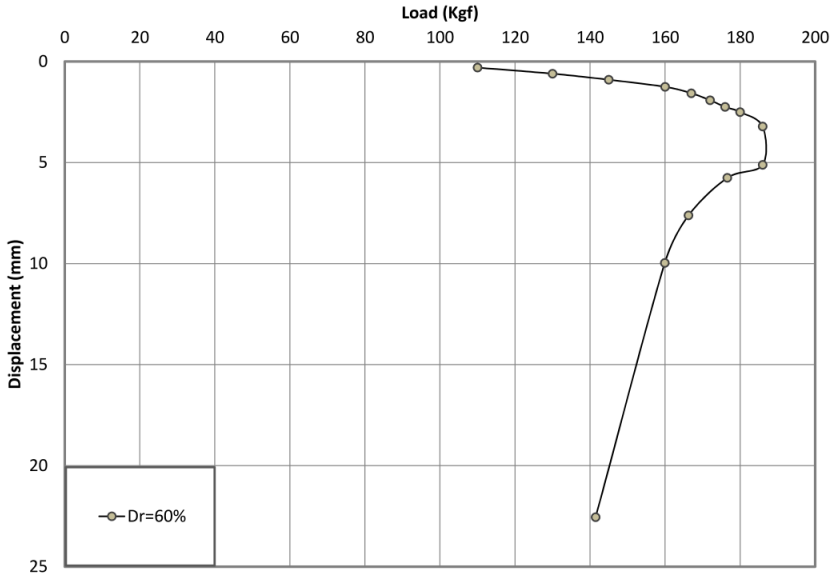

Figure 4-29 Test results on the shallow footing R10-60-40-10 (load-settlement curve)

R15-60-40-10

In this test, the trend of load-settlement curve is similar to the previous test; although, the R15 foundation provides greater bearing capacity.

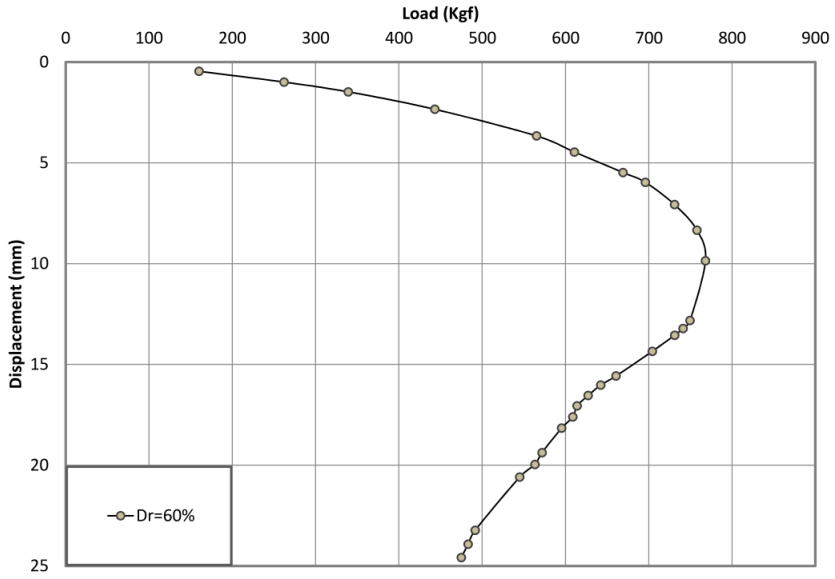

Figure 4-30 Test results on the shallow footing R15-60-40-10 (load-settlement curve)

DP60-40-10

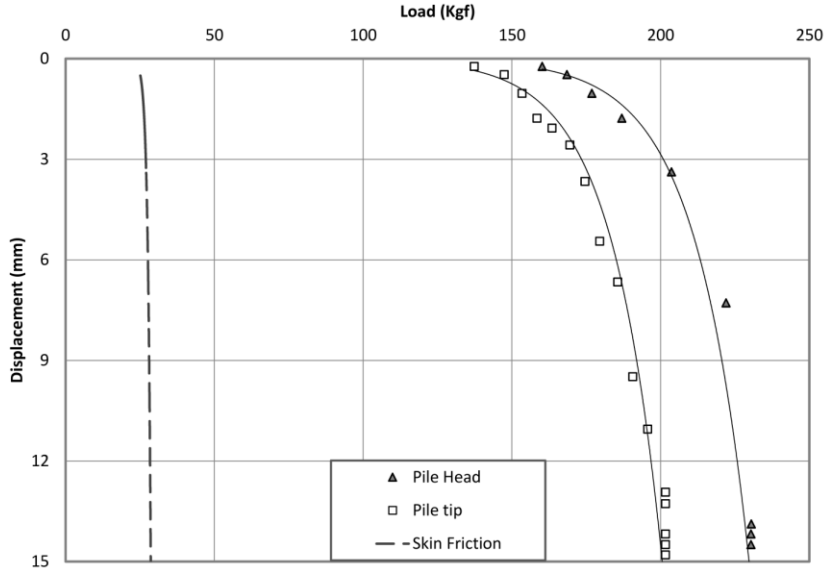

Figure 4-31 Test results on single displacement pile DP60-40-10 (load-settlement curve)

NDP60-40-10

The plunging occurred at 213.7kgf resulting into 3.35mm settlement.

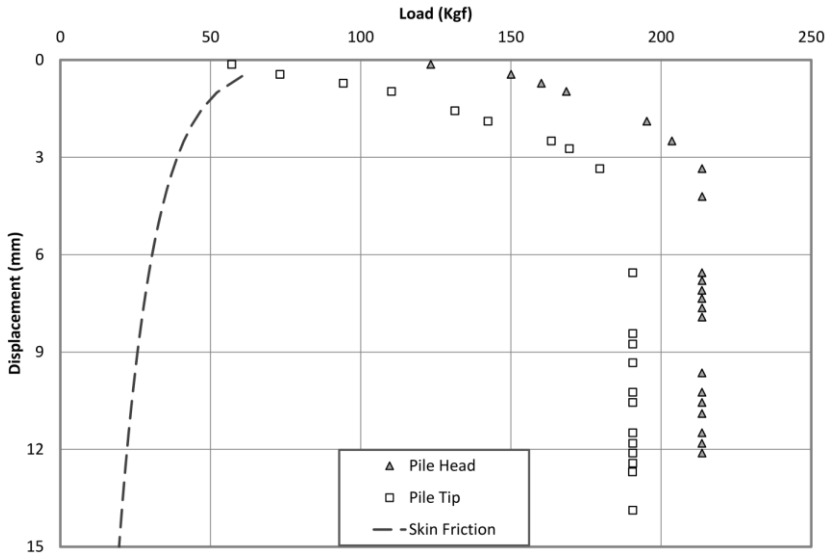

Figure 4-32 Test results on single non-displacement pile NDP60-40-10 (load-settlement curve)

DPR60-40-10-R10

The local shear failure was observed on displacement piled raft and the ultimate load of 355kgf was achieved.

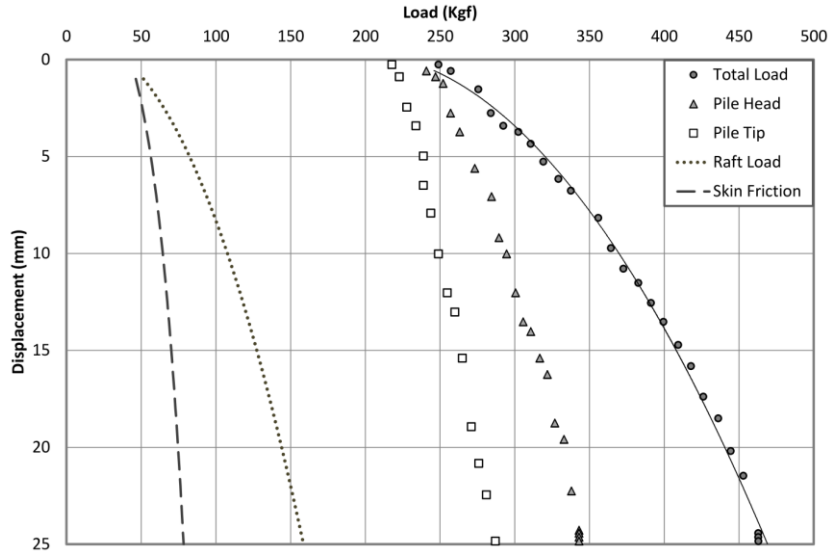

Figure 4-33 Test results on displacement piled raft DPR60-40-10-R10 (load-settlement curve)

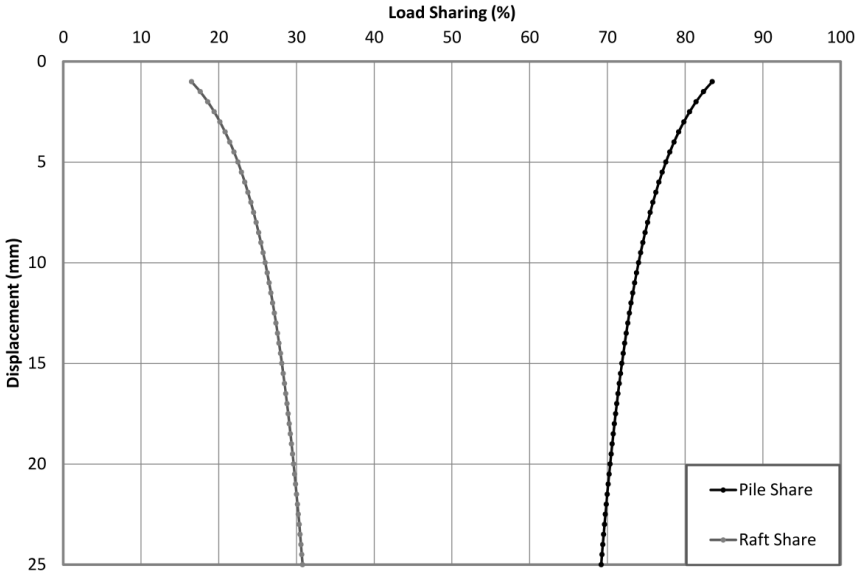

Figure 4-34 Test results on displacement piled raft DPR60-40-10-R10 (load sharing-settlement curve)

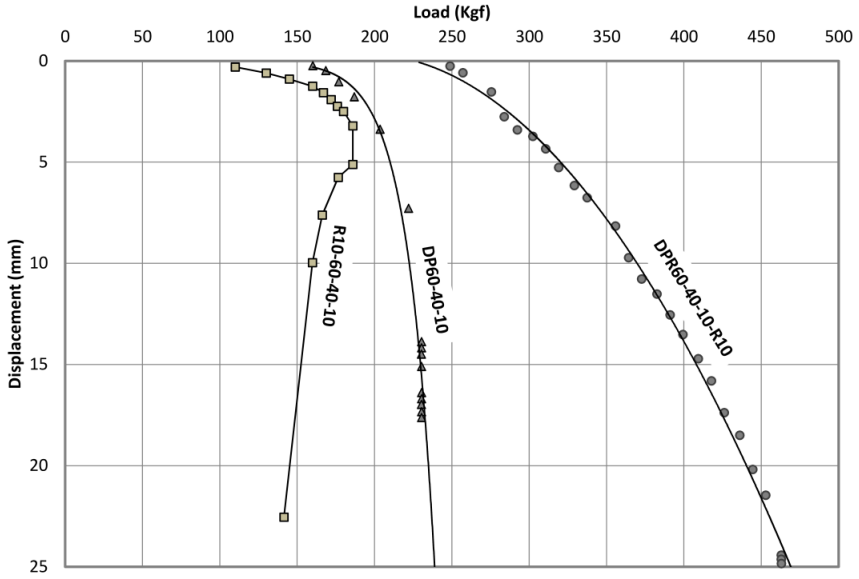

Figure 4-35 The load-settlement curves of shallow footing R10-60-40-10, single displacement pile DP60-40-10, and displacement piled raft DPR60-40-10-R10

NDPR60-40-10-R10

The non-displacement piled raft in dense sand experienced the general shear failure at settlement ratio of 3% (Figure 4-36).

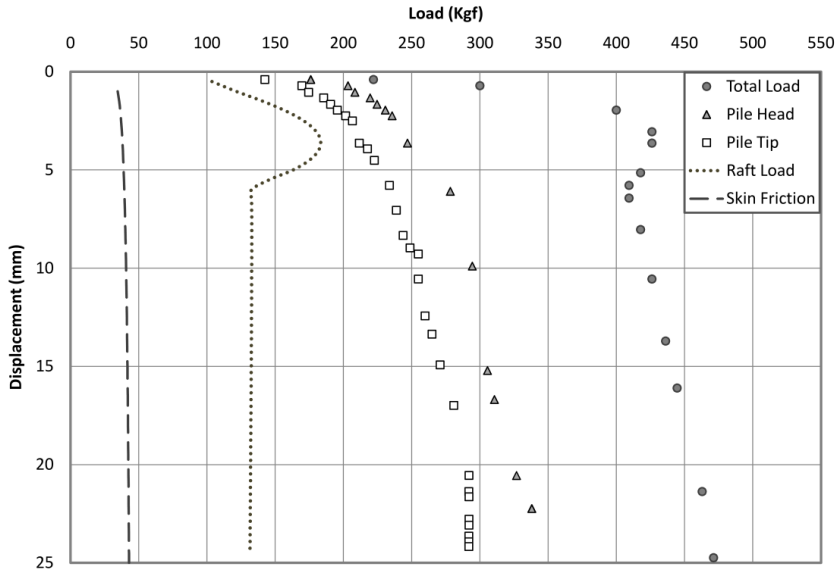

Figure 4-36 Test results on non-displacement piled raft NDPR60-40-10-R10 (load-settlement curve)

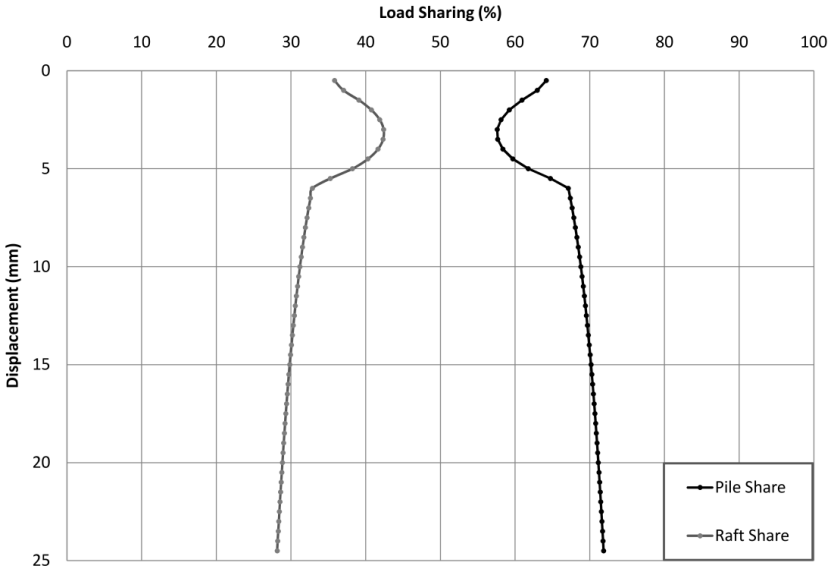

Figure 4-37 Test results on non-displacement piled raft NDPR60-40-10-R10 (load sharing-settlement curve)

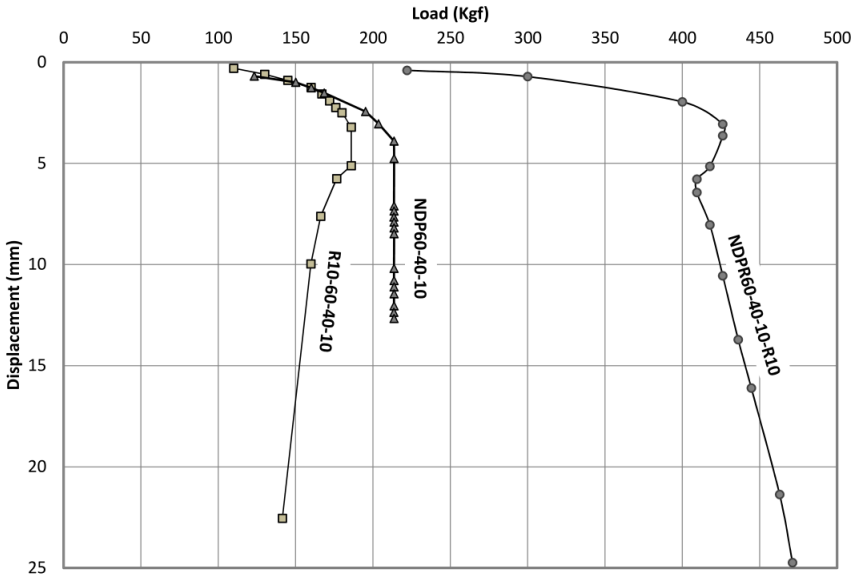

Figure 4-38 The load-settlement curves of shallow footing R10-60-40-10, single non-displacement pile NDP60-40-10, and non-displacement piled raft NDPR60-40-10-R10

NDPR60-40-10-R15

In this test, the S load cell was not mounted because the maximum capacity of S load cell was 500kgf and it was expected to exceed this capacity. Therefore, only the pile head, pile tip and corresponding settlement were measured. The total load was estimated for this test based on the assumption that the load sharing is exactly the same as non-displacement piled raft in medium sand.

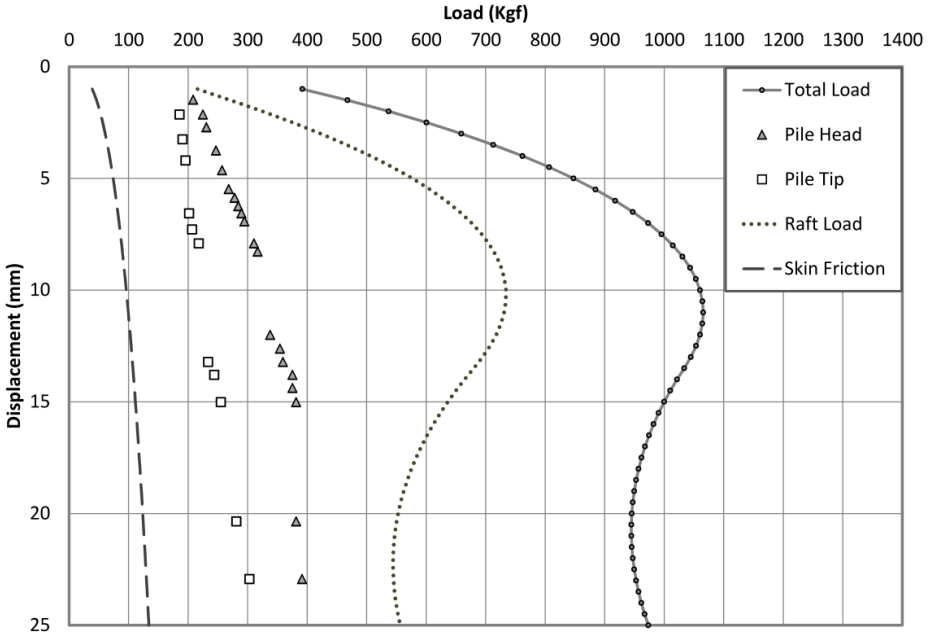

Figure 4-39 Test results on non-displacement piled raft NDPR60-40-10-R15 (load-settlement curve)

NDPR60-70-30-R10

The general shear failure was observed for the non-displacement piled raft in 70-30 Silica sand. The same behavior was noticed for non-displacement piled raft in 40-10 Silica sand.

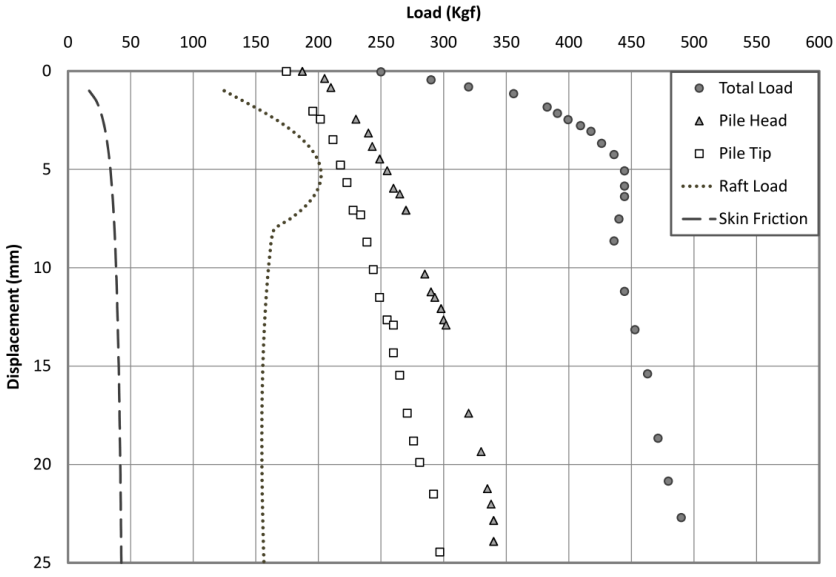

Figure 4-40 Test results on non-displacement piled raft NDPR60-70-30-R10 (load-settlement curve)

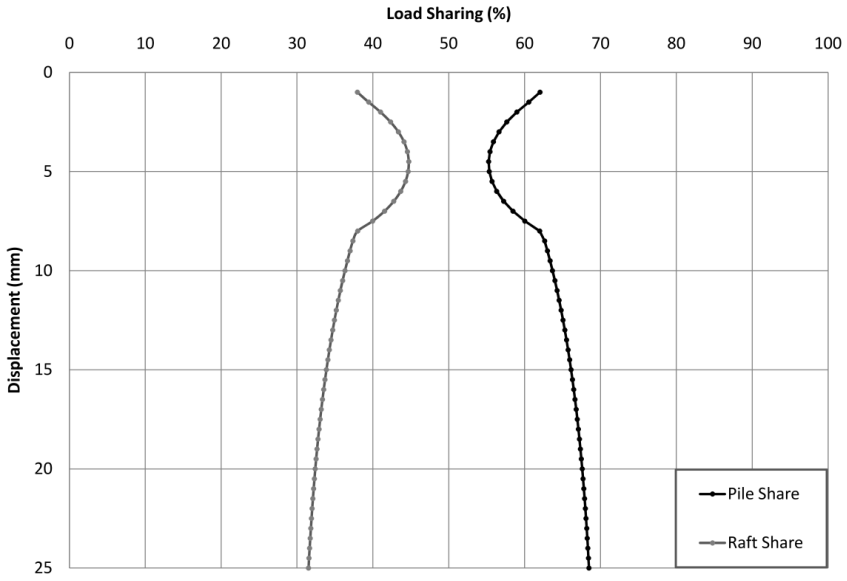

Figure 4-41 Test results on non-displacement piled raft NDPR60-70-30-R10 (load sharing-settlement curve)

4.3 Layered Sand

The experimental results on layered soil are categorized based on the soil density patterns, loose on medium, loose on dense and medium on dense sand (Figure 3-9), and are presented in the following subsections.

4.3.1 Loose on Medium sand

NDP30/45-40-10

In this test, the bearing capacity was mainly provided by the pile tip which was placed on medium sand. The failure happened by plunging and 116.6kgf was recorded as the ultimate bearing capacity (Figure 4-42).

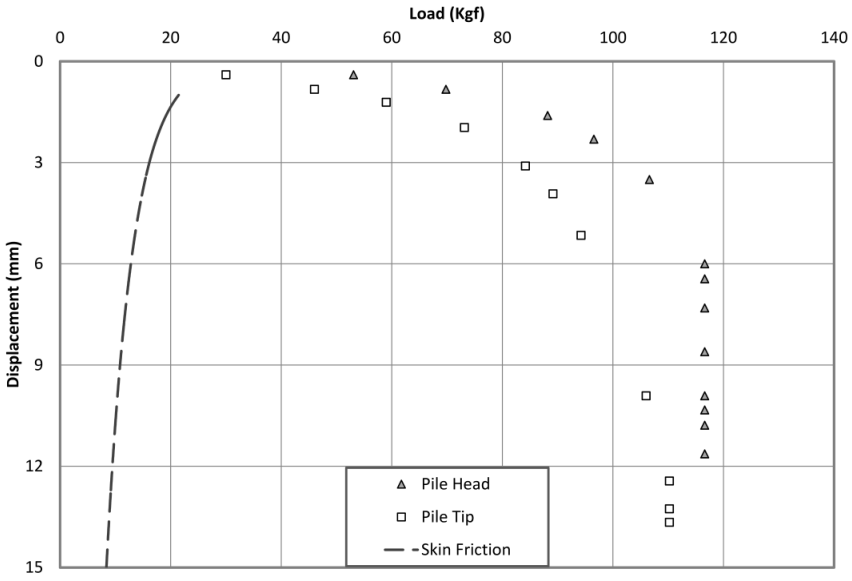

Figure 4-42 Test results on single non-displacement pile NDP30/45-40-10 (load-settlement curve)

NDPR30/45-40-10-R10

Figure 4-43 illustrates the occurrence of punching shear at the failure point. The load sharing trend is similar to that observed for the piled raft in homogenous soil and the pile share decreases by settlement until reaching the failure point (Figure 4-44). Figure 4-45 compares the load-settlement curves of shallow and deep foundation with pile raft footing demonstrating the efficiency of pile raft in reducing settlement.

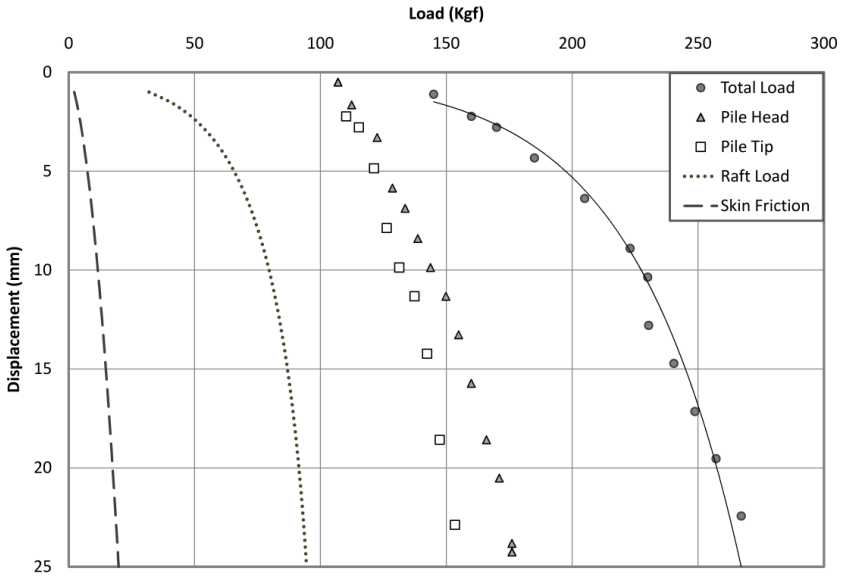

Figure 4-43 Test results on non-displacement piled raft NDPR30/45-40-10-R10 (load-settlement curve)

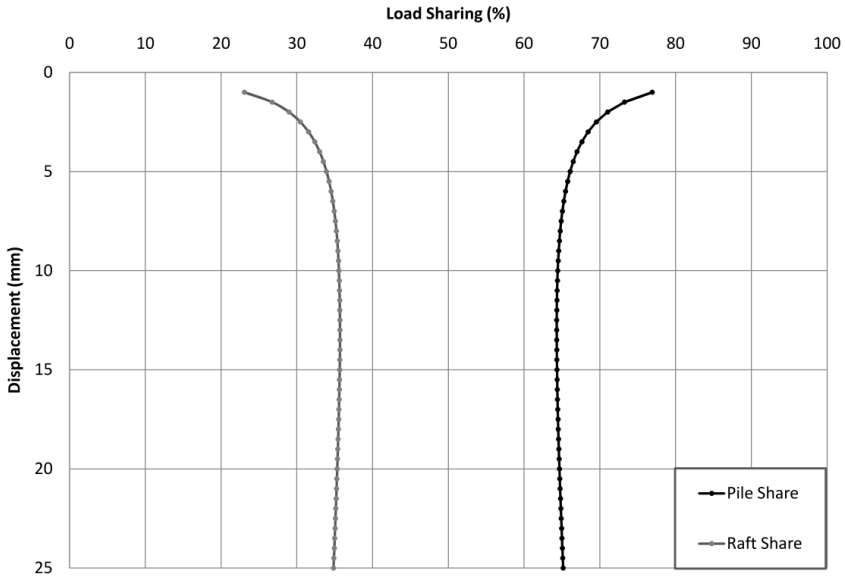

Figure 4-44 Test results on non-displacement piled raft NDPR30/45-40-10-R10 (load sharing-settlement curve)

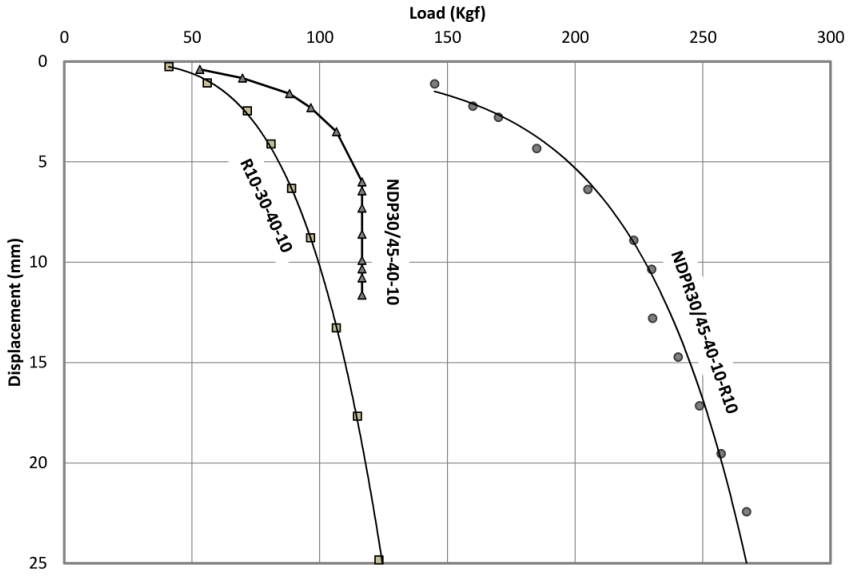

Figure 4-45 The load-settlement curves of shallow footing R10-30-40-10, single non-displacement pile NDP30/45-40-10, and non-displacement piled raft NDPR30/45-40-10-R10

NDPR30/45-40-10-R15

The failure mechanism is same as the previous test although the raft contribution in carrying the applied load increased significantly.

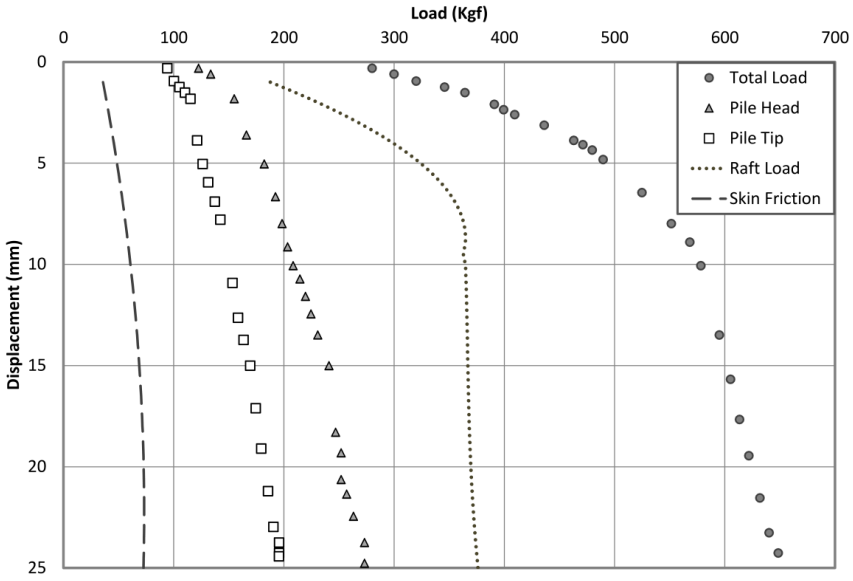

Figure 4-46 Test results on non-displacement piled raft NDPR30/45-40-10-R15 (load-settlement curve)

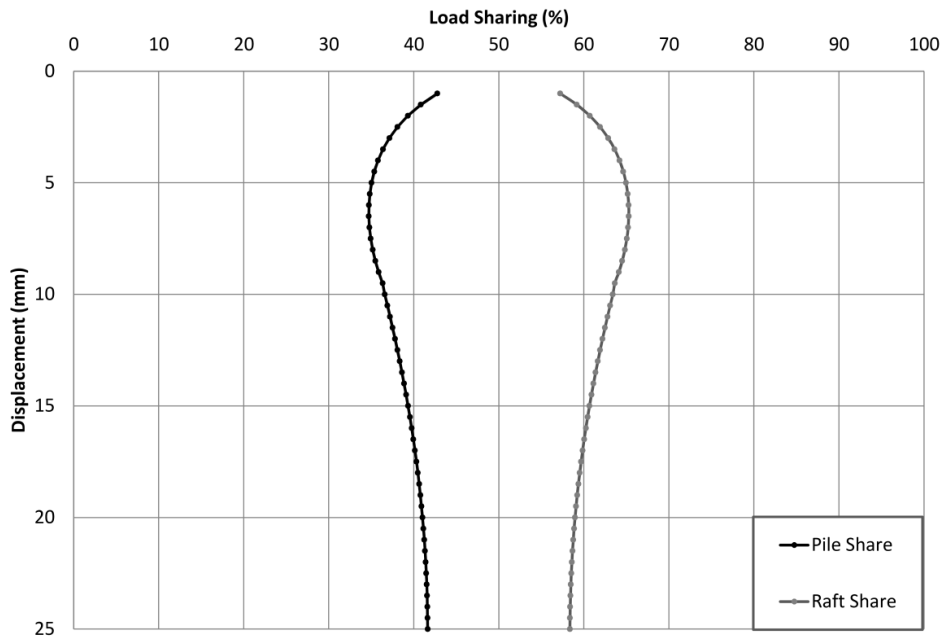

Figure 4-47 Test results on non-displacement piled raft NDPR30/45-40-10-R15 (load sharing-settlement curve)

4.3.2 Loose on dense sand

NDP30/60-40-10

Figure 4-48 shows the results of pile load test of founded pile on dense sand, surrounded by loose sand. The plunging defined the failure point at 148.33kgf.

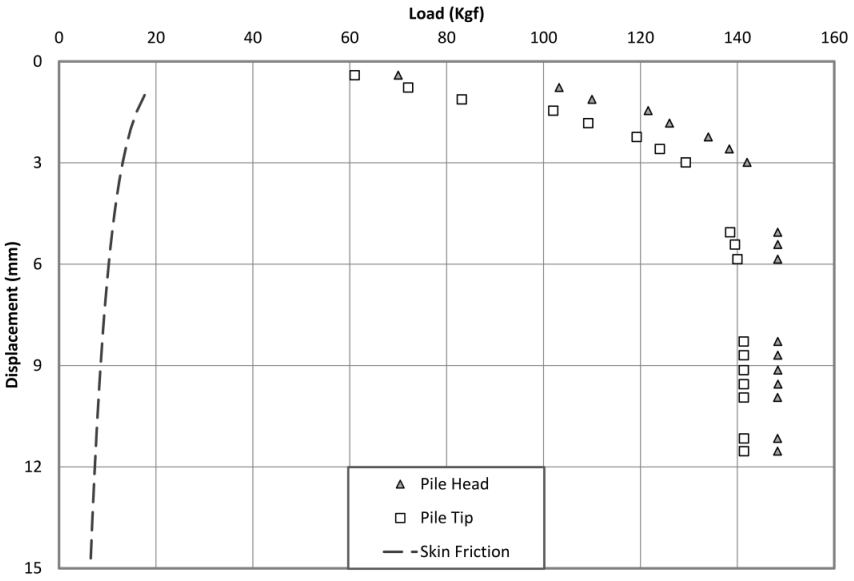

Figure 4-48 Test results on single non-displacement pile NDP30/60-40-10 (load-settlement curve)

NDPR30/60-40-10-R10

The load settlement curve of non-displacement piled raft is shown in Figure 4-49. Since the pile was founded on dense sand, it carried most of the applied load at the initial steps.

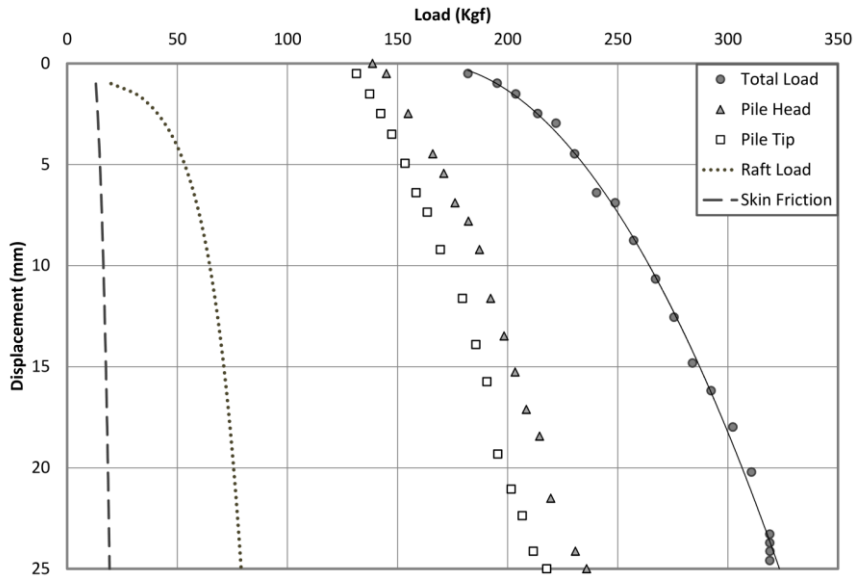

Figure 4-49 Test results on non-displacement piled raft NDPR30/60-40-10-R10 (load-settlement curve)

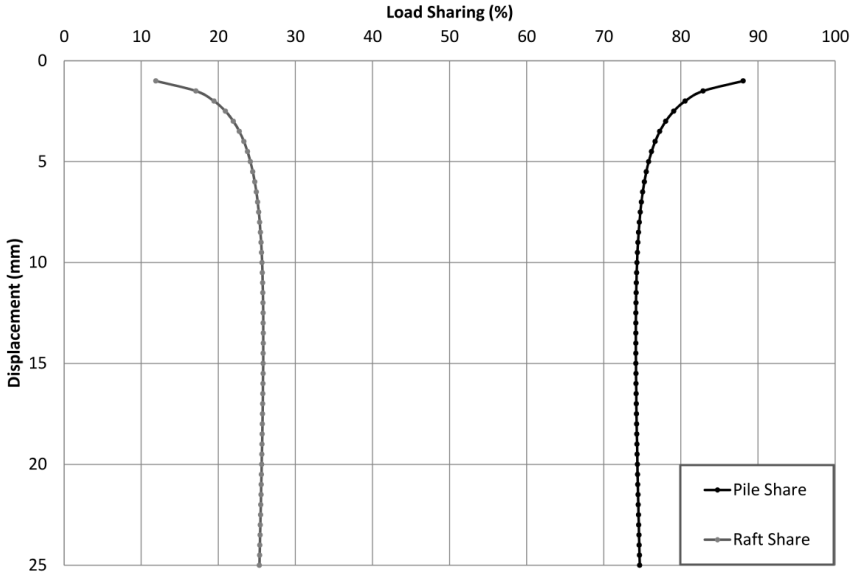

Figure 4-50 Test results on non-displacement piled raft NDPR30/60-40-10-R10 (load sharing-settlement curve)

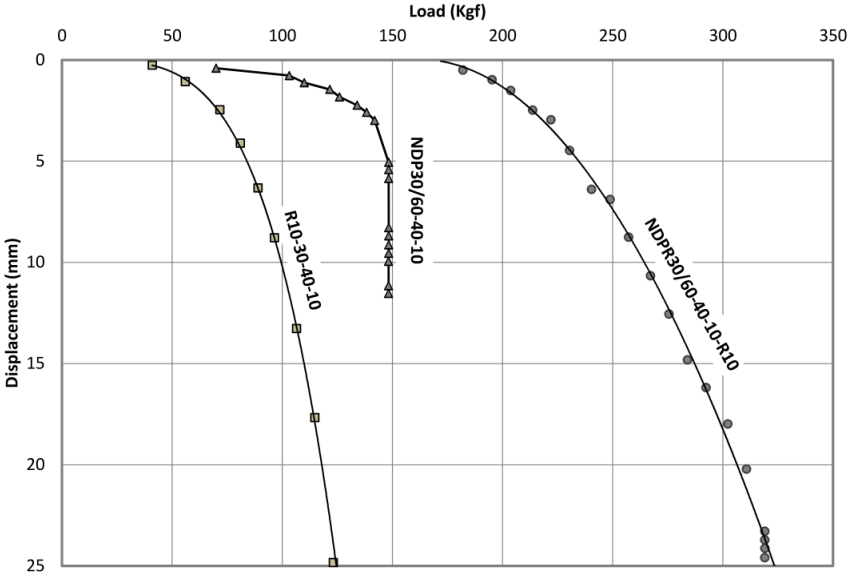

Figure 4-51 The load-settlement curves of shallow footing R10-30-40-10, single non-displacement pile NDP30/60-40-10, and non-displacement piled raft NDPR30/60-40-10-R10

NDPR30/60-40-10-R15

In this test, the 150x150mm raft was founded on loose sand while the pile tip was sitting on dense sand. The piled raft experienced the local shear failure and the point with minimum curvature on the load-settlement curve defined the failure point (Figure 4-52).

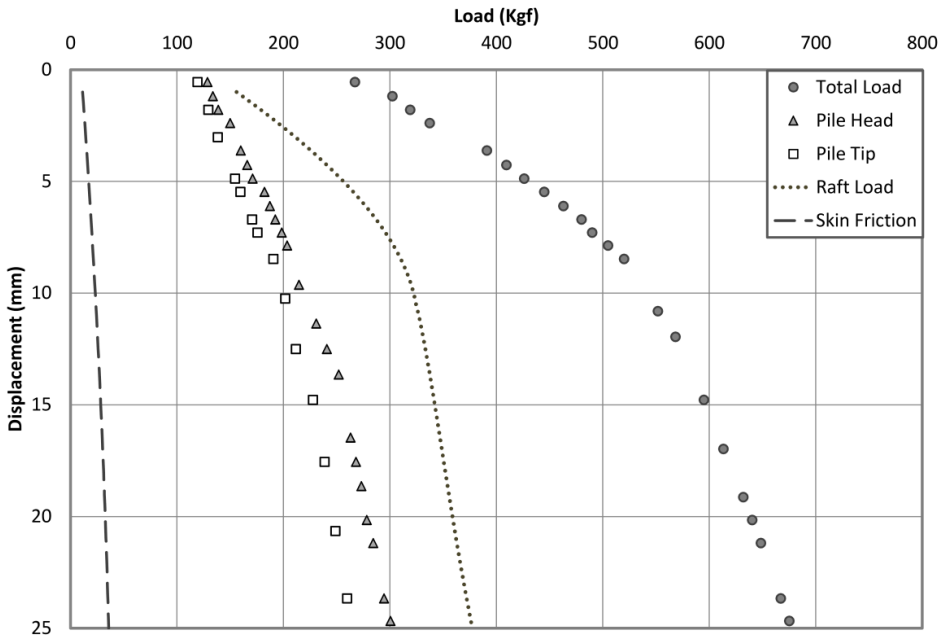

Figure 4-52 Test results on non-displacement piled raft NDPR30/60-40-10-R15 (load-settlement curve)

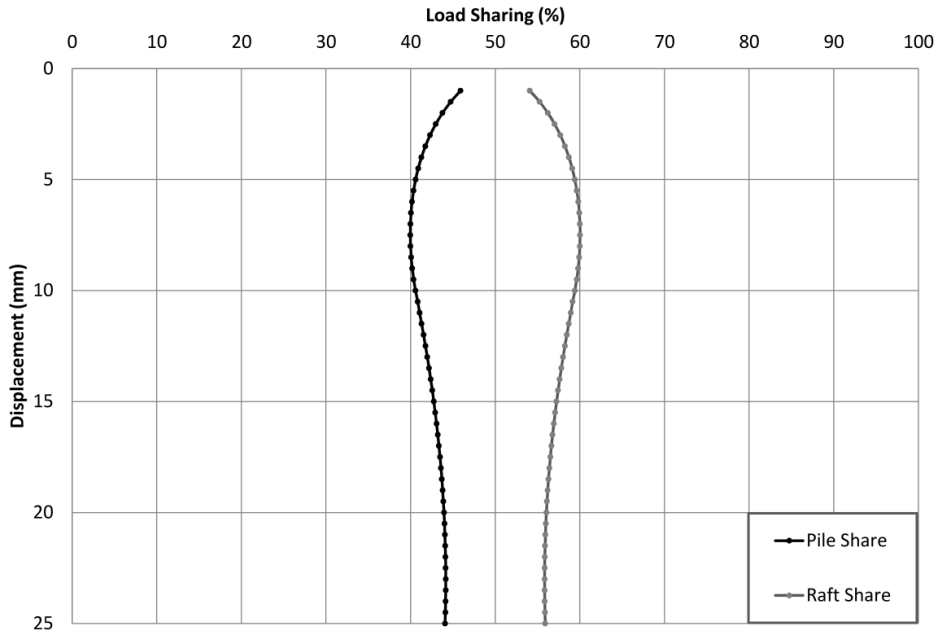

Figure 4-53 Test results on non-displacement piled raft NDPR30/60-40-10-R15 (load sharing-settlement curve)

4.3.3 Medium on dense sand

NDP45/60-40-10

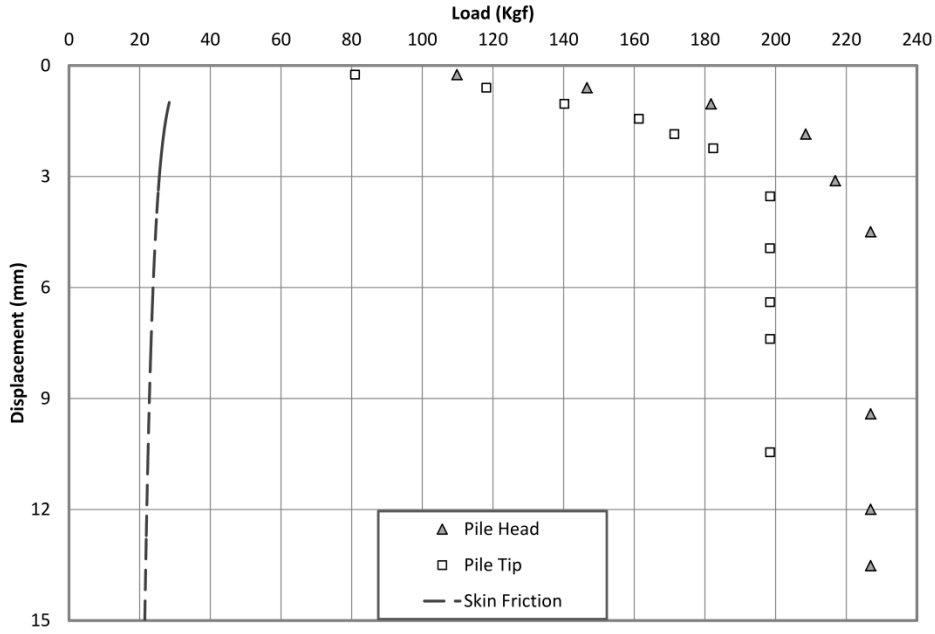

Figure 4-54 Test results on single non-displacement pile NDP45/60-40-10 (load-settlement curve)

NDPR45/60-40-10-R10

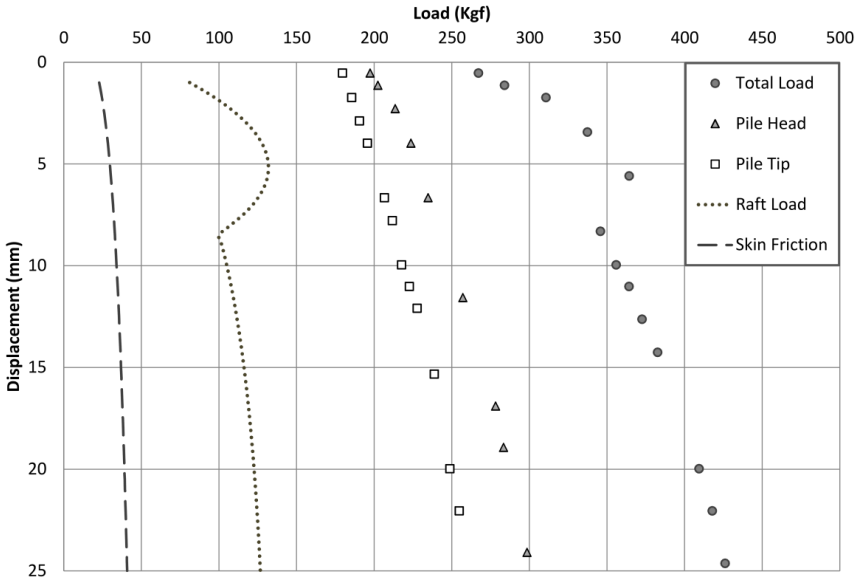

Figure 4-55 Test results on non-displacement piled raft NDPR45/60-40-10-R10 (load-settlement curve)

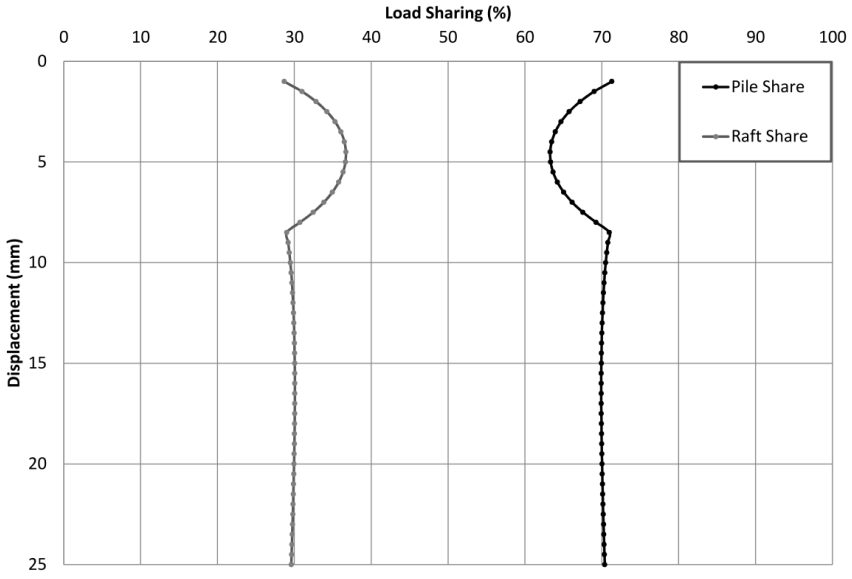

Figure 4-56 Test results on non-displacement piled raft NDPR45/60-40-10-R10 (load sharing-settlement curve)

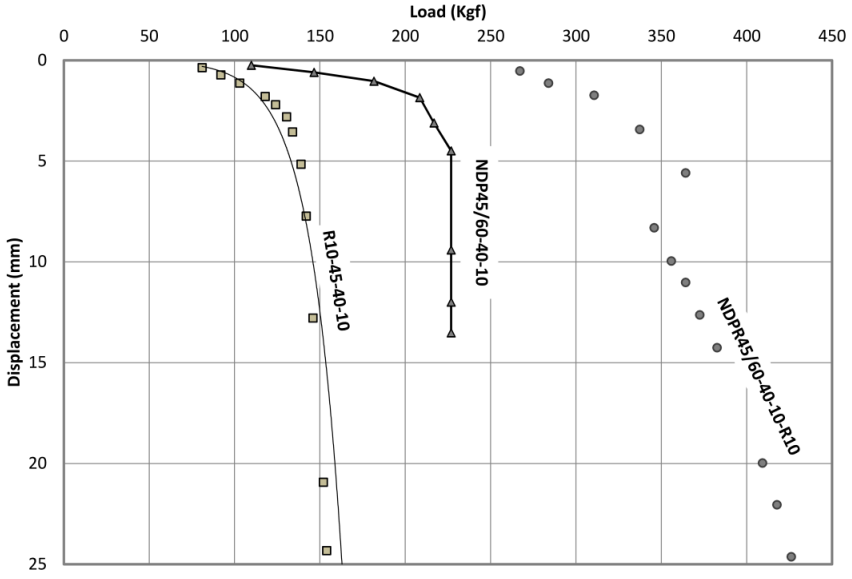

Figure 4-57 The load-settlement curves of shallow footing R10-45-40-10, single non-displacement pile NDP45/60-40-10, and non-displacement piled raft NDPR45/60-40-10-R10

NDPR45/60-40-10-R15

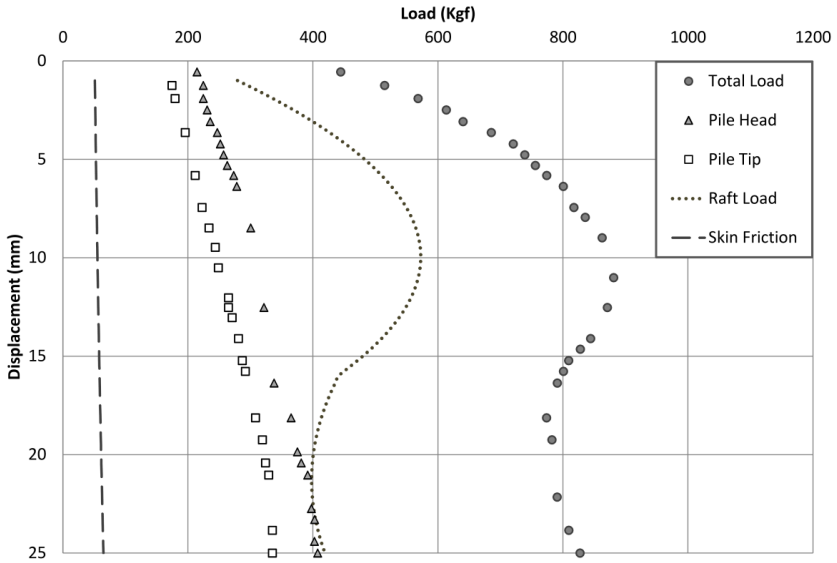

Figure 4-58 Test results on non-displacement piled raft NDPR45/60-40-10-R15 (load-settlement curve)

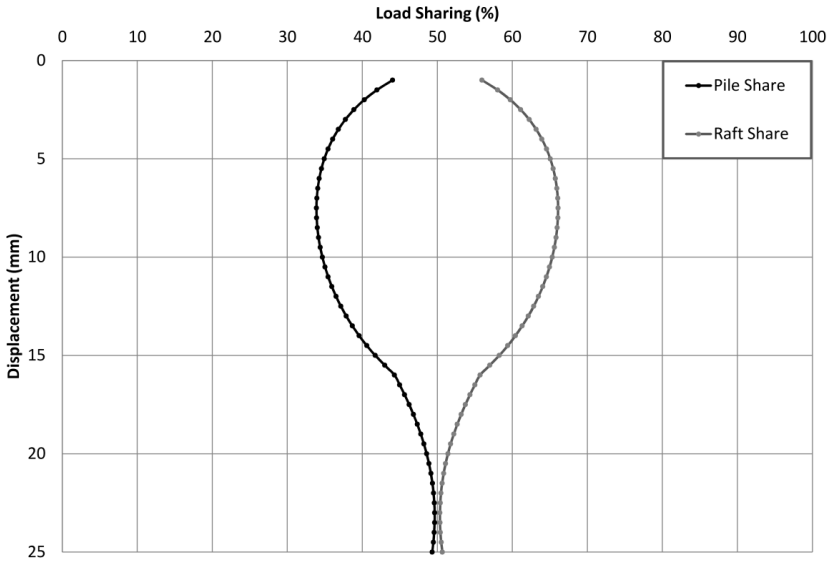

Figure 4-59 Test results on non-displacement piled raft NDPR45/60-40-10-R15 (load sharing-settlement curve)

4.4 Repeatability of Test Results

In this study, two tests were repeated to illustrate the repeatability of the test results. The tests on non-displacement pile in dense sand (NDP60-40-10) and non-displacement piled raft in medium density were repeated and compared with the original tests. The comparison shows acceptable consistency in the test results.

NDP60-40-10

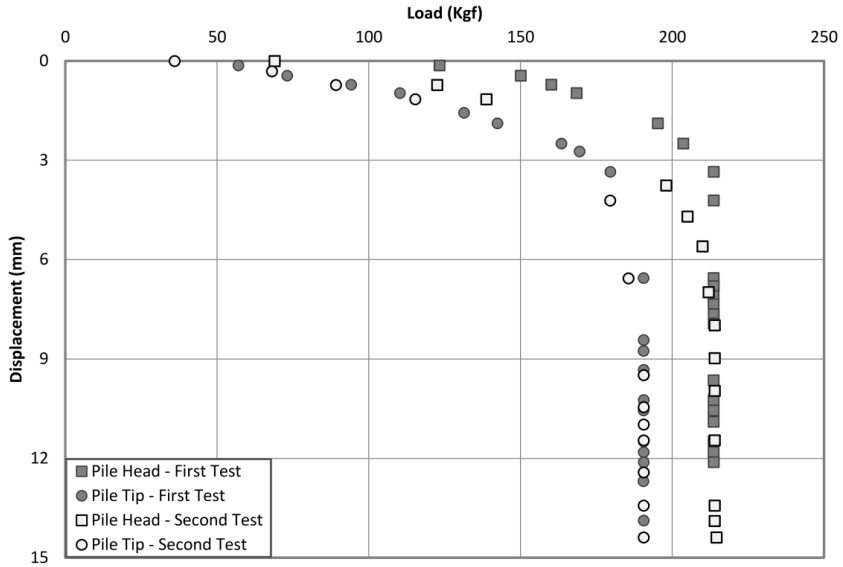

Figure 4-60 Results of the original and repeated test on non-displacement pile NDP60-40-10 (Load settlement curve)

NDPR45-40-10-R10

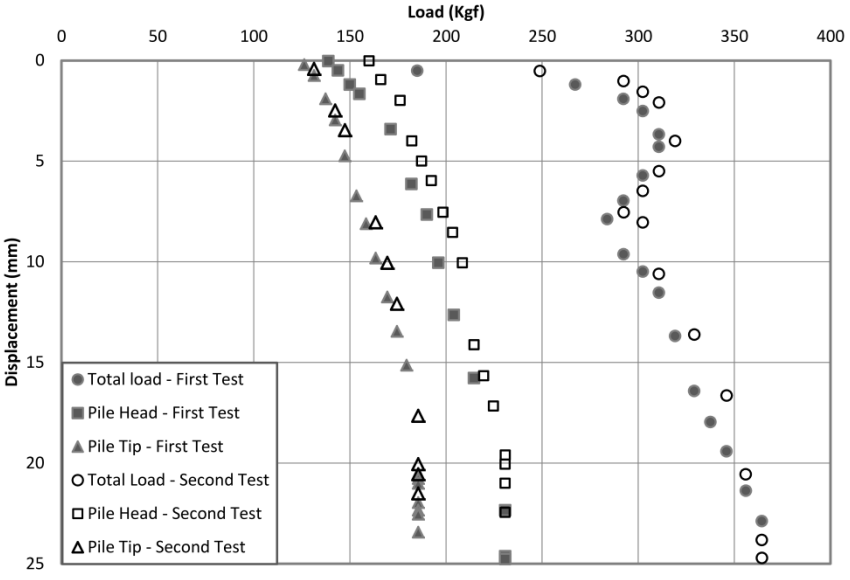

Figure 4-61 Results of the original and repeated test on non-displacement pile raft NDPR45-40-10-R10 (Load settlement curve)

4.5 Test Results

Tables 4-1, 4-2, and 4-3 present the ultimate capacity of shallow footing, single pile and piled raft footing in homogeneous sand, respectively. The ultimate loads of conducted tests in layered soil are reported in Tables 4-4 and 4-5. The recorded pile and raft share at $W/d_r = 1\%$ (W is settlement and d_r is the raft width) and at the failure point are reported in Table 4-6. Since the load sharing under the working load is the interest of this research, the average of pile and raft share from the beginning of the test until reaching the failure point is also included in this table. The calculated efficiency for the piled raft foundations are reported in Table 4-7.

Table 4-1 Analysis of shallow footing tests in homogeneous sand

Test name	Friction angle (ϕ)	Raft width, mm, (d_r)	Ultimate load, Kgf, (P_R)
R10-30-40-10	32.96	100	85
R10-45-40-10	34.93	100	139
R10-60-40-10	36.80	100	186
R15-30-40-10	32.96	150	242.4
R15-45-40-10	34.93	150	531.6
R15-60-40-10	36.80	150	768.1

Table 4-2 Analysis of pile load tests in homogeneous sand

Test name	Friction angle (ϕ)	Pile diameter, mm, (d_p)	Ultimate load, Kgf, (P_P)
DP30-40-10	32.96	28.6	96.4
DP45-40-10	34.93	28.6	171.1
DP60-40-10	36.80	28.6	215
NDP30-40-10	32.96	28.6	77.5
NDP45-40-10	34.93	28.6	141.7
NDP60-40-10	36.80	28.6	213.7

Table 4-3 Analysis of piled raft tests in homogeneous sand

Test name	Friction angle (ϕ)	Raft width, mm, (d_r)	Ultimate total load, Kgf, (P_{PR})	Ultimate pile resistance, Kgf, (P_P)
DPR30-40-10-R10	32.96	100	195.3	113.7
DPR45-40-10-R10	34.93	100	319.1	198.4
DPR60-40-10-R10	36.80	100	355	252
NDPR30-40-10-R10	32.96	100	187	105.6
NDPR45-40-10-R10	34.93	100	310.7	171.1
NDPR60-40-10-R10	36.80	100	426.1	235.8
NDPR30-40-10-R15	32.96	150	436.2	119.6
NDPR45-40-10-R15	34.93	150	764.1	219.6
NDPR60-40-10-R15	36.80	150	1065.6	316.7
NDPR30-70-30-R10	33.21	100	195.3	104
NDPR45-70-30-R10	37.59	100	319	166.1
NDPR60-70-30-R10	40.06	100	444.5	230

Table 4-4 Analysis of pile load test results in layered soil

Test name	Friction angle (ϕ)	Pile diameter, mm, (d_r)	Ultimate load, Kgf, (P_P)
NDP30/45-40-10	32.96	28.6	116.6
NDP30/60-40-10	34.93	28.6	148.33
NDP45/60-40-10	36.80	28.6	226.9

Table 4-5 Analysis of piled raft test results on layered sand

Test name	Raft width, mm, (d_r)	Ultimate load, Kgf, (P_{PR})	Ultimate pile resistance, Kgf, (P_P)
NDPR30/45-40-10-R10	100	230	122.6
NDPR30/60-40-10-R10	100	248	150
NDPR45/60-40-10-R10	100	364.3	223.7
NDPR30/45-40-10-R15	150	524.9	154.9
NDPR30/60-40-10-R15	150	540	203.4
NDPR45/60-40-10-R15	150	881.1	300.6

Table 4-6 Summary of test results on piled raft foundation

Test Name	Load sharing (%)					
	at W/d_r=1%		at failure point		Average in working load	
	Pile	Raft	Pile	Raft	Pile	Raft
DPR30-40-10-R10	78.4	21.6	63.9	36.1	69	31
DPR45-40-10-R10	80.4	19.6	70	30	73.7	26.3
DPR60-40-10-R10	83.5	16.5	75.2	24.8	78.5	21.5
NDPR30-40-10-R10	62.3	37.3	55.3	44.7	58.3	41.7
NDPR45-40-10-R10	61.3	38.7	54.8	45.2	56.6	43.4
NDPR60-40-10-R10	63	37	57.6	42.4	59.8	40.2
NDPR30-40-10-R15	42.1	57.9	31.3	68.7	34	66
NDPR45-40-10-R15	42	58	31.4	68.6	33.4	66.6
NDPR60-40-10-R15	42	58	31.4	68.6	33.4	66.6
NDPR30-70-30-R10	62.3	37.7	54.8	45.2	57.5	42.5
NDPR45-70-30-R10	61.5	38.5	56.5	43.5	57.5	42.5
NDPR60-70-30-R10	62	38	55.3	44.7	57.5	42.5
NDPR30/45-40-10-R10	77	23	64.4	35.6	67	33
NDPR30/60-40-10-R10	88	12	74.9	25.1	78	22
NDPR45/60-40-10-R10	71.3	28.7	63.7	36.3	65.6	34.4
NDPR30/45-40-10-R15	40.8	59.2	34.7	65.3	37	63
NDPR30/60-40-10-R15	44.7	55.3	40.4	59.6	41.4	58.6
NDPR45/60-40-10-R15	42	58	34.7	65.3	36.2	63.8

Table 4-7 The amount of group efficiency for piled raft foundation in different conditions

Test Name	Piled Raft Efficiency
DPR30-40-10-R10	2.03
DPR45-40-10-R10	1.86
DPR60-40-10-R10	1.65
NDPR30-40-10-R10	2.41
NDPR45-40-10-R10	2.19
NDPR60-40-10-R10	1.99
NDPR30-40-10-R15	5.63
NDPR45-40-10-R15	5.4
NDPR60-40-10-R15	4.99
NDPR30/45-40-10-R10	1.97
NDPR30/60-40-10-R10	1.67
NDPR45/60-40-10-R10	1.61
NDPR30/45-40-10-R15	4.5
NDPR30/60-40-10-R15	3.64
NDPR45/60-40-10-R15	3.88

Chapter 5

Analysis of Experimental Results

5.1 General

The presented experimental results in Chapter 4 clearly illustrate the nonlinear variation of load sharing versus settlement, which is in line with the observations of Lee et al. (2014)'s. In this chapter, the effect of other parameters such as soil relative density (D_r), raft width ratio (d_r/d_p), and pile installation method on load sharing and piled raft efficiency is investigated through a comprehensive parametric study. Since the mechanism of load sharing under working loads is of interest in engineering practice, the load sharing results before reaching failure are further studied in the following sections.

5.2 Effect of relative density

Conducting the experimental tests in different soil densities provides an opportunity to investigate the effect of relative density on the load sharing mechanism and ultimate bearing capacity of piled raft footings. The load-settlement curves of non-displacement piled rafts at different densities are compared in Figures 5-1 and 5-2. As expected, augmenting the soil relative density increases the ultimate bearing capacity. The experimental test results also illustrate that the non-displacement piled raft in loose sand experienced local shear failure; however, a general shear failure was observed for piled raft foundations in medium and dense sand. Under such failure, the soil experiences an extensive displacement once the foundation reaches the ultimate bearing capacity. Subsequently, the failure surface extends to the ground surface and the heave is observed around the raft. This phenomenon is observed through the

bended curves in Figures 5-1 and 5-2. After the sudden failure, the raft does not provide any more bearing capacity and the pile takes any additional load on the foundation. This fact could be observed in Figure 4-36 which shows the load-settlement curves of a non-displacement piled raft in dense sand.

The effect of relative density on group efficiency of the piled raft foundation is shown in Figure 5-3: the group efficiency increases by increasing the raft width ratio and decreases at higher densities. The piled raft efficiency was defined as the ratio of ultimate bearing capacity of the piled raft (P_{PR}) over the single pile's ultimate capacity (P_p). The 100x100mm and 150x150mm rafts represent the piled raft with $3.5d_p$ and $5.2d_p$ pile spacing, respectively.

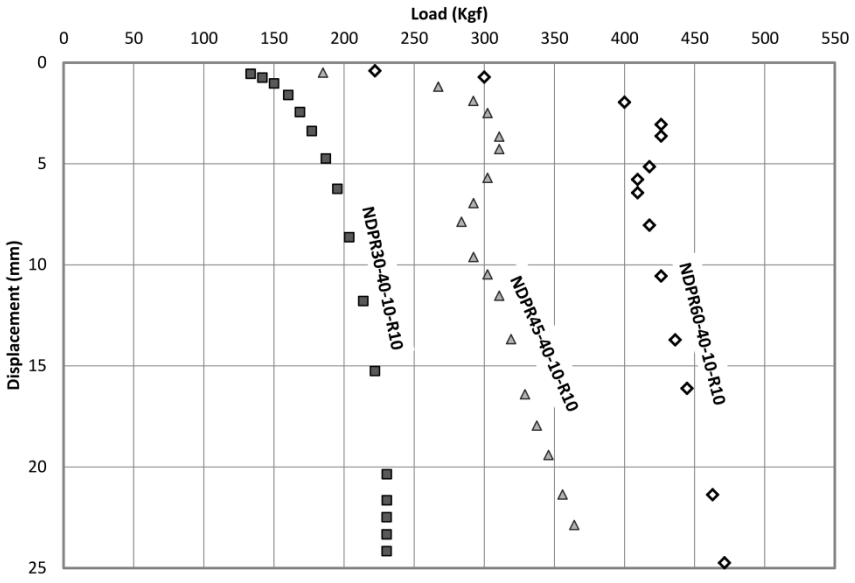

Figure 5-1 Load-settlement curves of non-displacement piled raft with 100x100mm raft at different densities

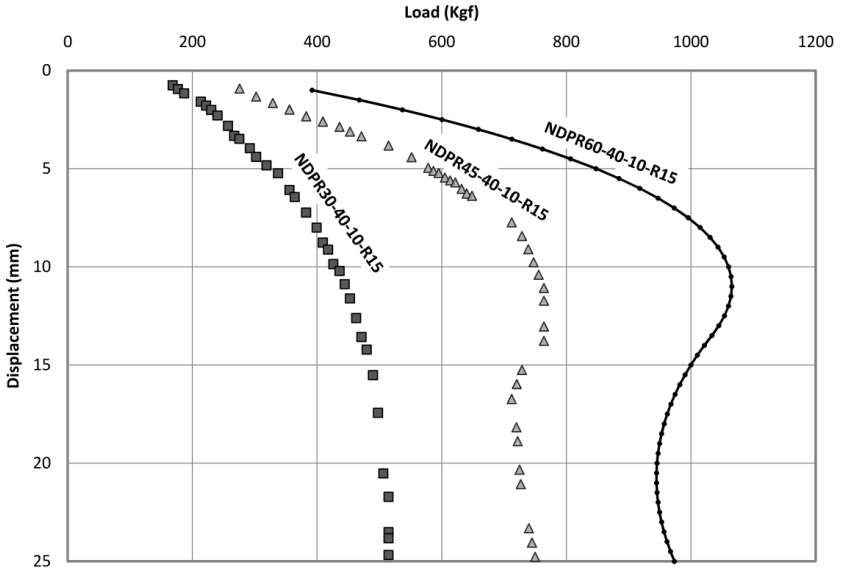

Figure 5-2 Load-settlement curves of non-displacement piled raft with 150x150mm raft at different densities

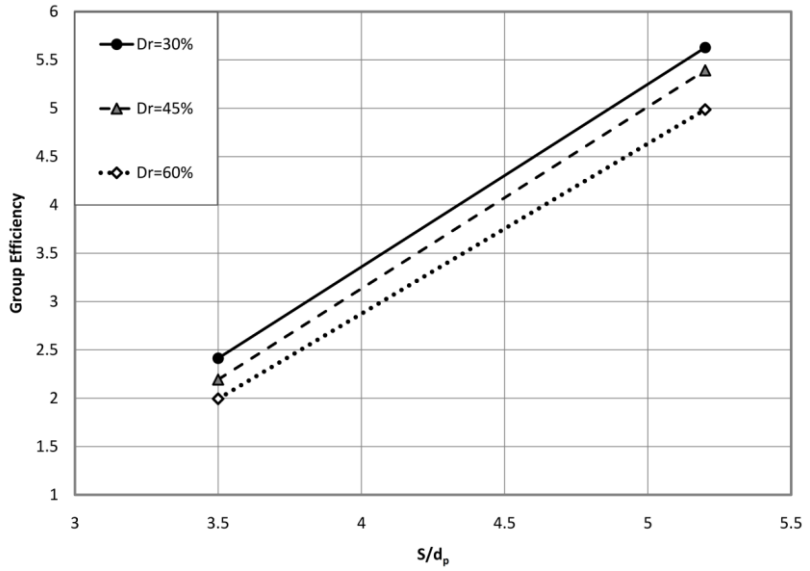

Figure 5-3 Group efficiency of non-displacement piled raft versus S/d_p ratio at different soil relative densities

The effect of settlement ratio (displacement over raft width) on load sharing of non-displacement piled raft is shown in Figures 5-4 and 5-5. This comparison reveals that the relative density changes do not have a significant impact on the load sharing mechanism of non-displacement piled raft.

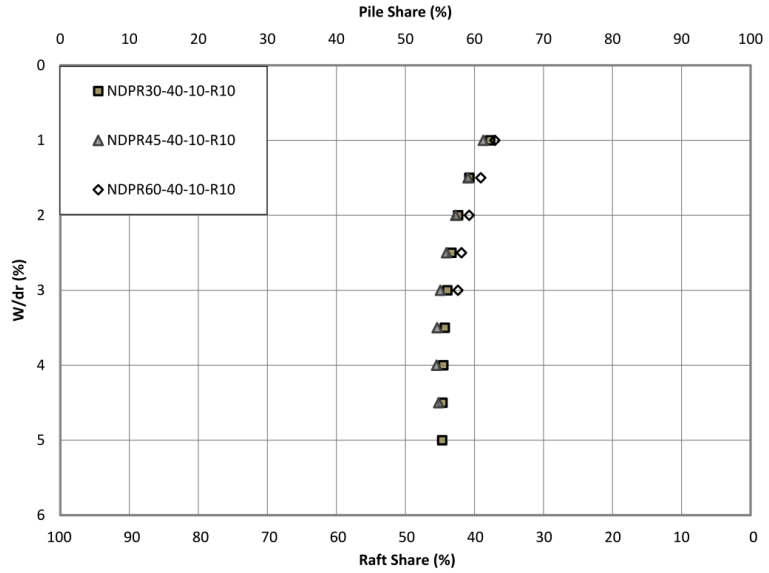

Figure 5-4 Load sharing versus settlement ratio for a non-displacement piled raft with 100x100mm raft at different densities

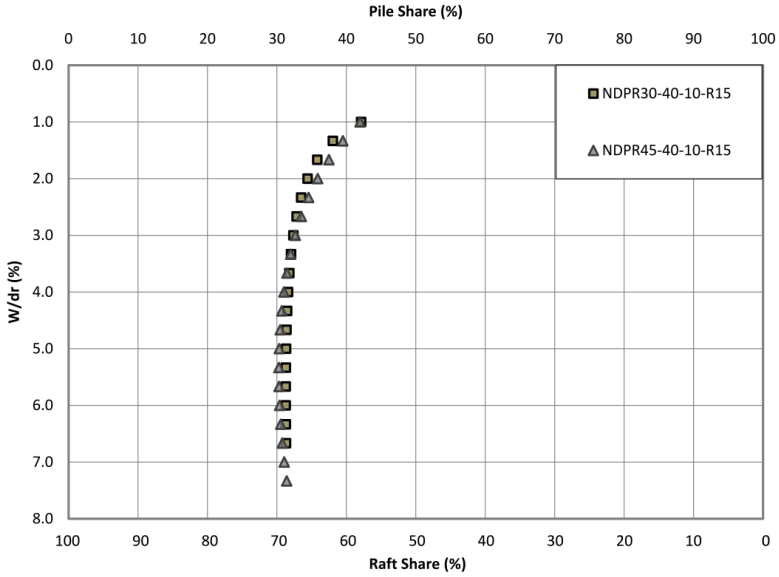

Figure 5-5 Load sharing versus settlement ratio for non-displacement piled raft with 150x150mm raft in different densities

The same charts were developed by analyzing the results of experimental tests on displacement piled raft foundation (Figures 5-6 and 5-7). It is observed in Figure 5-7 that the load sharing mechanism of the displacement piled raft is diverse for different densities: the pile share increases as a function of soil relative density. This observation could be explained by the effect of pile driving on the OCR of sandy soil which increases the pile sharing. This effect is more

significant when there is a greater interlocking between the particles; in other words, in denser sands.

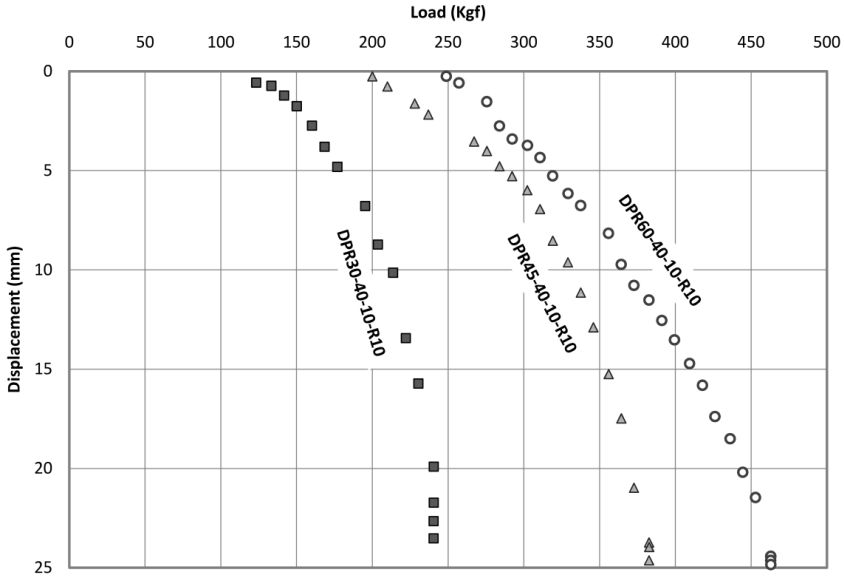

Figure 5-6 Load-settlement curves of displacement piled raft with 100x100mm raft in different densities

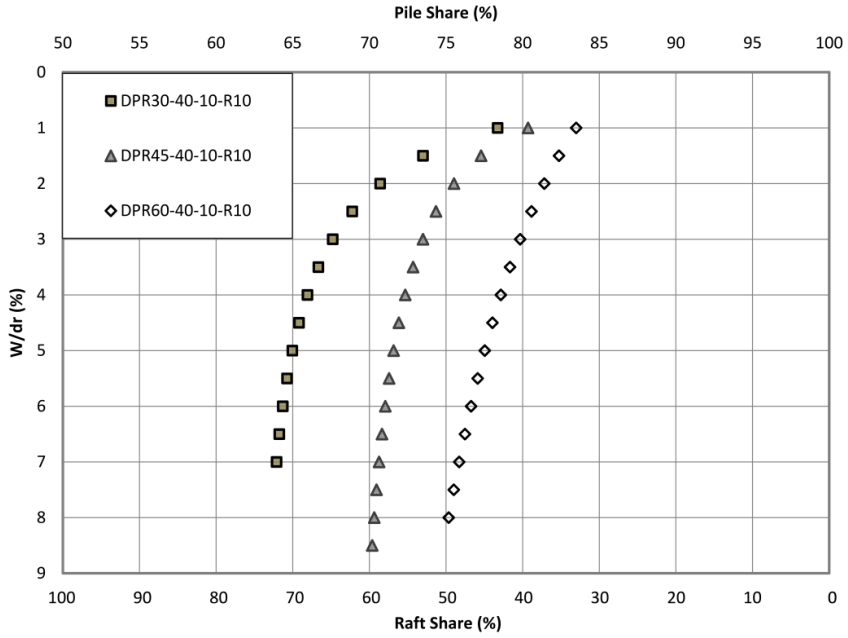

Figure 5-7 Load sharing versus settlement ratio for displacement piled raft with 100x100mm raft in different densities

5.3 Effect of particle size distribution

The effect of particle size distribution on ultimate bearing capacity of non-displacement piled raft was studied by comparing the test results in 40-10 Silica sand to those in 70-30 Silica sand (Figure 5-8). This comparison reveals that the variation of particle size distribution does not make any changes in the load-settlement curves of a non-displacement piled raft at different densities. As mentioned previously in Chapter 3, the 40-10 Silica sand has coarser particles than 70-30 Silica sand.

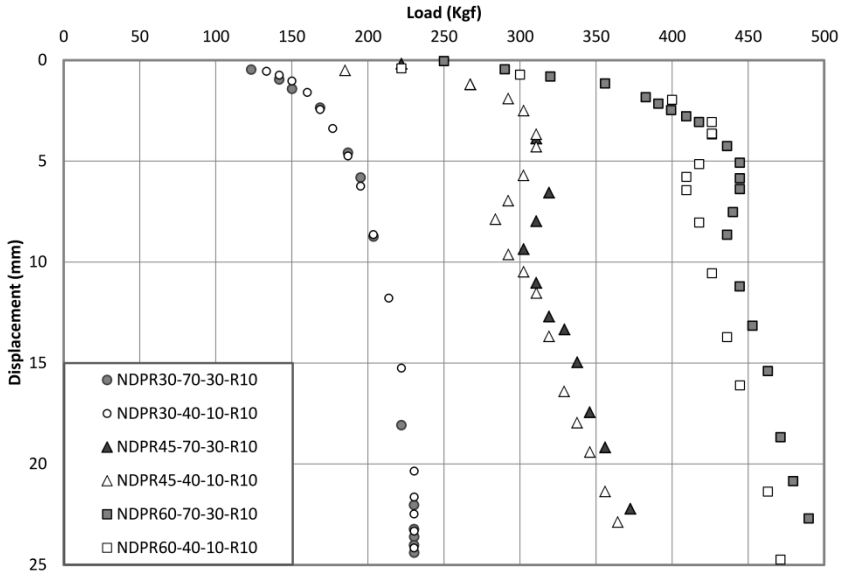

Figure 5-8 Load-settlement curves of non-displacement piled raft with 100x100mm raft in 40-10 and 70-30 Silica sand

Figure 5-9 illustrates the variation of load-sharing at different stages of settlement ratio for non-displacement piled raft in 40-10 and 70-30 Silica sands. It is observed that piled raft load sharing is independent of particle size distribution.

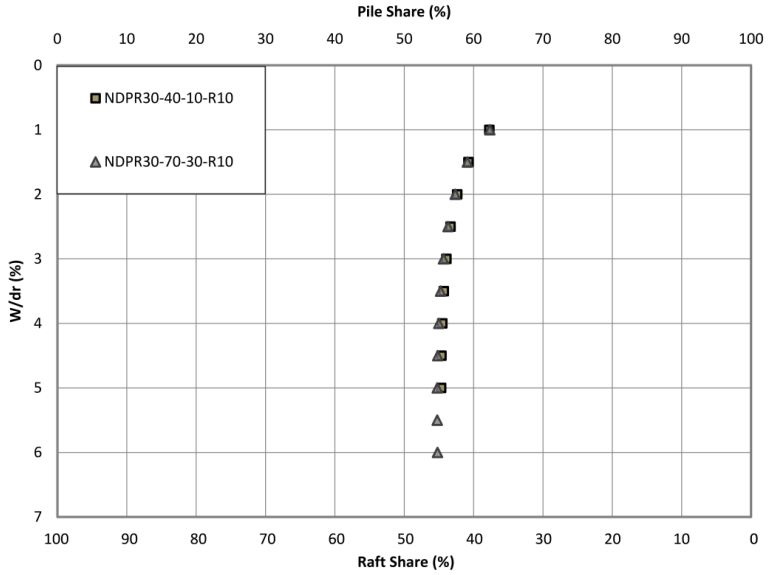

Figure 5-9 Load sharing versus settlement ratio for non-displacement piled raft with 100x100mm raft in relative density of 30%

5.4 Effect of pile spacing

The raft width in a single piled raft unit specifies the pile spacing in a pile group which is formed by placing the single piled raft units adjacent to each other. Therefore, the 100x100mm and 150x150mm rafts simulate the piled raft with pile spacing ratio (S/d_p) of 3.5 and 5.2, respectively. The fact that the bearing capacity of piled raft would increase by enlarging the pile spacing is illustrated in Figures 5-10 and 5-11.

Sinha (2013) and Yamashita et al. (1994) mentioned that the raft share increases by increasing the pile spacing and reaches a constant value when pile spacing is more than $6d_p$. The experimental tests also affirm the aforementioned correlation (Figure 5-12). The same behavior was observed on the conducted tests in layered soil (Figure 5-13). It could be concluded that the pile spacing in a pile group or the raft width in a single piled raft unit is the dominant factor in the load sharing mechanism.

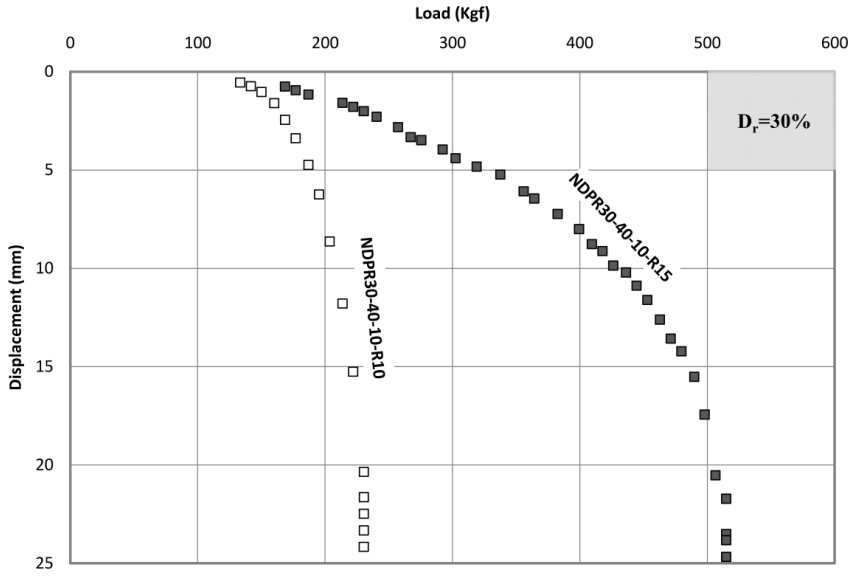

Figure 5-10 Load-settlement curve of non-displacement piled raft with 100x100mm raft and 150x150mm raft (D_r=30%)

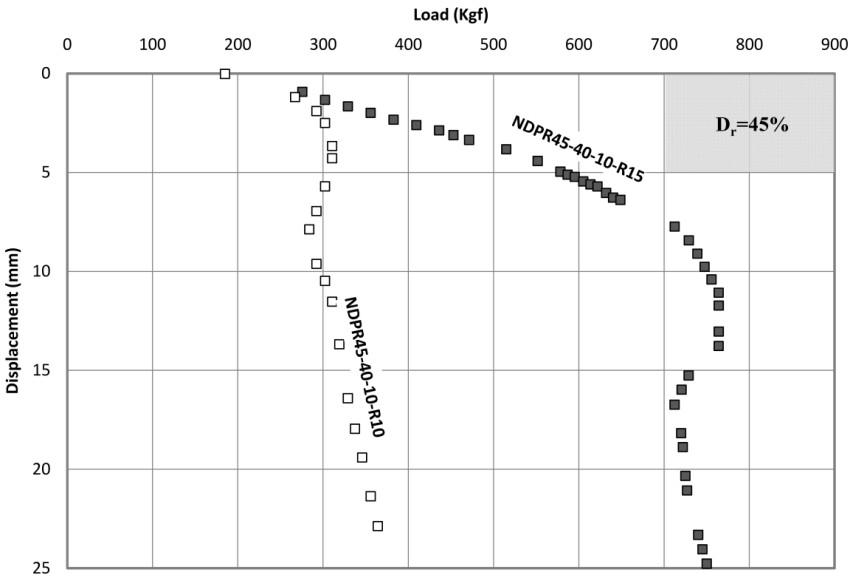

Figure 5-11 Load-settlement curve of non-displacement piled raft with 100x100mm raft and 150x150mm raft (D_r=45%)

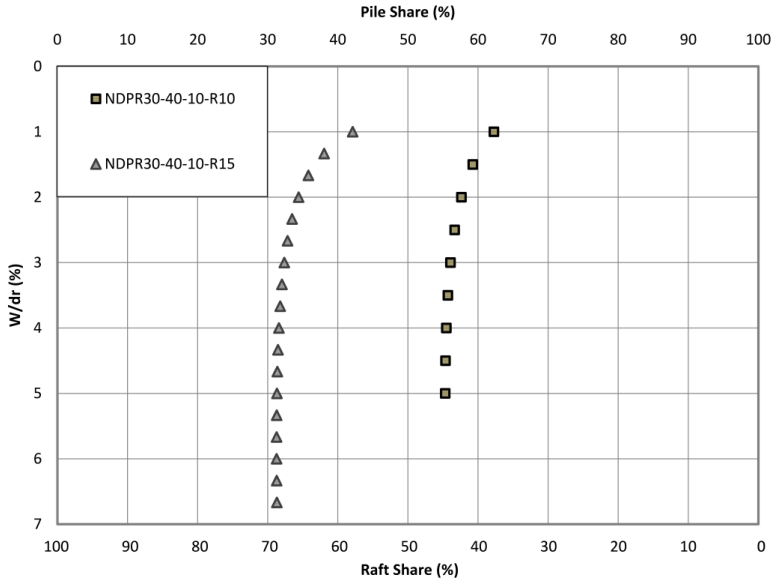

Figure 5-12 Load sharing versus settlement ratio for non-displacement piled raft with 100x100mm and 150x150mm raft in relative density of 30%

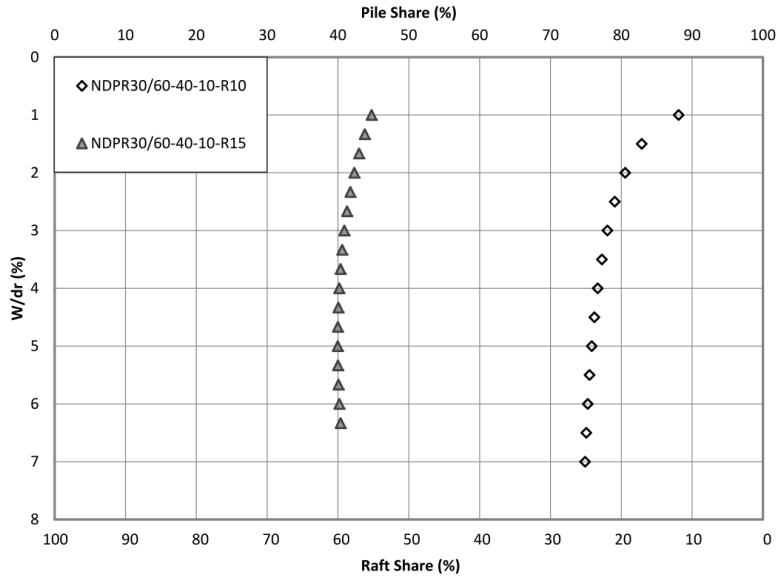

Figure 5-13 Load sharing versus settlement ratio (W/d_r>1%) for non-displacement piled raft with 100x100mm raft and 150x150mm raft in layered sand (loose on dense)

5.5 Effect of pile installation method

The experimental results on displacement and non-displacement piled raft reveals that the ultimate capacity of displacement piled raft was mobilized at higher load and larger settlement in comparison with non-displacement piled raft in loose and medium sand (Figures 5-14 and 5-15).

This observation is clearly the consequence of pile driving process, which increases the soil densification and the OCR of the sand. However, by driving the pile in dense sand the soil particles around the pile shaft are dragged down and a heave was observed on the ground surface (Figure 5-17). Rearrangement of soil particles below the raft cause a reduction in bearing capacity of displacement piled raft in comparison with the non-displacement piled raft in dense sand (Figure 5-16). The pile driving also changes the failure mechanism of the piled raft in medium and dense sand. Unlike the non-displacement piled raft, the displacement piled rafts did not experience general shear failure (Figure 5-15 and 5-16) simply because the failure surfaces were not extended to the shallow depths due to the soil densification around the pile caused by the driving process.

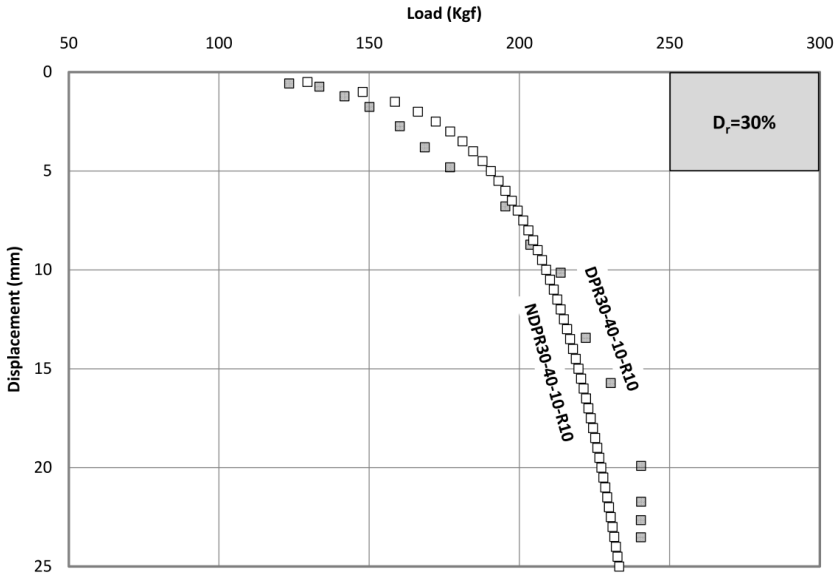

Figure 5-14 Load-settlement curves of displacement and non-displacement piled raft footing with 100x100mm raft in relative density of 30%

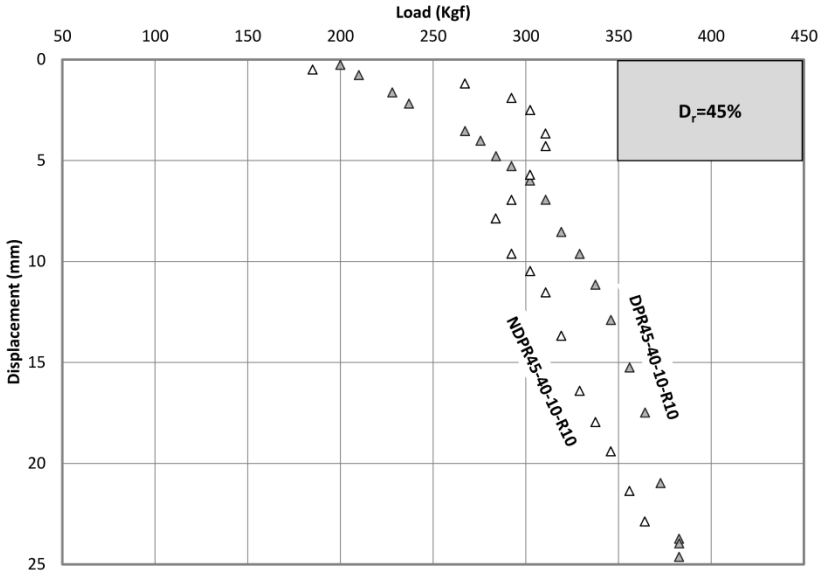

Figure 5-15 Load-settlement curves of displacement and non-displacement piled raft footing with 100x100mm raft in relative density of 45%

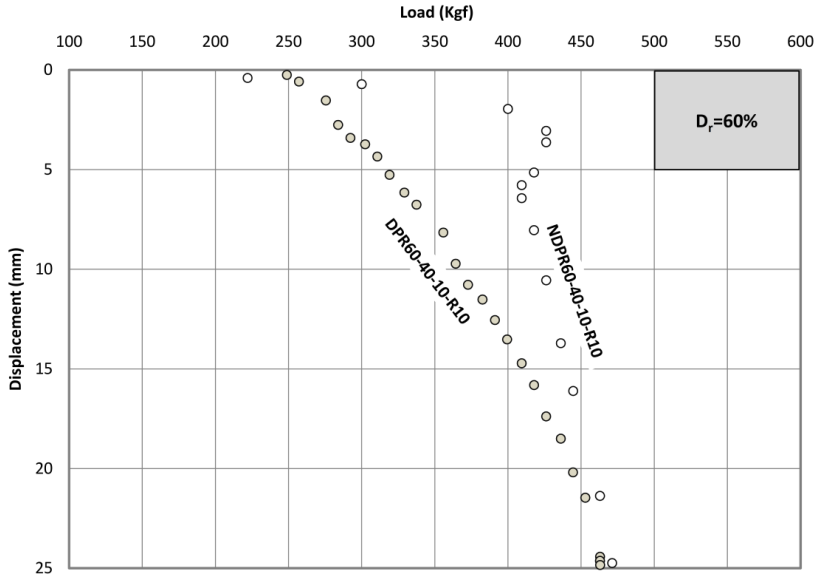

Figure 5-16 Load-settlement curves of displacement and non-displacement piled raft footing with 100x100mm raft in relative density of 60%

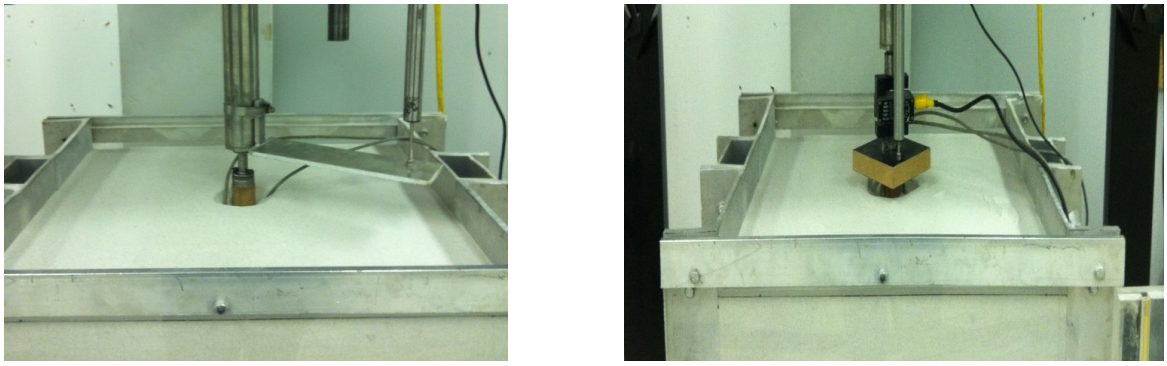

Figure 5-17 The heave around the driven pile in dense sand

The group efficiency of displacement and non-displacement piled rafts are compared in Figure 5-18. It is observed that the group efficiency is more than 1 for both cases at different densities; however, the non-displacement piled raft provides higher efficiencies. The difference between the efficiency of displacement and non-displacement piled raft originates from the noticeable difference between the ultimate capacities of driven and bored piles. The capacity of driven piles is much greater than non-displacement pile and the ultimate capacity of DPR and NDPR are close to each other; therefore, the estimated group efficiency for a displacement piled raft is less than non-displacement piled raft. Analyzing the experimental results demonstrates that the group efficiency of a DPR is 15% less than that of a NDPR.

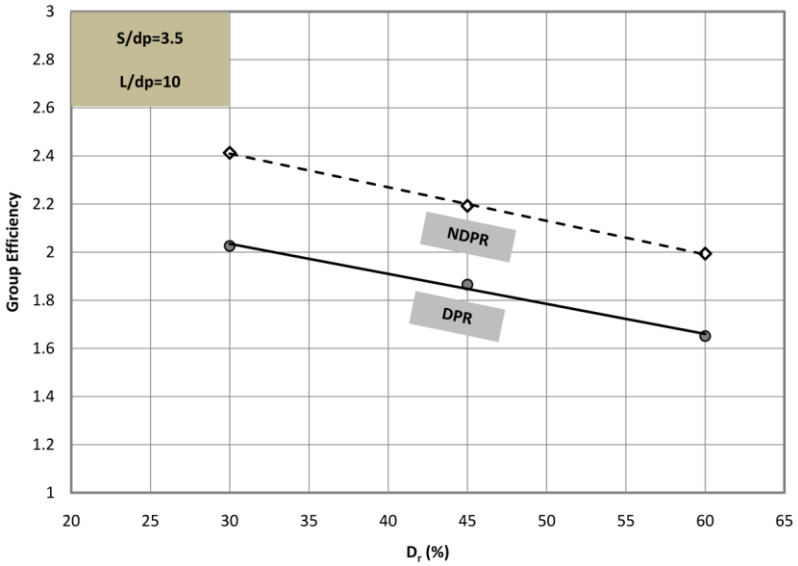

Figure 5-18 Group efficiency of displacement and non-displacement piled raft versus relative density

Figure 5-19 illustrates the difference between the load sharing of displacement and non-displacement piled rafts in loose sand. The amount of the pile share in displacement piled rafts is greater than that of non-displacement piled rafts due to the difference in pile installation techniques. The pile driving process made the sand around the pile over-consolidated which ultimately increased the pile sharing. The experimental test results show that the raft share of displacement piled raft in loose sand is approximately 75 percent of the raft share in non-displacement piled raft. Table 5-1 shows the amount of reduction in raft share of displacement piled raft in respect to non-displacement piled raft in different densities.

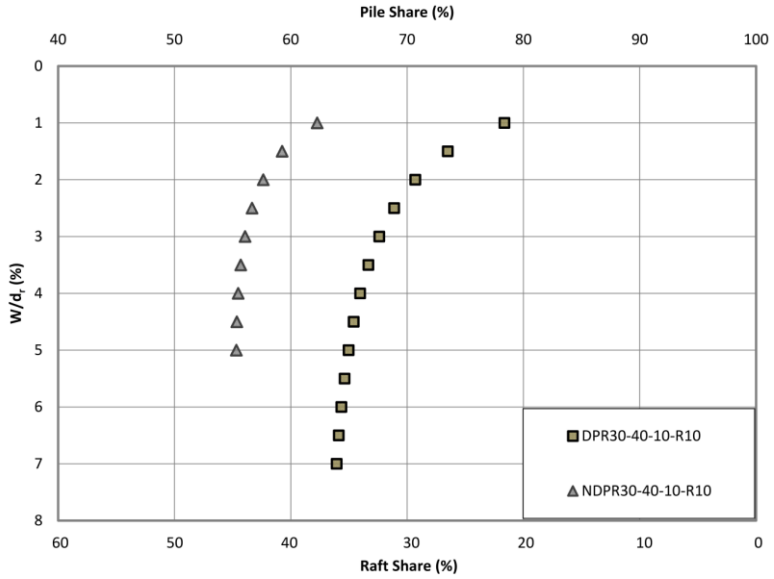

Figure 5-19 Load sharing versus settlement ratio for displacement and non-displacement piled raft with 100x100mm raft in relative density of 30%

Table 5-1 The ratio of raft share in displacement piled raft over non-displacement piled raft in different densities

D_r (%)	X_{DPR}/X_{NDPR} (%)
30	75
45	60
60	47

5.6 Piled raft in layered soil

The load-settlement curves of non-displacement piled raft in homogeneous and layered sands are compared in Figures 5-20 and 5-21. These figures show that increasing the soil density at the pile tip increases the ultimate bearing capacity but does not create any changes in the failure mechanism. It is illustrated in Figures 5-22 and 5-23 that increasing the soil density at the pile tip in layered soil decreases the group efficiency.

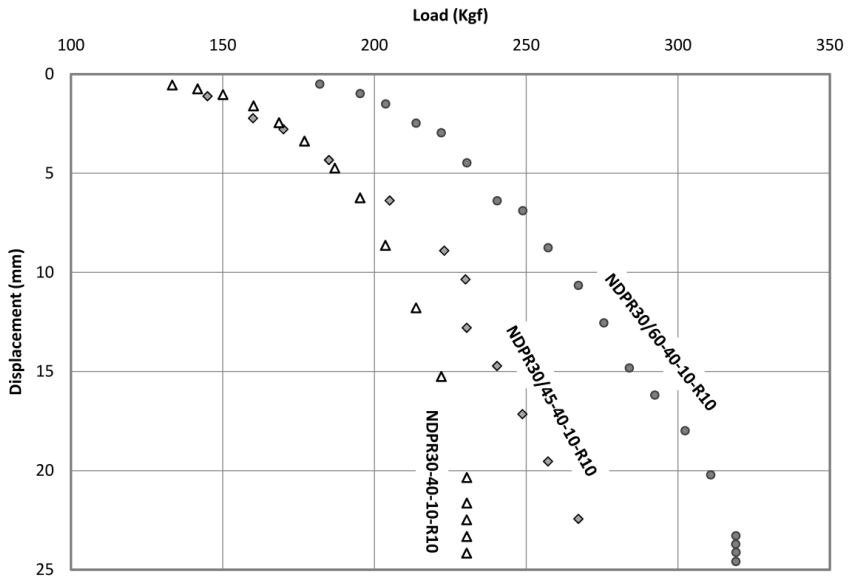

Figure 5-20 The load-settlement curves of piled raft with 100x100mm raft in homogeneous (D_r=30%) and layered sand (loose on medium and loose on dense)

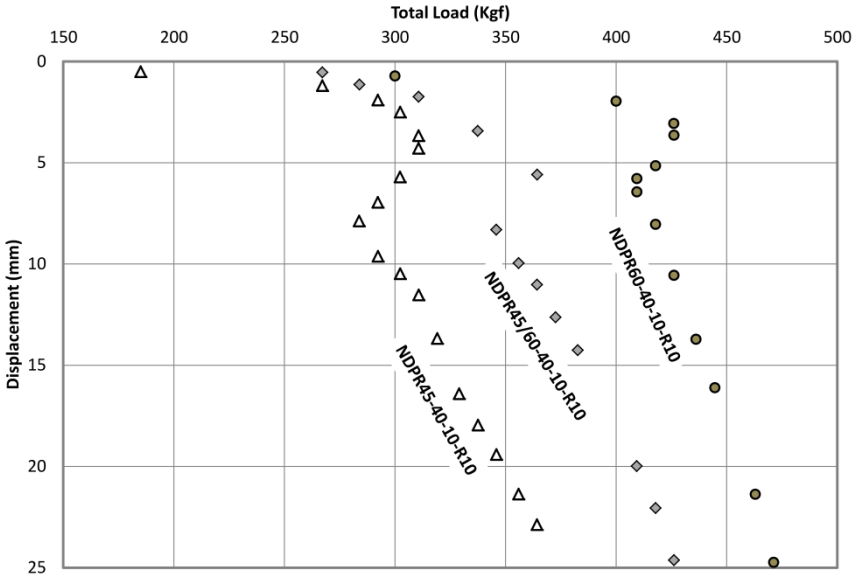

Figure 5-21 The load-settlement curves of piled raft with 100x100mm raft in homogeneous (D_r=45 and 60%) and layered sand (medium on dense)

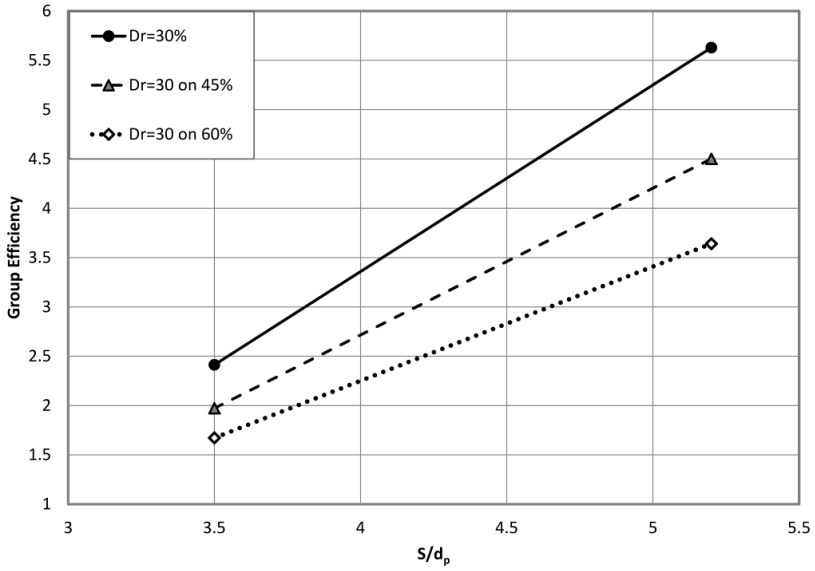

Figure 5-22 Group efficiency versus pile spacing ratio for non-displacement piled raft in homogeneous (D_r=30%) and layered sand (loose on medium and loose on dense)

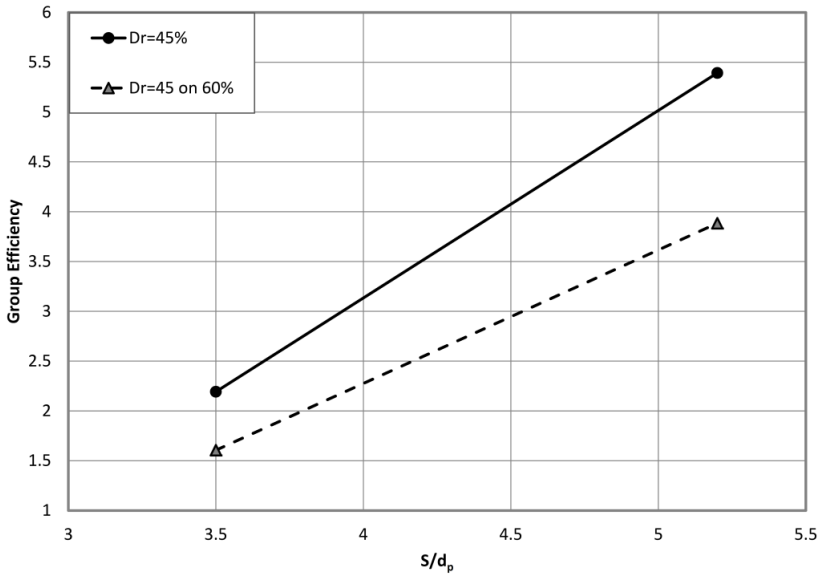

Figure 5-23 Group efficiency versus pile spacing ratio for non-displacement piled raft in homogeneous (D_r=45%) and layered sand (medium on dense)

The presence of denser layer at pile tip also changes the load sharing mechanism of piled raft footing. Since the pile tip sits on a denser layer in comparison with the soil below the raft, the pile behaves as an end-bearing pile and consequently the pile share increases. The load sharing mechanism of NDPR30/45-40-10-R10 and NDPR30/60-40-10-R10 are shown in Figure 5-24 and are compared with the non-displacement piled raft in loose condition. A direct correlation

between the soil density at pile tip and the pile share is clearly observed in Figure 5-24. The same behavior was observed by comparing the NDPR45/60-40-10-R10 and NDPR45-40-10-R10 (Figure 5-25). The conducted experimental tests on non-displacement piled raft with 150x150mm raft also show similar load sharing trend.

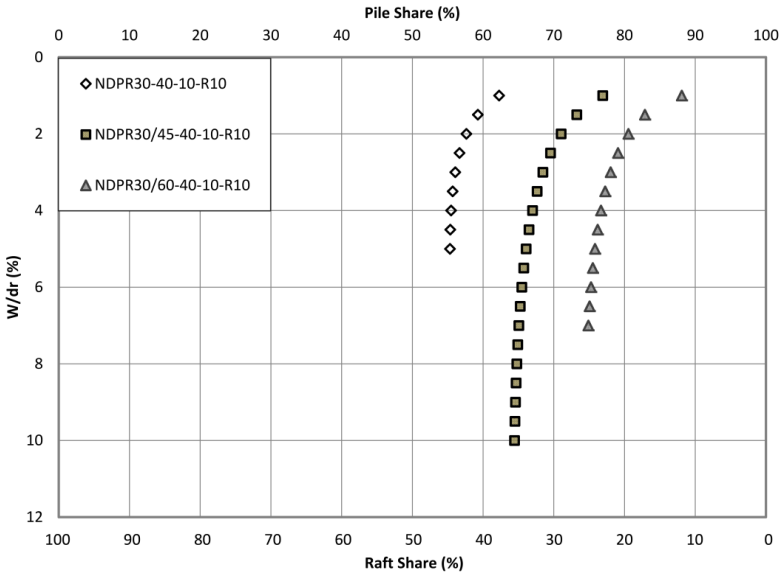

Figure 5-24 Load sharing versus settlement ratio (W/d_r>1%) for non-displacement piled raft with 100x100mm raft in homogeneous (D_r=30%) and layered sand (loose on medium and loose on dense)

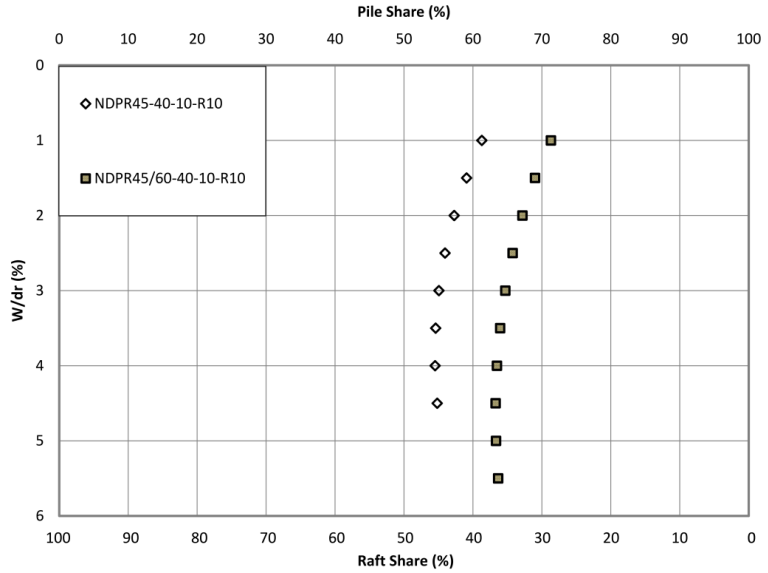

Figure 5-25 Load sharing versus settlement ratio (W/d_r>1%) for non-displacement piled raft with 100x100mm raft in homogeneous (Dr=45%) and layered sand (medium on dense)

5.7 Comparison between the experimental results and the studies in the literature

In this section, the validity of our experimental results is confirmed through comparison with related studies in the literature.

Phuong (1993) and Lee and Chung (2005) observed that the variation of raft share-settlement in a piled raft foundation closely follows the load-settlement curve of a shallow footing with the same geometry. This observation is confirmed by comparing our measured raft share for non-displacement piled raft in different settlement with the load-settlement curve of shallow footing (Figures 5-26 and 5-27).

Lee and Chung (2005) studied the effect of pile-soil-raft interaction on the pile behavior by running tests on displacement piled raft and pile group in dense sand. The authors concluded that the pile-soil-raft interaction generally increases the pile shaft friction. The results of the experimental tests in this study also show a significant raise in frictional resistance of pile in a piled raft system in comparison with single pile (Figure 5-28).

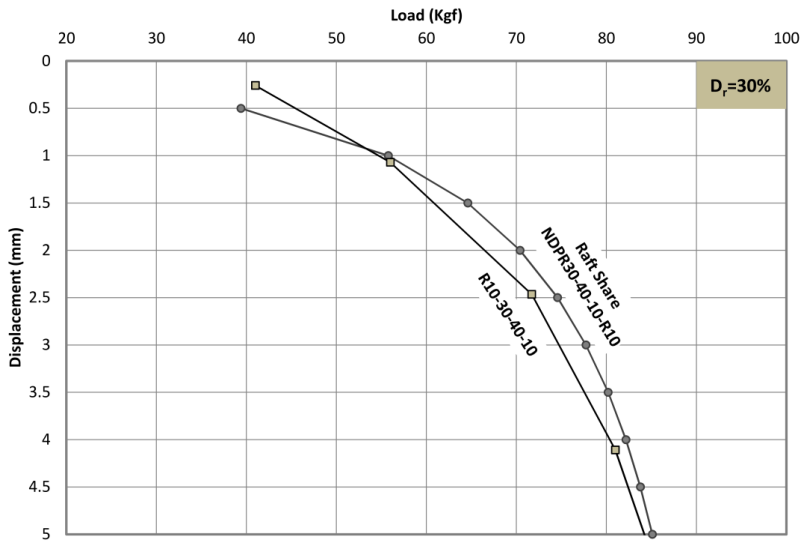

Figure 5-26 Load-settlement curves of raft share in NDPR30-40-10-R10 and shallow footing (R10-30-40-10)

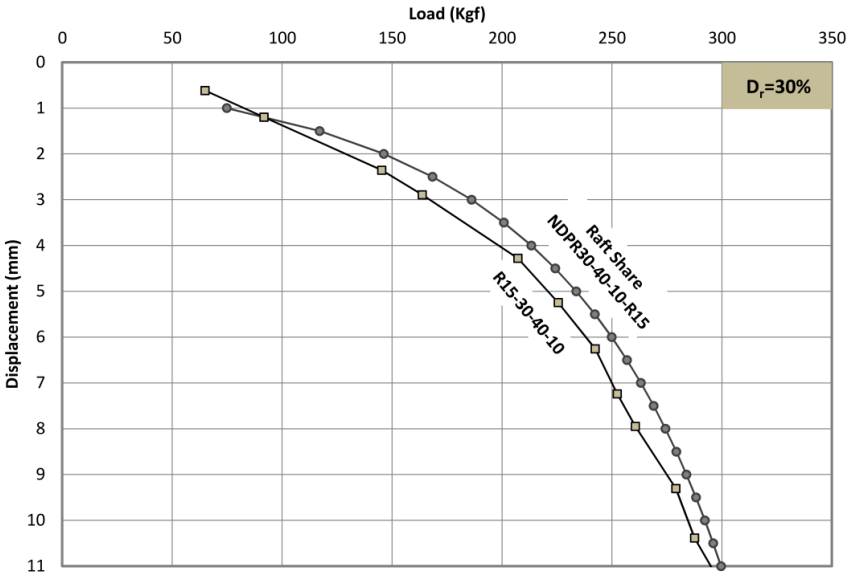

Figure 5-27 Load-settlement curves of raft share in NDPR30-40-10-R15 and shallow footing (R15-30-40-10)

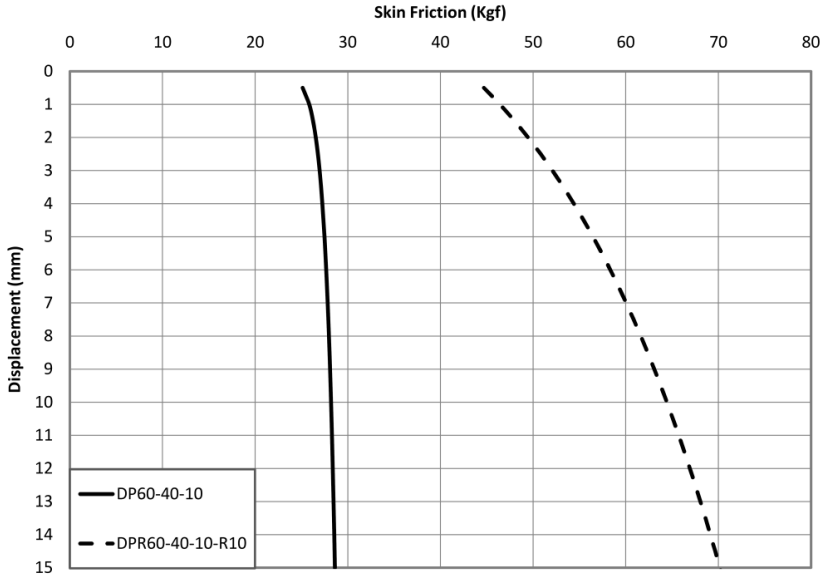

Figure 5-28 The skin friction of displacement pile versus settlement for single pile and displacement piled raft in relative density of 60%

Akinmusuru (1980) stated that the bearing capacity of piled raft in sand is more than the summation of pile group and shallow footing bearing capacities. Table 5-2 presents our measured ultimate capacity for non-displacement piled raft and compares these values with the

ultimate capacity of single pile and shallow footing. The results of this comparison is aligned with Akinmusuru's observation.

Table 5-2 Comparing the summation of recorded bearing capacity for single non-displacement pile and shallow footing with non-displacement piled raft bearing capacity

D_r	$Q_{u(NDP)}$	$Q_{u(R10)}$	$Q_{u(R15)}$	$Q_{u(NDP)}+Q_{u(R10)}$	$Q_{u(NDPR10)}$	$Q_{u(NDP)}+Q_{u(R15)}$	$Q_{u(NDPR15)}$
30	77.5	85	242.4	162.5	187	319.9	436.2
45	141.7	139	531.6	280.7	310.7	673.3	764.1
60	213.7	186	768.1	399.7	426.1	981.8	1065.6

Akinmusuru proposed Eq. 2.1 to determine the bearing capacity of piled raft foundation in sand and stated that the pile sharing factor (α′) is influenced by center-to-center pile spacing, soil condition and pile installation method. Our experimental results on non-displacement piled raft were applied to Eq. 2.1 to calculate α′ at different soil densities and pile spacing ratio. The results of this analysis is illustrated in Figure 5-29 and confirms that α′ is a function of these parameters. It was further confirmed that the calculated α′ for displacement piled raft foundations is less than non-displacement ones.

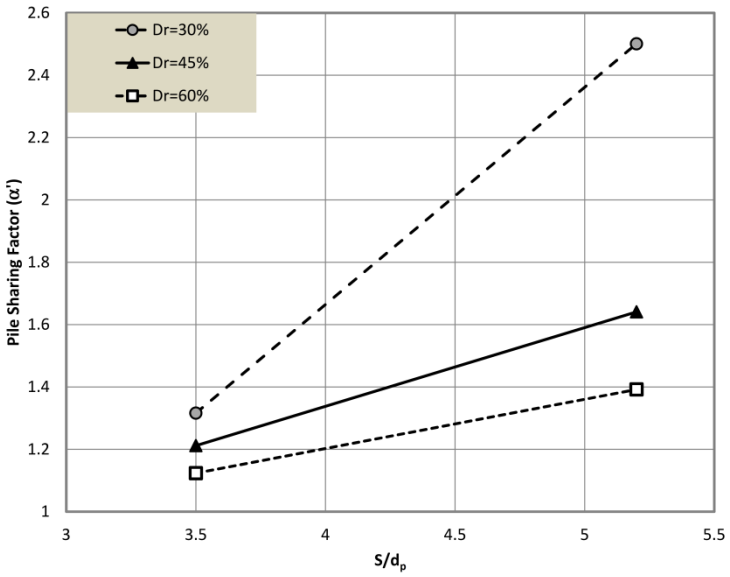

Figure 5-29 Pile sharing factor (proposed by Akinmusuru) versus pile spacing: calculated by applying the experimental results of this study

The 3D numerical analyses conducted by Sinha (2013) revealed that the raft share increases linearly by increasing the pile spacing and reaches to a constant value for S/d_p ratios more than six. The estimated load sharing of the above numerical study for a 16x16 piled raft with $4d_p$ and $6d_p$ pile spacing under 0.5MPa distributed stress is illustrated in Figure 5-30. This figure compares Sinha's results with our measured load sharing at failure point for non-displacement piled raft where a similar trend confirms the validity of our work. The gap between the two curves are expected due to the dissimilarity of the soil condition.

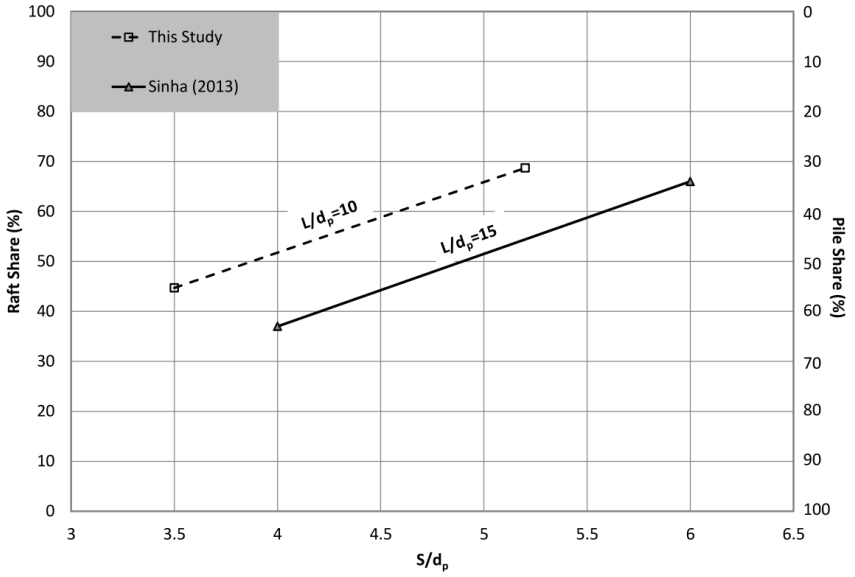

Figure 5-30 Load sharing versus pile spacing for non-displacement piled raft in loose soil

Omeman (2012) studied the effect of sand friction angle on load sharing variation of non-displacement piled raft foundation while the L/d_p and S/d_p ratios were kept constant. The 2D numerical analyses revealed that the soil friction angle has inconsiderable effect on load sharing of piled raft foundation. Our experimental results in this study confirm this observation as illustrated in Figure 5-31.

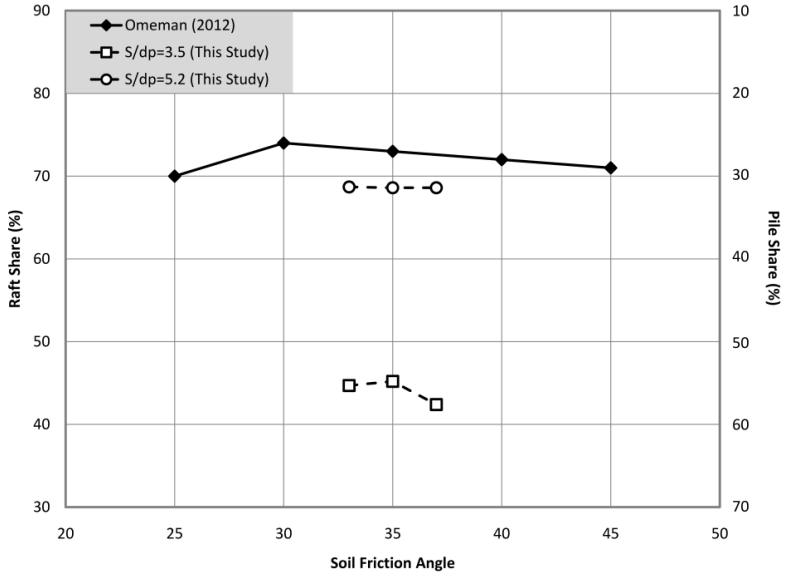

Figure 5-31 Load sharing versus soil friction angle in homogeneous sand

5.8 Comparison between Randolph's simplified method and experimental results

In this subsection, the experimental test results on shallow footing, non-displacement pile and non-displacement piled raft are applied to determine the piled raft interaction factor (α_{cp}) which was proposed by Randolph (1983). In order to be consistent with Randolph estimation method, the stiffness of shallow footing (100x100mm) and non-displacement pile, along with load sharing of non-displacement piled raft were determined based on our experimental results at the piled raft failure point. The above measured values were applied to Eq. 2.4 to back calculate the interaction factor (α_{rp}). The calculated interaction factors in different densities are presented in Table 5-3 which shows a fairly close agreement with Clancy and Randolph (1996)'s results.

Table 5-3 Comparison between estimated interaction factor by back calculation at failure point and proposed value of interaction factor for S/d_p=3.5

Relative Density (%)	Back calculated value of α_{rp} in this study	Suggested value for α_{rp} by Clancy and Randolph (1996)
30	0.62	0.645
45	0.62	0.645
60	0.64	0.645

The experimental tests are widely used in academia and industry as a means of understanding the effect of various parameters on foundation behavior. This study achieved this goal by conducting a series of experimental tests on single piled raft. The results were applied to calibrate the numerical model in order to extend the scope of this study to multi piled raft configurations.

Chapter 6

Numerical Analyses

6.1 General

The aim of this chapter is to investigate the effect of number of piles on the non-displacement piled raft load-sharing. To this end, a series of three dimensional numerical analyses were performed using the ABAQUS 6.11 finite element software. The numerical model was calibrated with conducted experimental test on a non-displacement piled raft. The validated model was employed to estimate the load sharing of pile raft with two different configurations (2x2 and 3x3) in homogenous sand. The pile spacing and pile length were kept constant through the numerical analyses. More information about the numerical models is provided in the Table 6-1.

Table 6-1 Numerical analyses program

Name	pile Number	Raft size (mm^3)	Pile size (mm^3)	Soil block size (mm^3)	Soil density (%)	Pile Spacing (S/d_p)
1x1 piled raft	1	100x100x25.4	22.4x22.4x290	500x500x600	45	3.5*
2x2 piled raft	4	200x200x25.4	22.4x22.4x290	1000x1000x600	45	3.5
3x3 piled raft	9	300x300x25.4	22.4x22.4x290	1500x1500x600	45	3.5

* the ratio of d_r over d_p for 1x1 piled raft

6.2 Finite element Model

6.2.1 Defining the geometry

As the first step of the modeling process, the geometry of the piled raft and the soil block were defined. The piled raft was established by attaching the square pile(s) to the bottom surface of the raft and the soil was created as a block with the sufficient number of holes to a depth of 290mm. The defined parts were assembled by situating the pile group in the pre-made holes in the soil block.

6.2.2 Element type

Different element types are available in ABAQUS software (i.e., beam, shell, and solid elements) which are implemented based on the nature of projects. Solid elements were applied in this study to model the piled raft footing as well as the sandy soil. Assigning the same element to the piled raft and the soil would facilitate the interaction modeling process.

The software provides different types of solid elements (Tetrahedral, triangular wedge and hexahedra element) which are schematically shown in Figure 6-1. It is a common practice to apply the hexahedra element to execute three-dimensional analyses as it provides accurate results with minimum computational cost (Sinha 2013). The hexahedra element has 6 faces and could be used with 8 or 20 nodes. The number of nodes in hexahedra element is selected based on the type of project; for instance, the software's manual recommends the hexahedra element with 8 nodes for the problems with complicated interactions and the elements with 20 nodes for the bending dominated problems. In the light of these recommendations, the hexahedra element with 8 nodes was used in this study.

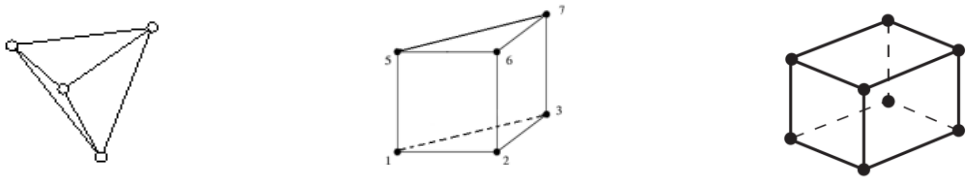

(a) (b) (c)

Figure 6-1 Different types of solid elements: (a) Tetrahedral, (b) Triangular wedge, and (c) Hexahedra

6.2.3 Mesh generation

A collection of elements which are connected to each other by shared nodes form a mesh in a finite element model. A trade-off exists between the level of accuracy and the computational complexity–higher density mesh produces more accurate result at the cost of additional complexity. In the available teaching version of ABAQUS 6.11, the number of nodes is limited to 100,000. By considering this limitation, a uniform fine mesh was generated in this study for the piled raft and the soil. The automatic mesh generation option in ABAQUS is not available for complicated geometries; therefore, the piled raft and the soil were partitioned into simpler forms before applying the mesh generation function.

6.2.4 Boundary condition

Transitions of bottom nodes were restricted in all three directions (X, Y and Z) and the lateral movement was avoided for the nodes on the sides of the soil block.

6.2.5 Material properties

The linear elastic constitutive model was applied to predict the behavior of the foundation elements and soil in this study. Although the soil is not an elastic material, the behavior of homogeneous sand at working (serviceability) loads could be simulated by an elastic constitutive model.

The stress-strain relationship for one dimensional isotropic elastic material is defined as follows:

$$\sigma = E\varepsilon \tag{6.1}$$

Where σ represents the normal stress which is directly proportional to the normal strain (ε), and E is the modulus of elasticity. This relationship, known as Hooke's law, was named after Robert Hooke (1635-1703) and later extended to three-dimensional spaces including the shear stresses. A three-dimensional cubic element subjected to normal and shear stresses is shown in Figure 7-2. The following equations represent Hooke's law for a general stress condition:

$$\begin{aligned}
\varepsilon_{11} &= \frac{1}{E}\left(\sigma_{11} - \nu\sigma_{22} - \nu\sigma_{33}\right) & \varepsilon_{12} &= \frac{(1+\nu)}{E}\tau_{12} \\
\varepsilon_{22} &= \frac{1}{E}\left(\sigma_{22} - \nu\sigma_{11} - \nu\sigma_{33}\right) & \varepsilon_{23} &= \frac{(1+\nu)}{E}\tau_{23} \\
\varepsilon_{33} &= \frac{1}{E}\left(\sigma_{33} - \nu\sigma_{11} - \nu\sigma_{22}\right) & \varepsilon_{31} &= \frac{(1+\nu)}{E}\tau_{31}
\end{aligned} \tag{6.2}$$

Where ν is the Poisson's ratio and is defined as the ratio of lateral strain over axial strain ($\nu = -\frac{\varepsilon_{22}}{\varepsilon_{11}} = -\frac{\varepsilon_{33}}{\varepsilon_{11}}$).

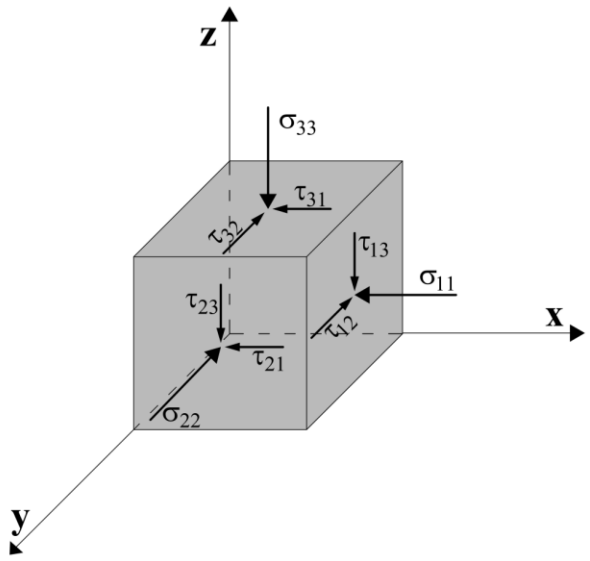

Figure 6-2 Three dimensional cubic element subjected to combined shear and normal stresses

The aforementioned equations could be combined in a matrix form as follows:

$$\begin{bmatrix} \sigma_{11} \\ \sigma_{22} \\ \sigma_{33} \\ \tau_{12} \\ \tau_{13} \\ \tau_{23} \end{bmatrix} = \frac{E}{(1+\nu)(1-2\nu)} \begin{bmatrix} 1-\nu & \nu & \nu & 0 & 0 & 0 \\ \nu & 1-\nu & \nu & 0 & 0 & 0 \\ \nu & \nu & 1-\nu & 0 & 0 & 0 \\ 0 & 0 & 0 & 1-2\nu & 0 & 0 \\ 0 & 0 & 0 & 0 & 1-2\nu & 0 \\ 0 & 0 & 0 & 0 & 0 & 1-2\nu \end{bmatrix} \begin{bmatrix} \varepsilon_{11} \\ \varepsilon_{22} \\ \varepsilon_{33} \\ \varepsilon_{12} \\ \varepsilon_{13} \\ \varepsilon_{23} \end{bmatrix} \tag{6.3}$$

Based on the Eq. 6.3, the required parameters for the elastic constitutive model are the modulus of elasticity (E) and Poisson's ratio (ν).

6.2.6 Interface element

The soil structure interaction is the main driving factor of the load sharing mechanism that requires proper modeling to achieve accurate numerical results. Therefore, we first specified the locations where two different surfaces meet (i.e., soil and foundation elements) and applied the surface-to-surface discretization technique to model the soil-structure interaction. The aforementioned technique connects the nodes on one of the two surfaces (master surface) to the

face of the other one (slave surface). Each node on the slave surface is constrained to have the same motion as the closest point on the master surface. It is a common practice to consider the surface with higher rigidity as the master surface. In this study, the pile and raft surfaces were treated as master surface and the soil in contact with foundation elements represented the slave surface.

The "mechanical contact property" function in ABAQUS software was used to specify tangential (friction) and normal interaction between the soil and the structures. The pile peripheral surfaces represented the tangential interaction whereas the soil contact with the raft and the pile tip represented the normal interaction. Furthermore, the stiffness of contact surfaces was simulated by "frictional constraint enforcement" feature within the software. The frictional coefficient for tangential interaction (μ) and the stiffness of normal interaction was assumed to be 0.3 and 1, respectively.

6.2.7 Loading steps

The numerical analyses were conducted in two steps. Initially, the numerical model was run under gravity load and subsequently, a uniformly distributed load was applied on the raft surface and increased incrementally until it reached 41.8kN/m^2. The output data was requested for forces, stresses and displacements in each load increments. The load-settlement curve and the load sharing at settlement ratio of 2% were obtained from the numerical results.

6.3 Model validation

The conducted experimental test on non-displacement piled raft in medium sand was simulated by ABAQUS software to calibrate the numerical model. Figure 6-3 shows the geometry of soil block and the single piled raft unit (1x1 piled raft). The 1x1 piled raft was configured by

attaching the square pile with 290mm length to the rigid raft (100x100mm) with 25.4mm thickness. The circular pile in the experimental test was replaced with a square pile with a same peripheral surface area in the numerical model to reduce the number of elements. Sinha (2013) demonstrated that this replacement has no effect on numerical results.

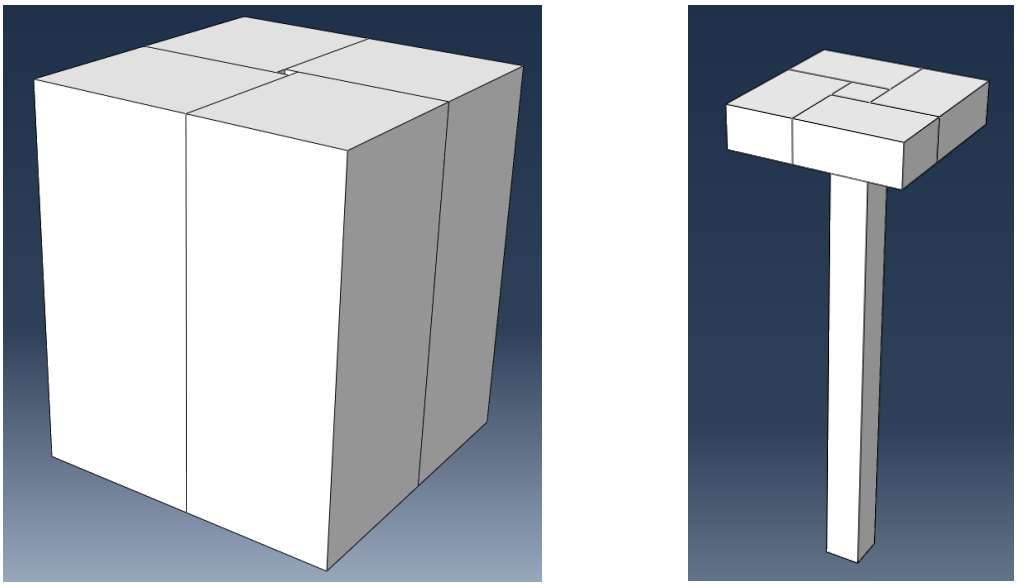

(a) (b)

Figure 6-3 Soil block and 1x1 piled raft model

Table 6-2 presents the material properties assigned to the foundation elements and the soil in the numerical model. Reviewing the available studies in the literature revealed that the Poisson ratio (ν) and elasticity modulus (E) of sand vary in the range of 0.25-0.4 and 10-50MPa, respectively. Accordingly, the Poisson's ratio of the test sand was considered to be 0.25 and the soil elasticity modulus was calculated based on the soil friction angle (Eq. 6.4).

$$E_{sand(kPa)} = 500(N_{60} + 15) \quad \text{(Bowels 1982)}$$

$$\phi = \sqrt{20N_{60}} + 20 \quad \text{(Hatanaka and Uchida 1996)} \qquad (6.4)$$

Where N_{60} represents the SPT blow-count corrected for energy, equipment, and procedure effects. Furthermore, the Poisson ratio and elasticity modulus of pile and raft were assigned based on steel properties equal to 0.3 and $2x10^{11}N/m^2$, respectively.

Table 6-2 Material properties in the numerical models

	Sandy soil	**Pile**	**Raft**
Poisson ratio	0.25	0.3	0.3
Elasticity modulus (N/m^2)	$1.3x10^7$	$2x10^{11}$	$2x10^{11}$
Density (kg/m^3)	1554	7800	7800
Load	Self-weight	Self-weight	Self-weight & 41.8 N/cm^2

After assigning the material properties, the piled raft and the soil were assembled and a uniform mesh was generated for the model. The generated mesh before and after applying external load are illustrated in Figure 6-4. In general, the boundary conditions should be selected in a fashion that the major displacements caused by the applied load is captured within the model. The above condition is respected in our model as shown in Figure 6-5 where the boundaries are extended far enough such that the impact of the last loading step ($41.8kN/m^2$) is insignificant towards the edge of the soil.

The obtained load-settlement curve from the conducted numerical analysis is shown in Figure 6-6. The result of the experimental test on non-displacement piled raft in medium sand is also included in this figure. A reasonable consistency is observed between the predicted and measured load-settlement curve at small settlements (under working loads).

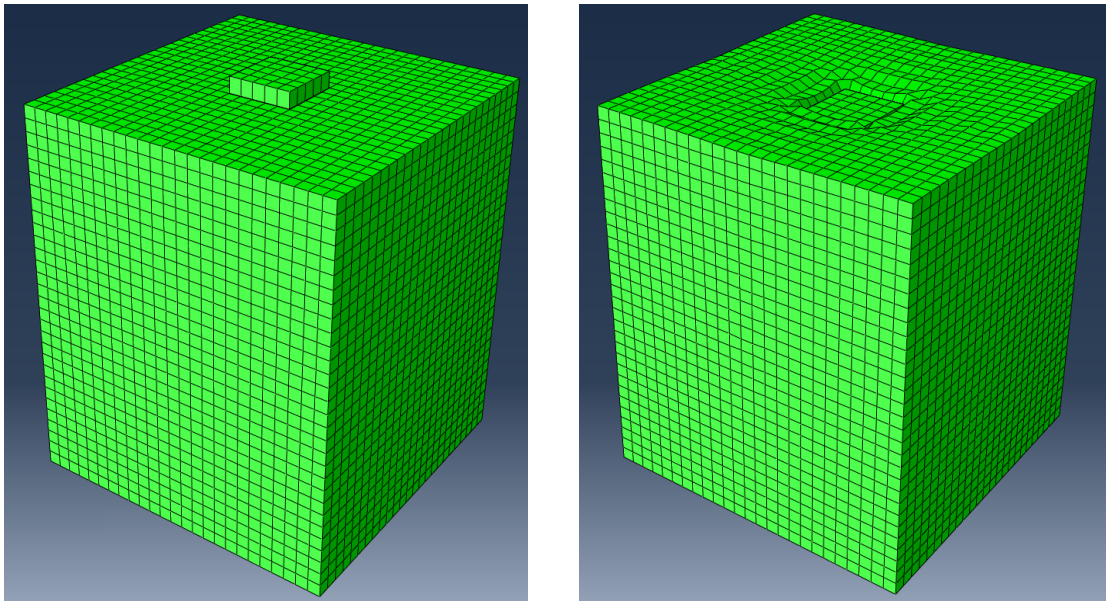

Figure 6-4 General view of un-deformed and deformed mesh for the 1x1 piled raft model

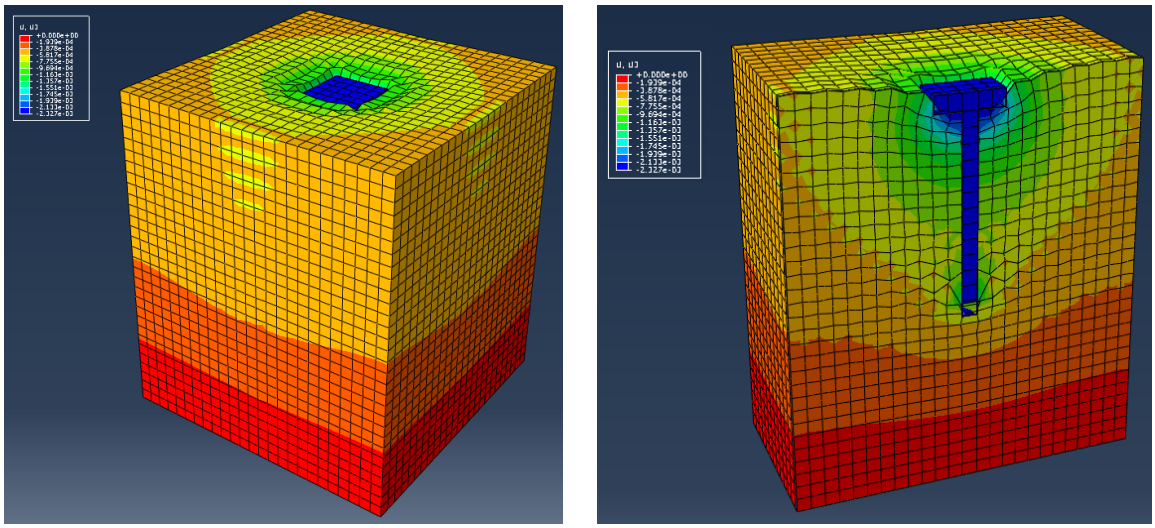

(a) (b)

Figure 6-5 (a) 3D view and (b) 3D axial cut view of vertical displacement contours in meters (U3)

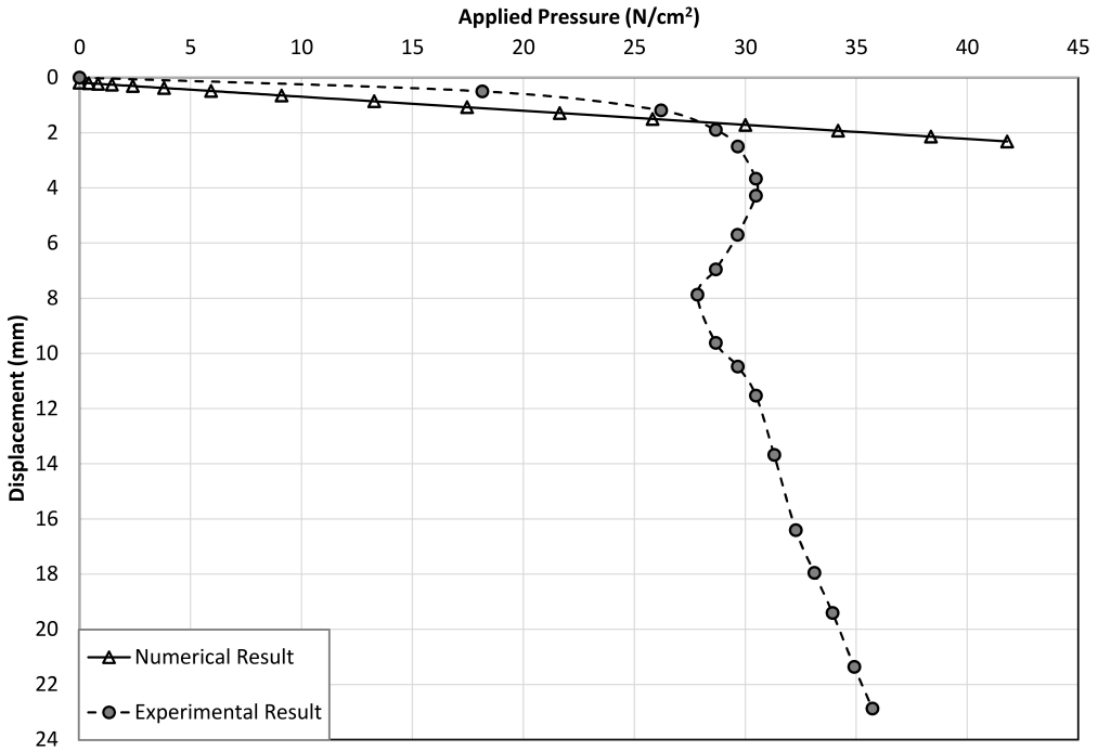

Figure 6-6 Load-settlement curve of 1x1 piled raft, experimental and numerical results

The raft contribution in carrying the applied load on 1x1 piled raft footing was defined as the ratio of average pressure below the raft to the applied distributed pressure on the raft in each loading step. The unknown pressure below the raft was estimated as the average of recorded pressures along the length of the raft. Based on the above definition, the raft share of 1x1 piled raft at 2% settlement ratio was found to be 54% which was aligned with present experimental results, 43%, at the same settlement ratio. This comparison reveals that the numerical model has an acceptable level of accuracy in the load sharing estimation.

6.4 2x2 piled raft

The 2x2 piled raft footing was produced by placing the piles in $3.5d_p$ spacing below a 200x200mm raft. The size of the soil block increased to 1000x1000mm to mitigate the boundary effects on the numerical results. The parts were partitioned to facilitate the mesh generation

(Figure 6-7) and the generated mesh before and after applying the load are illustrated in Figure 6-8. Figure 6-9 demonstrates the general and axial cut view of vertical displacement contours at the last loading step.

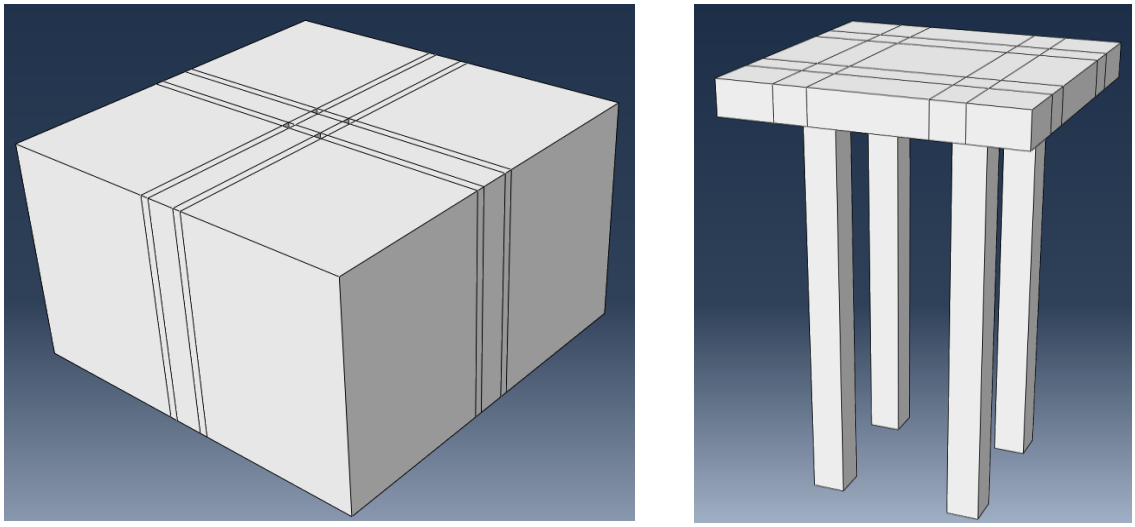

(a) (b)

Figure 6-7 The defined parts for the 2x2 piled raft model: (a) soil block and (b) 2x2 piled raft

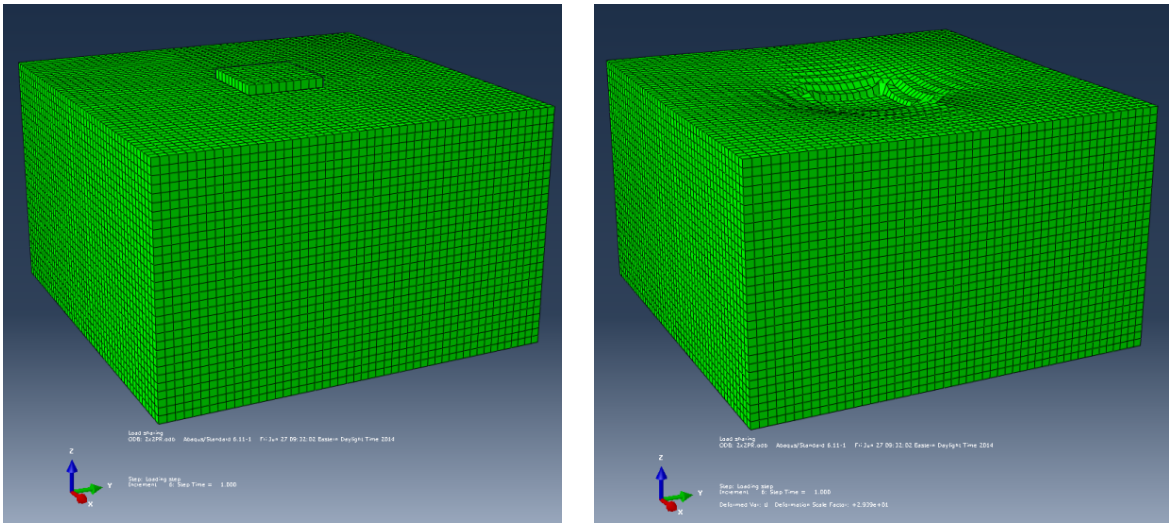

(a) (b)

Figure 6-8 General view of (a) un-deformed and (b) deformed mesh of 2x2 piled raft model

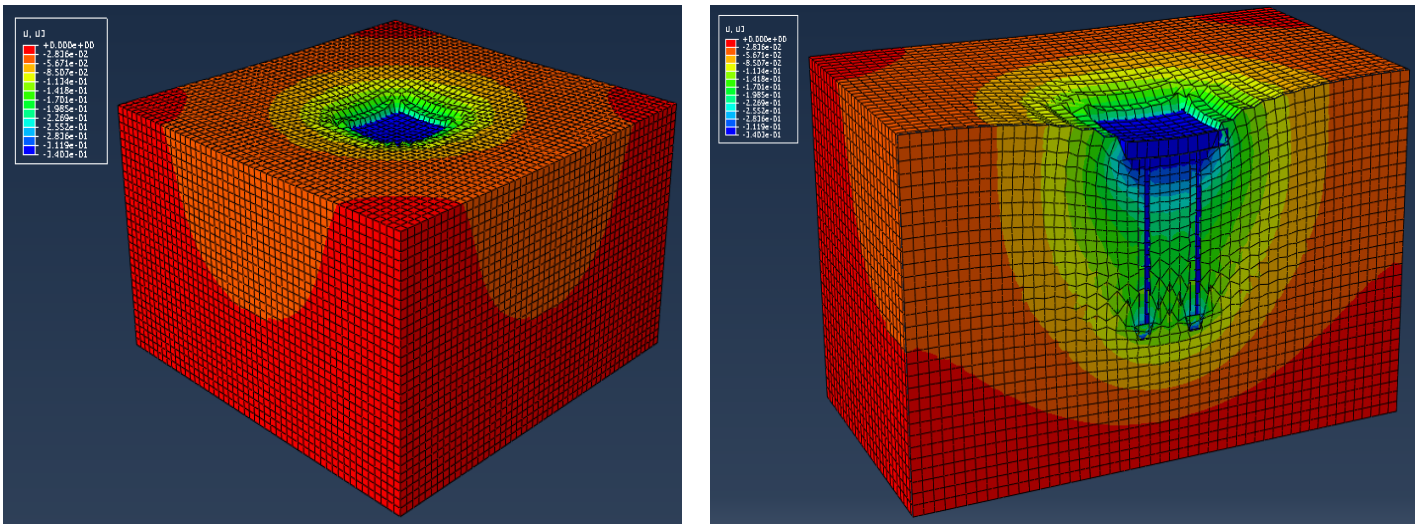

(a) (b)

Figure 6-9 Vertical displacement contours of 2x2 piled raft model at the last loading step in centimeters

6.5 3x3 piled raft

The 3x3 piled raft model was built with nine identical piles connected to the bottom surface of 300x300mm raft (Figure 6-10) and placed at the center of the soil block in the pre-made holes (Figure 6-11). The generated mesh for this model before and after applying external load is illustrated in Figure 6-12. The load-settlement curve and load sharing of the numerical analyses are compared in the subsequent section.

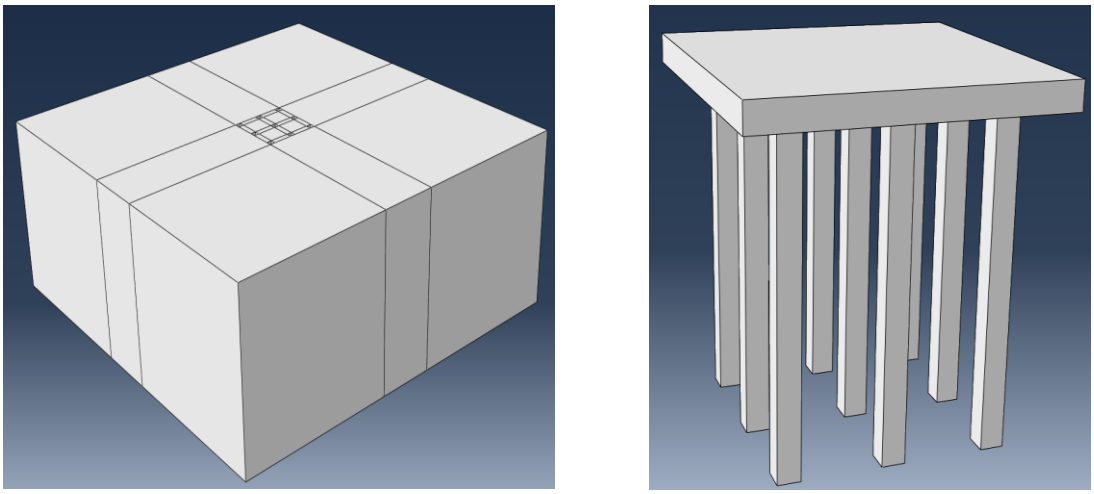

(a) (b)

Figure 6-10 The defined 3x3 piled raft and the soil block for the numerical analysis

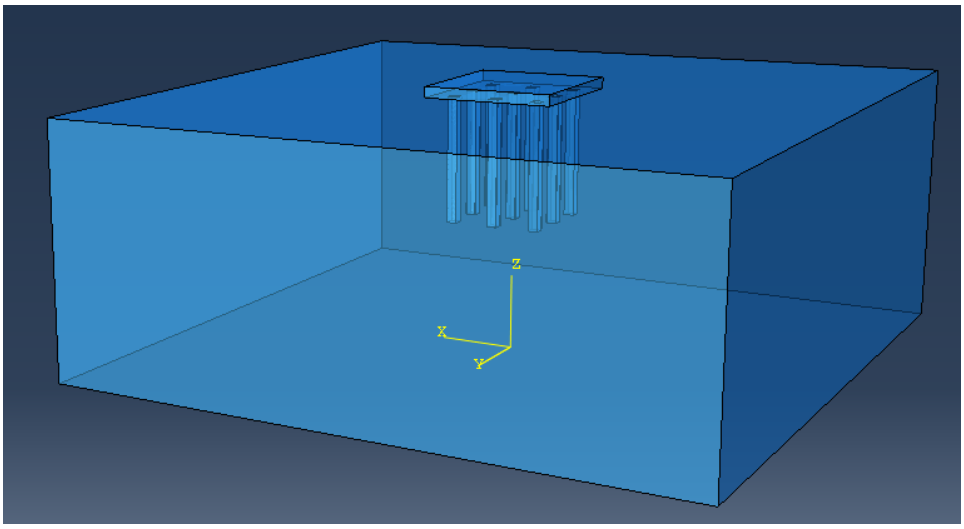

Figure 6-11 3x3 piled raft model and the soil block after assembling

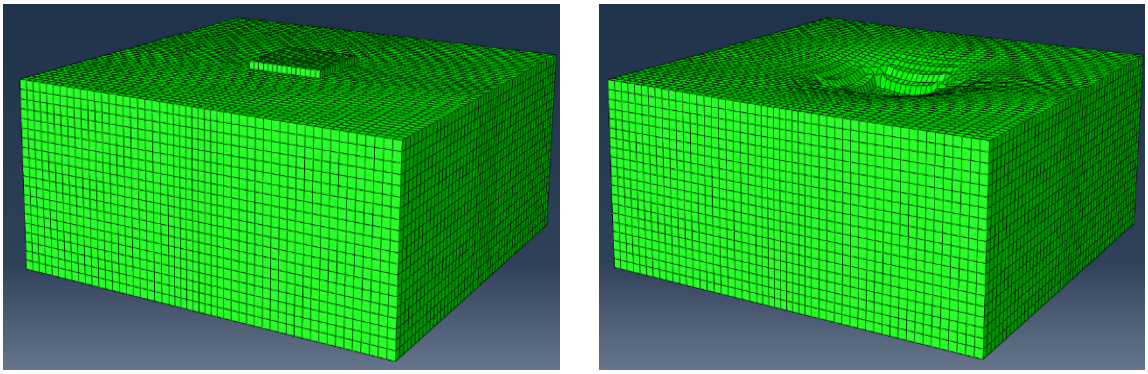

Figure 6-12 Un-deformed and deformed generated mesh for 3x3 non-displacement piled raft

6.6 Comparing the numerical results

The load-settlement behaviors of piled raft with different number of piles are compared in Figure 6-13. As expected, significant reduction in settlement is observed by enhancing the number of piles. The estimated loads sharing at settlement ratio of 2% for the numerical models are compared in Figure 6-14. It is observed that increasing the number of piles has inconsiderable impact on the load sharing of non-displacement piled raft. The observed behavior is due to the inconsiderable effect of pile-soil-pile interaction on the load sharing mechanism of non-displacement piled raft when the minimum pile spacing is $3.5d_p$. Therefore, the load sharing and group efficiency of non-displacement piled raft with multiple identical piles could be estimated

by analyzing a single piled raft unit given that the raft is rigid and the minimum pile spacing is respected. In the light of this observation, the empirical and analytical models are developed in the following chapters based on conducted experimental tests on a single piled raft unit.

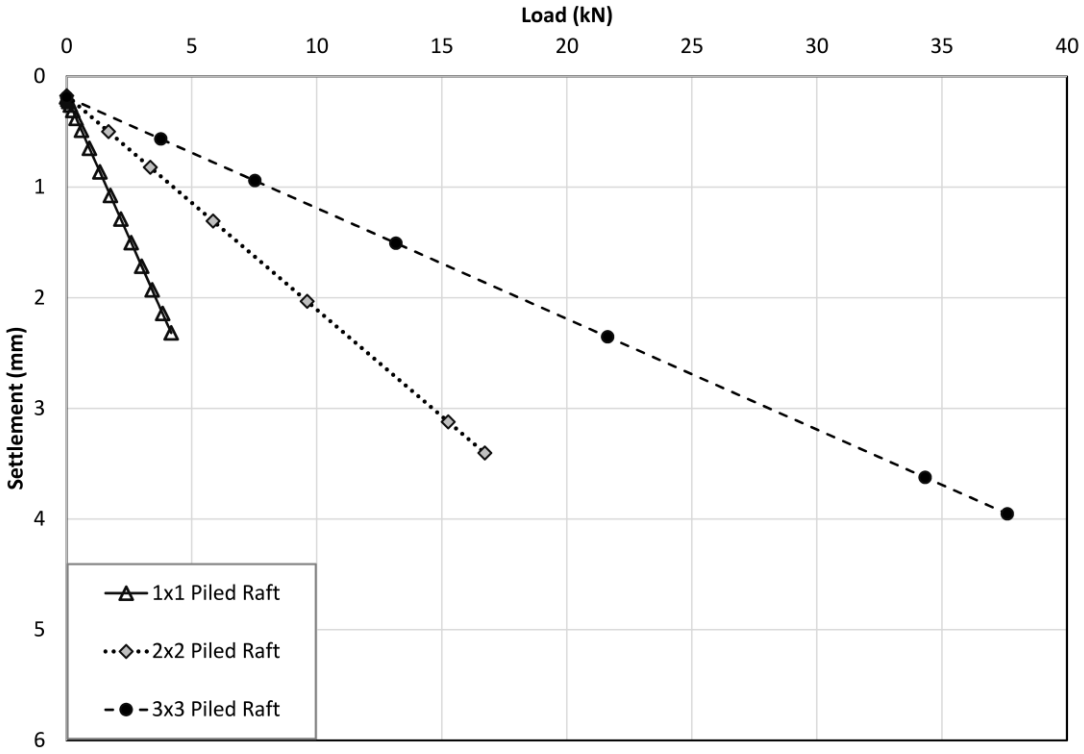

Figure 6-13 Load-settlement behavior of 1x1, 2x2, and 3x3 non-displacement piled raft

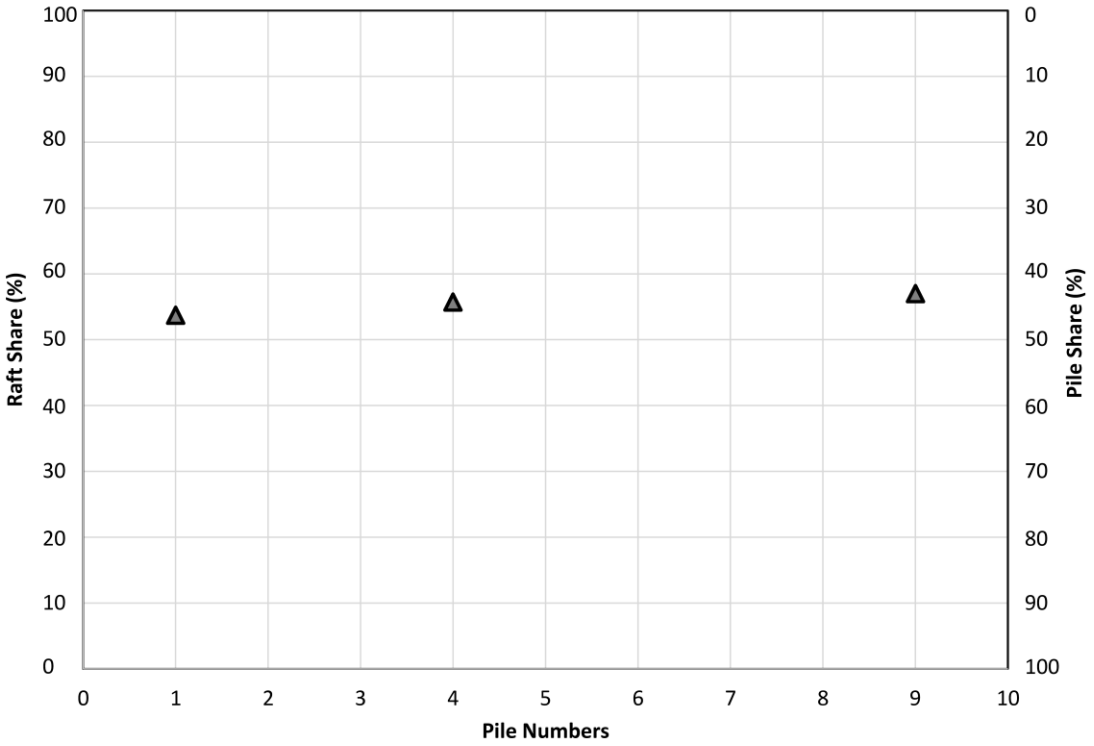

Figure 6-14 Estimated load sharing for 1x1, 2x2, and 3x3 at settlement ratio of 2% (w/dr=2%)

Chapter 7

Developing Empirical Models

7.1 General

As concluded in the previous chapter, the behavior of non-displacement piled raft with rigid raft, identical piles, and minimum pile spacing of 3.5dp (Figure 7-1), is not affected by pile-soil-pile interaction and could be analyzed as a single piled raft unit. Following this fact, our conducted experimental tests on single piled raft unit were employed to develop empirical models on piled raft load sharing and group efficiency in homogenous and layered sands. The empirical models for piled raft load sharing are based on settlement ratio (W/d_r) and pile spacing ratio (S/d_p) with the addition of soil density in the case of layered soil. The empirical models for piled raft efficiency are developed as a function of pile spacing ratio and soil relative density. The proposed models are validated by employing the available experimental results and field measurements in the literature at the end of this chapter.

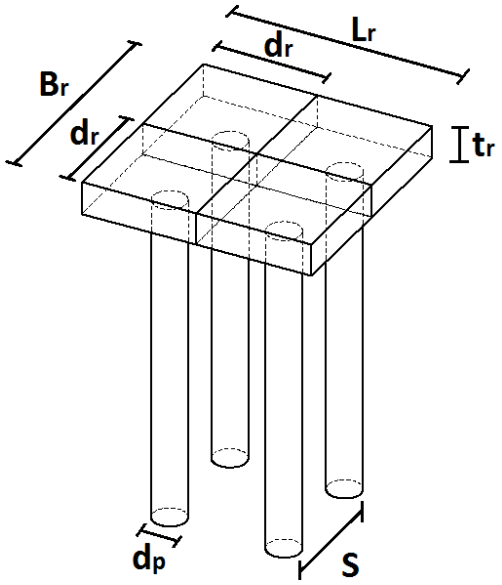

Figure 7-1 Schematic view of piled raft with identical piles in grid pattern

7.2 Load sharing model

The settlement-based load sharing models for non-displacement piled raft are presented in the following:

7.2.1 Homogeneous sand

Our experimental and numerical results analyses along with the conducted literature review revealed that the load sharing of non-displacement piled raft foundation in homogeneous sand is a function of two variables, S/d_p and W/d_r ratios, but independent of soil relative density, number of piles, and pile slenderness ratio. In the light of the above observation, our experimental tests on non-displacement piled raft foundations in medium sand were employed herein to develop the load sharing empirical model. Figure 6-2 shows the empirical design charts for the pile spacing ranges from $3.5d_p$ to $6d_p$ under working load. The two load sharing curves at $3.5d_p$ and $5.2d_p$ pile spacing, shown in Figure 6-2, correspond to our experimental results; whereas, the other curves were obtained by performing a linear interpolation or extrapolation between the recorded experimental data. The basis of linear interpolation was the work of Sinha (2013) which proved the existence of a linear relationship between pile spacing ratio and load sharing. Furthermore, Yamashita et al. (2011) and Sinha (2013) demonstrated that the relationship between the load sharing and pile spacing reaches a saturation point at $S/d_p \geq 6$ where the pile spacing has no further effect on load sharing. Therefore, for any pile spacing greater than 6, the proposed load sharing curve at $S/d_p=6$ should be employed. The empirical curves in Figure 7-2 were extended up to $W/d_r=10\%$ to widely cover the variation of load sharing by settlement ratio before the failure as also seen in previous studies such as Cerato and Lutenegger (2006) and Lee and Salgado (2005).

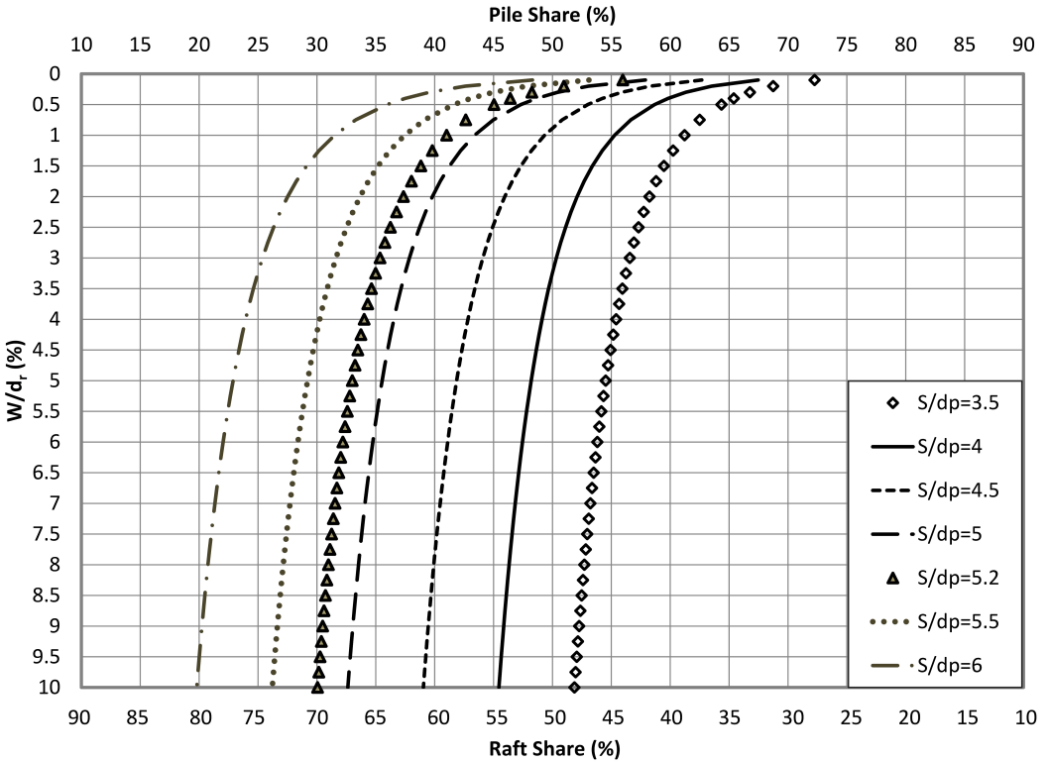

Figure 7-2 The proposed empirical curves for estimating the load sharing of non-displacement piled raft in homogeneous sand as the function of W/d_r and S/d_p

7.2.2 Layered sand

As mentioned previously in Chapter 3, the experimental results on non-displacement piled raft were performed on three different compaction patterns: loose on medium, loose on dense, and medium on dense soil (Figure 3-9). The results of these experiments revealed that the compaction pattern, settlement ratio, and pile spacing ratio have a considerable impact on the piled raft load sharing; however, the pile length is not a major contributing factor. In the following, the developed empirical charts for non-displacement piled rafts in layered soil are presented under two different scenarios: raft on loose sand and raft on medium sand.

Raft on loose sand

Figures 7-3 and 7-4 illustrate the variation of load sharing versus settlement ratio where the raft is founded on loose sand (D_r=30%) and the soil density at pile tip is varied from 30% to 60% at

3.5d_p and 5.2d_p pile spacing, respectively. Referring to these figures, the load sharing curves with soil density of 30, 45, and 60% at the pile tip represent our experimental tests; whereas, the other curves were estimated by linear interpolation of the experimental data. The presented charts could be extended to other pile spacing ratios (up to S/d_p=6) using linear interpolation/extrapolation techniques. Bear in mind that the load sharing of piled raft with pile spacing greater than 6d_p is equal to the load sharing value at 6d_p.

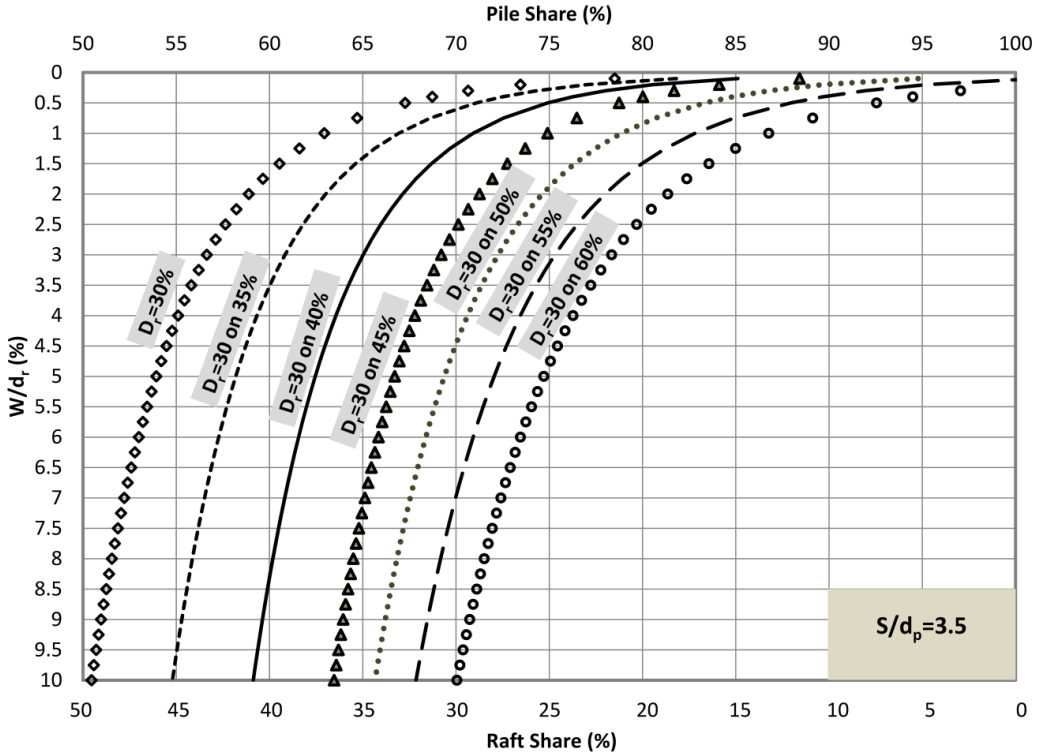

Figure 7-3 Proposed empirical curves for estimating the load sharing of non-displacement piled raft in layered soil when the raft was founded on loose sand, and S/d_p=3.5

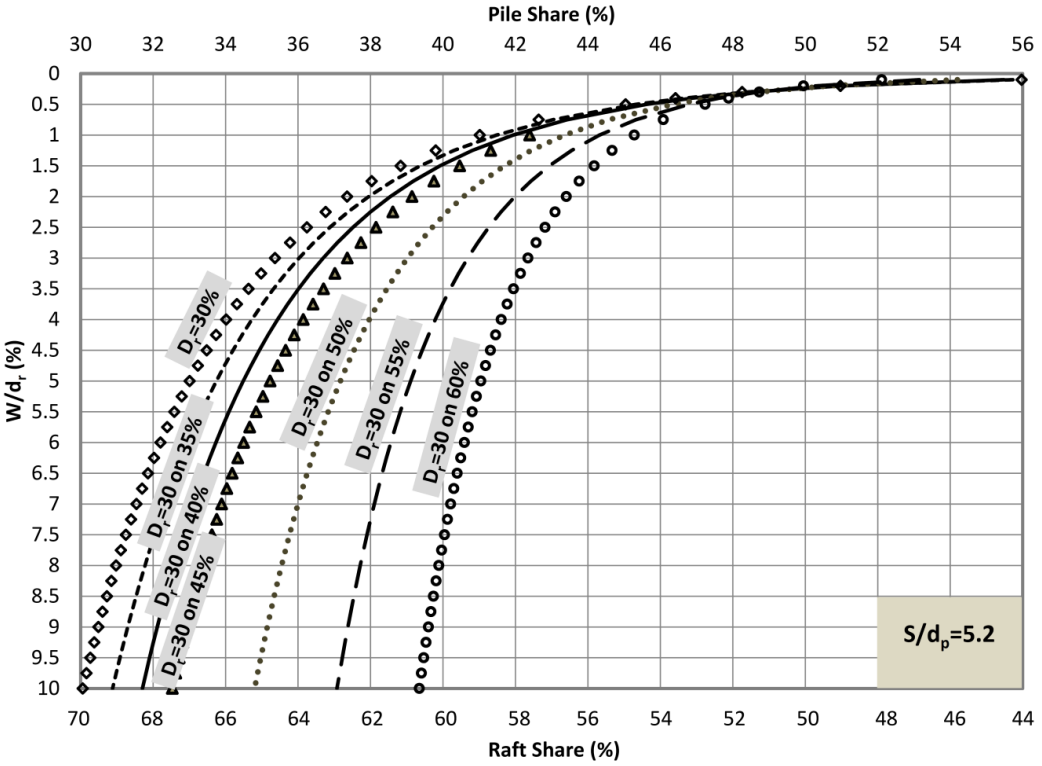

Figure 7-4 Proposed empirical curves for estimating the load sharing of non-displacement piled raft in layered soil when the raft was founded on loose sand, and S/d_p=5.2

Raft on medium sand

The same procedure was followed to develop the empirical charts for non-displacement piled raft when the raft is founded on medium sand and the soil density at pile tip is varied from 45% to 60%. Figure 7-5 and 7-6 show the load sharing empirical charts when S/d_p is equal 3.5 and 5.2, respectively. Similar to the previous scenario, the experimental measurements were interpolated to obtain the load sharing curves with the soil density of 50% and 55% at the pile tip. The load sharing of piled raft with pile spacing other than $3.5d_p$ and $5.2d_p$ should be calculated by applying a linear interpolation/extrapolation technique on the presented results.

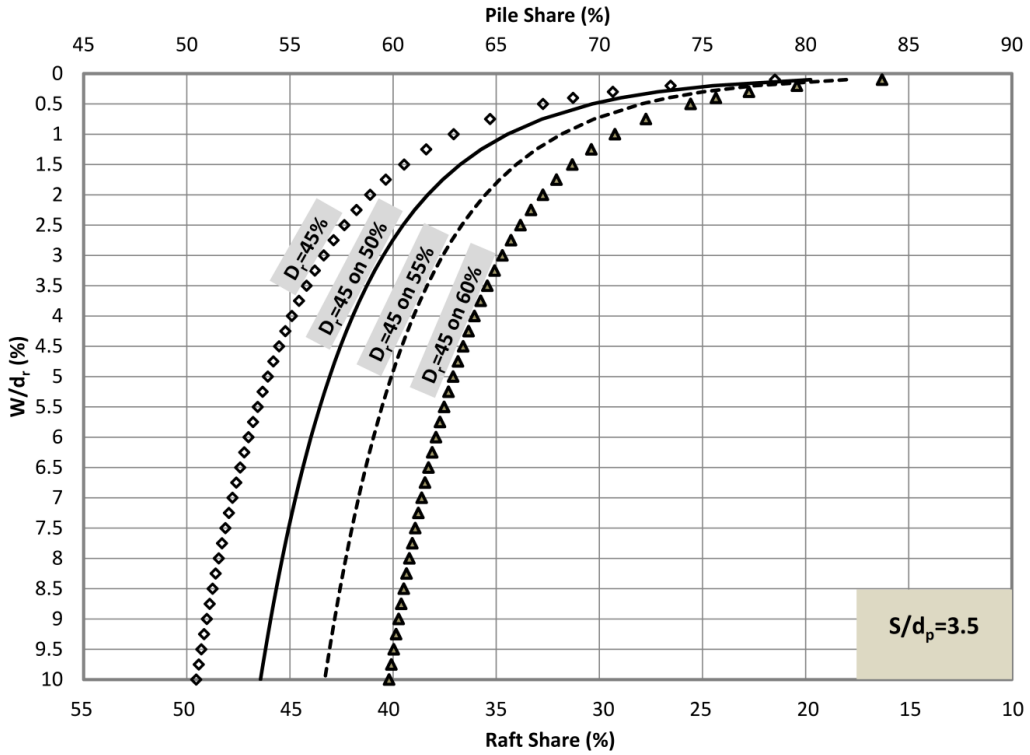

Figure 7-5 Proposed empirical curves for estimating the load sharing of non-displacement piled raft in layered soil when the raft was founded on medium sand, and S/d_p=3.5

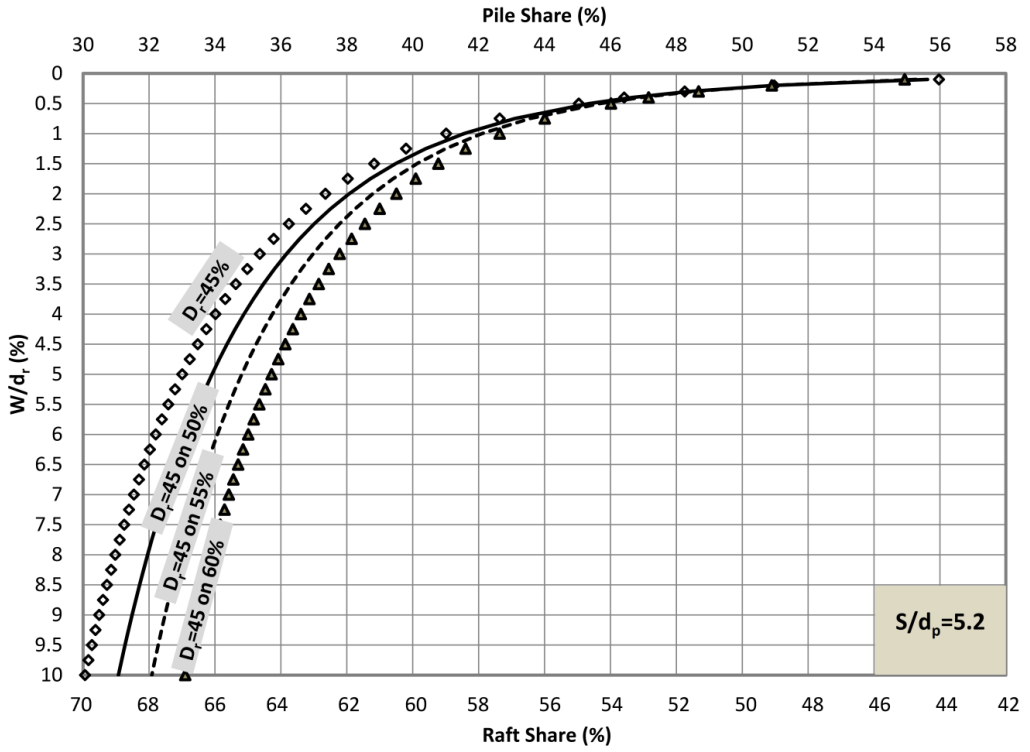

Figure 7-6 Proposed curves for estimating the load sharing of non-displacement piled raft in layered soil when the raft was founded on medium sand, and S/d_p=5.2

7.2.3 Validation

The empirical models are compared with the available centrifuge test results and field measurements to confirm their accuracy and reliability.

Homogeneous sand

The centrifuge test results, executed by Giretti (2010), on non-displacement piled raft were used to validate the developed load sharing model in homogeneous sand. Two centrifuge tests shown in Figure 7-7, PR1 and PR3(a), are used herein to be compared with the results of the proposed empirical model. Test PR1 was conducted on a single non-displacement piled raft unit in loose sand whereas test PR3(a) was performed on three non-displacement piles arranged in a circular pattern and placed in the middle of the raft. More information about the dimensions of pile raft model are provided in Table 7-1 and also in section 2.2.2. Figure 2-12 shows the variation of load sharing versus settlement ratio for the aforementioned tests. It is noticeable in this figure that the applied load was entirely carried by the pile(s) for small settlements due to the existence of a gap between the raft and the soil. Therefore, the starting point was the point where load-sharing variation begins. Figure 7-8 and 7-9 illustrate the comparison between the results of centrifuge test and the empirical model values under working condition ($W/d_r<5\%$). The measured and estimated load sharing values are in a fairly close agreement with each other.

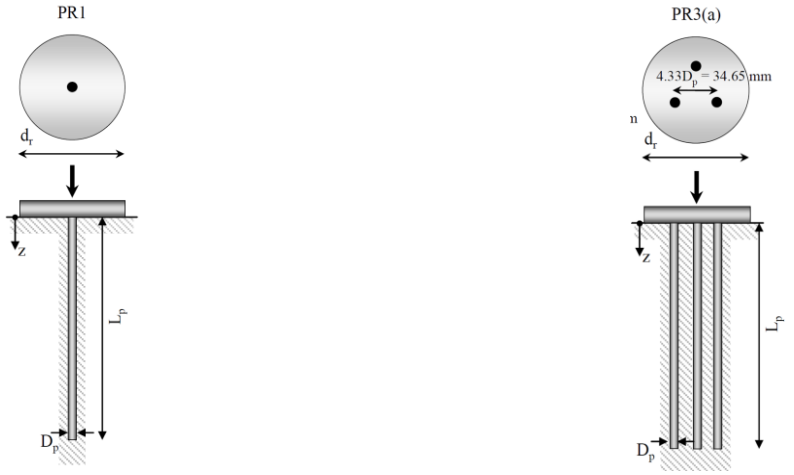

Figure 7-7 Plan and side view of piled raft in test PR1 (left side) and PR3(a) (right side), adapted from Giretti (2010)

Table 7-1 The information about geometry of pile and raft in the tests PR1 and PR3(a)

Test Name	D_r (%)	No. of piles	Pile diameter (d_p)	Pile spacing (S)	Pile length (L)	L/d_p	Raft diameter (d_r)
PR1	35	1	8mm	-	160mm	20	88mm
PR3(a)	31	3	8mm	$4.33d_p$	160mm	20	88mm

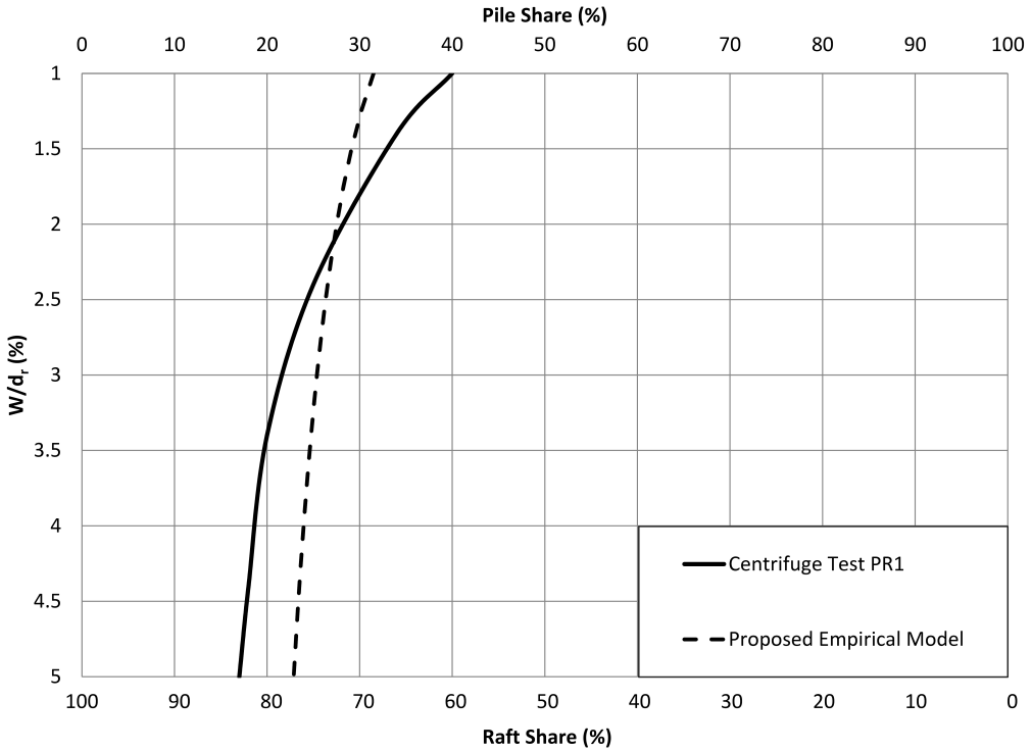

Figure 7-8 Comparison between the measured load sharing in centrifuge test PR1 and the estimated values by the proposed empirical model

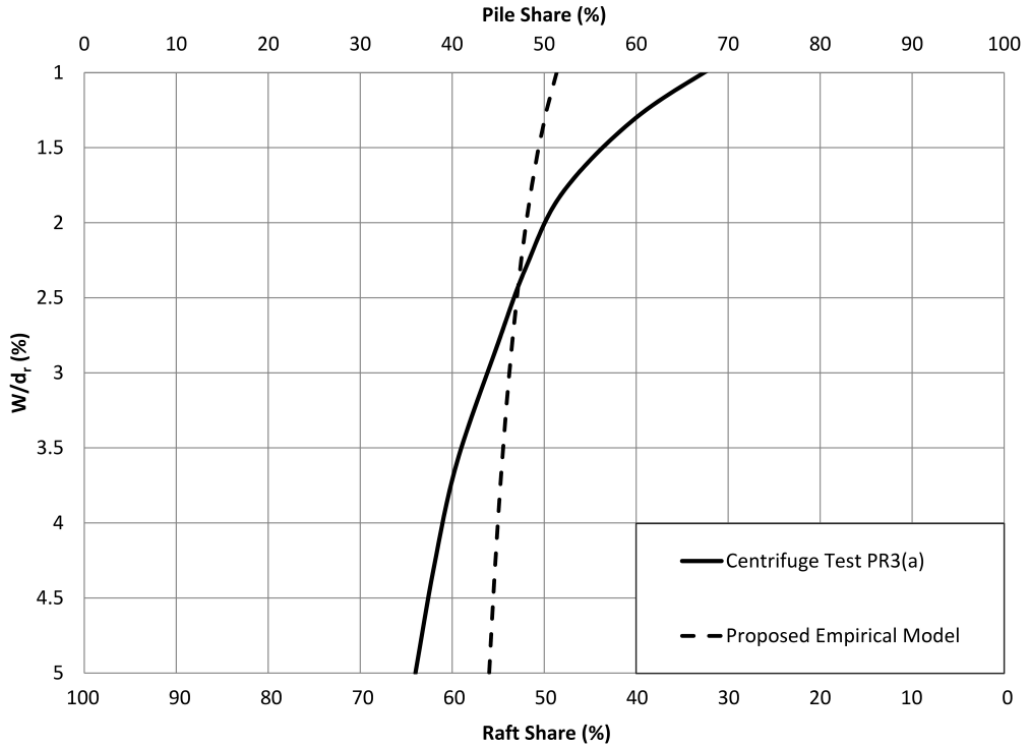

Figure 7-9 Comparison between the measured load sharing in centrifuge test PR3(a) and estimated load sharing by the proposed empirical model

Layered sand

The case study reported by Yamashita et al. (2011), forty-seven story residential tower in Nagoya, was employed to validate the developed empirical model for piled raft foundation in layered sand. This case study was selected due to its similarity with our empirical model in soil material and the availability of foundation settlement. In this building, the raft was founded on medium sand and the pile group, with grid pattern and various pile spacing in different directions, was embedded on very dense sand. The measured load sharing and settlement for the instrumented pile with average pile spacing of $3.96d_p$, 8 months after the end of construction, was reported to be 87% and 24mm, respectively. The field pile sharing measurement and the empirical model result are compared in Table 7-2. As discussed in chapter 5, increasing the sand density at the pile tip results into pile sharing enhancement. This phenomenon is also seen through this comparison where the soil density in field is greater than that of empirical model.

Table 7-2 The measured pile sharing for instrumented pile (7D) in 47 story residential tower in comparison with estimated pile sharing value from empirical models for layered sand

Instrumented pile	Foundation settlement (mm)	S/d_p (average)	W/d_r (%)	Pile share (field observation)	Pile share (empirical model)
				Raft on medium sand and pile in very dense sand	Raft on medium sand and pile in dense sand
7D	24	3.96	0.3	87%	71%

7.3 Piled raft efficiency model

7.3.1 Homogeneous sand

The efficiency of a piled raft is defined as the ratio of piled raft ultimate bearing capacity over pile group ultimate capacity. As discussed in the previous chapter, the effect of pile-soil-pile interaction is insignificant in non-displacement piled raft with pile spacing greater than or equal

to $3.5d_p$. Therefore, the efficiency of a piled raft with multiple piles is similar to that of a single piled raft unit given that the minimum pile spacing (i.e., $3.5d_p$) is respected. The efficiency of single piled raft unit at different pile spacing and soil relative density were obtained from our experimental results and extrapolated over a range of 3.5-6dp as shown in Figure 7-10.

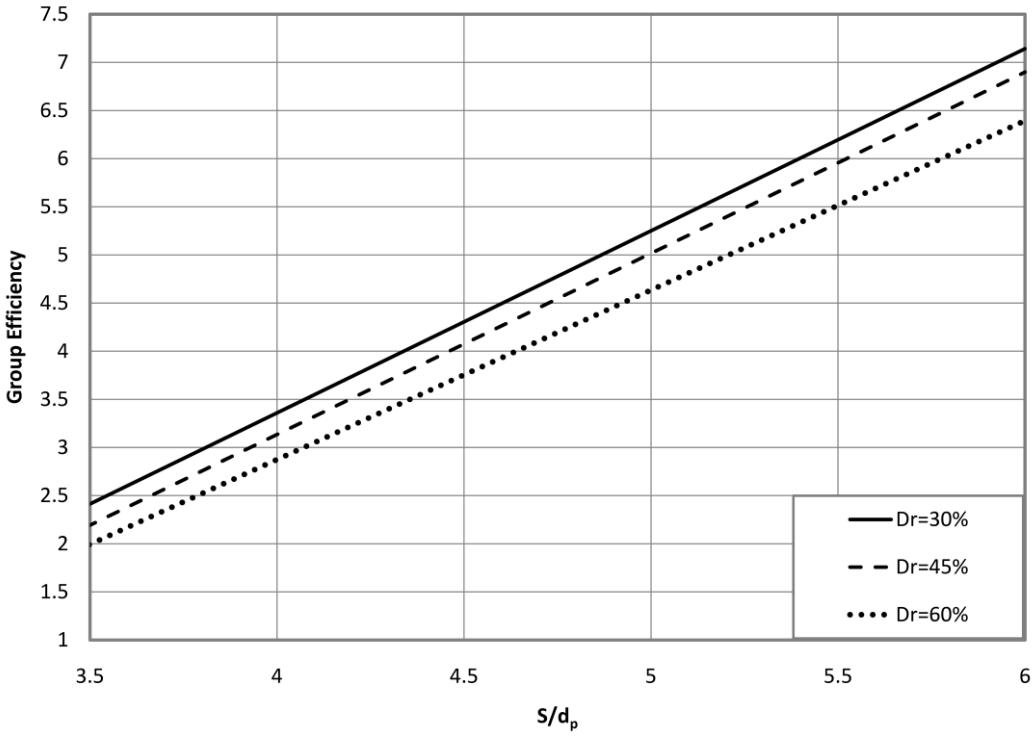

Figure 7-10 Variation of non-displacement piled raft group efficiency in homogeneous sand versus S/d_p ratio and soil relative density

7.3.2 Layered Sand

Similar procedure was followed to develop the empirical charts for estimating the piled raft efficiency in layered sand. Figure 7-11 shows the group efficiency when the raft is founded on the upper layer with 30% soil density and the pile tip is placed on the lower sand layer with higher density. A similar model was generated for the case that the raft is founded on medium sand as shown in Figure 7-12. It is observed that by increasing the soil density at the pile tip the group efficiency of piled raft drops.

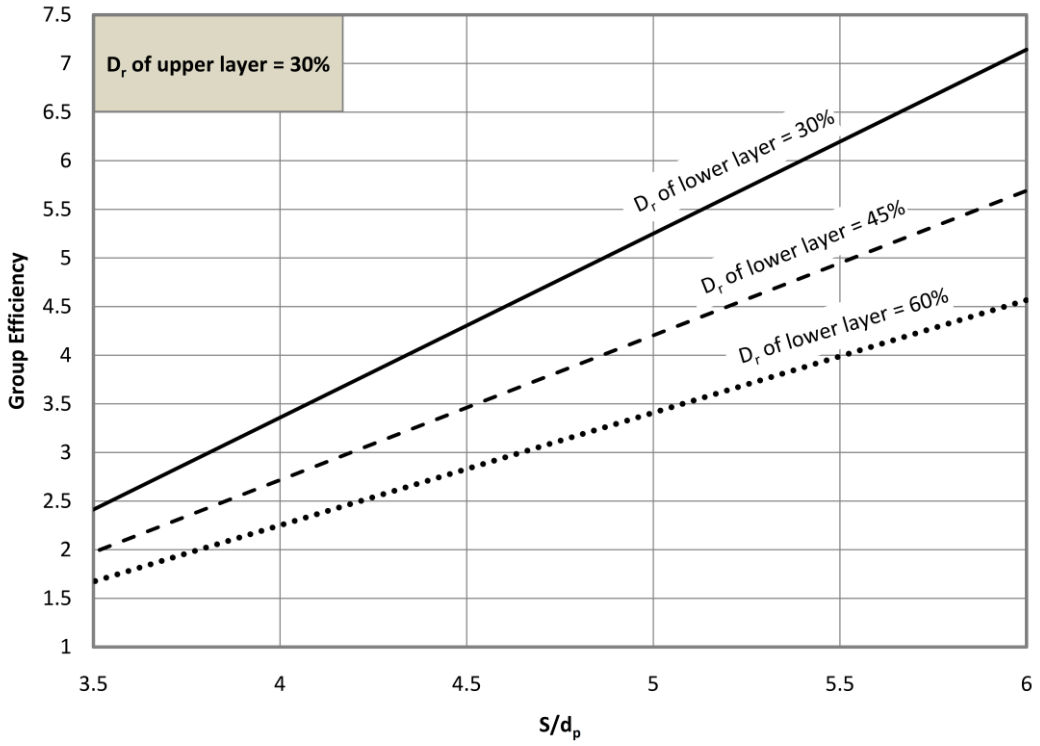

Figure 7-11 Group efficiency of piled raft in layered sand when the raft was founded on loose sand and the soil relative density at pile tip changes by 30, 45 and 60%

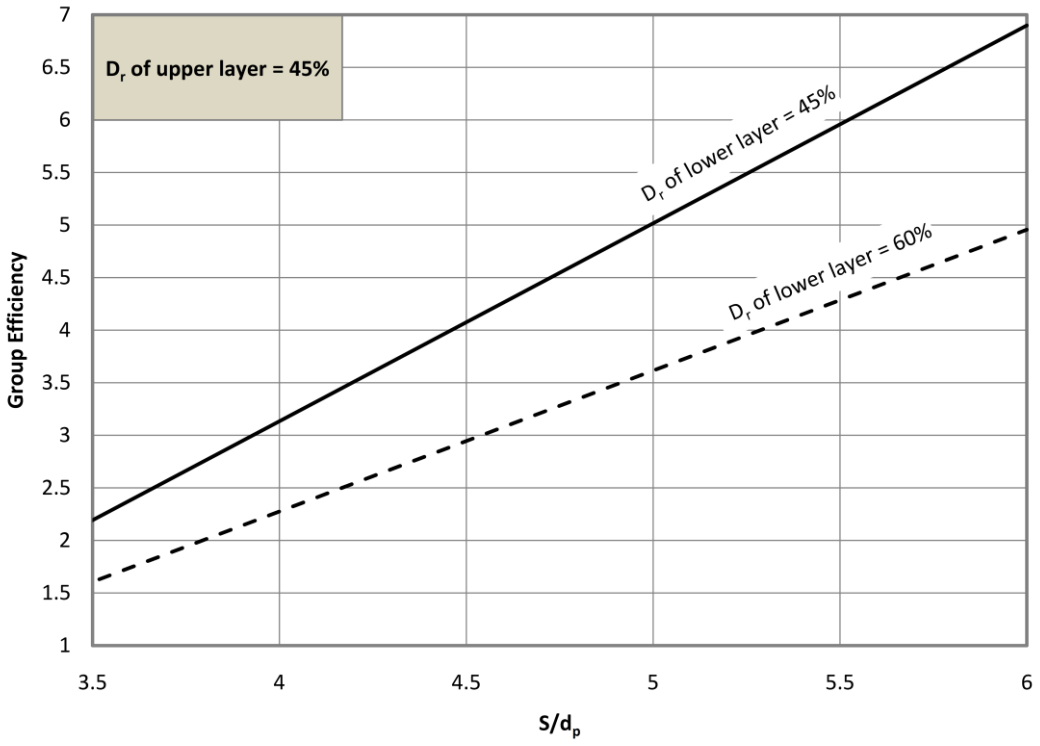

Figure 7-12 Group efficiency of piled raft in layered sand when the raft was founded on medium sand and the soil relative density at pile tip changes by 45 and 60%

7.3.3 Validation

The results of field tests on piled raft foundation in sand (Liu et al. 1985) were used to validate the proposed empirical model for piled raft group efficiency. Liu et al. (1985) performed a series of field tests on non-displacement pile group and piled raft in loose sand and determined the piled raft efficiency based on the experimental results. The field tests were conducted on 3x3 pile group configurations with $3d_p$ pile spacing and varied pile slenderness ratios. The obtained group efficiencies from our empirical model for soil density of 30% (Figure 7-10), and the experimental tests are compared in Table 7-3 and a close consistency is observed between the two values.

Table 7-3 The soil and piled raft condition in the performed field tests with Liu et al. (1985) for determining the group efficiency of piled raft footing

Soil Condition	L/d_p	S/d_p	Pile configuration	The measured efficiency by Liu et al. (1985)	The obtained efficiency by the empirical model
Loose	8	3	3x3	1.64	1.5
Loose	13	3	3x3	1.69	1.5

Chapter 8

Developing Analytical Model

8.1 General

Randolph (1983) proposed a simplified method for the piled raft load sharing estimation, previously described in Section 2.3.1, which is a commonly accepted method of piled raft foundation design. This method is based on the theory of elasticity and estimates the load sharing according to pile stiffness (K_p), raft stiffness (K_r), and pile-raft interaction factor (α_{rp}). Clancy and Randolph (1996) recommended a design chart for estimating the α_{rp} as a function of pile spacing and number of piles (Figure 2-16) while the effect of foundation settlement on piled raft load sharing was completely omitted in their study. In this chapter, Randolph's method is adjusted to incorporate the effect of settlement on piled raft load sharing in homogeneous and layered soil. In this regard, the conducted experimental results on raft (100x100mm), single pile, and non-displacement piled raft unit with 100x100mm raft, were employed to back-calculate the interaction factor (α_{rp}) in different settlement. The experimental results of shallow footing and single pile tests were used to calculate K_r and K_p as the ratio of load over settlement; whereas, the experimental results on piled raft provided the load sharing at different settlement. Subsequently, the unknown α_{rp} in different settlement was calculated and the best fit curve was applied to estimate the correlation between interaction factor and settlement. Furthermore, a correction factor was applied to the best fit equation to include the effect of pile spacing on interaction factor (α_{rp}). The pile slenderness ratio (L/d_p) and number of piles were excluded

from the proposed pile-raft interaction factor equation; since, their effects on load sharing are inconsiderable. The results of the conducted experimental tests on non-displacement piled raft with 150x150mm raft, were applied to validate the proposed analytical model. A good agreement was observed between the predicted values by the proposed analytical model and the measured ones from the experimental tests.

8.2 Randolph's analytical solution for a single piled raft unit

The original idea of Randolph's analytical method was derived from Randolph and Wroth (1978)'s study. The authors considered a rigid pile with a radius of $r_\circ$, which transmits the load to the surrounding elastic medium by the means of lateral friction only. Under this condition, the induced shear stress around the pile is a function of radial distance from the pile axis (r) and has the maximum value at pile-soil interface ($r = r_\circ$). The shear stress (τ_r) and corresponding shear strain (γ) induced around the pile under axial load are determined by the following equations:

$$\tau_r = \frac{\tau \times r_\circ}{r} \tag{8.1}$$

$$\gamma = \frac{\tau_r}{G} \tag{8.2}$$

Where G is the shear modulus of the elastic medium and is obtained as follows:

$$G = \frac{E}{2(1+\upsilon)} \tag{8.3}$$

Where υ and E represent the Poisson's ratio and elastic modulus of the medium around the pile, respectively.

Randolph and Wroth (1978) conducted experimental tests on single pile and illustrated that the displacement around a pile reduces logarithmically as a function of radial distance from the center of the pile. Subsequently, they proposed the following equation for determining the shear strain around an axially loaded pile:

$$\gamma = \frac{\delta w}{\delta r} \tag{8.4}$$

By combining the Eqs. 8.2, and 8.4, the soil displacement (w) around the pile is obtained as follows:

$$w_p(r) = \int_{r_0}^{r_m} \frac{\tau \times r_0}{Gr} dr = \frac{\tau \times r_0}{G} \ln\left(\frac{r_m}{r}\right) \tag{8.5}$$

Where $w_p(r)$ is the soil displacement in a radial distance of r from the pile center and r_m is the influence radius of the pile. The influence radius, r_m, is the distance from the center of the pile where displacement beyond that point is negligible. Randolph (1983) stated that r_m depends on the pile geometry and the relative homogeneity of the soil as follows:

$$r_m = 2.5\rho l(1-\upsilon) \tag{8.6}$$

Where l is the pile length and ρ represents the homogeneity of the soil with 1 corresponding to homogeneous soil and 0.5 corresponding to the cases that soil stiffness is proportional to the depth.

The maximum pile deformation occurs at the pile-soil interface (i.e., $r = r_0$) and is determined by inserting r_0 in Eq. 8.5:

$$w_{p0} = \frac{\tau_0 \times r_0}{G} \ln\left(\frac{r_m}{r_0}\right) = \frac{\tau_0 \times r_0}{G} \varsigma \tag{8.7}$$

The following equation provides soil displacement around the pile as a function of maximum deformation and is obtained by combining Eq. 8.5 and Eq. 8.7:

$$w_p = w_{p0} \frac{\ln\left(r_m / r\right)}{\ln\left(r_m / r_0\right)} \tag{8.8}$$

Randolph (1983) claimed that the soil displacement around the rafted pile ($\overline{w}_{rp}$) is less than that of single pile (w_{p0}) and proposed Eq. 8.9 to estimate the maximum displacement of piled raft:

$$\overline{w}_{rp} = w_{p0} \frac{\ln\left(r_m / nr_0\right)}{\ln\left(r_m / r_0\right)} \tag{8.9}$$

Where $n = \frac{r_r}{r_0}$ and r_r represents the radius of raft. Randolph (1983) defined the raft-pile interaction factor (α_{rp}) as the ratio of Eq. 8.9 over Eq. 8.8:

$$\alpha_{rp} = \frac{\ln\left(r_m / nr_0\right)}{\ln\left(r_m / r_0\right)} \tag{8.10}$$

α_{rp} represents the effect of pile-soil-raft interaction on reduction of soil displacement around the pile in a piled raft system. As the next step, the effect of pile-soil-raft interaction on the raft behavior should be taken into consideration.

Timoshenko and Goodier (1970) used the theory of elasticity to determine the settlement of a shallow footing under a uniform contact pressure (q) on the surface of an elastic half space. Based on their study, the displacement at the center of a raft sitting on the ground surface is given by the following equation:

$$w_r = qd_r \frac{1-\upsilon^2}{E} = qr_r \frac{(1-\upsilon)}{G} \tag{8.11}$$

Where d_r and r_r represent the diameter and radius of raft, respectively.

Randolph (1983) claimed that the settlement of piled raft is less than shallow footing and the average of vertical displacement below a piled raft over the depth of pile (l) is obtained by the following equation:

$$\overline{w}_{pr} = qr_r \frac{(1-\upsilon)}{G} \frac{r_r}{2l}\left[\left(1-\frac{1}{2(1-\upsilon)}\right)\frac{l}{r_r}\times\left(\left(1+\frac{l^2}{r_r^{\,2}}\right)^{\frac{1}{2}}-\frac{l}{r_r}\right)+\left(1+\frac{1}{2(1-\upsilon)}\right)\sinh^{-1}\left(\frac{l}{r_r}\right)\right] \tag{8.12}$$

Assuming that $\left(\left(1+\frac{l^2}{r_r^{\,2}}\right)^{\frac{1}{2}}-\frac{l}{r_r}\right)$ is equal to 0.5 and replacing r_r with nr_0, Randolph (1983) defined the pile-raft interaction factor as follows:

$$\alpha_{pr} = \frac{nr_0}{4l}\left[\left(\left(1-\frac{1}{2(1-\upsilon)}\right)+\left(2+\frac{1}{(1-\upsilon)}\right)\sinh^{-1}\left(\frac{l}{nr_0}\right)\right)\right] \tag{8.13}$$

Randolph (1983) applied the flexibility matrix method to combine the individual stiffness of pile and raft and presented the following matrix:

$$\begin{bmatrix} 1/k_p & \alpha_{pr}/k_r \\ \alpha_{rp}/k_p & 1/k_r \end{bmatrix} \begin{bmatrix} P_p \\ P_r \end{bmatrix} = \begin{bmatrix} w_p \\ w_r \end{bmatrix} \tag{8.14}$$

Where P_p and P_r represent the acting load on pile and cap individually and w is the corresponding settlement. Moreover, k_p and k_r represent the pile and raft stiffness, respectively. The presented matrix in Eq. 8.14 could be written in the format of linear equations as follows:

$$\begin{aligned} P_p/k_p + \alpha_{pr} P_r/k_r &= w_p \\ \alpha_{rp} P_p/k_p + P_r/k_r &= w_r \end{aligned} \tag{8.15}$$

In a piled raft system with a rigid raft, the pile and the raft settle by the same amount ($w_p = w_r$). Therefore, a relationship between P_r and P_p can be obtained by equating w_p to w_r in equation 7.15:

$$P_p = P_r \frac{k_p}{k_r} \frac{(1-\alpha_{pr})}{(1-\alpha_{rp})} \tag{8.16}$$

Based on Eq. 8.16, the overall stiffness of the piled raft foundation (k_f) was given by the following equation:

$$k_f = \frac{P_r + P_p}{w_f} = \frac{P_r + P_r \dfrac{k_p}{k_r} \times \dfrac{1-\alpha_{pr}}{1-\alpha_{rp}}}{\dfrac{P_p}{k_p} + \alpha_{pr} \dfrac{P_r}{k_r}} = \frac{P_r \left[k_r \left(1-\alpha_{rp}\right) + k_p \left(1-\alpha_{pr}\right) \right]}{k_r \left(1-\alpha_{rp}\right) \left(\dfrac{P_r \dfrac{k_p}{k_r} \times \dfrac{1-\alpha_{pr}}{1-\alpha_{rp}}}{k_p} + \alpha_{pr} \dfrac{P_r}{k_r} \right)} \qquad (8.17)$$

$$k_f = \frac{k_r \left(1-\alpha_{rp}\right) + k_p \left(1-\alpha_{pr}\right)}{1-\alpha_{pr}\alpha_{rp}}$$

Eq. 8.16 was also used to determine the raft share in a piled raft unit as follows:

$$\frac{P_r}{P_r + P_p} = \frac{k_r \left(1-\alpha_{rp}\right)}{k_r \left(1-\alpha_{rp}\right) + k_p \left(1-\alpha_{pr}\right)} \qquad (8.18)$$

Where the summation of P_r and P_p shows the total applied load on piled raft foundation, and P_r is the load carried by the raft. Clancy and Randolph (1993) applied the flexibility matrix method to two adjacent unequal piles and demonstrated that the off-diagonal terms of the flexibility matrix (Eq. 8.14) are equal (i.e., $\alpha_{pr}/k_r = \alpha_{rp}/k_p$). Hence, by replacing the α_{pr} by $\alpha_{rp} \dfrac{k_r}{k_p}$ in Eq. 8.18, the raft share was determined as a function of α_{rp} alone as follows:

$$\frac{P_r}{P_r + P_p} = \frac{k_r \left(1-\alpha_{rp}\right)}{k_p + k_r \left(1-2\alpha_{rp}\right)} \qquad (8.19)$$

Accordingly, the pile share could be obtained by the following equation:

$$\frac{P_p}{P_r + P_p} = 1 - \frac{k_r \left(1-\alpha_{rp}\right)}{k_p + k_r \left(1-2\alpha_{rp}\right)} \qquad (8.20)$$

Eq. 8.19 and Eq. 8.20 were proposed by the Randolph (1983) to obtain the load sharing of piled raft foundation. Clancy and Randolph (1996) illustrated the variation of interaction factor (α_{rp})

versus pile spacing and number of piles while the effect of settlement on piled raft load sharing was neglected. However, it was shown through our conducted experimental tests that the load-sharing varies non-linearly with settlement such that the pile endures most of the applied load at small settlement and pile share decreases by increasing settlement. Accordingly, the interaction factor (α_{rp}) should be close to 1 at small settlement and decreases with increasing settlement. The variation of interaction factor with settlement is shown in the subsequent section for the non-displacement piled rafts in homogenous and layered soil.

8.3 Effect of settlement on pile-raft interaction factor

8.3.1 Homogenous sand

As mentioned previously in Chapter 3, our experimental tests on non-displacement piled raft and shallow footing were conducted on two rafts with different sizes: 100x100mm and 150x150mm. The experimental test results of the former case on a piled raft and shallow footing in addition to the pile load test measurements are used herein to develop a relationship between the pile-raft interaction factor (α_{rp}) and settlement ratio ($\frac{W}{d_r}$). The interaction factor was back-calculated for different settlements by inserting the pile stiffness, raft stiffness, and raft share obtained from the experimental results in Eq. 8.19. Figure 8-1 illustrates the variation of α_{rp} with $\frac{W}{d_r}$ for non-displacement piled raft at different densities under working loads. It is observed in this figure that the interaction factor varies non-linearly with settlement; however, the soil relative density has little impact on pile-raft interaction factor. Therefore, the medium density was used as the base of this analysis and the following equation was obtained by applying the best fitted curve through the calculated interaction factors:

$$\alpha_{rp\left(S/d_p=3.5\right)} = -0.104\ln\left(\frac{W}{d_r}\right) + 0.75 \tag{8.21}$$

The above equation corresponds to a piled raft with $3.5d_p$ pile spacing, as the raft size and pile diameter are 100x100mm and 28.6mm, respectively. A correction factor is applied to the above equation in order to account for the effect of pile spacing on pile-raft interaction factor:

$$\alpha_{rp} = \alpha_{rp\left(S/d_p=3.5\right)} \times C_{ps} \tag{8.22}$$

Where C_{ps} is the pile spacing coefficient and is determined in the subsequent section based on the results of Clancy and Randolph (1996)'s study.

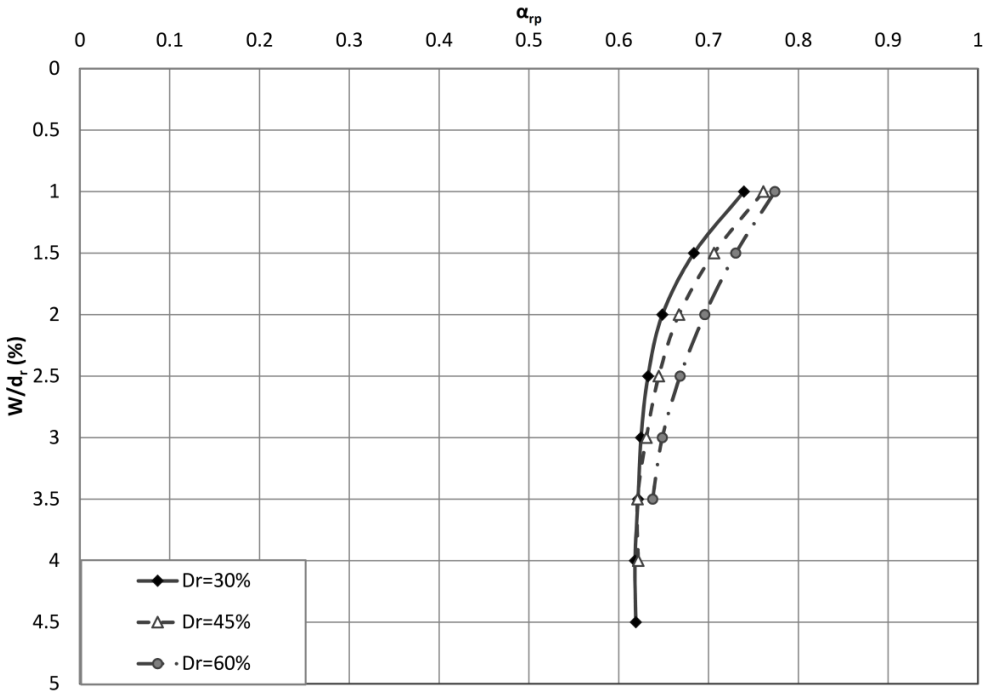

Figure 8-1 Back-calculated values of pile-raft interaction factor versus settlement ratio in different densities

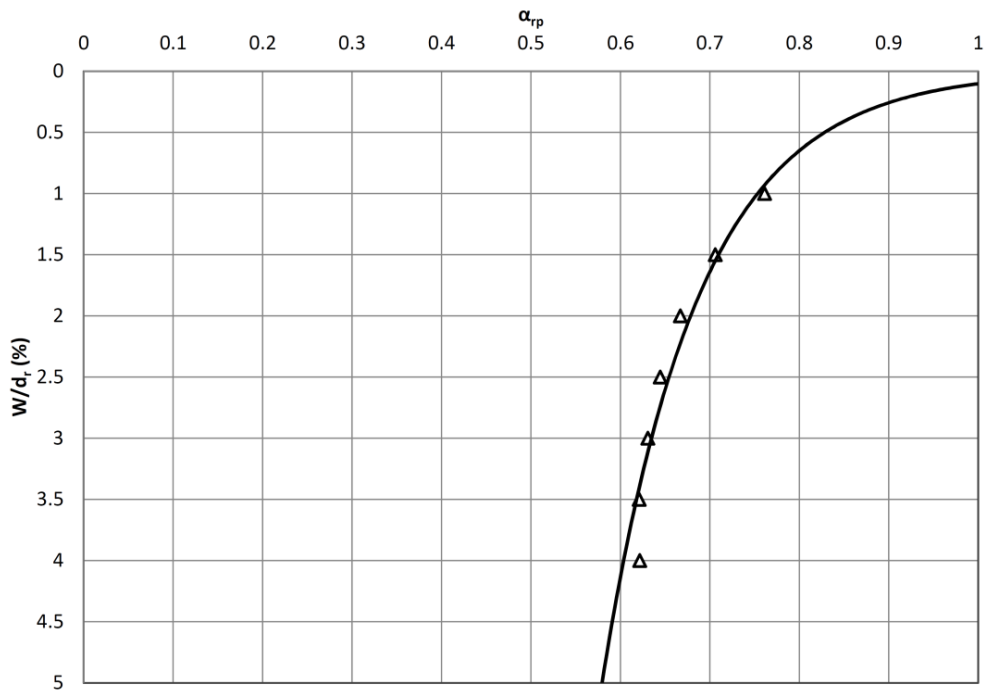

Figure 8-2 The pile-raft interaction factor versus settlement ratio when S/d_p=3.5

8.3.2 Layered sand

A similar procedure was followed to back-calculate the pile-raft interaction factor of non-displacement piled raft in layered sands. Figures 8-3 and 8-4 present the variation of pile-raft interaction factor versus settlement under two different scenarios: raft founded on loose sand and raft founded on medium sand. It is observed in these figures that α_{rp} increases by densifying the soil at the pile tip while maintaining the soil density below the raft intact.

The three equations corresponding to the interaction factor curves of layered sand in Figures 8-3 and 8-4 are captured in the following general format:

$$\alpha_{rp\left(S/d_p=3.5\right)} = a\ln\left(\frac{W}{d_r}\right)+b \qquad (8.23)$$

The values of coefficients a and b are presented in Table 8-1 for different soil density conditions.

Table 8-1 The values of coefficients a and b in Eq. 8.23

	Loose on Medium Sand	Loose on Dense Sand	Medium on Dense Sand
a	-0.097	-0.075	-0.12
b	0.79	0.81	0.83

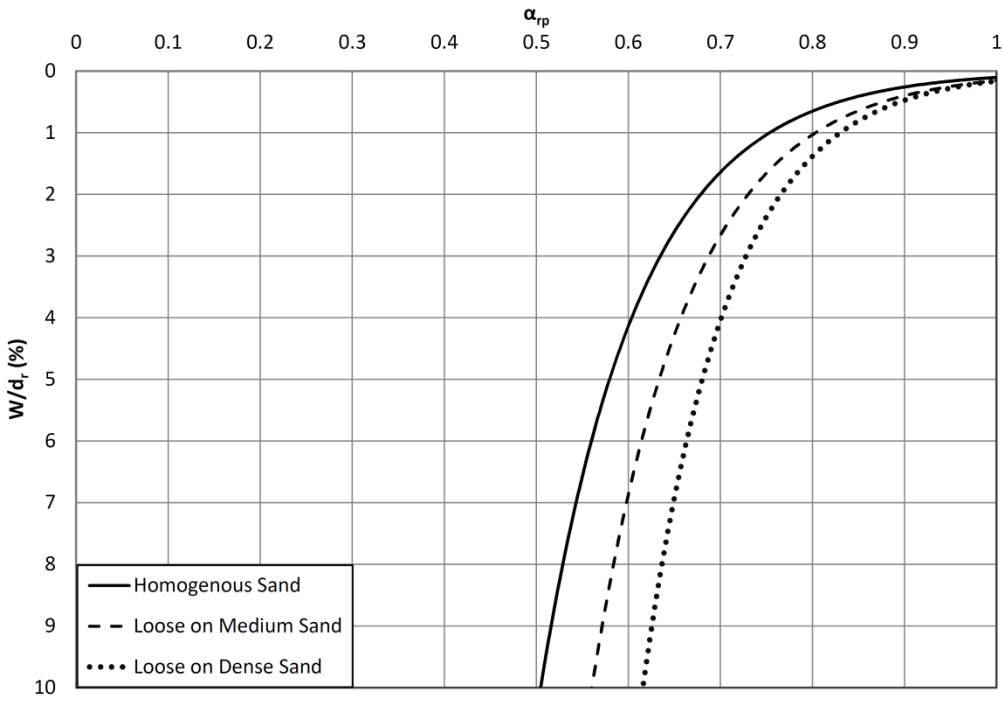

Figure 8-3 The interaction factor versus settlement ratio (W/d_r) when the raft founded on loose sand and the sand density at pile tip varies from loose to dense condition

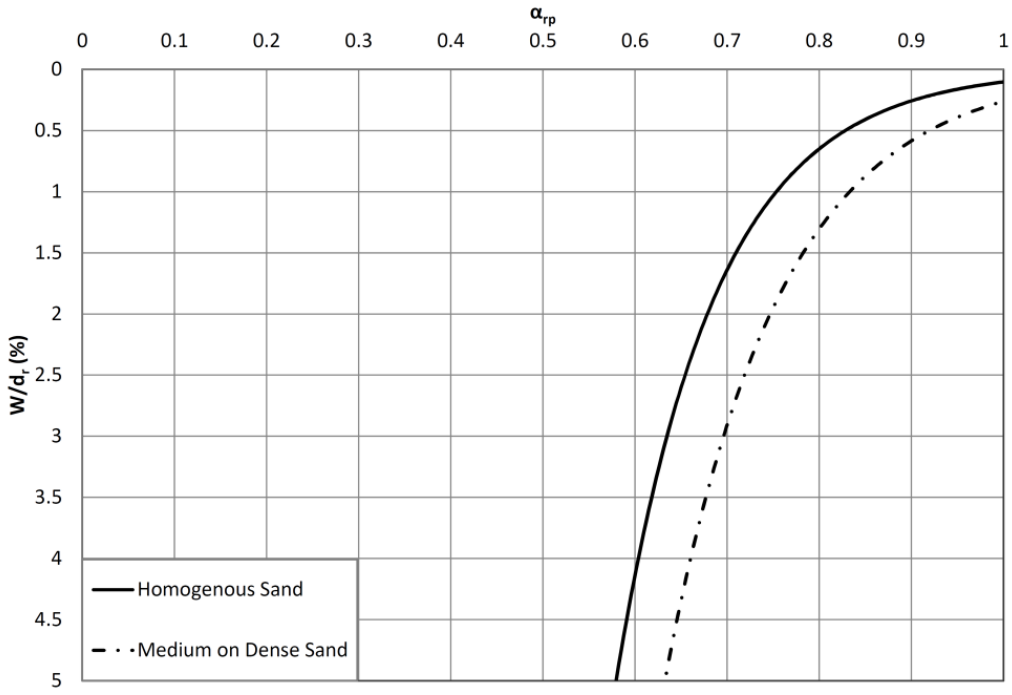

Figure 8-4 The interaction factor versus settlement ratio (W/d_r) when the raft founded on medium sand and the sand density at pile tip varies from medium to dense condition

The behavior of shallow footing on layered soil is governed by the ratio of tangent of upper layer friction angle ($\tan\phi_U$) over lower layer friction angle ($\tan\phi_L$). This fact was shown by Hanna (1981) and Hanna (1982) by conducting experimental tests on model strip footing in layered sands. The following two figures illustrate the variation of a and b coefficients with $\tan(\phi_U)/\tan(\phi_L)$. Figure 8-5 illustrates that the coefficient a varies linearly by $\tan(\phi_U)/\tan(\phi_L)$ ratio however coefficient b is not showing a significant dependency to the pattern of layered soil (Figure 8-6). Therefore, Eq. 8.23 is rewritten as follows:

$$\alpha_{rp\left(S/d_p=3.5\right)} = \left(-0.540\frac{\tan\phi_U}{\tan\phi_L} + 0.394\right)\ln\left(\frac{W}{d_r}\right) + 0.810 \tag{8.24}$$

Similar to the equation of interaction factor in homogenous sand, the pile spacing coefficient (C_{ps}) should be applied to the above equation to consider the effect of pile spacing on pile-raft

interaction factor in layered soil. The next section will discuss the pile spacing coefficient in more details.

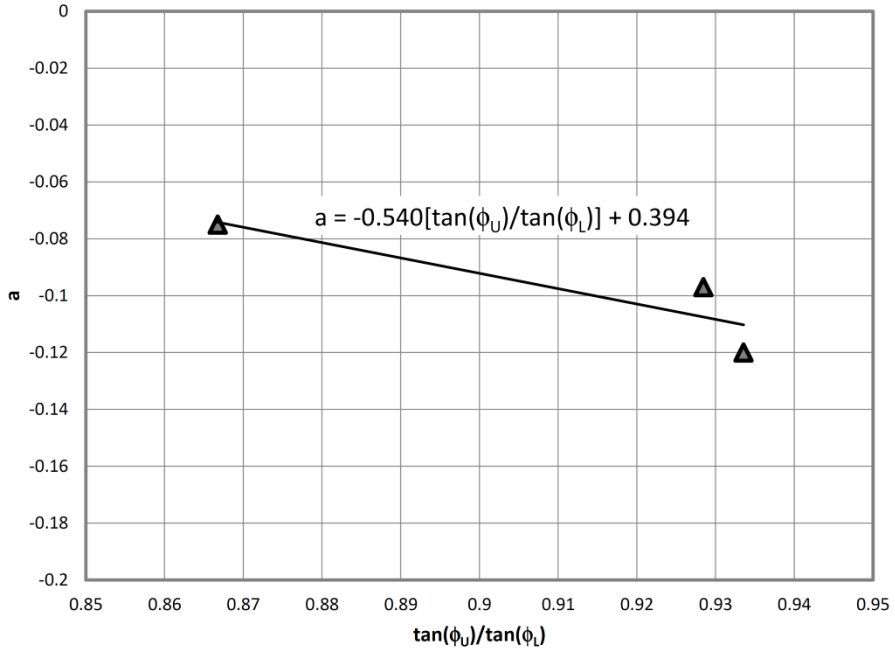

Figure 8-5 Coefficient a versus $\tan(\phi_U)/\tan(\phi_L)$

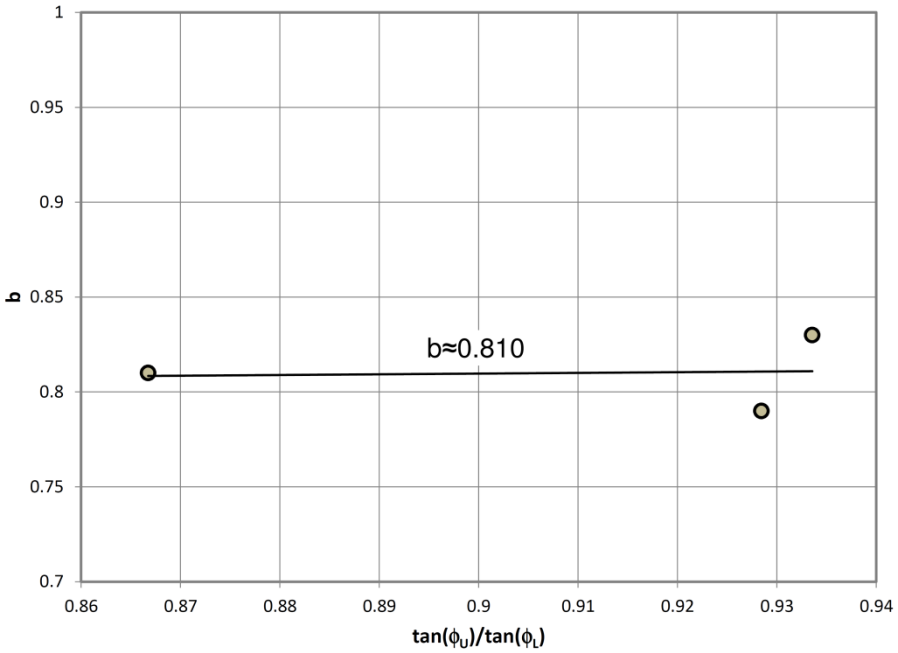

Figure 8-6 Coefficient b versus $\tan(\phi_U)/\tan(\phi_L)$

8.4 Determination of pile spacing coefficient (C_{cp})

Clancy and Randolph (1996) studied the effect of pile spacing on the interaction factor of single piled raft unit as shown in Figure 8-7. The results of this analysis was normalized by the value of interaction factor at $3.5d_p$ pile spacing in order to obtain the variation of pile spacing coefficient at different S/d_p ratio (Figure 8-8). The equation corresponding to the obtained curve represent the pile spacing coefficient as follows:

$$C_{ps} = 1.5679 \times \left(\frac{S}{d_p} \right)^{-0.359} \tag{8.25}$$

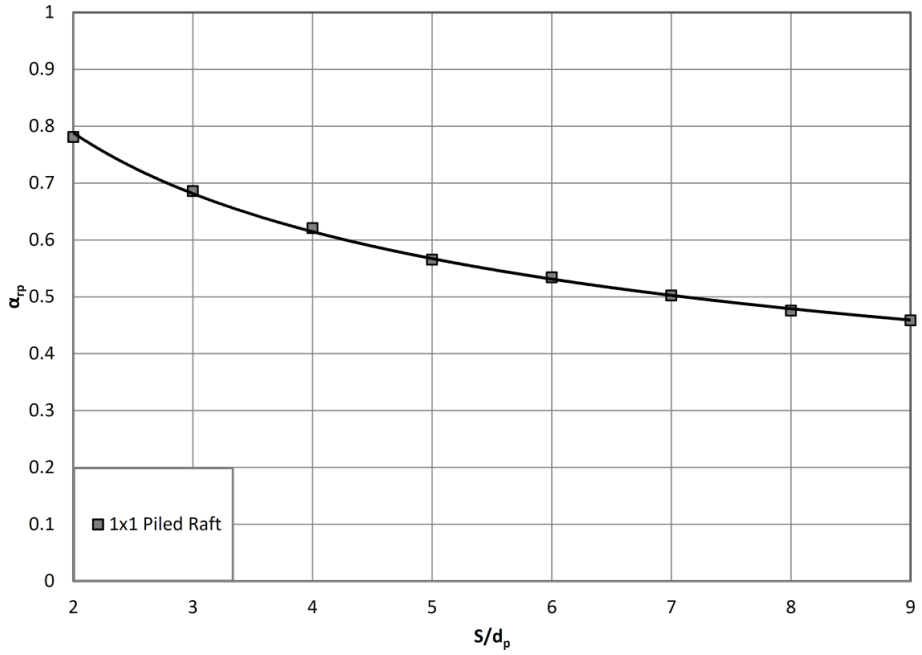

Figure 8-7 Interaction factor versus S/d_p ratio for a single piled raft unit (L/d_p=25, K_{ps}=1000, K_{rs}=10), after Clancy and Randolph (1996)

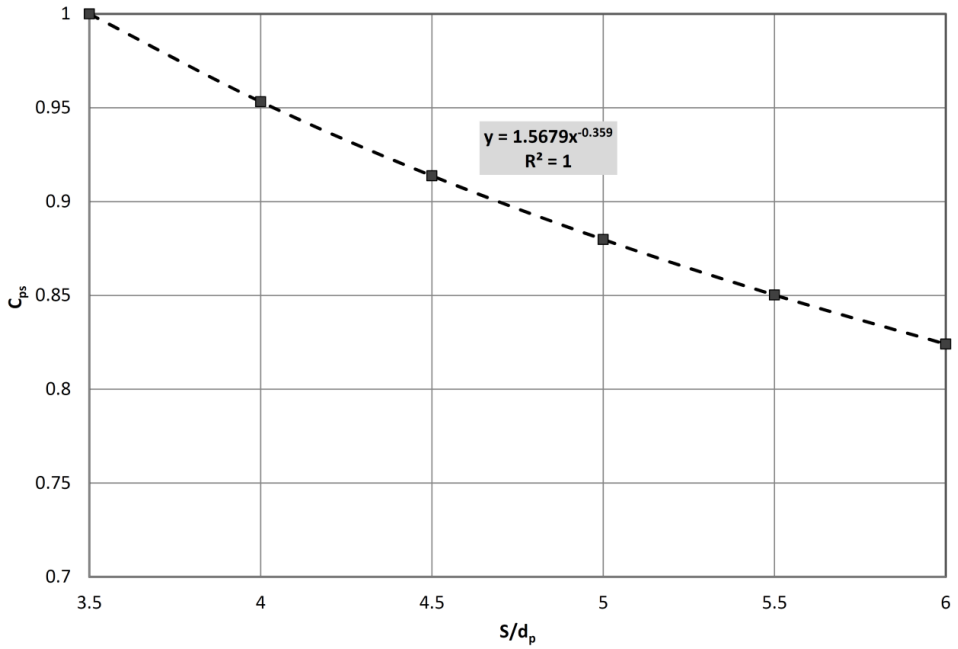

Figure 8-8 Pile spacing correction factor (C_{ps}) versus S/d_p ratio

The pile spacing coefficient is applied to Eq. 8.21 and Eq. 8.24 to incorporate the effect of S/d_p on pile-raft interaction factor and the resulting equations for homogenous and layered sand are shown in Eq. 8.26 and Eq. 8.27, respectively.

$$\alpha_{rp} = \left[-0.104 \ln\left(\frac{W}{d_r}\right) + 0.75 \right] \times \left[1.568 \times \left(\frac{S}{d_p}\right)^{-0.359} \right] \tag{8.26}$$

$$\alpha_{rp} = \left[\left(-0.540 \frac{\tan\phi_U}{\tan\phi_L} + 0.394 \right) \ln\left(\frac{W}{d_r}\right) + 0.810 \right] \times \left[1.568 \times \left(\frac{S}{d_p}\right)^{-0.359} \right] \tag{8.27}$$

The proposed equations are applicable for load sharing estimation of non-displacement piled raft under working loads when the pile spacing is more than or equal to $3.5d_p$; however, it should be noted that the pile spacing greater than $6d_p$ has no further effect on load sharing of non-

displacement piled raft (Sinha 2013). Figure 8-9 illustrates α_{rp} family curves produced by Eq. 8.26 for piled raft in homogenous sand with various pile spacing ratios. In the next section, the validity of the proposed equations is confirmed through comparison with our experimental results on non-displacement piled raft with 150x150mm raft.

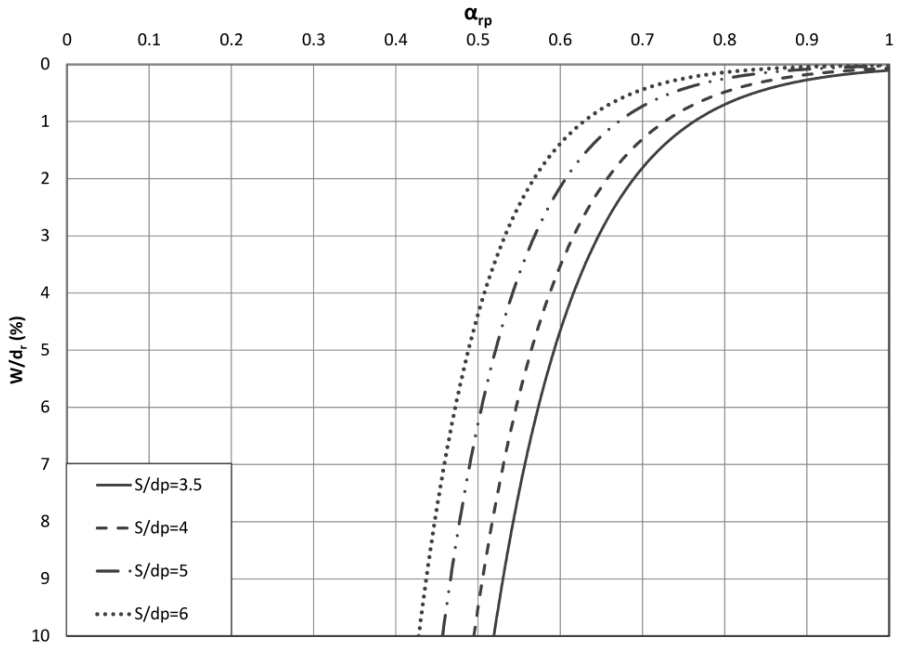

Figure 8-9 Interaction factor versus settlement ratio in different S/d_p ratios for a piled raft footing in homogenous sand

8.5 Model Validation

The results of the experimental tests on non-displacement piled raft with 150x150mm raft were employed to validate the developed analytical model. The proposed analytical model was first used to determine the load sharing of a piled raft unit with the same dimensions and soil condition as our experimentally modeled piled raft. In this regard, the unknown parameters of the analytical model, pile and raft stiffness, were determined based on the available empirical equations in the literature. Subsequently, our experimental results were compared with the obtained load sharing to validate the analytical model. The available experimental, numerical and

case studies in the literature were also used for validating the analytical model. The following presents the empirical equations used to determine the pile and raft stiffness in the analytical model.

8.5.1 Stiffness of single pile

The stiffness of axially loaded single pile was estimated based on the following equation which was originally proposed by Viggiani and Viggiani (2008):

$$w_s = \frac{d}{M}\frac{Q}{Q_{\lim}} \tag{8.28}$$

Where Q is the applied load on the pile, Q_{lim} is the bearing capacity of the single pile, d is the pile diameter, and M is a coefficient which depends on pile installation method (Table 8-2).

Table 8-2 Values of M, adapted from Viggiani et al. (2012)

Pile type	Soil type	M
Displacement	Cohesionless	80
Replacement	Cohesionless	25

Based on this equation, the stiffness of a single pile is estimated as follows:

$$K_p = \frac{Q}{w_s} = \frac{M}{d}Q_{\lim} \tag{8.29}$$

Where Q_{lim} is determined based on Meyerhof (1976)'s study.

8.5.2 Stiffness of shallow footing

The following empirical equation which was developed originally by Meyerhof (1956) and modified later by Bowles (2002), was applied in this study to determine the raft stiffness:

$$q_{all} = 19.16 N_{60} \left(\frac{S_e}{25.4} \right) \qquad B \le 1.22m$$

$$q_{all} = 11.98 N_{60} \left(\frac{3.28B + 1}{3.28B} \right)^2 \left(\frac{S_e}{25.4} \right) \qquad B > 1.22m \tag{8.30}$$

Where q_{all} is the allowable bearing capacity in kPa, N_{60} is the corrected standard penetration resistance in a depth of 2B to 3B below the foundation, B is the footing width in m, and S_e is the tolerable settlement in mm. Therefore, the raft stiffness with a safety factor (FS) of 2 is obtained as follows:

$$k_{r\left(\frac{kgf}{mm}\right)} = \frac{q_{all} \times FS \times A}{S_e} = \left(\frac{19.16 N_{60}}{25.4} \right) \times A \times 2 \times \frac{1000}{9.81} \qquad B \le 1.22m \tag{8.31}$$

Where A is the area of shallow footing in meter. The raft stiffness with a width greater than 1.22m was not shown as it surpasses the width of the raft in our experimental model. The sand SPT blow-count (N_{60}) is required to obtain the raft stiffness in different densities. Several empirical equations and tables are available in the literature to estimate the sand SPT blow-count such as Eq. 6.4 presented in Chapter 6 and the work of Knowles (1991) and Bowles (2002) presented in Tables 8-3 and 8-4, respectively. Since SPT blow-count with 60% energy ratio (N_{60}) is of interest in this study, the following scaling factor was applied to the results of Table 8-4:

$$N_{60} = \frac{70}{60} \times N_{70} \tag{8.32}$$

N_{60} was first calculated by Eq. 6.4 for loose ($\phi = 33^{\circ}$), medium ($\phi = 35^{\circ}$), and dense ($\phi = 36.8^{\circ}$) conditions and the obtained values were further confirmed against the results of Table 8-3 and adjusted Table 8-4. In the case of discrepancies between the two values, a fudge factor was applied. Based on the above methodology, N_{60} was found to be 7.5, 11, and 18 in loose, medium, and dense condition, respectively. Subsequently, the stiffness of 150x150mm raft on homogeneous loose, medium, and dense sand were calculated as 26.4, 38.7, and 63.2 kgf/mm, respectively. As Eq. 8.30 was developed for N_{60} at 2B to 3B below the foundation, the stiffness of the raft on layered soil is determined by N_{60} of the lower layer.

Table 8-3 The suggested values for estimating the corrected SPT blow-count as a function of relative density and friction angle, adapted from Knowles (1991)

Corrected SPT Blow-count	Relative Density (%)	ϕ
0-5	0-5	26-30
5-10	5-30	28-35
10-30	30-60	35-42
30-50	60-95	38-46

Table 8-4 The common range of SPT values in different densities, adapted from Bowles (2002)

Description	Very Loose	Loose	Medium	Dense	Very Dense
Relative Density (%)	0	15	35	65	85
SPT N_{70}					
Fine	1-2	3-6	7-15	16-30	?
Medium	2-3	4-7	8-20	21-40	>40
Coarse	3-6	5-9	10-25	26-45	>45
ϕ					
Fine	26-28	28-30	30-34	33-38	
Medium	27-28	30-32	32-36	36-42	<50
Coarse	28-30	30-34	33-40	40-50	

8.5.3 Comparing the predicted and measured values

To complete the analytical model validation, the raft share obtained from Eq. 8.19 is compared with that of experimental tests in different settlements for homogenous and layered sand. Figures 8-10 and 8-11 illustrate the ratio of estimated over measured raft sharing for piled raft in homogenous and layered sand, respectively. It is observed in these figures that the estimated and measured values are in close agreement and the average error of 7.5% and 7.7% in homogenous and layered soil, respectively.

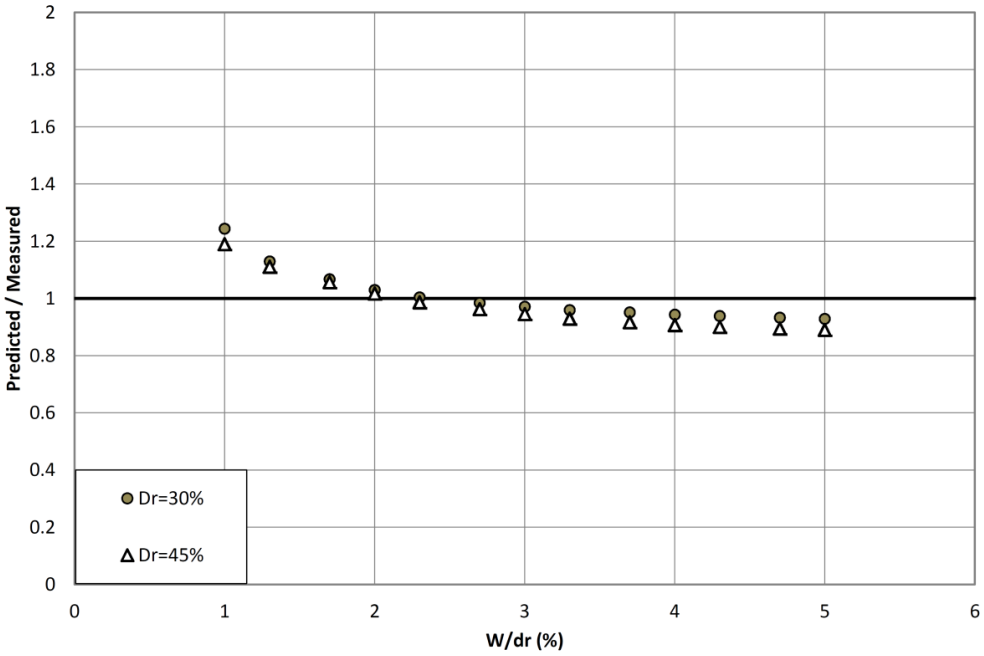

Figure 8-10 The ratio of predicted over measured load sharing in different settlement ratio for non-displacement piled raft in homogeneous sand

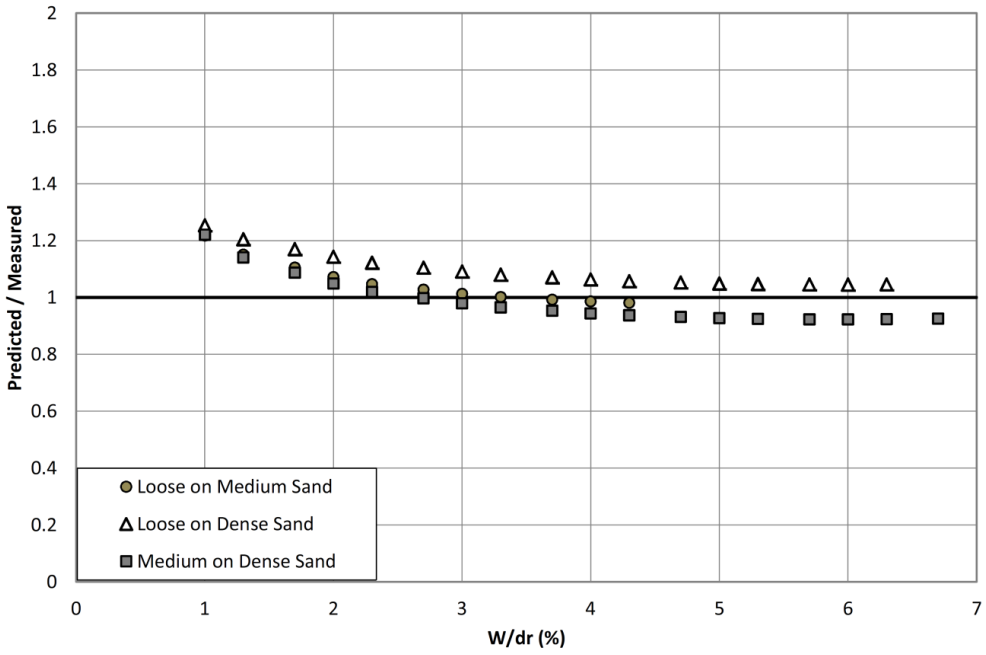

Figure 8-11 The ratio of predicted over measured load sharing in different settlement ratio for non-displacement piled raft in layered sand

The centrifuge test result, executed by Giretti (2010), on single non-displacement piled raft in loose sand (PR1) was also used to validate the developed analytical model. The information about dimensions of piled raft model and sand properties were provided previously in Table 7.1 and section 2.2.2. In order to calculate the piled raft load sharing by the proposed analytical model, the soil friction angle, SPT blow count and soil unit weight were considered equal to 33, 10, and 12 kN/m^3, respectively. Figure 8-12 illustrates the comparison between the results of centrifuge test and the analytical model values for load sharing under working load. The measured and estimated values show an acceptable consistency by following each other closely. The average error of 24% was observed in the prediction of piled raft load sharing under working load. The error between the predicted and measured values derives from the fact that the centrifuge test was conducted on piled raft in saturated sand whereas the analytical model was developed for estimation of piled raft load sharing in dry sand.

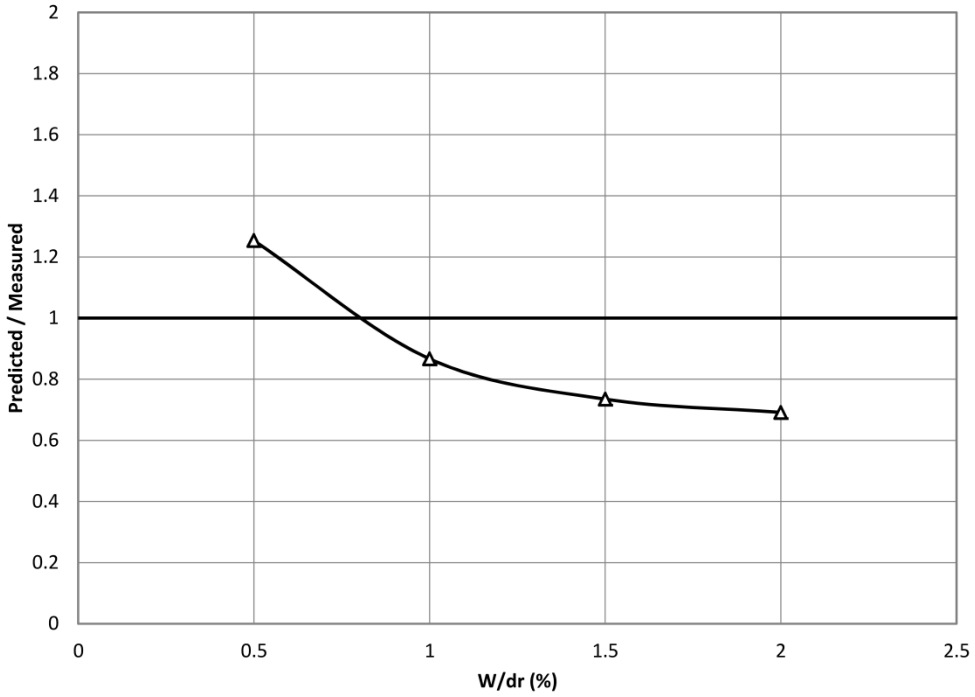

Figure 8-12 The ratio of predicted over measured load sharing in different settlement ratio for PR1 centrifuge test

The three dimensional numerical analyses, carried out by Sinha (2013), were applied herein to evaluate the accuracy of the proposed analytical model in determining the piled raft load sharing. The load sharing of non-displacement piled raft under 0.5MPa axial load were determined through Sinha's numerical study. More information about the simulated piled raft by Sinha (2013) are provided in Table 8.5. The soil modulus of elasticity was considered equal to 250MPa through the numerical analysis which simulated a very dense condition. Consequently, the soil friction angle, SPT blow count and soil unit weight were assumed as 45, 31, and 18 $kN.m^3$, respectively. The determined load sharing from numerical analyses and the developed analytical model are compared in Table 8.6. A good consistency is observed through this comparison.

Table 8-5 Specification of piled raft models in Sinha (2013)'s numerical analyses

Pile Spacing	Raft Size (LxDxt)	No. of Piles	Length of Pile (m)	Pile Diameter (m)
$4d_p$	24x24x2	36	15	1
$6d_p$	24x24x2	16	15	1

Table 8-6 Comparison between the estimated values of load sharing by the numerical analyses and the determined ones from the proposed analytical model

Pile Spacing	Reported load Share (%)		Predicted load sharing (%)	
	Raft	Pile	Raft	Pile
$4d_p$	37	63	28	72
$6d_p$	66	34	62	38

Among the available case studies, reported by Yamashita et al. (2011), the forty-seven story residential tower was employed to validate the analytical model. The building was constructed on non-displacement piled raft in a way that the raft was founded on medium sand and the pile group was embedded on dense sand. The pile group was arranged in a grid pattern with average pile spacing of $3.96d_p$. This case was described in more details previously in Chapter 2 (section 2.4.4). To calculate the piled raft load sharing by the proposed analytical model, the friction angle, SPT blow count, and unit weigh of the soil around the pile were assumed equal to 35, 11.25, and 15.25kN/m^3. Since the piles were founded on dense sand, the soil friction angle and soil unit weight at pile tip were considered as 39 and 16.24kN/m^3. The predicted and measured load sharing for the aforementioned case study is presented in Table 8.7. The consistency of the predicted and measured raft share values are in acceptable level.

Table 8-7 Comparison between the measured load sharing with the estimated one from the proposed analytical model

Instrumented pile	Foundation settlement (mm)	W/d_r (%)	Measured load sharing (%)		Predicted load sharing (%)	
			Raft	Pile	Raft	Pile
7D	24	0.3	13	87	10	90

8.6 Design procedure

A series of design procedures are proposed based on the analytical and empirical models. The procedure is applicable to non-displacement piled raft with identical piles in grid pattern where the pile spacing is greater than or equal to $3.5d_p$.

Step 1: With the knowledge of maximum acceptable settlement, pile spacing ratio, and soil properties, determine the raft share of a single piled raft unit based on the empirical or analytical model introduced in Chapter 7 and Chapter 8, respectively.

Step 2: Apply Eq. 8.30 to determine the allowable raft load for the given settlement and width of d_r (B).

Step 3: Divide the result of step 2 by the raft share determined in step 1 to find the total allowable load on the single piled raft unit.

Step 4: Multiply the determined load for a single piled raft unit by the number of piles to determine the total allowable load on the piled raft.

Step 5: Compare the total allowable load from step 4 with the applied load on the foundation for design validation: if the applied load on foundation is less than or equal to the allowable load, the design is acceptable.

Chapter 9

Conclusion and Recommendations

This dissertation addressed implications of various parameters in the problem of piled raft load sharing determination. In particular, the effect of foundation settlement, soil density in homogenous and layered sand, raft width ratio, number of piles, and pile installation method were investigated through experimental and numerical analyses. The analyses results were applied to develop empirical and analytical models to estimate the load sharing of piled raft foundations in sandy soil. This chapter provides a summary of the work and suggested directions for continuing research in this area.

9.1 Thesis summary

This research stemmed from various experimental tests performed on shallow foundation, single pile, and single piled raft unit. Throughout the experiments, the pile length, pile diameter, and raft thickness were constant while the raft width, soil condition and pile installation method were variable. Due to the single piled raft nature of our experimental set-up, we further investigated the effect of number of piles through three dimensional numerical analyses. The following conclusions were drawn from these analyses:

- The piled raft footing is more capable of controlling settlement in comparison with single pile and shallow footing.
- The ultimate bearing capacity of piled raft is more than summation of bearing capacity of shallow footing and single pile.
- The load sharing of piled raft footing varies non-linearly with settlement: raft share increases as a function of settlement ratio (W/d_r).

- Load sharing of displacement piled raft before reaching failure varies by relative soil density–the pile share increases as a function of soil density. Whereas, the load sharing of non-displacement piled raft under working loads is independent of soil density.
- The pile share of non-displacement piled raft in loose sand is approximately 75 percent of the pile share in displacement piled raft.
- Particle size distribution of sand has inconsiderable effect on the load sharing of piled raft footing.
- Raft thickness and pile length have inconsiderable impact on the piled raft load sharing.
- The raft share increases noticeably by increasing the raft width ratio.
- The pile group takes the majority of the applied load on the piled raft footing when the pile spacing is less or equal $3d_p$.
- The raft share increases by increasing the pile spacing until it reaches a constant value at $S/d_p=6$.
- Dissimilarity in the soil density has considerable impact on the load sharing of non-displacement piled raft–increasing the soil density at pile tip in layered soil increases the pile share.
- Increasing the number of identical piles in a non-displacement piled raft when the pile spacing is more than or equal to $3.5d_p$, does not greatly impact the load sharing.
- The amount of carried load by the piles in a rigid piled raft is not a function of pile position.

Based on the above observations, two settlement-based empirical and analytical models were developed to estimate the load sharing between foundation elements of non-displacement piled raft in homogeneous and layered soils. The proposed empirical model was validated based on the

available experimental and field observations in the literature. The analytical model was developed by incorporating the effect of settlement on the interaction factor introduced by Randolph (1983). Our experimental test results on non-displacement piled raft (100x100mm raft), single pile and shallow footing were used to generate a novel interaction factor as a function of settlement ratio in homogenous and layered sand. The effect of pile spacing on interaction factor was applied as a correction factor to the newly generated function. The experimental test results on non-displacement piled raft with 150x150mm raft were used to validate the proposed analytical model. The analytical model results followed closely the measured experimental values. The proposed models were also validated against the available centrifuge and field test results in the literature.

The developed models are applicable to routine practices where the following assumptions are reasonable:

- The pile and raft are rigid
- Pile-soil-pile interaction is negligible
- The pile group is uniformly distributed on the raft area
- The piles are identical.

9.2 Future research directions

This study provides valuable insights on load sharing mechanism of piled raft foundations and sets the ground for future research directions in this area:

1. In this thesis, the load sharing mechanism of piled raft was studied under vertical load at the center of raft; however, the effect of load eccentricity and load inclination on load sharing is still an open area of research.

2. The effect of raising ground water table on load sharing mechanism could be studied by executing small scale tests.
3. All the available tests in the literature, including this study, reported the load sharing instantly after applying the load. Therefore, the long term behavior of piled raft foundation under working load (creep) could be studied in small scale or field tests.
4. The load sharing mechanism of piled raft in layered sand was investigated in this thesis where the higher density sand was placed at the pile tip. However, the effect of lower density sand at the pile tip could be also investigated.
5. The effect of variable pile length and non-uniform distribution of pile could be further investigated.

References

Akinmusuru, J.O. 1980. Interaction of piles and cap in piled footings. Journal of the Geotechnical Engineering Division, ASCE, 106(11), pp. 1263-1268.

Al-Mahdi, A.I. 2004. Effect of Loading Rate on Pile Groups in Sand. Proceeding of International Conference on Geotechnical Engineering, Sharjah – UAE.

Al-Mahdi, A.I. 2006. Experimental investigation of the behavior of pile groups in sand under different loading rates. Geotechnical and Geological Engineering, 24, pp. 889–902.

Anagnostopoulos, C. and Georgiadis, M. 1998. A simple analysis of piles in raft foundations. Journal of Geotechnical Engineering, 29 (1), pp. 71-83.

Bowles, J.E. 2002. Foundation Analysis and Design, McGraw-Hill, New York.

Borland, J. B. 1995. Piles as Settlement Reducers. In Proceedings of the 18th Italian National Geotechnical Congress, Pavia, Italy, Vol. 2. pp. 21-34.

Borland, J. B., Broms, B.B., De Mello, V.F.B 1977. Behaviour of foundations and structures. In Proceedings of the 9th International Conference on Soil Mechanics and Foundation Engineering, Tokio, Japan, Vol. 2, pp.495-546.

Cao, X.D., Wong, I.H., and Chang, M.F. 2004. Behavior of model rafts resting on pile-reinforced sand. Journal of Geotechnical and Geotechnical Engineering, ASCE, 130(2), pp. 129-138.

Cerato A.B., and Lutenegger, A.J. 2006. Bearing capacity of square and circular footings on a finite layer of granular soil underlain by a rigid base. Journal of Geotechnical and Geoenvironmental Engineering, ASCE, 132(11), pp. 1496–501.

Clancy, P., and Randolph, M.F. 1993. An approximate analysis procedure for piled raft foundations. International Journal for Numerical and Analytical Methods in Geomechanics, 17(12), pp. 849–869.

Clancy, P., and Randolph, M.F. 1996. Simple Design Tools for Piled Raft Foundations. Géotechnique, 46(2), pp. 313-328.

Comodromos, E.M., Papadopoulos, M.C., and Rentzeperis, I.K. 2009. Pile foundation analysis and design using experimental data. Computers and Geotechnics, 36, pp. 819–36.

Cooke, R.W., Smith, D.W.B., Gooch, M.N., and Sillet, D.F. 1981. Some observations of the foundation loading and settlement of a multi-story building on a piled raft foundation in London Clay. Proc. ICE, 107(1), 433-460.

El Sawwaf, M. 2010. Experimental study of eccentrically loaded raft with connected and unconnected short piles, Journal of Geotechnical and Geoenvironmetnal Engineering, ASCE, 136(10), pp. 1394-1402.

El-Garhy, B., Galil, A.A., Youssef, A.F. and Raia, M.A. 2013. Behavior of raft on settlement reducing piles: Experimental model study. Journal of Rock Mechanics and Geotechnical Engineering, Vol. 5, pp. 389-399.

El-Mossallamy, Y., Lutz, B., and Richter, T. 2006. Innovative application of piled raft foundation to optimize the design of high-rise buildings and bridge foundations. Proceedings of 10th International Conference on Piling and Deep Foundations (DFI/EFFC - Amsterdam, 31 May-2 June), Eds. J. Lindberg, M. Bottiau & A.F. VanTol, 269-278.

Fioravante,V. 2011. Load transfer from a raft to a pile with an interposed layer. Geotechnique, 61(2), pp. 121-132.

Fioravante,V., and Giretti, D. 2010. Contact versus noncontact piled raft foundation. Canadian Geotechnical Journal, 47, pp. 1271-1287.

Fioravante,V., Giretti, D., and Jamiolkowski, M. 2008. Physical modeling of raft on settlement reducing piles, Proceeding, Research to Practice in Geotechnical Engineering Congress, ASCE, 206-229.

Fleming, W.G.K., Weltman, A.J., Randolph, M.F., and Elson, W.K. 2009. Piling Engineering. London, 398p.

Franke, E. 1991. Measurements beneath piled rafts. Keynote Lecture, ENPC Conf., Paris, pp. 1-28.

Franke, E., Lutz, B. and El-Mossallamy, Y. 1994. Measurements and Numerical Modelling of High-Rise Building Foundations on Frankfurt Clay. Vertical and Horizontal Deformation of Found. And Embankments, Geotech. Spec. Pub. 40, ASCE, 2, pp. 1325-1336.

Giretti, D. 2010. Modeling of piled raft foundation in sand. Ph.D. thesis, University of Ferrara, Italy.

Hanna, A.M. 1982. Bearing capacity of foundations on a weak sand layer overlying a strong deposit. Canadian Geptechnical Journal, 19(3), 392-396.

Hanna, A.M. 1981. Foundation on strong sand overlying weak sand. Journal of the geotechnical engineering Division, ASCE, 107(GT7), 915-927.

Hanson, S. 1993. Interaction Problems Related to the Installation of Pile Groups. Seminar on Deep Foundations on Bored and Auger Piles, BAP2, Ghent, pp. 59-66.

Hanson, S., Hofmannn, E., and Mosesson, J. 1973. ÖstraNordstaden, Gothenburg. Experience concerning a difficult foundation problem and its unorthodox solution. Proc. 8th ICSMFE, Moscow, Vol. 2, pp. 105-110.

Hartmann, F., and Jahn, P. 2001. Boundary element analysis of raft foundations on piles", International Journal of Theoretical and Applied Mechanics, Vol- 36, pp 351-366.

Hatanaka, M. and Uchida, A. 1996. Empirical correlation between penetration resistance and internal friction angle of sandy soils. Soils and Foundations, 36(4), pp. 1-10.

Horikoshi, K. and Randolph, M.F. 1997. On the definition of raft-soil stiffness ratio for rectangular raft. Geotechnique, 47(5), pp. 1055-1061.

Katzenbach, R., Arslan, U. and Moormann, C. 2000. Piled raft foundation projects in Germany. Design Application of Raft Foundations. J.A. Hemsley Ed., Telford. pp. 323-390.

Lee J, and Salgado, R. 2005. Estimation of bearing capacity of circular footings on sands based on cone penetration test. Journal of Geotechnical and Geoenvironmental Engineering, ASCE, 131(4), pp. 442–52.

Lee, J., Park, D., and Choi, K. 2014. Analysis of load sharing behavior for piled rafts using normalized load response model. Computers and Geotechnics, 57, pp. 65–74.

Lee, S.H., and Chung, C.K. 2005. An experimental study of the interaction of vertically loaded pile groups in sand. Canadian Geotechnical Journal, 42, pp. 1485–1493.

Liu, J.L., Yuan, Z.L., and Shang, K.P., 1985. Cap–pile–soil interaction of bored pile groups. In Proceedings of the 11th International Conference on Soil Mechanics and Foundation Engineering, San Francisco, Calif., 12–16 August 1985. A.A. Balkema, Rotterdam, The Netherlands. Vol. 3, pp. 1433–1436.

Lv, Y., Liu, H., Ng, C.W.W., Ding, X. and Gunawan, A. 2014. Three-dimensional numerical analysis of the stress transfer mechanism of XCC piled raft foundation. Computers and Geotechnics, 55, pp. 365–377.

Mandolini, A. 2003. Design of Piled Raft Foundations: Practice and Development. In Proceedings of the 4th International Geotechnical Seminar on Deep Foundations on Bored and Auger Piles, Ghent, Van Impe, W.F. Ed. Millpress, Rotterdam, pp. 59-80.

Mayne, P.W., and Poulson, H.G. 1999. Approximate Displacement Influence Factors for Elastic Shallow Foundations. Journal of Geotechnical and Geoenvironmental Engineering, ASCE, 125(6), pp. 453-460.

Meyerhof, G.G. 1956. Penetration Tests and Bearing Capacity of Cohessionless Soils. JSMFD, ASCE, vol. 82, SM 1, pp. 1-19.

Meyerhof, G.G. 1976. Bearing Capacity and Settlement of Pile Foundations. Journal of the Geotechnical Engineering Division, ASCE, 102(GT3), pp. 197–228.

Neto, O.D.F., Cunha, R.P., Santos, O.F., Albuquerque, P.J.R. and Garcia, J.R. 2014. Comparison of Numerical Methods for Piled Raft Foundations. Advanced Materials Research Vols. 838-841, pp. 334-341.

Oh, E.Y.N., Bui, Q.M., Surarak, C., and Balasurbamaniam, A.S. 2008b. Parametric study on piled raft foundation in sand using numerical modeling. In 20th Australasian Conference on the Mechanics of Structures and Materials (ACMSM20).

Oh, E.Y.N., Huang, M., Surarak, C., Adamec, R., and Balasurbamaniam, A.S. 2008a. Finite element modeling for piled raft foundation in sand. Eleventh East Asia-Pacific Conference on Structural Engineering& Construction (EASEC-11), Taipei, Taiwan.

Omeman, Z.M. 2012. Load sharing of piled-raft foundations in sand subjected to vertical loads. Ph.D. Thesis. Concordia University, Montreal, Quebec.

Phuong, D.L. 1993. Footings with settlement-reducing piles in non-cohesive soil. Ph.D Thesis. University of Technology, Göteborg, Sweden.

Phuong, DL. 2010. Piled raft – a cost-effective foundation method for high-rises. Geotechnical Engineering Journal of the SEAGS&AGSSEA, 41(3), pp. 1–12.

Poulson, H.G. 1991. Analysis of piled strip foundations. Computer Methods & Advances in Geomechanics, Beer et al Ed., Balkema, Rotterdam, Vol. 1, pp. 183- 191.

Poulson, H.G. 1994. An approximate numerical analysis of pile-raft interaction. International Journal for Numerical and Analytical Methods in Geomechanics, London, 18(2), pp. 73–92.

Poulson, H.G. 2001a. Piled Raft Foundations: Design and Applications. Geotechnique, 51(2), pp. 95-113.

Poulson, H.G. 2001b. Methods of Analysis of Piled Raft Foundations. A Report Prepared on Behalf of Technical Committee TC18 on Piled Foundations. International Society of Soil Mechanics and Geotechnical Engineering.

Poulson, H.G. and Davis, E.H. 1980. Pile Foundation Analysis and Design. Wiley, New York.

Poulson, H.G., Small, J.C., Ta, L.D., Sinha, J. and Chen, L. 1997. Comparison of some methods for analysis of piled rafts. In Proceedings of the 14th International Conference on Soil Mechanics and Foundation Engineering, Hamburg, Vol. 2, pp. 1119-1124.

Prakoso, W.A., and Kulhawy, F.H. 2001.Contribution to piled raft foundation design. Journal of Geotechnical and Geoenvironmental Engineering, ASCE, 127(1), pp. 17-24.

Randolph, M.F. 1983. Design of Piled Raft Foundations. Proc. Int. Symp. on Recent Developments in Laboratory and Field Tests and Analysis of Geotechnical Problems, Bangkok, pp 525-537.

Randolph, M.F. 1994. Design methods for pile groups and piled rafts. S.O.A. Report, 13 ICSMFE, New Delhi, 5, pp. 61-82.

Randolph, M.F. and Worth, C.P. 1978. A simple approach to pile design and the evaluation of pile tests. Behaviour of Deep Foundations, ASTM STP 670, pp. 484-499.

Randolph, M.F., Jamiolkowski M.B. and Zdravkovic, L. 2004. Load carrying capacity of foundations. Advances in Geotechnical Engineering, The Skempton Conference, Institution of Civil Engineers London, Jardine, R. J., Potts, D.M. Higgins, K.G. Eds Thomas Telford London, Vol. 1, pp. 207-240.

Sedran, G., Stolle, D. F.E., and Horvath R.G. 2001. An investigation of scaling and dimensional analysis of axially loaded piles. Canadian Geotechnical Journal, 38, pp. 530-541

Sinha, A. 2013. 3-D modeling of piled raft foundation. PhD Thesis, Concordia University, Montreal, Quebec.

Sinha, J. 1997. Piled Raft Foundations Subjected to Swelling and Shrinking Soils. PhD Thesis, University of Sydney, Australia.

Ta, L.D., and Small, J.C. 1996. Analysis of piled raft systems in layered soils. International Journal for Numerical and Analytical Methods in Geomechanics, 20(1), pp. 57–72.

Timoshenko, S.P. and Goodier, J.N. 1970. Theory of elasticity. 3rd edition, McGraw-Hill, New York.

Van Impe, W.F., and Clerq, L. 1995. A Piled Raft Interaction Model. Geotechnica, No.73, pp. 1-23.

Viggiani, C. 1998. Pile groups and piled rafts behaviour. Deep Foundations on Bored and Auger Piles, BAP III, van Impe and Haegman (eds), Balkema, Rotterdam, pp. 77-90.

Viggiani, C. 2001. Analysis and design of piled foundations.1st Arrigo Croce Lecture, RivistaItaliana di Geotecnica, No.1, pp. 47-75.

Viggiani, C., and Viggiani, G.M.B. 2008. Il ruolo dell'osservazione delle opera nell'Ingegneria Geotecnica, Diagnostica per la tutela e la conservazione dei materiali nel costruito, Diacomast 2, Acos srl, S. Leucio.

Viggiani, C., Mandolini, A., and Russo, G. 2012. Piles and piles foundations. Taylor & Francis, London & New York.

Wang, A. 1996. Three dimensional finite element analysis of pile groups and piled-rafts. PhD dissertation, University of Manchester, U.K.

Yamashita, K., and Yamada, T. 2007. Settlement and load sharing of a piled raft foundation combined with grid-form soil-cement walls on soft ground. Proc. IWDPF 07, pp. 299-305.

Yamashita, K., Hamada, J., and Soga, Y., 2010. Investigation of settlement and load sharing on piled raft by monitoring full-scale structures. GeoShanghai 2010 International Conference, Geotechnical Special Publication No. 205, ASCE, pp. 26-33.

Yamashita, K., Kakurai, M., and Yamada, T. 1994. Investigation of a piled raft foundation on stiff clay. Proc. 13th ICSMFE, Vol. 2, pp. 543-546.

Yamashita, K., Yamada, T., and Hamada, J. 2009. Recent case histories on monitoring settlement and load sharing of piled rafts in Japan." Deep Foundation on Bored and Auger Piles, Taylor & Francis Group, London, pp. 181-203.

Yamashita, K., Yamada, T., and Hamada, J. 2011. Investigation of settlement and load sharing on piled raft by monitoring full-scale structures. Soils and Foundations, 51(3), pp. 513-532.

Sievert, L. 1957. Compensated Friction-pile Foundation to Reduce the Settlement of Buildings on Highly Compressible Volcanic Clay of Mexico City. Proc. 4 ICSMFE, London, V.2.

Appendices

Appendix A

Friction angle between soil and sand paper (Direct Shear Test)

Definition

The angle of friction between soil particles and other materials (δ) is defined as follows:

$$\delta = \tan^{-1}\left(\frac{\tau}{\sigma_v'}\right)$$

where σ_v' and τ are the effective vertical stress and shear stress, respectively.

Same as the soil friction angle, the δ is also a function of relative density and size, shape and distribution of soil mass. In order to find the appropriate sand paper grit for covering the surface of the pile and raft, a series of direct shear test were run to determine the friction angle between the sand and different grits of sand paper.

Applicable ASTM Standard:

- ASTM D-3080- Standard Method for Direct Shear Test on Soils under Consolidated Drained Conditions.

Equipment

1. Direct shear box and machine
2. Caliper

3. Tamper for compacting soil
4. Different grades of sand paper
5. Wood blocks

Procedure

The volume of upper and lower half of the direct shear box was measured with the use of a caliper. The height of the lower part of shear box was measured as 18.54mm. Therefore, the wood blocks were cut in the size of $60 \times 60 \times 18.54 mm$ to fit exactly in the lower half. The top surface of the wood blocks was covered by sand paper. Different grades of sand paper (80, 150, 220, and 400) were tested to find the appropriate sand paper grade which simulates the concrete roughness. The height of the soil sample was considered to be 15mm in all of the tests. Therefore, the volume of the sample is $54cm^3$. The direct shear tests were done at three different relative densities (30, 45, and 60%).

Based on the dry density of soil for each relative density, the weight of the soil sample was calculated. The wood block was used to fill the lower half of the shear box and the weighted sample used to fill the upper part of shear box and compacted until it reached the 15cm height. The procedure of this test is visualized in the following figure.

Figure A-1 The procedure for preparing the wood blocks, covering with different sand papers, preparing the direct shear test sample

The direct shear tests were run under a strain control condition. The upper half of the direct shear box was moving at a constant rate of 10mm/min. The shear force (S) was recorded for every 0.05mm of horizontal displacement. By plotting the shear stress (τ) over horizontal displacement, the shear stress at failure was determined. Each soil specimen was tested at three different normal forces (0.133, 0.267, and 0.4 kN). A graph of shear stress at failure (τ_f) versus normal stress (σ_v') was plotted for each soil specimen. The friction angle between the sand paper and sand particles (δ) has been determined from the slope of the straight line plot of τ_f versus σ_v'. Two of these graphs are shown in Figures A-2 and A-3 as samples:

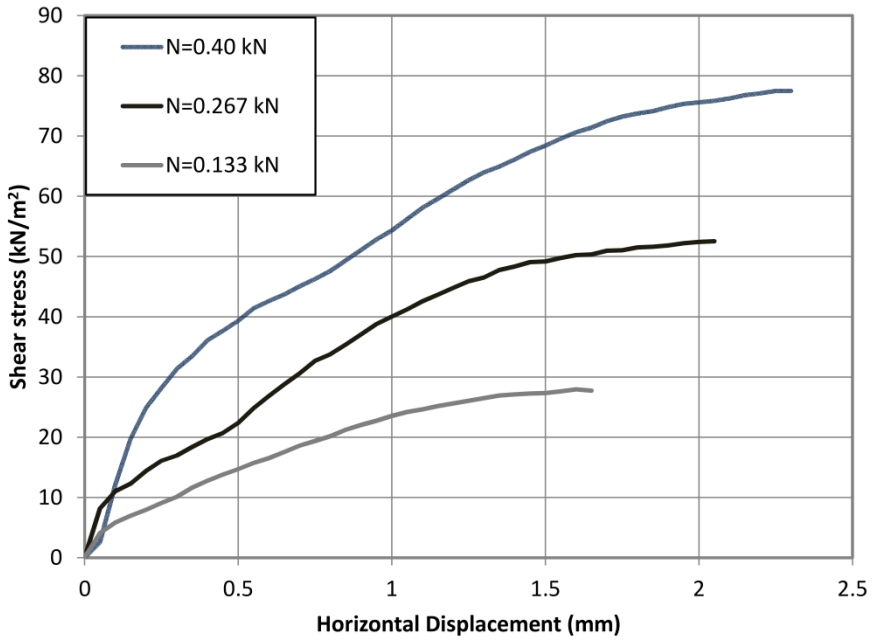

Figure A-2 Variation of horizontal displacement with shear stress in different vertical stress for clean silica sand 40-10 (Dr=30%) and sand paper 150

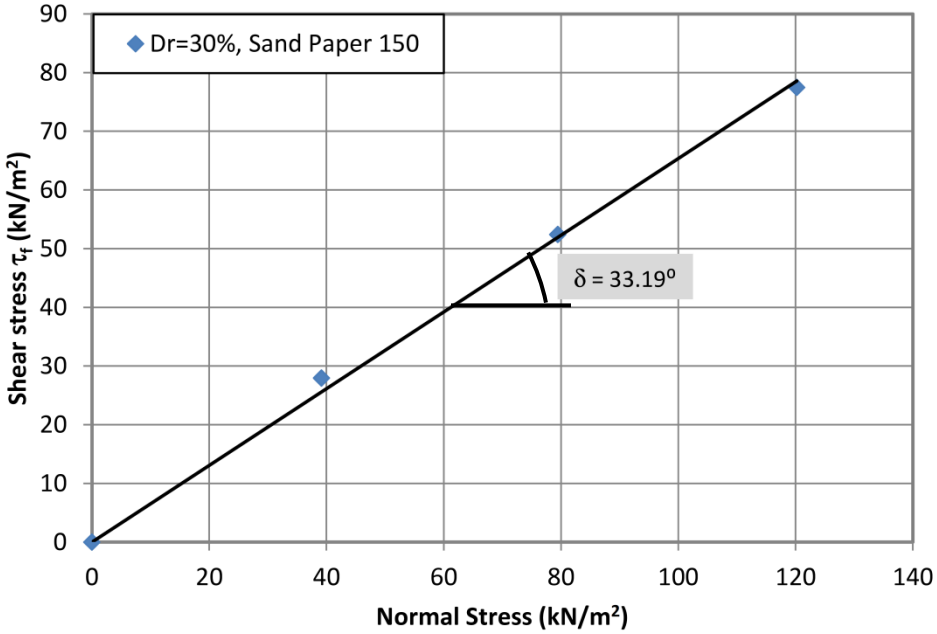

Figure A-3 Variation of shear stress with normal stress for clean silica sand 40-10 (Dr=30%) and sand paper 150

The friction angle between concrete and sand particles is almost equal to soil friction angle (ϕ). The following figure shows the variation of δ / ϕ with increasing the sand paper grade for a relative density of 30% in clean silica sand 40-10.

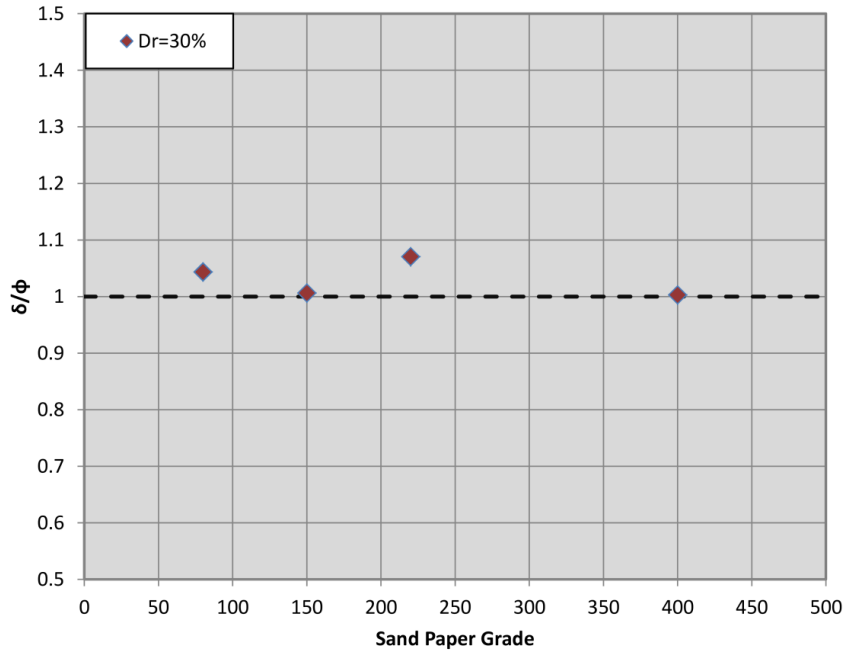

Figure A-4 Determined δ/ϕ ratio with different grades of sand paper and 40-10 Silica sand in 30% density

Based on the results of these tests, the sand paper with grade of 150 was selected for covering the surface of the pile and raft.

In the second phase of this study, the friction angle between soil particles at different relative densities with sand paper (150) has been determined. The results of these tests are shown in the following figure.

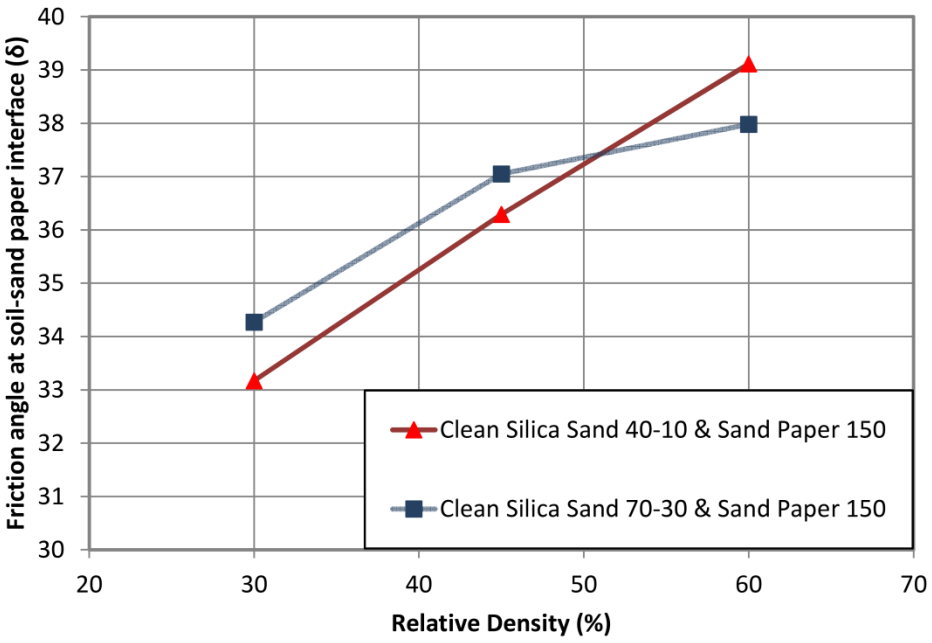

Figure A-5 Variation of friction angle between sand particles and sand paper 150 with relative density for 40-10 and 70-30 Silica sand

By combining the results of these tests with direct shear test results on clean silica sand, the variation of ϕ and δ with relative density are shown in the following figures.

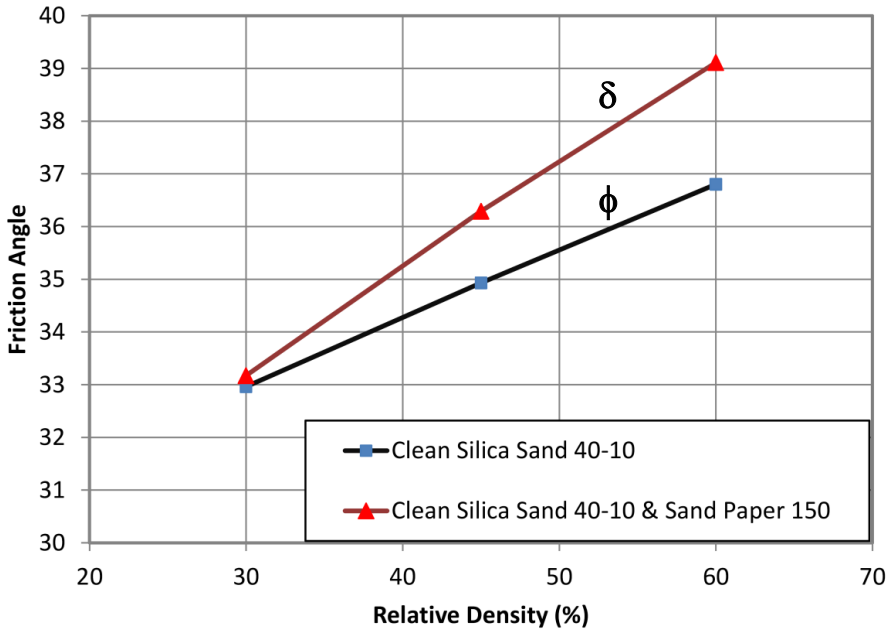

Figure A-6 Variation of ϕ and δ with relative density in Silica sand 40-10

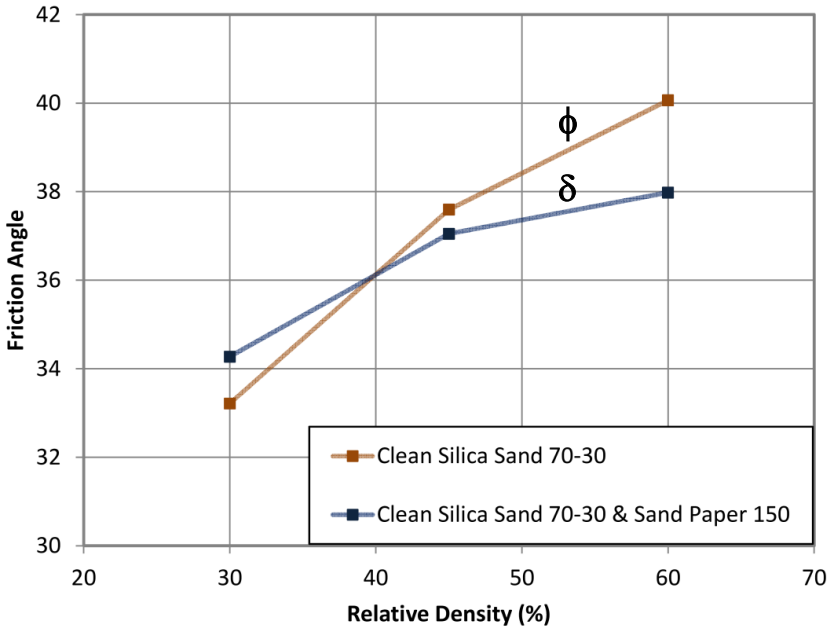

Figure A-7 Variation of ϕ and δ with relative density in Silica sand 70-30

Appendix B

Compaction Test

Definition

In order to deposit the dry sand mass in the test tank, two different methods could be implemented: 1) Pluviation of dry sand in air from a given height; the relative density of soil in this method could be controlled by changing the height of fall, 2) Compacting the soil in relatively thin layers; the density of soil is a function of compaction energy which is applied to each layer. The energy of compaction per unit volume could be calculated by the following equation.

$$\frac{E}{V} = \frac{W \times H \times N}{V}$$

Where, W is the weight of hammer, H is the height of fall, N is the number of drops, and V is the volume of compacted layer. The second method has been employed in this study. In this method, by tamping the surface of each layer, some of the applied energy would be transferred to the underlying layers. Therefore, for reaching to a constant relative density in the whole sand mass, all the layers could not be compacted with a same number of drops. It could be predicted that the number of drops should be increased by moving from lower layer to upper layers in the tank. To determine the number of drops pattern, a series of compaction tests were done in this study. Different patterns have been tried to find the appropriate ones that provide a homogenous sand deposit with relative density of 30, 45, and 60%. The same study had been done for layered soil.

Equipment

1. Compaction plate

2. Unit weight cans
3. Electronic scale

The weight of hammer and the height of fall were fixed at 7.12kg and 200mm, respectively. The height of each layer is 150mm; therefore, the volume of layer is 500x500x150mm. The only complication is finding the appropriate pattern for number of drops for each layer to reach to the desired density.

Procedure

1. Fill the sand distribution tank and pour the sand in the tank by the hose (Figure B-1a) until the sand level reaches to the height of 75mm (middle of the fourth layer).
2. Make the surface of the soil completely level (Figure B-1b).
3. Place the unit weight can at the corner of the tank (Figure B-1c).
4. Keep pouring the sand until it reaches to the top of the fourth layer (Figure B-1d).
5. Make the surface of the soil level (Figure B-1e).
6. Place the compaction plate on the soil surface and compact it with the specified number of drops.
7. Repeat this procedure for the other three layers.
8. Start emptying the tank and take the cans out carefully (Figure B-1h).
9. Weight the known volume unit weight cans and determine the unit weight of the soil.
10. By implementing the following equation, determine the relative density of soil in each layer.

$$D_r = \left(\frac{\gamma_d - \gamma_{d\_\min}}{\gamma_{d\_\max} - \gamma_{d\_\min}} \right) \times \frac{\gamma_{d\_\max}}{\gamma_d}$$

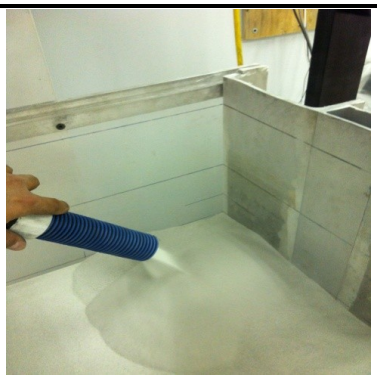

(a)

(b)

(c)

(d)

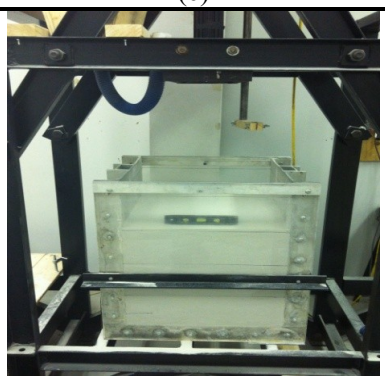

(e)

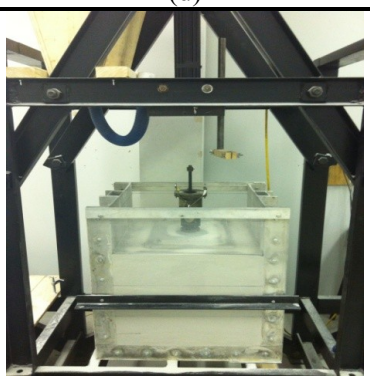

(f)

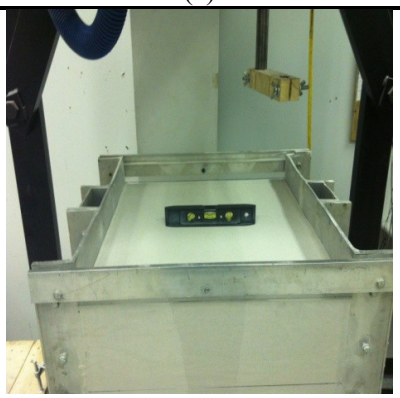

(g)

(h)

Figure B-1 Step by step procedure of the compaction test

Compaction tests results on homogenous soil

- Relative Density of 30% (Loose condition)

Five different compaction patterns have been tried for loose condition. The number of drops for each trial has been reported in Table B-1.

Table B-1 Number of drops for each trial of compaction test on homogenous loose sand

	First Trial	Second Trial	Third Trial	Forth Trial	Fifth Trial
Layer No. 1	34	34	32	33	**33**
Layer No. 2	28	28	28	28	**28**
Layer No. 3	22	17	24	24	**24**
Layer No. 4	16	8	20	17	**16**

The Figure B-2 illustrates the variation of relative density in the depth of tank for different trials. It is clear that the values of the fifth trial are close to 30% provide an average density of 31.75% in the test tank.

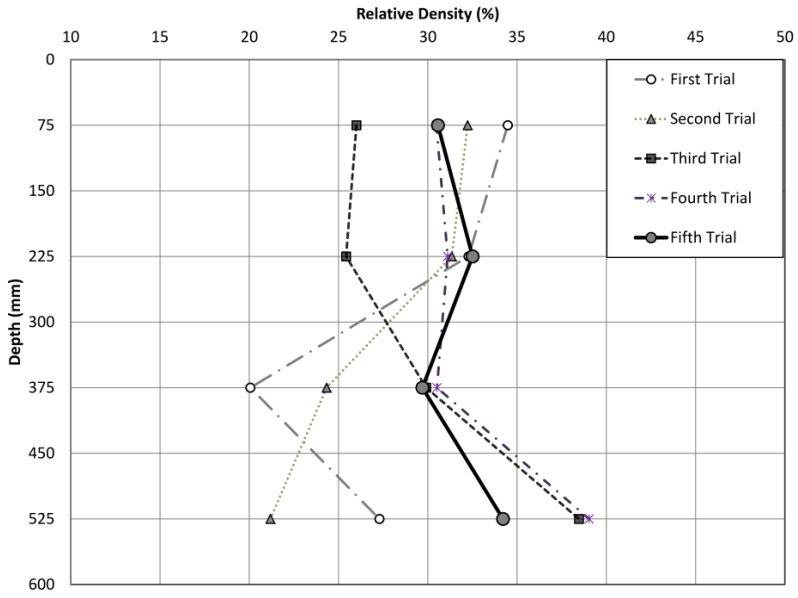

Figure B-2 Variation of relative density by depth in the test tank in loose condition (40-10 Silica Sand)

- Relative Density of 45% (Medium condition)

Five different compaction patterns have been tried for medium condition. The number of drops for each trial has been reported in Table B-2.

Table B-2 Number of drops for each trial of compaction test on homogenous medium sand

	First Trial	Second Trial	Third Trial	Forth Trial	Fifth Trial
Layer No. 1	56	63	69	72	**74**
Layer No. 2	50	58	65	68	**68**
Layer No. 3	44	50	54	57	**60**
Layer No. 4	38	30	20	22	**24**

The Figure B-3 shows the variation of relative density in the depth of tank for different trials. It is obvious that the values of the fifth trial are close to 45% and provide an average density of 45.43% in the test tank.

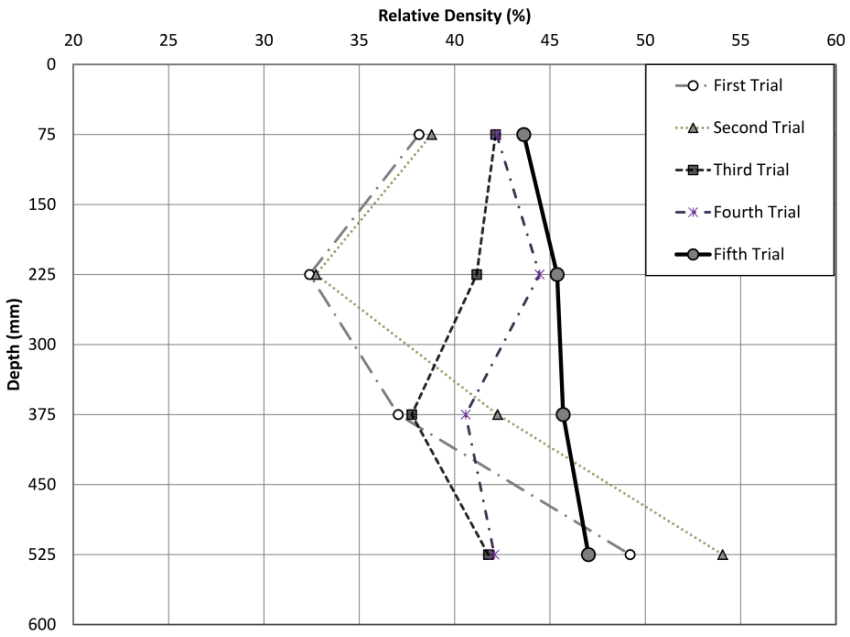

Figure B-3 Variation of relative density by depth in the test tank in medium condition (40-10 Silica Sand)

- Relative Density of 60% (Dense condition)

Three different compaction patterns have been tried for dense condition. The number of drops for each trial has been reported in Table B-3.

Table B-3 Number of drops for each trial of compaction test on homogenous dense sand

	First Trial	Second Trial	Third Trial
Layer No. 1	125	172	**188**
Layer No. 2	113	160	**175**
Layer No. 3	92	126	**137**
Layer No. 4	32	42	**45**

The Figure B-4 shows the variation of relative density in the depth of tank for different trials. It is obvious that the values of the fifth trial are close to 60% and provide an average density of 60.18% in the test tank.

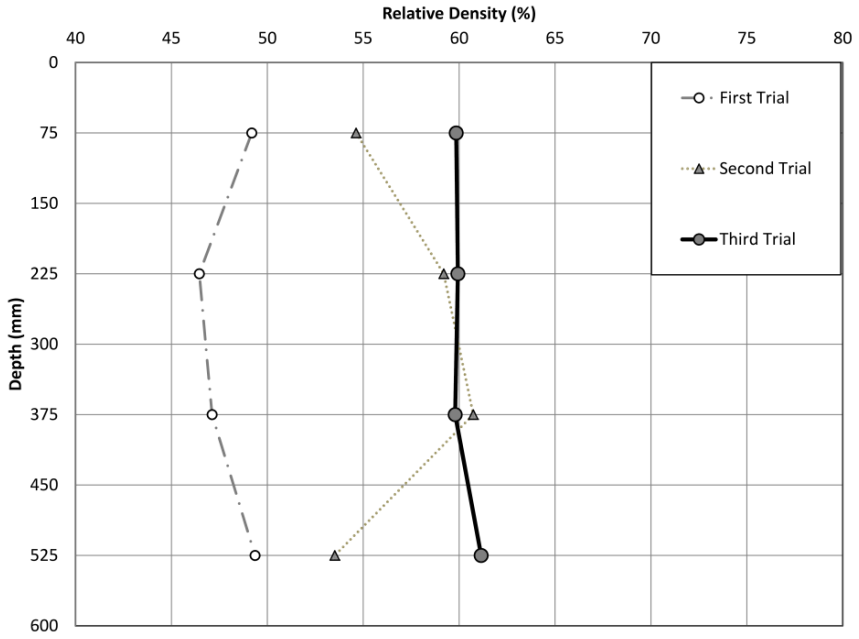

Figure B-4 Variation of relative density by depth in the test tank in dense condition (40-10 Silica Sand)

All the tests were done on 40-10 silica sand and it was expected that changing the particle size distribution would not change the compaction pattern. To verify this assumption, the 70-30 silica sand got compacted with the compaction pattern of 30% relative density. The results are presented in the Figure B-5 that proofs the initial assumption.

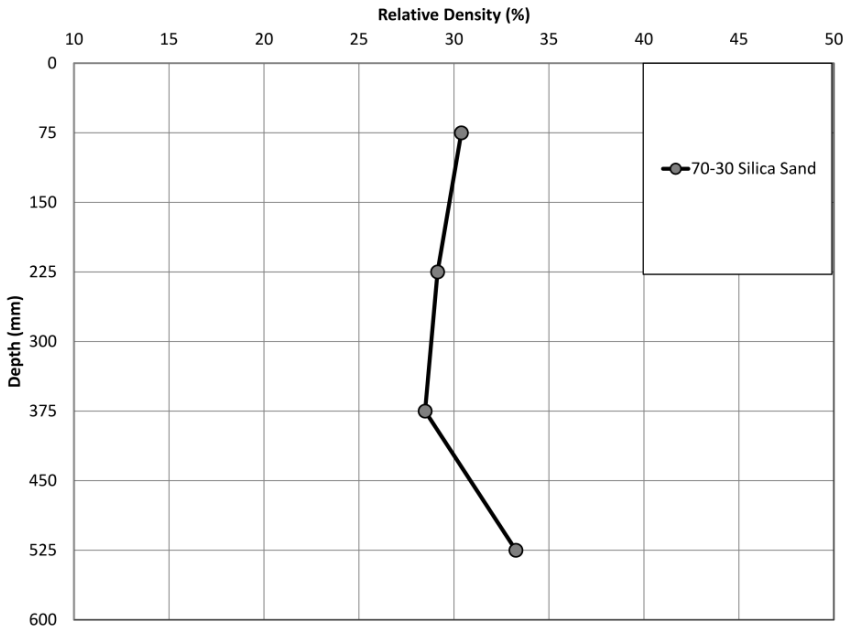

Figure B-5 Variation of relative density by depth in the test tank in loose condition (70-30 Silica Sand)

Compaction tests results on layered soil

- Relative density of 30 on 45% (Loose on Medium)

Three different compaction patterns have been tried for finding the appropriate number of drops which provides loose on medium condition. The number of drops for each trial has been reported in Table B-4.

Table B-4 Number of drops for each trial of compaction test on layered sand (loose on medium)

	First Trial	Second Trial	Third Trial
Layer No. 1	33	33	**33**
Layer No. 2	28	29	**28**
Layer No. 3	60	68	**74**
Layer No. 4	24	26	**24**

The Figure B-6 shows the variation of relative density in the depth of tank for different trials. The density of two top layers are fairly close to 30% that simulate the loose condition and density of two bottom layers are around 45% that represent medium condition.

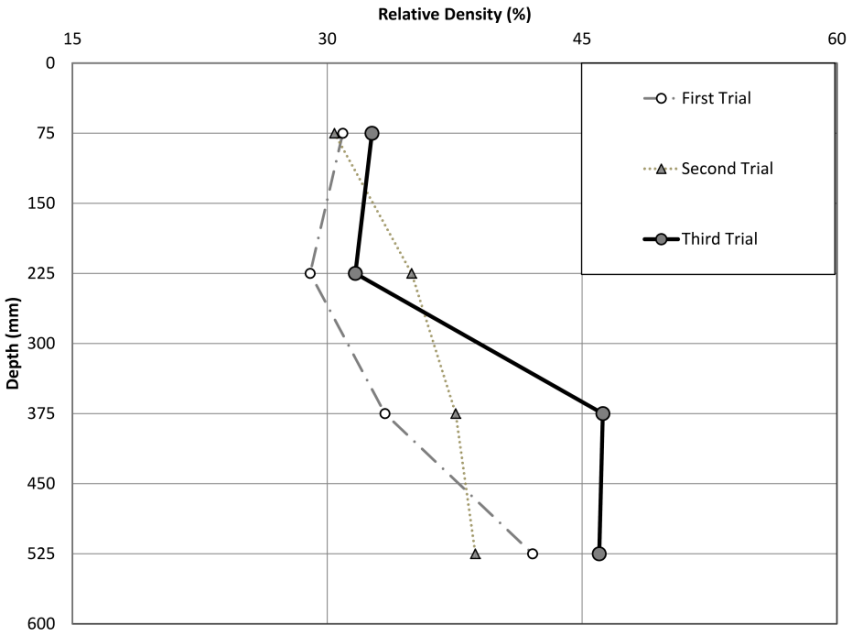

Figure B-6 Variation of relative density by depth in the test tank for loose on medium condition (40-10 Silica Sand)

- Relative density of 30 on 60% (Loose on Dense)

Four different compaction patterns have been tried for finding the appropriate number of drops which provides loose on dense condition. The number of drops for each trial has been reported in Table B-5.

Table B-5 Number of drops for each trial of compaction test on layered sand (loose on dense)

	First Trial	Second Trial	Third Trial	Forth Trial
Layer No. 1	33	25	25	**22**
Layer No. 2	28	23	22	**20**
Layer No. 3	175	188	193	**203**
Layer No. 4	45	45	50	**50**

The Figure B-7 shows the variation of relative density in the depth of tank for different trials. The density of two top layers are fairly close to 30% that simulate the loose condition and density of two bottom layers are around 60% that represent dense condition.

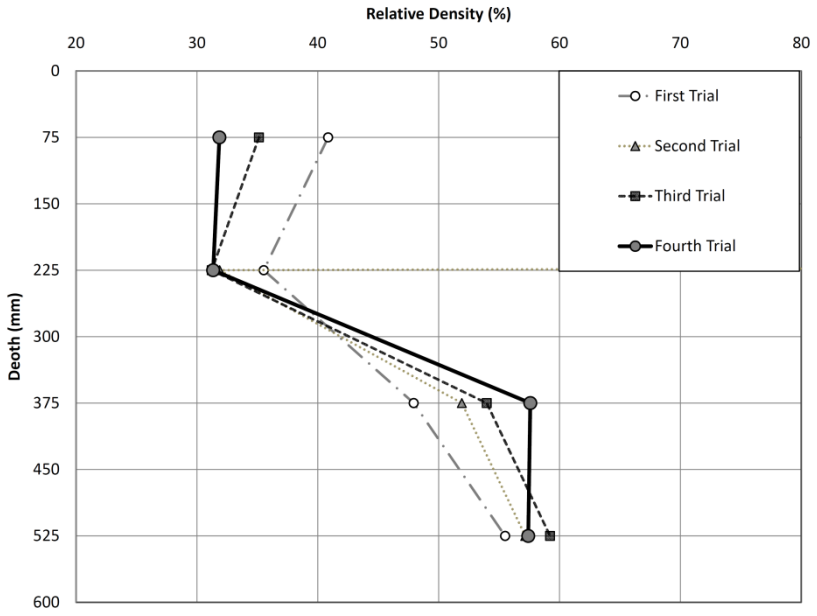

Figure B-7 Variation of relative density by depth in the test tank for loose on dense condition (40-10 Silica Sand)

- Relative density of 45 on 60% (Medium on Dense)

Two different compaction patterns have been tried for finding the appropriate number of drops which provides medium on dense condition. The number of drops for each trial has been reported in Table B-6.

Table B-6 Number of drops for each trial of compaction test on layered sand (medium on dense)

	First Trial	Second Trial
Layer No. 1	74	**73**
Layer No. 2	68	**68**
Layer No. 3	193	**200**
Layer No. 4	45	**49**

The Figure B-8 shows the variation of relative density in the depth of tank for different trials. The density of two top layers are fairly close to 45% that simulate the medium condition and density of two bottom layers are around 60% that represent dense condition.

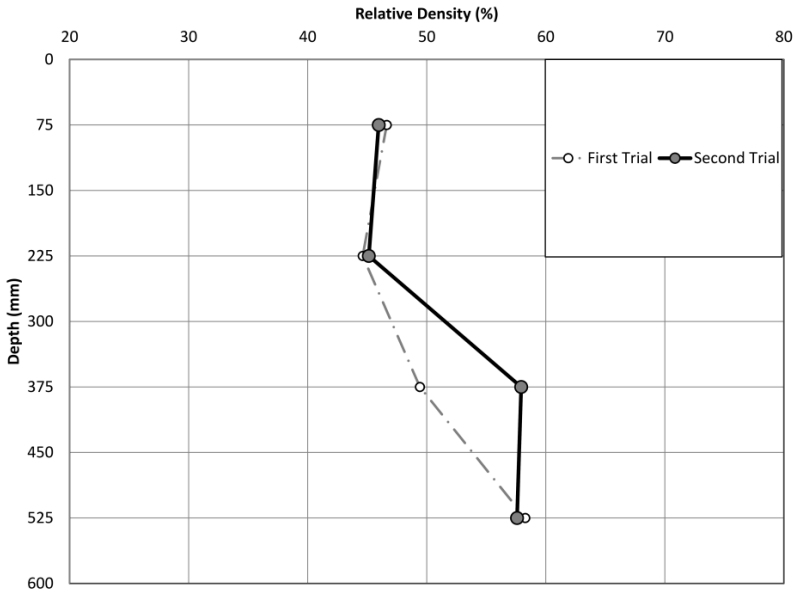

Figure B-8 Variation of relative density by depth in the test tank for medium on dense condition (40-10 Silica Sand)

Appendix C

VEE Program